water

Special Issue Reprint

Advances in Management and Optimization of Urban Water Networks

Edited by
Mohsen Hajibabaei, Robert Sitzenfrei, Mohsen Shahandashti and Milad Latifi

mdpi.com/journal/water

MDPI

Advances in Management and Optimization of Urban Water Networks

Advances in Management and Optimization of Urban Water Networks

Guest Editors

Mohsen Hajibabaei
Robert Sitzenfrei
Mohsen Shahandashti
Milad Latifi

MDPI

Basel • Beijing • Wuhan • Barcelona • Belgrade • Novi Sad • Cluj • Manchester

Guest Editors

Mohsen Hajibabaei
Department of Infrastructure Engineering
University of Innsbruck
Innsbruck
Austria

Robert Sitzenfrei
Department of Infrastructure Engineering
University of Innsbruck
Innsbruck
Austria

Mohsen Shahandashti
Department of Civil Engineering
University of Texas at Arlington
Arlington
USA

Milad Latifi
WSP
Exeter
UK

Editorial Office
MDPI AG
Grosspeteranlage 5
4052 Basel, Switzerland

This is a reprint of the Special Issue, published open access by the journal *Water* (ISSN 2073-4441), freely accessible at: https://www.mdpi.com/journal/water/special_issues/3RZ9M9675N.

For citation purposes, cite each article independently as indicated on the article page online and as indicated below:

Lastname, A.A.; Lastname, B.B. Article Title. *Journal Name* **Year**, *Volume Number*, Page Range.

ISBN 978-3-7258-8577-0 (Hbk)
ISBN 978-3-7258-8578-7 (PDF)
https://doi.org/10.3390/books978-3-7258-8578-7

© 2026 by the authors. Articles in this reprint are Open Access and distributed under the Creative Commons Attribution (CC BY) license. The reprint as a whole is distributed by MDPI under the terms and conditions of the Creative Commons Attribution-NonCommercial-NoDerivs (CC BY-NC-ND) license (https://creativecommons.org/licenses/by-nc-nd/4.0/).

Contents

About the Editors . . . . . **vii**

Preface . . . . . **ix**

Mohsen Hajibabaei, Robert Sitzenfrei, Mohsen Shahandashti and Milad Latifi
Advances in Management and Optimization of Urban Water Networks
Reprinted from: *Water* **2026**, *18*, 1476, https://doi.org/10.3390/w18121476 . . . . . **1**

Iman Bahrami Chegeni, Mohammad Mehdi Riyahi, Amin E. Bakhshipour, Mohamad Azizipour and Ali Haghighi
Developing Machine Learning Models for Optimal Design of Water Distribution Networks Using Graph Theory-Based Features
Reprinted from: *Water* **2025**, *17*, 1654, https://doi.org/10.3390/w17111654 . . . . . **14**

Paweł Suchorab, Dariusz Kowalski and Małgorzata Iwanek
Fractal-Based Approach to Simultaneous Layout Routing and Pipe Sizing of Water Supply Networks
Reprinted from: *Water* **2025**, *17*, 2745, https://doi.org/10.3390/w17182745 . . . . . **47**

Maria Cunha, João Marques and Enrico Creaco
Water Networks Management: Assessment of Heuristic and Exact Approaches for Optimal Valve Location and Operation Settings Schedule
Reprinted from: *Water* **2025**, *17*, 3249, https://doi.org/10.3390/w17223249 . . . . . **69**

Samer El-Zahab, Eslam Mohammed Abdelkader, Ali Fares and Tarek Zayed
Comparative Analysis of Machine Learning Techniques in Enhancing Acoustic Noise Loggers' Leak Detection
Reprinted from: *Water* **2025**, *17*, 2427, https://doi.org/10.3390/w17162427 . . . . . **101**

Milad Latifi, Shahab Sharafodin and MohammadAmin Gheibi
Predictive Rehabilitation of Clean Water Customer Connections Leveraging Machine Learning Algorithms and Failure Time Series Data
Reprinted from: *Water* **2026**, *18*, 110, https://doi.org/10.3390/w18010110 . . . . . **119**

Jefferson S. Rocha, José Gescilam S. M. Uchôa, Bruno M. Brentan and Iran E. Lima Neto
Key Calibration Strategies for Mitigation of Water Scarcity in the Water Supply Macrosystem of a Brazilian City
Reprinted from: *Water* **2025**, *17*, 883, https://doi.org/10.3390/w17060883 . . . . . **136**

Ying Tang, Yujie Zhao, Zhaoguang Li, Jinjun Zhou and Hao Wang
A Method to Determine the Design Flow of Stormwater Pipe Networks Based on Dynamic Wave Simulation
Reprinted from: *Water* **2024**, *16*, 3532, https://doi.org/10.3390/w16233532 . . . . . **152**

Mohsen Rezaee, Peter Melville-Shreeve and Hussein Rappel
Probabilistic Forecasting and Anomaly Detection in Sewer Systems Using Gaussian Processes
Reprinted from: *Water* **2025**, *17*, 2357, https://doi.org/10.3390/w17162357 . . . . . **171**

Francisco Javier García-Martínez, Francisco Osorio and Francisco González-Gómez
Challenges of Urban Water Cycle Management in Small Spanish Municipalities: The Case of the Province of Granada
Reprinted from: *Water* **2025**, *17*, 1750, https://doi.org/10.3390/w17121750 . . . . . **193**

About the Editors

Mohsen Hajibabaei

Mohsen Hajibabaei is a Postdoctoral Researcher at the Unit of Environmental Engineering and a Lecturer at the Institute of Design, University of Innsbruck, Austria. His research focuses on urban water management and infrastructure systems, with particular expertise in complex network analysis, sustainability assessment, resilience analysis, and environmental impact assessment. His work addresses the planning, design, modelling, and optimization of water distribution, stormwater, and reclaimed water systems, aiming to support more resilient, sustainable, and efficient urban water networks.

Robert Sitzenfrei

Robert Sitzenfrei is a Professor for Urban Water Management and Head of the Unit of Environmental Engineering at the University of Innsbruck, Austria. His research focuses on urban water management, water distribution systems, urban drainage systems, infrastructure resilience, digitalization, and the sustainable planning and operation of urban water infrastructure. He has contributed extensively to research on the analysis, modelling, optimization, and management of urban water networks and related infrastructure systems.

Mohsen Shahandashti

Mohsen Shahandashti is a Professor of Civil Engineering and Associate Dean at the University of Texas at Arlington, USA. His research focuses on infrastructure systems, resilient infrastructure, disaster engineering, vulnerability assessment, construction engineering, and the application of data-driven and analytical methods to improve the performance and resilience of civil infrastructure. His work supports the development of safer, more reliable, and more sustainable infrastructure systems under changing environmental and operational conditions.

Milad Latifi

Milad Latifi is affiliated with WSP, UK. His research interests include water engineering, water distribution networks, asset management, pipe failure prediction, machine learning, digital twins, and smart water systems. His work combines data-driven modelling, sensor-based approaches, and water infrastructure analysis to support predictive maintenance, failure assessment, and improved management of urban water systems.

Preface

This Reprint brings together selected contributions from the Special Issue "Advances in Management and Optimization of Urban Water Networks". The collected papers address key challenges in the planning, design, operation, monitoring, rehabilitation, and management of urban water systems, including water distribution networks, stormwater and sewer systems, and broader urban water cycle management. The aim of this Reprint is to present recent methodological developments and practical applications that support more efficient, resilient, and sustainable urban water infrastructure. We hope that this collection will be useful for researchers, engineers, water utilities, practitioners, and decision-makers working in the field of urban water management.

Mohsen Hajibabaei, Robert Sitzenfrei, Mohsen Shahandashti, and Milad Latifi
Guest Editors

water

MDPI

Editorial

Advances in Management and Optimization of Urban Water Networks

Mohsen Hajibabaei [1], Robert Sitzenfrei [1,*], Mohsen Shahandashti [2] and Milad Latifi [3]

[1] Unit of Environmental Engineering, Department of Infrastructure Engineering, University of Innsbruck, Innsbruck 6020, Austria; mohsen.hajibabaei@uibk.ac.at
[2] Department of Civil Engineering, University of Texas at Arlington, Arlington, TX 76019, USA; mohsen@uta.edu
[3] WSP, 3rd Floor, Longbrook House, New North Road, Exeter EX4 4GL, UK; milad.latifi@wsp.com
* Correspondence: robert.sitzenfrei@uibk.ac.at

1. Introduction

The effective management and optimization of urban water networks is essential for addressing the growing challenges posed by aging infrastructure, population growth, urbanization, and climate change. Given the complexity of these systems, such challenges increasingly require advanced analytical and data-driven methods, innovative technologies, and strategic planning approaches.

This Special Issue brings together contributions that address key challenges in urban water networks. At a broader level, it responds to urban water challenges from different but complementary perspectives, including advanced modeling, new optimization techniques, innovative monitoring approaches, and practical management strategies. Each contribution highlights a particular advance, and together they reflect broader progress toward improving urban water systems' efficiency, reliability, and sustainability.

With particular focus on three main domains—(1) water distribution networks (WDNs), (2) urban drainage networks (UDNs), and (3) broader urban water management perspectives—the included studies span different stages of system lifecycles, ranging from network design to operation, rehabilitation, and governance. More specifically, they reflect current research on network design and optimization (e.g., pipe sizing and layout generation), operational decision-making (e.g., control optimization), abnormal condition monitoring and detection (e.g., leak detection and overflow prediction), predictive maintenance and rehabilitation planning (e.g., failure prediction), and governance-related challenges in urban water systems.

The introduction is therefore structured around these three thematic domains of (1) WDNs, (2) UDNs, and (3) broader urban water management perspectives. For each domain, it outlines the broader background, key research gaps, and emerging needs across the relevant stages of the system lifecycle, thereby providing the context for the contributions included in this Special Issue.

1.1. Water Distribution Networks

WDN research has progressed significantly in recent decades, reflecting growing interest in both the design of new systems and the operation and management of existing ones. In this Special Issue, the contributions concerning WDNs can be broadly organized into two main areas: network design, and operation and management.

1.1.1. Network Design

WDN design encompasses both network layout, including structural arrangement and component routing, and hydraulic design, which involves selecting physical characteristics such as pipe diameters. The evolution of hydraulic design reflects the broader trajectory of the field, moving from early linear and nonlinear programming approaches focused on cost minimization and basic hydraulic constraints [1] to increasingly advanced optimization frameworks capable of addressing multiple, often competing, objectives [2]. In particular, metaheuristic and multi-objective algorithms have enabled the inclusion of performance criteria such as resilience and reliability alongside cost [3]. However, these approaches remain heavily dependent on repeated hydraulic simulations, which limit their efficiency, particularly for large or complex systems [4]. As a result, computational demand continues to represent a major challenge in the search for optimal hydraulic designs.

In response, alternative approaches have gained increasing attention. Graph theory, for example, has been applied to different types of WDN analysis to capture structural characteristics in a computationally efficient manner [4,5], while data-driven methods, particularly machine learning, have shown strong potential for modeling complex system behavior [6]. More recently, interest has grown in combining graph-based representations with machine learning techniques in order to exploit both structural insight and data-driven pattern recognition for various types of WDN analysis [7]. Such integration appears particularly promising for hydraulic design tasks such as pipe sizing, which are inherently complex and computationally intensive. However, despite this potential, the application of these combined approaches to hydraulic design remains largely unexplored. This makes their further investigation and application in WDN design a clear and emerging research direction, as reflected in this Special Issue.

A further key aspect of WDN design concerns network layout generation, a factor inherently connected to hydraulic sizing, as network configuration directly influences hydraulic performance and, consequently, pipe-sizing decisions [8]. However, many existing methods still address these aspects sequentially, assuming a predefined layout before carrying out hydraulic design [9], and although simultaneous layout and sizing approaches have been proposed [10], they are computationally intensive and difficult to apply to large-scale and real-world systems. These challenges point to another important research direction in WDN design which is also explored in this Special Issue.

1.1.2. Operation and Management

Beyond design, the effective operation and management of WDNs require maintaining system performance under varying dynamic and often uncertain conditions. This stage encompasses several interconnected tasks, including operational optimization, system monitoring, predictive maintenance, and rehabilitation planning, which together frame the contributions presented in this Special Issue.

A first major challenge in WDN operation concerns the optimization of control strategies and system interventions in order to balance competing objectives. However, operational problems, particularly in design-for-control applications, are often highly nonlinear, combinatorial, and strongly coupled with hydraulic behavior [11,12]. For instance, they could involve the simultaneous determination of structural interventions, such as valve or pipe placement, and operational policies, such as valve settings over time, to achieve competing objectives, including pressure-induced leakage reduction and resilience enhancement. Although optimization techniques ranging from global exact approaches [13] to heuristic methods [14] have been explored as decision-support tools for such tasks, they are often applied in isolation, limiting understanding of their comparative performance and practical implications. In particular, while exact methods often rely on model simplifi-

https://doi.org/10.3390/w18121476

cations, metaheuristic approaches can better accommodate real-world complexity but do not guarantee global optimality [12,13]. Addressing these challenges and improving optimization mechanism understanding in complex operational problems, therefore, remain important research directions addressed in the contributions of the Special Issue.

In addition to control strategy optimization, effective WDN management also depends on the ability to monitor system behavior and identify abnormal conditions. In this context, leak detection remains a major challenge in many aging WDNs because of its impact on water loss, network reliability, and operational costs. At the same time, conventional methods based on visual inspection or pressure monitoring are often labor-intensive and insufficient for identifying small or intermittent leaks [15]. In response, various sensing technologies, such as acoustic, vibration, ultrasonic, and fiber-optic systems, have been developed [15,16], with acoustic-based techniques appearing particularly promising given their ability to capture leak-induced signals [17]. When combined with data-driven approaches [18], sensing technologies improve detection capability by enabling the analysis of complex and noisy data. However, many existing acoustic-based studies are based on controlled laboratory conditions [19] or focus only on isolated aspects of acoustic behavior, such as the effects of pipe diameter and material on leak-induced signals [20], limiting their applicability to real-world and large-scale networks. Moreover, the comparative performance and integration of different data-driven models for such acoustic-based techniques remain insufficiently explored. This highlights the need for comprehensive evaluation frameworks that leverage real operational data to assess and combine machine learning techniques for reliable, real-time leak detection in WDNs, an aspect further explored in this Special Issue.

Building on operational optimization and system monitoring, another key direction in WDN management involves predictive maintenance and failure forecasting to support rehabilitation and asset management decisions. Failure prediction in WDNs, particularly for pipes, has evolved from traditional statistical formulations [21] toward more advanced machine learning approaches [22], driven by the need to better capture complex deterioration patterns and support proactive asset management. Rehabilitation planning must, however, extend beyond deterioration-driven failure prediction to also account for sudden and large-scale serviceability loss caused by extreme events such as earthquakes, which demand a system-level perspective beyond what is possible with pipe-level failure forecasting alone. In this context, research has advanced from early single-objective formulations toward multi-objective and risk-averse frameworks, including approaches that optimize rehabilitation strategies while explicitly accounting for decision-makers' risk attitudes [23] and game-theoretic models that identify Pareto-optimal rehabilitation plans under competing objectives [24]. The interaction between pipe degradation and seismic vulnerability adds a further layer of complexity, as deteriorating pipes exhibit increasing seismic fragility over time, altering the relative criticality of rehabilitation targets and rendering static rehabilitation plans insufficient [25]. To address the high computational cost of hydraulic-simulation-based optimization at the city scale, topology-based surrogate methods have been proposed that substantially reduce runtimes while preserving solution quality [26]. Alongside these hazard-driven challenges, failure prediction efforts have concentrated mainly on water mains [27], whereas failures in service lines remain comparatively less studied, despite their substantial contribution to total network failures in some regions and their direct impact on customer service [28]. This highlights the need for more reliable predictive frameworks that can identify high-risk service lines and support proactive, data-driven maintenance planning, a consideration further addressed by one of the contributions presented in this Special Issue.

https://doi.org/10.3390/w18121476

Underpinning the majority of operational and management challenges, especially in some of the tasks discussed above, is the need for reliable and well-calibrated hydraulic models. In this context, the calibration of large-scale water supply macrosystems remains a major challenge, particularly when applied to real networks characterized by limited data availability, complex operational rules, and uncertain topology. For this reason, many calibration studies have focused on hypothetical or benchmark models [29], which offer methodological simplicity but may not adequately represent real systems' complexity. Although several advanced calibration techniques have been proposed, including graph-based metamodels and artificial neural networks [30,31], their application to large, dynamic, real-world systems is still difficult in practice. This highlights the need for practical calibration strategies that can improve the reliability of large-scale hydraulic models while incorporating prior knowledge of actual system behavior and operational conditions, an important gap addressed by a contribution in this Special Issue.

1.2. Urban Drainage Networks

Similar to WDNs, research on UDNs, including both separate stormwater systems and combined sewer networks, can be broadly grouped into two main areas: network design, and operation and management.

1.2.1. Network Design

As in WDNs, the UDN design process typically involves defining the network layout (often assumed to be predefined) followed by the estimation of hydraulic parameters such as pipe diameter and slope, which are functions of the design flow. Traditionally, the Rational Method (RM) has been widely used to estimate design flow rates from sub-catchments due to its simplicity and limited data requirements, while Manning's equation is applied for hydraulic calculations [32]. However, the RM assumes steady and uniform flow conditions and only provides peak flow values limiting its ability to represent actual unsteady hydraulic behavior, particularly in large-scale systems. To improve design accuracy, hydrological and hydraulic-simulation-based approaches have been increasingly adopted, including SWMM-based iterative design methods [33] and various optimization techniques such as genetic algorithms [34], cellular automata [35], and ant colony optimization [36]. While these approaches enhance design precision, many still rely on RM-based assumptions for estimating design flows. Moreover, when employing detailed hydraulic models such as SWMM to estimate design flows, they must be calibrated with extensive, reliable, and complete data, which are often uncertain or unavailable in practice [37]. In addition, optimization-based methods typically depend on evaluating multiple design alternatives, leading to high computational demand as system scale increases.

These limitations highlight the need for more efficient approaches to estimating design flows that can better capture unsteady hydraulic behavior while reducing data requirements and computational complexity, a research gap addressed in this Special Issue.

1.2.2. Operation and Management

Moving beyond UDN design, effective management and operation, particularly in combined sewer systems, require reliable flow condition and overflow event predictions, which are critical for mitigating urban flooding and protecting public health. To address this, a range of modeling approaches has been developed, including physics-based simulators [38], data-driven surrogate approaches [39], and hybrid frameworks [40]. While physical models provide a detailed representation of hydrological and hydraulic processes through governing equations, they often require significant simplifications, are computationally expensive [41], and depend on detailed and frequently uncertain system information such as network topology and condition [42]. In contrast, data-driven models

https://doi.org/10.3390/w18121476

offer higher computational efficiency and the ability to capture complex relationships directly from data [43], but they often lack physical interpretability and reliability [44]. Hybrid or physics-informed models attempt to combine these advantages [45], yet their complexity and implementation challenges limit their practical applicability. Despite these advances, there remains a lack of efficient and uncertainty-aware approaches capable of providing real-time prediction and anomaly detection in complex and data-scarce UDNs. Addressing this gap is essential for improving operational decision-making and is the focus of one of the contributions presented in this Special Issue.

1.3. Broader Urban Water Management Perspectives

While recent advances in WDNs and UDNs have primarily focused on technological and data-driven solutions, such as optimization, simulation, and machine learning for leakage detection, flow prediction, and anomaly identification, these efforts largely address the physical and operational dimensions of urban water systems. However, effective urban water management also depends on institutional, economic, and governance structures, which have received comparatively less attention and require further systematic investigation. In particular, practice-based and diagnostic approaches that examine how governance arrangements and managerial processes shape urban water services at the municipal level remain limited. This highlights the need for more integrated analyses that complement technical developments with institutional perspectives, an aspect explored by the final contribution to this Special Issue.

The research gaps and emerging needs outlined in the Introduction are addressed in this Special Issue through the contributions presented in the following sections. Section 2 provides an initial overview of these papers, which are then summarized in more detail in Section 3. Finally, Section 4 reflects on the main insights emerging from these contributions and highlights important directions for future research.

2. Overview of Contributions

From the various submissions received for this Special Issue, a total of nine high-quality papers were accepted and published. Table 1 provides a concise overview of these contributions, summarizing them according to our three main identified domains: WDNs, UDNs, and broader urban water management perspectives. In addition, it highlights each paper's main contribution type, methodological approach, and practical applications. Collectively, these contributions reflect the research gaps and emerging needs identified in the Introduction and illustrate the diversity of current approaches being developed to address key challenges in urban water systems.

Table 1. Overview of the contributions included in this Special Issue.

Contribution No.	Main Domain	Contribution Type	Research Methods	Potential Application
1	WDN	Network design (pipe sizing)	Graph-theoretic and hydraulic feature extraction, feature selection, and ensemble machine learning	Optimal diameter design with reduced computational burden
2	WDN	Network design (layout and pipe sizing)	Fractal-based simultaneous routing and sizing with modified Murray's law	Generation of network layouts and pipe-sizing decisions
3	WDN	Operational optimization (design-for-control)	Comparative assessment of heuristic and exact optimization for optimal valve location and operation settings	Leakage reduction and resilience enhancement through design-for-control

https://doi.org/10.3390/w18121476

Table 1. *Cont.*

Contribution No.	Main Domain	Contribution Type	Research Methods	Potential Application
4	WDN	Monitoring (leak detection)	Wireless acoustic noise loggers combined with machine learning and ensemble models	Real-time leak detection and leak management
5	WDN	Predictive maintenance (rehabilitation planning)	Machine learning algorithms using service-line attributes and failure history	Identification of high-risk service lines and proactive rehabilitation planning
6	WDN	Calibration (hydraulic modeling)	PSO-based calibration combined with operational-rule adjustment and engineering judgment	Improving reliability of large-scale hydraulic models for real system operation
7	UDN	Network design (hydraulic design)	Dynamic-wave-simulation-based method coupled with SWMM and iterative design	More realistic estimation of design flow, pipe diameters, and slopes
8	UDN	Operation (forecasting and anomaly detection)	Gaussian Process Regression with probabilistic prediction	Real-time flow/depth prediction and anomaly detection in sewer systems
9	UWM	Governance and institutional analysis	Case-study-based diagnostic assessment using documentary evidence and stakeholder insights	Identification of governance and institutional constraints in small municipalities

Note(s): WDN: Water Distribution Network; UDN: Urban Drainage Network; UWM: Urban Water Management; PSO: Particle Swarm Optimization; SWMM: Storm Water Management Model.

3. Summary of Contributions

3.1. Water Distribution Systems

3.1.1. Network Design

The first contribution addresses a research gap in integrating graph-theoretic approaches with machine learning methods for the optimal design of WDNs. Their goal was to approximate optimal pipe diameters without repeatedly solving computationally intensive hydraulic equations. To build a robust training dataset, the authors generated 600 synthetic WDNs and determined the optimal pipe diameter configuration for each network using a conventional single-objective genetic algorithm. From these optimized networks, they then extracted 80 diverse features, including hydraulic attributes (e.g., flow rate, flow velocity) and graph-theoretical descriptors (e.g., shortest-path metric, clustering coefficients). To refine the input space, six different feature-selection techniques were applied to identify the most influential predictors for optimal design. Using these selected features, the authors trained four machine learning models (Random Forest, Support Vector Machine, Bagging, and Light Gradient Boosting Machine), resulting in a total of 24 ensemble model combinations. The best-performing model was subsequently applied to the well-known Hanoi benchmark network, demonstrating strong predictive capability for estimating optimal pipe diameters.

The second contribution introduces a simultaneous routing and sizing (SRS) method for WDNs, adopting a cooperative approach that integrates layout routing and pipe diameter assignment. The layout generation is based on fractal geometry principles, enabling the creation of hierarchical, branching network structures that resemble patterns observed in natural systems. For pipe sizing, the method incorporates a modified form of Murray's

https://doi.org/10.3390/w18121476

law [46], providing a scaling relationship that links pipe diameters to flow distribution. In this approach, routing decisions are guided by multiple criteria, including total pipe length and construction cost, with the latter being dependent on pipe diameter. This creates an interaction between layout and sizing during the iterative design process, although the method remains rule-based rather than building a global optimization framework. The approach was applied to both single- and multi-source configurations using synthetic case studies. The results suggest that the SRS method can reduce design complexity and provide a structured procedure for generating feasible network layouts.

3.1.2. Operation and Management

The third contribution addresses the need to better understand the underlying mechanisms of metaheuristic and exact optimization approaches for the design-for-control of water distribution networks. To this end, it investigates the simultaneous determination of structural interventions, such as the installation of valves and/or pipes, together with valve operational settings in existing networks, with the aim of optimizing two conflicting objectives: minimizing pressure-induced background leakage and maximizing network resilience. The authors apply an upgraded Multi-Objective Simulated Annealing with new Generation and Reannealing procedures (MOSA-GR) [47] and compare its performance with the exact global optimization spatial branch-and-bound method previously proposed for the same problem [13]. Using the same case studies and evaluation framework, the paper provides a structured comparison of the two approaches and offers insight into their mathematical and hydraulic implications. The results show that the metaheuristic approach can generate high-quality solutions in a shorter computational time while avoiding the model simplifications required by the exact method, thereby demonstrating strong potential for addressing complex real-world design-for-control problems.

The fourth contribution addresses the limited real-world applicability of many existing leak detection studies by integrating wireless acoustic noise loggers with machine learning models for real-time leakage detection in water pipelines. Unlike earlier work, which often relied on laboratory or testbed datasets, this study is based on 2110 acoustic signals collected in real urban environments in Hong Kong, comprising 992 leak and 1118 non-leak cases. The authors evaluate several machine learning algorithms, with Random Forest achieving the highest accuracy (93.68%) and K-Nearest Neighbors and Multi-Layer Perceptron also performing strongly, offering robust alternative approaches. An ensemble model combining these top-performing methods further improved detection performance. By contrast, YamNet, a general-purpose deep audio classification model based on pre-trained deep learning for sound recognition [47], showed weaker results, likely due to its sensitivity to urban background noise and its lack of adaptation to leak-specific acoustic patterns. Overall, the study demonstrates the strong potential of data-driven acoustic monitoring for practical and sustainable leak management in WDNs.

The fifth contribution presents a machine learning-based rehabilitation framework for forecasting the likelihood of failures in service lines within WDNs, with the aim of supporting proactive decision-making. Using 11 years of service-line data, including variables such as diameter, length, age, material, pressure, and demand, together with more than 88,000 recorded failures, the study evaluated three predictive models: Random Forest (RF), Extreme Gradient Boosting (XGB), and Long Short-Term Memory (LSTM). The first nine years of data were used for training, while the final two years were reserved for validation, and the analysis was repeated to examine the effect of training data length on prediction performance. It was shown that the tree-based models, RF and XGB, outperformed LSTM, mainly because the available inputs were dominated by static service-line attributes rather than rich temporal signals. Overall, the study highlights the potential of machine learning

https://doi.org/10.3390/w18121476

for identifying high-risk service lines and supporting predictive asset management. The authors also indicated that future improvements could be achieved by incorporating measured pressure data, environmental variables such as soil conditions, and more detailed information on failure type and severity into the models.

The sixth contribution addresses the challenge of calibrating large-scale real water supply macrosystems by considering not only physical parameters, but also the influence of actual operational behavior on model performance. Focusing on the metropolitan water supply system of Fortaleza, Brazil, the authors calibrated absolute pipe roughness and base demand multiplication factors using 50 pressure-head monitoring points and 40 flow-rate monitoring points over a 48 h period. In addition, the calibration process accounted for the operating rules of several pressure-reducing valves, reflecting the complexity of real system operation. To achieve a realistic model, pre-calibration operational adjustments were carried out by reviewing model outputs, revising valve control settings, and evaluating their effects on network behavior before applying Particle Swarm Optimization (PSO) to minimize the objective function. By combining engineering judgment with optimization, the study achieved acceptable agreement between simulated and observed data, highlighting the importance of practical calibration strategies for improving the reliability of large-scale hydraulic models in water-scarce urban systems.

3.2. Urban Drainage Networks

3.2.1. Network Design

The seventh contribution addresses key UDN design limitations by proposing a dynamic-wave-simulation-based method that aims to improve design flow estimation while reducing reliance on the simplifying assumptions of the Rational Method (RM). The approach bridges the gap between simple empirical methods and data-intensive hydraulic simulations by transforming traditional RM input parameters into an equivalent time-varying runoff hydrograph. This is achieved through the development of a runoff yield and flow concentration model that preserves consistency with RM while enabling unsteady flow simulation. The generated hydrograph is then used within the dynamic wave module of SWMM to compute pipe flows more realistically, and an iterative procedure is applied to determine pipe diameters and slopes across the network. The method was validated on two case studies, where results showed that design flow rates obtained using the dynamic approach were generally higher than those from the RM. Overall, the study demonstrates that incorporating unsteady hydraulic behavior into design flow estimation can enhance the reliability of UDN design while maintaining practical applicability for engineering use.

3.2.2. Operation and Management

The eighth contribution introduces an uncertainty-aware, data-driven framework for probabilistic forecasting and anomaly detection in sewer networks. The study employs Gaussian Process Regression to predict flow and water depth in a (combined) sewer system while simultaneously identifying abnormal conditions such as blockages. A key innovation lies in the design of a customizable composite kernel (i.e., the core function that defines how the model learns patterns), which is tailored to reflect underlying physical processes. The approach is demonstrated on a hypothetical sewer network, where time and precipitation are used as primary inputs, enabling the model to effectively capture both dry- and wet-weather dynamics. Results show that the model performs well even with limited training data, achieving high predictive accuracy and reliable uncertainty bounds. In addition, anomaly detection is achieved by identifying deviations beyond confidence thresholds, allowing early detection of abnormal events. Overall, the study highlights the potential of

https://doi.org/10.3390/w18121476

probabilistic, uncertainty-aware models for real-time monitoring and decision support in urban drainage systems.

3.3. Broader Urban Water Management Perspectives

The ninth contribution to this Special Issue shifts the focus from technological advancements to the institutional and governance dimensions of urban water management, with particular attention on small municipalities. The study addresses the limited consideration of small and rural service areas in both the literature and policy debates by contrasting their conditions with those of larger, better-resourced systems. Using a case-study-based diagnostic approach supported by documentary evidence, expert input, and stakeholder insights, the authors systematically analyze the structural, financial, and institutional challenges affecting water services. The findings reveal that deficiencies, such as low hydraulic performance, inadequate infrastructure, limited human capacity, and conflicts of interest, are not isolated technical issues but are deeply interconnected with governance and resource constraints. These challenges are organized into six key domains—regulation, resource availability, infrastructure, financing, stakeholder involvement, and innovation. Based on this integrated diagnosis, the authors propose a set of coordinated measures, ranging from infrastructure improvement to institutional reform. Overall, the paper highlights governance as a central lever for addressing systemic challenges and calls for a reassessment of regulatory and institutional frameworks to improve water service delivery in small municipalities.

4. Discussion and Conclusions

This Special Issue's overall aim was to respond to urban water network challenges from different but complementary perspectives. Taken together, the contributions reflect broader progress toward improving the efficiency, reliability, and sustainability of urban water systems. Across the papers, several recurring challenges emerged, including high computational demands, limited data availability and quality, the need for more accurate and transferable data-driven approaches, and difficulties in representing real-world system complexity. The following discussion highlights some of the main remaining research gaps and future directions that emerge from the Special Issue:

- **Integrating Topology, Data-Driven Methods, and Design:** The contributions in this Special Issue reflect a broader shift toward more integrated approaches to network design, combining structural, data-driven, and generative methodologies. The integration of graph theory with machine learning techniques is increasingly recognized as a powerful strategy for supporting design decisions; however, key challenges remain, particularly regarding the robustness and generalizability of such models, which depend strongly on the quality and representativeness of training data. While the Special Issue's first contribution demonstrates promising results, it is based on synthetic networks, and future work should therefore focus on improving transferability through the inclusion of real-world systems with diverse configurations, operational conditions, and components such as pumps and valves.

At the same time, these developments point toward a broader need to move beyond simplified and sequential design practices. In particular, the network design involves not only pipe sizing but also layout configuration, two inherently interconnected processes. Emerging approaches that address layout and pipe sizing simultaneously demonstrate the potential to improve efficiency while capturing the interaction between network structure and hydraulic performance. Nevertheless, further research is required to enhance these methods by incorporating hydraulic simulation, real-world constraints, and more complex network configurations, ultimately moving toward more reliable and globally

https://doi.org/10.3390/w18121476

optimal design solutions. In this context, the integration of design strategies with advanced data-driven techniques, including graph neural networks, together with improved model transparency through explainable AI tools, could offer promising directions for developing more robust, interpretable, and practical design frameworks.

- **Bridging Exact and Heuristic Optimization:** The contributions in the Special Issue show that neither metaheuristics nor exact global optimization can be viewed as a universal solution for complex network management problems. While exact (global) methods offer mathematical rigor, they often rely on simplifications that may affect hydraulic realism; metaheuristics, in turn, can better accommodate real-world complexity but do not provide formal guarantees of global optimality. This suggests an important future direction: the development of hybrid frameworks that combine the strengths of both paradigms—global rigor, hydraulic realism, and flexibility. In particular, for complex design-for-control and operational tasks, cooperative schemes integrating exact and heuristic methods could offer more reliable and practically meaningful solutions, as also suggested in [12]. Further research could therefore focus on understanding problem structure and exploiting combinatorial properties to build more efficient and intelligent optimization strategies for network management.
- **Toward More Transferable Acoustic Leak Detection:** A key direction emerging from this Special Issue's fourth contribution is the need to improve the transferability of data-driven leak detection methods across real-world systems. Although the study demonstrates strong results using a large set of real acoustic measurements, further validation is still needed under a wider range of network characteristics, operating conditions, and background noise environments. The weaker performance of general-purpose deep audio models such as YamNet also shows that models trained on broad audio datasets, which include many types of sounds but not specifically leak-induced signals in pressurized pipelines, may not be directly suitable for this task. Future research should therefore focus on more representative datasets, improved robustness under diverse field conditions, and better tailoring of data-driven models to sensing-based leak detection tasks. This would support the development of more reliable and practically deployable real-time monitoring systems for WDNs.
- **Advancing Efficient Stormwater Design:** While the seventh contribution to this Special Issue proposes a promising approach to reducing reliance on fully calibrated and data-intensive inputs for estimating dynamic design flows, its broader applicability still requires validation across diverse catchment characteristics and rainfall patterns. Thus, future research should focus on testing such approaches under varying real-world conditions to enhance their robustness. In addition, coupling dynamic flow estimation with more computationally efficient approaches, such as physics-guided graph-based methods [48], which have recently shown strong potential for efficient flow routing in pipes, offers a promising direction.
- **Integrating Governance Frameworks and Technical Innovation**: This Special Issue primarily focuses on technological innovations and emerging approaches for urban water system management, including AI-driven optimization and related advancements. While these contributions highlight the transformative potential of technical solutions, future research should move beyond purely technology-centered perspectives. Increasingly, there is a need to integrate institutional governance and policy dimensions into urban water management frameworks. As emphasized in the final contribution, many existing challenges, particularly in small municipalities, are rooted in structural and organizational constraints that can hinder the effective implementation of technological solutions. Addressing these challenges requires bridging

https://doi.org/10.3390/w18121476

engineering innovations with governance frameworks alongside fostering meaningful stakeholder engagement.

Author Contributions: Writing—original draft preparation, M.H.; writing—review and editing, R.S., M.L. and M.S. All authors have read and agreed to the published version of the manuscript.

Funding: This research was funded in part by the Austrian Science Fund (FWF) [10.55776/P36737]. For open access purposes, the author has applied a CC BY public copyright license to any accepted manuscript version arising from this submission.

Acknowledgments: The Guest Editors sincerely thank all reviewers for their time, effort, and thoughtful comments, which helped enhance the quality and clarity of the contributions included in this Special Issue. During the preparation of this Editorial, the authors used ChatGPT 5.5 to edit the language. The authors have reviewed and edited the output and take full responsibility for the content of this publication.

Conflicts of Interest: Author Milad Latifi was employed by the company WSP. The remaining authors declare that the research was conducted in the absence of any commercial or financial relationships that could be construed as a potential conflict of interest.

Abbreviations

The following abbreviations are used in this manuscript:

AI	Artificial Intelligence
LSTM	Long Short-Term Memory
MOSA-GR	Multi-Objective Simulated Annealing with Generation and Reannealing procedures
PSO	Particle Swarm Optimization
RF	Random Forest
RM	Rational Method
SRS	Simultaneous Routing and Sizing
SWMM	Storm Water Management Model
UDN	Urban Drainage Network
UWN	Urban Water Network
WDN	Water Distribution Network
XGB	Extreme Gradient Boosting

List of Contributions:

1. Bahrami Chegeni, I.; Riyahi, M.M.; Bakhshipour, A.E.; Azizipour, M.; Haghighi, A. Developing Machine Learning Models for Optimal Design of Water Distribution Networks Using Graph Theory-Based Features. *Water* **2025**, *17*, 1654.
2. Suchorab, P.; Kowalski, D.; Iwanek, M. Fractal-Based Approach to Simultaneous Layout Routing and Pipe Sizing of Water Supply Networks. *Water* **2025**, *17*, 2745.
3. Cunha, M.; Marques, J.; Creaco, E. Water Networks Management: Assessment of Heuristic and Exact Approaches for Optimal Valve Location and Operation Settings Schedule. *Water* **2025**, *17*, 3249.
4. El-Zahab, S.; Abdelkader, E.M.; Fares, A.; Zayed, T. Comparative Analysis of Machine Learning Techniques in Enhancing Acoustic Noise Loggers' Leak Detection. *Water* **2025**, *17*, 2427.
5. Latifi, M.; Sharafodin, S.; Gheibi, M. Predictive Rehabilitation of Clean Water Customer Connections Leveraging Machine Learning Algorithms and Failure Time Series Data. *Water* **2026**, *18*, 110.
6. Rocha, J.S.; Uchôa, J.G.S.M.; Brentan, B.M.; Neto, I.E.L. Key Calibration Strategies for Mitigation of Water Scarcity in the Water Supply Macrosystem of a Brazilian City. *Water* **2025**, *17*, 883.
7. Tang, Y.; Zhao, Y.; Li, Z.; Zhou, J.; Wang, H. A Method to Determine the Design Flow of Stormwater Pipe Networks Based on Dynamic Wave Simulation. *Water* **2024**, *16*, 3532.
8. Rezaee, M.; Melville-Shreeve, P.; Rappel, H. Probabilistic Forecasting and Anomaly Detection in Sewer Systems Using Gaussian Processes. *Water* **2025**, *17*, 2357.
9. García-Martínez, F.J.; Osorio, F.; González-Gómez, F. Challenges of Urban Water Cycle Management in Small Spanish Municipalities: The Case of the Province of Granada. *Water* **2025**, *17*, 1750.

https://doi.org/10.3390/w18121476

References

1. Karmeli, D.; Gadish, Y.; Meyers, S. Design of optimal water distribution networks. *J. Pipeline Div.* **1968**, *94*, 1–10. [CrossRef]
2. Creaco, E.; Franchini, M. Low level hybrid procedure for the multi-objective design of water distribution networks. *Procedia Eng.* **2014**, *70*, 369–378. [CrossRef]
3. Riyahi, M.M.; Bakhshipour, A.E.; Haghighi, A. Probabilistic warm solutions-based multi-objective optimization algorithm, application in optimal design of water distribution networks. *Sustain. Cities Soc.* **2023**, *91*, 104424. [CrossRef]
4. Diao, K.; Berardi, L.; Laucelli, D.B.; Ulanicki, B.; Giustolisi, O. Topological and hydraulic metrics-based search space reduction for optimal re-sizing of water distribution networks. *J. Hydroinform.* **2022**, *24*, 610–621. [CrossRef]
5. Hajibabaei, M.; Hesarkazzazi, S.; Minaei, A.; Dastgir, A.; Sitzenfrei, R. Using complex network theory for missing data reconstruction in water distribution networks. *Sustain. Cities Soc.* **2024**, *101*, 105114. [CrossRef]
6. Pei, S.; Hoang, L.; Fu, G.; Butler, D. Real-time multi-objective optimization of pump scheduling in water distribution networks using neuro-evolution. *J. Water Process Eng.* **2024**, *68*, 106315. [CrossRef]
7. Zhou, X.; Guo, S.; Xin, K.; Tang, Z.; Chu, X.; Fu, G. Network embedding: The bridge between water distribution network hydraulics and machine learning. *Water Res.* **2025**, *273*, 123011. [CrossRef] [PubMed]
8. Suchorab, P.; Kowalski, D. Designing Water Distribution Networks in Quasi-Real and Real-World Scenarios Using the Fractal-Based Approach. *Water* **2026**, *18*, 828. [CrossRef]
9. Wang, Q.; Savić, D.A.; Kapelan, Z. G ALAXY: A new hybrid MOEA for the optimal design of Water Distribution Systems. *Water Resour. Res.* **2017**, *53*, 1997–2015. [CrossRef]
10. Vertommen, I.; Mitrović, D.; van Laarhoven, K.; Piens, P.; Torbeyns, M. Optimization of water network topology and pipe sizing to aid water utilities in deciding on a design philosophy: A real case study in Belgium. *Water* **2022**, *14*, 3973. [CrossRef]
11. Ulusoy, A.-J.; Mahmoud, H.A.; Pecci, F.; Keedwell, E.C.; Stoianov, I. Bi-objective design-for-control for improving the pressure management and resilience of water distribution networks. *Water Res.* **2022**, *222*, 118914. [CrossRef]
12. Ulusoy, A.; Stoianov, I. Hybrid evolutionary-exact optimization method for the bi-objective design-for-control of water distribution networks. *Water Resour. Res.* **2026**, *62*, e2025WR040688. [CrossRef]
13. Ulusoy, A.-J.; Pecci, F.; Stoianov, I. Bi-objective design-for-control of water distribution networks with global bounds. *Optim. Eng.* **2022**, *23*, 527–577. [CrossRef]
14. De Paola, F.; Galdiero, E.; Giugni, M. Location and setting of valves in water distribution networks using a harmony search approach. *J. Water Resour. Plan. Manag.* **2017**, *143*, 4017015. [CrossRef]
15. El-Zahab, S.; Zayed, T. Leak detection in water distribution networks: An introductory overview. *Smart Water* **2019**, *4*, 5. [CrossRef]
16. Awwad, A.; Yahyia, M.; Albasha, L.; Mortula, M.M.; Ali, T. Communication network for ultrasonic acoustic water leakage detectors. *IEEE Access* **2020**, *8*, 29954–29964. [CrossRef]
17. Martini, A.; Troncossi, M.; Rivola, A. Leak detection in water-filled small-diameter polyethylene pipes by means of acoustic emission measurements. *Appl. Sci.* **2016**, *7*, 2. [CrossRef]
18. Ullah, N.; Siddique, M.F.; Ullah, S.; Ahmad, Z.; Kim, J.-M. Pipeline leak detection system for a smart city: Leveraging acoustic emission sensing and sequential deep learning. *Smart Cities* **2024**, *7*, 2318–2338. [CrossRef]
19. Shukla, H.; Piratla, K.R.; Atamturktur, S. Influence of soil backfill on vibration-based pipeline leakage detection. *J. Pipeline Syst. Eng. Pract.* **2020**, *11*, 4019055. [CrossRef]
20. Lobato de Almeida, F.C.; Brennan, M.J.; Joseph, P.F.; Dray, S.; Whitfield, S.; Paschoalini, A.T. Measurement of wave attenuation in buried plastic water distribution pipes. *Stroj.-Vestn.-J. Mech. Eng.* **2014**, *60*, 298–306. [CrossRef]
21. Dehghan, A.; McManus, K.J.; Gad, E.F. Probabilistic failure prediction for deteriorating pipelines: Nonparametric approach. *J. Perform. Constr. Facil.* **2008**, *22*, 45–53. [CrossRef]
22. Latifi, M.; Beig Zali, R.; Javadi, A.A.; Farmani, R. Efficacy of tree-based models for pipe failure prediction and condition assessment: A comprehensive review. *J. Water Resour. Plan. Manag.* **2024**, *150*, 3124001. [CrossRef]
23. Sharveen, S.; Shahandashti, M. Identifying Pareto-optimal seismic rehabilitation strategies for water distribution networks considering decision maker's risk attitudes. *Nat. Hazards* **2024**, *120*, 11743–11764. [CrossRef]
24. Sharveen, S.; Ryu, K.R.; Shahandashti, M. Multiobjective Game Theory Model for Identifying Proactive Pipeline Rehabilitation Strategies in Water Distribution Systems. *J. Infrastruct. Syst.* **2025**, *31*, 4025024. [CrossRef]
25. Roy, A.; Shahandashti, M. Effects of degradation of pipes on seismic rehabilitation decision-making for water distribution networks. *J. Pipeline Syst. Eng. Pract.* **2024**, *15*, 4024032. [CrossRef]
26. Pudasaini, B.; Shahandashti, M. Topological surrogates for computationally efficient seismic robustness optimization of water pipe networks. *Comput. Civ. Infrastruct. Eng.* **2020**, *35*, 1101–1114. [CrossRef]
27. Barton, N.A.; Hallett, S.H.; Jude, S.R.; Tran, T.H. An evolution of statistical pipe failure models for drinking water networks: A targeted review. *Water Supply* **2022**, *22*, 3784–3813. [CrossRef]

https://doi.org/10.3390/w18121476

28. International Water Association Water Loss Specialist Group (IWA WLSG). *Service Pipe Leakage Initiative Report; International Water Association*; IWA WLSG: London, UK, 2004.
29. Moasheri, R.; Ghazizadeh, M.J.; Tashayoei, M. Leakage detection in water networks by a calibration method. *Flow Meas. Instrum.* **2021**, *80*, 101995. [CrossRef]
30. Zanfei, A.; Menapace, A.; Brentan, B.M.; Sitzenfrei, R.; Herrera, M. Shall we always use hydraulic models? A graph neural network metamodel for water system calibration and uncertainty assessment. *Water Res.* **2023**, *242*, 120264. [CrossRef]
31. Meirelles, G.; Manzi, D.; Brentan, B.; Goulart, T.; Luvizotto, E., Jr. Calibration model for water distribution network using pressures estimated by artificial neural networks. *Water Resour. Manag.* **2017**, *31*, 4339–4351. [CrossRef]
32. Kuichling, E. The relation between the rainfall and the discharge of sewers in populous districts. *Trans. Am. Soc. Civ. Eng.* **1889**, *20*, 1–56. [CrossRef]
33. Shao, Z.; Zhang, X.; Li, S.; Deng, S.; Chai, H. A novel SWMM based algorithm application to storm sewer network design. *Water* **2017**, *9*, 747. [CrossRef]
34. Haghighi, A.; Bakhshipour, A.E. Optimization of sewer networks using an adaptive genetic algorithm. *Water Resour. Manag.* **2012**, *26*, 3441–3456. [CrossRef]
35. Afshar, M.; Shahidi, M.; Rohani, M.; Sargolzaei, M. Application of cellular automata to sewer network optimization problems. *Sci. Iran.* **2011**, *18*, 304–312. [CrossRef]
36. Moeini, R.; Afshar, M.H. Constrained Ant Colony Optimisation Algorithm for the layout and size optimisation of sanitary sewer networks. *Urban Water J.* **2013**, *10*, 154–173. [CrossRef]
37. Hajibabaei, M.; Hesarkazzazi, S.; Sitzenfrei, R. Filling data gaps in urban drainage networks: An automated graph theory framework for data collection and reconstruction. *Water Res.* **2025**, *287*, 124272. [CrossRef]
38. Perez, G.; Gomez-Velez, J.D.; Grant, S.B. The sanitary sewer unit hydrograph model: A comprehensive tool for wastewater flow modeling and inflow-infiltration simulations. *Water Res.* **2024**, *249*, 120997. [CrossRef]
39. Zhang, Q.; Li, Z.; Snowling, S.; Siam, A.; El-Dakhakhni, W. Predictive models for wastewater flow forecasting based on time series analysis and artificial neural network. *Water Sci. Technol.* **2019**, *80*, 243–253. [CrossRef]
40. Li, S.; Tian, W.; Yan, H.; Zeng, W.; Tao, T.; Xin, K. Modeling transient mixed flows in sewer systems with data fusion via physics-informed machine learning. *Water Res. X* **2024**, *25*, 100266. [CrossRef]
41. Machac, D.; Reichert, P.; Rieckermann, J.; Albert, C. Fast mechanism-based emulator of a slow urban hydrodynamic drainage simulator. *Environ. Model. Softw.* **2016**, *78*, 54–67. [CrossRef]
42. Troutman, S.C.; Schambach, N.; Love, N.G.; Kerkez, B. An automated toolchain for the data-driven and dynamical modeling of combined sewer systems. *Water Res.* **2017**, *126*, 88–100. [CrossRef]
43. Ge, J.; Li, J.; Qiu, R.; Shi, T.; Zhang, C.; Huang, Z.; Yuan, Z. A data-driven method for estimating sewer inflow and infiltration based on temperature and conductivity monitoring. *Water Res.* **2024**, *261*, 122002. [CrossRef] [PubMed]
44. Swiler, L.P.; Gulian, M.; Frankel, A.L.; Safta, C.; Jakeman, J.D. A survey of constrained Gaussian process regression: Approaches and implementation challenges. *J. Mach. Learn. Model. Comput.* **2020**, *1*, 119–156. [CrossRef]
45. Raissi, M.; Perdikaris, P.; Karniadakis, G.E. Physics-informed neural networks: A deep learning framework for solving forward and inverse problems involving nonlinear partial differential equations. *J. Comput. Phys.* **2019**, *378*, 686–707. [CrossRef]
46. Murray, C.D. The physiological principle of minimum work: I. The vascular system and the cost of blood volume. *Proc. Natl. Acad. Sci. USA* **1926**, *12*, 207–214. [CrossRef]
47. Cunha, M.; Marques, J. A new multiobjective simulated annealing algorithm—MOSA-GR: Application to the optimal design of water distribution networks. *Water Resour. Res.* **2020**, *56*, e2019WR025852. [CrossRef]
48. Rajabi, M.; Hajibabaei, M.; Dastgir, A.; Sitzenfrei, R. Functional and structural resilience assessment in urban drainage networks: A physics-guided graph-based surrogate model. *Water Res.* **2025**, *289*, 124784. [CrossRef] [PubMed]

Disclaimer/Publisher's Note: The statements, opinions and data contained in all publications are solely those of the individual author(s) and contributor(s) and not of MDPI and/or the editor(s). MDPI and/or the editor(s) disclaim responsibility for any injury to people or property resulting from any ideas, methods, instructions or products referred to in the content.

https://doi.org/10.3390/w18121476

water

MDPI

Article

Developing Machine Learning Models for Optimal Design of Water Distribution Networks Using Graph Theory-Based Features

Iman Bahrami Chegeni [1], Mohammad Mehdi Riyahi [1], Amin E. Bakhshipour [2,*], Mohamad Azizipour [1] and Ali Haghighi [1,2]

[1] Department of Civil Engineering, Faculty of Civil Engineering and Architecture, Shahid Chamran University of Ahvaz, Ahvaz 61357-83151, Iran; iman78bc@gmail.com (I.B.C.); mo_riyahi@yahoo.com (M.M.R.); azizipour@scu.ac.ir (M.A.); a.haghighi@scu.ac.ir (A.H.)

[2] Department of Urban Water Management, RPTU in Kaiserslautern, Paul-Ehrlich-Straße 14, D-67663 Kaiserslautern, Germany

* Correspondence: amin.bakhshipour@rptu.de

Abstract: This study presents an innovative data-driven approach to optimally design water distribution networks (WDNs). The methodology comprises five key stages: Generation of 600 synthetic WDNs with diverse properties, optimized to determine optimal component diameters; Extraction of 80 topological and hydraulic features from the optimized WDNs using graph theory; preprocessing and preparing the extracted features using established data science methods; Application of six feature selection methods (Variance Threshold, k-best, chi-squared, Light Gradient-Boosting Machine, Permutation, and Extreme Gradient Boosting) to identify the most relevant features for describing optimal diameters; and Integration of the selected features with four machine learning models (Random Forest, Support Vector Machine, Bootstrap Aggregating, and Light Gradient-Boosting Machine), resulting in 24 ensemble models. The Extreme Gradient Boosting-Light Gradient-Boosting Machine (Xg-LGB) model emerged as the optimal choice, achieving R^2, MAE, and RMSE values of 0.98, 0.017, and 0.02, respectively. When applied to a benchmark WDN, this model accurately predicted optimal diameters, with R^2, MAE, and RMSE values of 0.94, 0.054, and 0.06, respectively. These results highlight the developed model's potential for the accurate and efficient optimal design of WDNs.

Keywords: water distribution networks; graph theory; machine learning; feature engineering; network optimization

1. Introduction

Water distribution networks (WDNs) are a complex set of connected components, including water resources, pipes, and other process equipment like pumps, valves, etc. The WDNs are a fundamental part of supplying water from storage to consumers at the required pressure and quality. Given the high costs associated, the design of WDNs has attracted considerable interest from researchers and designers [1].

The evolution of WDN design approaches has been marked by several key developments categorized as follows:

- 1960s–1980s: Early efforts focused on linear and nonlinear programming methods to minimize design costs under hydraulic constraints [2–7].

- 1990s–2000s: Metaheuristic algorithms (e.g., genetic algorithms, particle swarm optimization) have gained prominence for cost-effective solutions [8–10].
- 2000s–Present: Multi-objective optimization algorithms have emerged to address additional factors such as reliability, water quality, and resilience in more complex WDNs [11–16].

While these traditional and metaheuristic optimization methods have advanced WDN design, they fundamentally rely on iterative hydraulic simulations and can be computationally expensive, particularly for large-scale or complex WDNs.

In parallel with these optimization method developments, in recent years, machine learning models have proven highly effective tools in WDNs, offering innovative solutions to complex problems traditionally addressed through conventional hydraulic modeling approaches. A critical observation on prior studies shows that few have explored the application of machine learning in WDN design [17,18], while most have focused on applying machine learning methods to the operational aspects of WDNs, such as demand forecasting [19,20], WDN monitoring [21,22], leakage detection [23,24], and pump operation [25]. The limited application of machine learning methods in designing WDNs serves as a key motivation for the current study.

Concurrently, graph theory has proven to be an indispensable tool for representing and analyzing the structural properties of WDNs. This approach represents WDNs as nodes (consumers or hydraulic control components) connected by links (pipes) [26]. The application of graph theory to WDNs began in the 1970s, initially focusing on understanding fundamental concepts and analyzing water flow and pressure [27,28]. Over time, researchers have adopted a more topological perspective, integrating graph theory with analytical tools to develop innovative solutions for WDN analysis and design [29,30].

Graph theory has various applications in WDN research, including reliability analysis [31], network dimension reduction [32,33], robustness enhancement [34–38], leak detection [39–41], network segmentation [42–45], and pump operation planning [46–48].

The integration of graph theory and machine learning has given rise to powerful new approaches in WDN analysis and management [49,50]. This combination allows for the extraction of topological features and the identification of complex patterns within WDNs. Applications of this synergy include leak detection and localization [51–55], water quality monitoring and prediction [56,57], pressure and demand forecasting [58], sensor and valve placement optimization [59], district metered area design [60,61], and asset management and failure prediction [62–65]. Nevertheless, similar to the standalone ML applications, graph theory and machine learning integration in WDN research has primarily focused on analysis/operational support for WDNs, without directly addressing the challenge of discovering the relationship between network properties and optimal design parameters like pipe diameters. Table 1 presents a comparative summary categorizing previous machine learning applications in WDNs by application domain, model type, feature set, dataset source, and reference.

Based on the literature review presented earlier, and to the best of the authors' knowledge, there is no study that has developed machine learning models for the optimal design of WDNs. In this research, a large dataset comprising 600 synthetic WDNs is created to feed machine learning methods, which has not been done in previous studies. Graph theory is used to extract 80 features from 600 synthetic WDNs (with a total of 85,745 samples), thereby creating a connection between the machine learning method and graph theory. Unlike traditional methods that use hydraulic equations to design WDNs and determine the optimal pipe diameter, this study aims to reshape the optimal design of WDNs by integrating graph theory with machine learning models. The approach involves generating

synthetic WDNs, optimizing their design, extracting topological and hydraulic features, and applying machine learning techniques to identify patterns for optimal diameter design. The process encompasses data preparation, feature selection through six methods, and the development of 24 ensemble machine learning models. The best-performing model is subsequently applied to the Hanoi WDN, showcasing the effectiveness of this innovative approach in optimizing WDN design.

Table 1. Comparative summary of machine learning model applications in WDNs.

Application	Machine Learning Model	Features Used	Dataset	Reference
Rehabilitation/Design of WDN	Feed-Forward Neural Network (FFNN)	Length, material, age, diameter, depth, and wall thickness	Real-world WDN (Shaker Al-Bahery WDN)	[17]
Rehabilitation/Design of WDN	Hybrtid based model (GLR-LR-RBFNN-SVR-ANFIS-FFNN)	Age, pipe depth, number of failures, diameter, and length	Real-world WDN (Gorgan WDN)	[18]
Water demand forecasting	Six machine learning models (LS, DT, KNN, SVR, RF, and RNN)	Air temperature, water consumption, precipitation,	The Battle of Water Demand Forecasting (WDSA-CCWI-2024) dataset	[19]
Water demand forecasting	One-Dimensional convolutional neural network (1D CNN)	Hourly water demand dat	Real-world WDN (Shiraz WDN)	[20]
WDN monitoring	XGBoost	Free residual chlorine concentration (FRC), Total Organic Carbon (TOC), pH, and distance from water treatment plants (WTPs)	Real-world WDN (Maragheh WDN)	[21]
WDN monitoring	Artificial neural network (ANN)	Pressure values, demand values, and number of users.	The benchmark network (Fossolo WDN)	[22]
Pump operation	Artificial neural network (ANN)	Water levels in tanks	The benchmark network (Anytown network)	[25]
WDN analysis and management	KNN, SVM, and RF	Demand variations and structural relationships	The benchmark network (M town)	[50]
Leak detection	RF	Structure and network attribute	Two case studies	[51]
Leak detection	SVM-CNN	Flow rate, pressure, and tempreture	Real-world WDN	[55]
Failure prediction	Gradient Boosted Trees (GBTs), and RF	19 features such as pipe diameter, pipe material, pipe length, pipe age, etc.	Real-world WDN	[62]
Failure prediction	Reinforcement learning algorithm based on Q-learning	Location ID, time to repair, and cost	Arlington County's water network	[63]
Failure prediction	Random Forest-Hierarchical Clustering (RF-HC)	Time-domain features of flow data (Peak value, mean, variance, Form factor, etc.)	Real-world WDN	[64]

2. Methodology

This section introduces an innovative approach to WDN design utilizing supervised machine learning regression models. The method leverages topological and hydraulic features to achieve optimal WDN design without relying on traditional hydraulic equation-solving techniques. Figure 1 illustrates the flowchart of the innovative approach comprising five essential steps. These steps are summarized as follows:

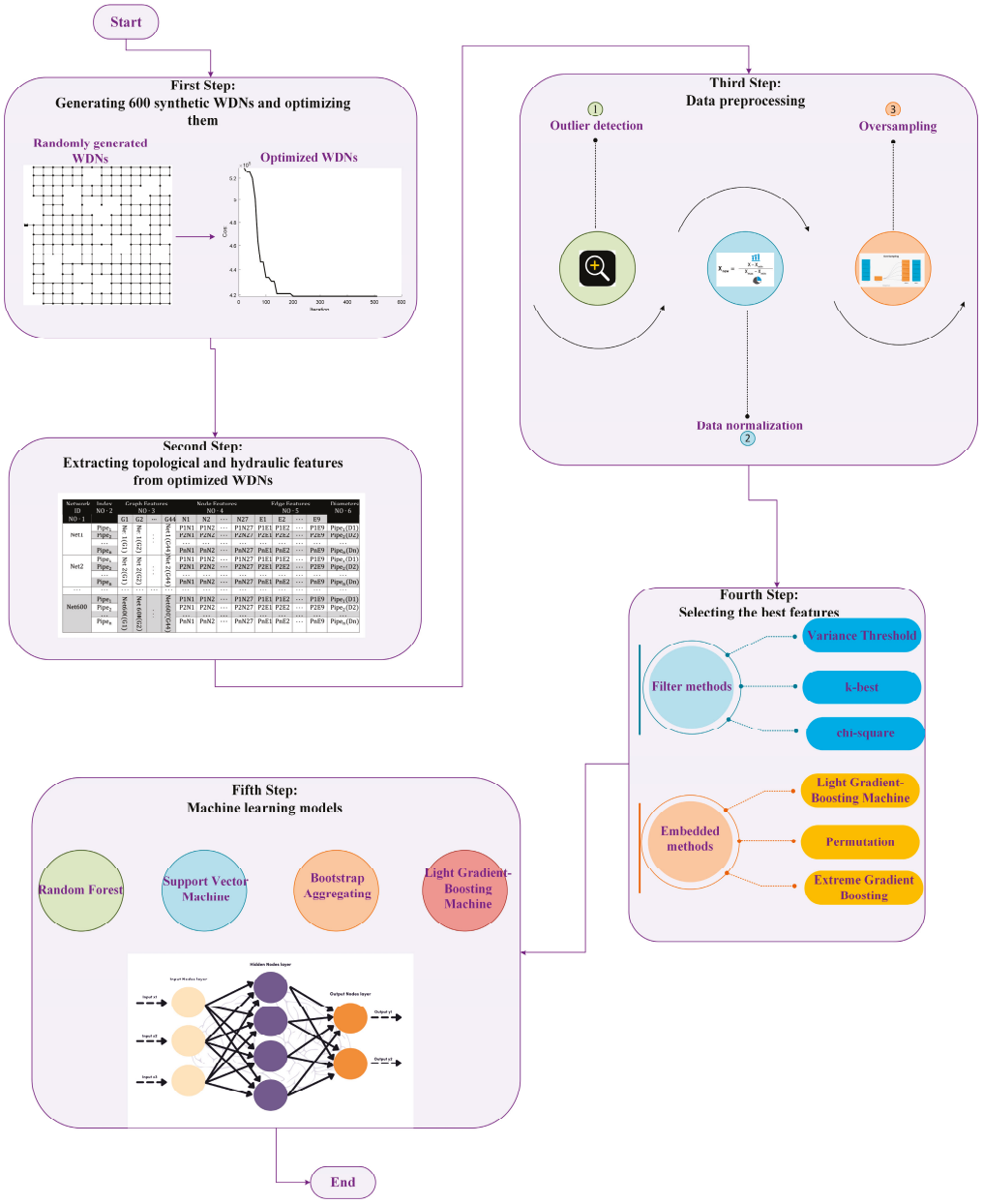

Figure 1. Flowchart of the developed machine learning model based on graph theory for WDN design.

1. Generation and optimization of 600 synthetic WDNs to determine optimal pipe diameters.

2. Extraction of topological and hydraulic features for WDN components (pipes, nodes, and the overall network graph).

3. Preparation of a database using the features obtained in step two.

4. Application of six feature selection methods to identify the most relevant features.

5. Combination of the feature selection methods with four machine learning models, creating 24 ensemble machine learning models to detect optimal WDN design patterns.

6. The methodology concludes by employing the most effective ensemble machine learning model to determine the optimal diameters for the Hanoi WDN, a real-world case study.

This approach signifies a notable shift from conventional WDN design methods, potentially enhancing efficiency in identifying optimal pipe diameters. The subsequent sections of the paper will provide detailed explanations of each stage in the proposed methodology.

2.1. Synthetic Water Distribution Network Generation

Diverse datasets of WDNs are essential for simulating and evaluating machine learning and graph theory-based methods. To achieve this, a specialized algorithm was developed to randomly generate synthetic WDNs replicating real-world network characteristics. The algorithm for generating synthetic WDNs involves the following procedures:

1. Creating a 2D initial raw graph representing a synthetic WDN, where nodes are linked to nearby neighbors in a network formation.
2. Introducing randomness into the initial graph by randomly eliminating nodes and their associated pipes.
3. Verifying the connectivity of the graph and repeating step 2 if it is not fully connected.
4. Assigning random allowable values, such as nodal demands, pipe lengths, pipe roughness coefficients, reservoir elevation levels, and others, to the components of the synthetic WDNs generated.
5. Continuing the process until the required number of synthetic WDNs is reached.

The synthetic WDN generation algorithm ensures the generated networks are valid and functional by adhering to the structural rules defining actual WDNs. For example, the algorithm produces planar graphs in which all connections (i.e., pipes) are joined exclusively at nodal points. This feature prevents unrealistic pipe connections and closely resembles the structure of real WDNs.

Additionally, the number of pipes connected to a single node is limited to a maximum of four, enhancing the resemblance to real networks by avoiding nodes with excessive connections. These constraints, along with other critical characteristics like pipe lengths and friction coefficients, help create synthetic WDNs that resemble real-world networks. In this study, 600 synthetic WDNs were generated, with each network component having the following characteristics:

Number of nodes: Between 16 and 141 nodes
Number of pipes: Between 24 and 252 pipes
Pipe lengths: Between 20 and 100 m
Hazen-Williams friction coefficient: In the 80 to 130 range
Reservoir head height: Between 20 and 90 m
Number of loops: Between 9 and 112 loops

In generating synthetic WDNs, the following points have been considered to align the topological rules with the hydraulics of WDNs: (1) The generated synthetic WDNs are in the form of a planar graph, (2) each synthetic WDN represents a connected graph, and there is a path between every pair of nodes, and (3) each node is connected to a maximum of four pipes, preventing unrealistic and overly complex connections, (4) The random removal of nodes or pipes introduces variability in the configurations of the generated WDNs, resulting in diverse topologies, (5) Assigning realistic random hydraulic values to nodes/pipes (such as pipe length, Hazen-Williams coefficient, and reservoir head) ensures the synthetic WDNs act as real-world WDNs, and (6) the generated WDNs are evaluated for performance, including topological and hydraulic control, using hydraulic simulation software. It is also important to note that the elevation of all nodes in these synthetic WDNs is set to zero. By incorporating these features, the generated datasets provide a robust

foundation for evaluating machine learning models and graph theory-based approaches in WDN analysis.

2.2. Water Distribution Network Optimization

One of the main goals in WDN design is to meet consumers' water demands at a desirable pressure while minimizing the design cost. One of the typical approaches widely used to achieve this goal is single-objective optimization, where the goal of the objective function is the minimization of WDN construction costs. The basic intent of this optimization procedure is to determine the values of the decision variables (pipe diameters) that minimize the objective function (WDN cost) while satisfying the system's technical and hydraulic constraints. The objective function and pressure constraint employed in the optimization problem are presented as follows.

$$f = \sum_{i=1}^{Np} C(d_i)L_i; \qquad i = 1, \ldots, Np \tag{1}$$

$$H_j \geq H_{min}; \qquad j = 1, \ldots, Nn \tag{2}$$

Equation (1) represents the objective function of the single-objective optimization algorithm. Here, $C(d_i)$ is the cost of diameter d_i per unit of pipe length, and L_i is the pipe length. Equation (2) is the optimization problem constraint, where H_j is the pressure at node (j), which must be greater than or equal to the minimum pressure (H_{min}). Table 2 presents the commercial diameters used in the optimization problem along with their corresponding costs. Hydraulic simulation of the synthetic WDNs is performed in EPANET software [66]. To this end, the synthetic graphs created in Python 3.8 are first introduced to EPANET 2.2 using the EPANET Toolkit in Python [67]. Next, specifications for components, such as pipe diameter, pipe length, and nodal demands, are assigned to these components, and the hydraulic simulation is performed [67]. A single-objective genetic algorithm is used in this study to optimize the synthetic WDNs. A self-adaptive method is utilized to satisfy the pressure constraint. Please refer to the article by Makaremi [68] for further study of the self-adaptive method.

Table 2. Commercial diameters and their corresponding costs.

Diameter Number	Diameter (mm)	Cost of Pipes (€/m)	Diameter Number	Diameter (mm)	Cost of Pipes (€/m)
1	16	10.34	11	125	35.38
2	20	11.18	12	160	48.84
3	25	12.22	13	200	66.80
4	32	13.69	14	250	95.25
5	40	15.36	15	315	141.83
6	50	17.45	16	400	216.60
7	63	20.17	17	500	327.50
8	75	22.67	18	600	438.40
9	90	25.81	19	800	660.20
10	110	30.89	20	1000	882.00

2.3. Topological and Hydraulic Features

The integration of topological and hydraulic features significantly enhances the application of machine learning models in WDN analysis. Topological features, such as node degree, clustering coefficient, and shortest path, define the network structure and connections, providing crucial insights into its fundamental organization and stability. Complementing these are hydraulic features that reflect WDN performance, including average flow velocity in pipes, piezometric head at nodes, and flow rates under various conditions.

This study incorporates 80 diverse features as critical input variables for various machine learning algorithms. These features enable supervised machine learning models to learn complex relationships within WDNs, facilitating optimal design without directly solving hydraulic equations. The features used in this research encompass nodes, pipes, and the overall network graph.

Feature assignment follows a specific methodology:

- Node and overall network graph features are assigned to pipes.
- For each pipe, the average of features from connecting nodes is calculated and assigned as a descriptive feature.
- Features derived from the overall network graph are uniformly applied to all pipes within that network, aiding in network differentiation during the learning process.

The study employs both directed and undirected graph representations:

- Undirected graphs are used for features such as square clustering coefficient, node eccentricity, and pipe length index.
- Directed graphs are necessary for features like degree of centrality and shortest path from the reservoir to nodes.
- Some features, including node closeness centrality index and betweenness centrality indices, require examination of both directed and undirected graphs.

Water flow direction determines the directionality of the graph in WDNs. For features requiring graph weight attributes, either the pipe length or the pipe resistance coefficient from the Hazen-Williams equation is used:

$$\mathrm{R} = \frac{10.67 \times L_i}{C^{1.85} \times d_i^{4.87}} \tag{3}$$

where:

R = Pipe resistance

L_i = Pipe length

C = Hazen-Williams coefficient

d_i = Pipe diameter

The target feature in this study is the optimal commercial diameters in WDNs, obtained through the optimization process. Table 3 presents a schematic of the features derived from 600 synthetic WDNs. The dataset represented in Table 3 comprises 80 columns showing the features and 85,745 rows describing the attributes of nodes, pipes, and the overall network graph assigned to the pipes. For a comprehensive list of features used in this study, please refer to Table A1 in the Appendix A.

Table 3. The features obtained from synthetic WDNs.

Network ID No. 1	Index No. 2	Graph Features No. 3				Node Features No. 4				Edge Features No. 5				Diameters No. 6
		G1	G2	…	G44	N1	N2	…	N27	E1	E2	…	E9	
Net 1	$Pipe_1$	Net 1(G1)	Net 1(G2)	⋮	Net 1(G44)	P1N1	P1N2	…	P1N27	P1E1	P1E2	…	P1E9	$Pipe_1$(D1)
	$Pipe_2$					P2N1	P2N2	…	P2N27	P2E1	P2E2	…	P2E9	$Pipe_2$(D2)
	…					…	…	…	…	…	…	…	…	…
	$Pipe_n$					P_nN1	P_nN2	…	P_nN27	P_nE1	P_nE2	…	P_nE9	$Pipe_n$(Dn)
Net 2	$Pipe_1$	Net 2(G1)	Net 2(G2)	⋮	Net 2(G44)	P1N1	P1N2	…	P1N27	P1E1	P1E2	…	P1E9	$Pipe_1$(D1)
	$Pipe_2$					P2N1	P2N2	…	P2N27	P2E1	P2E2	…	P2E9	$Pipe_2$(D2)
	…					…	…	…	…	…	…	…	…	…
	$Pipe_n$					P_nN1	P_nN2	…	P_nN27	P_nE1	P_nE2	…	P_nE9	$Pipe_n$(Dn)
…	…	…	…	…	…	…	…	…	…	…	…	…	…	…
Net 600	$Pipe_1$	Net 600(G1)	Net 600(G2)	⋮	Net 600(G44)	P1N1	P1N2	…	P1N27	P1E1	P1E2	…	P1E9	$Pipe_1$(D1)
	$Pipe_2$					P2N1	P2N2	…	P2N27	P2E1	P2E2	…	P2E9	$Pipe_2$(D2)
	…					…	…	…	…	…	…	…	…	…
	$Pipe_n$					P_nN1	P_nN2	…	P_nN27	P_nE1	P_nE2	…	P_nE9	$Pipe_n$(Dn)

2.4. Database Preparation

The crucial stage of database preparation comes after randomly generating synthetic WDNs and extracting their topological and hydraulic characteristics. This procedure is vital for producing an appropriate dataset for machine learning models and consists of two primary steps:

1. **Outlier Data Detection:** Identifying and handling outliers is crucial, as these anomalous values can significantly impact model training, reducing accuracy and generalizability. In this study, outliers are defined as data points whose distance from the same dataset's mean exceeds four times the standard deviation. Once identified, outliers are removed from the final database.
2. **Data Normalization:** Normalization is performed using the Min-max normalization method. This step is vital for (1) aligning features with different scales and (2) preventing the disproportionate impact of varying value ranges (e.g., pipe lengths vs. node pressures) on machine learning model performance.

By carefully addressing outliers and normalizing the data, we ensure that the machine learning models have a clean, well-prepared dataset to work with. This will ultimately lead to more reliable and accurate results in WDN analysis and design. To prevent data leakage between train/test sets, each WDN is considered as an independent entity during training, and all pipes in a WDN belong exclusively to either the training dataset or the testing dataset. This data-splitting procedure prevents data leakage and allows the machine learning model to be evaluated on unseen WDNs, increasing the model's generalizability.

2.5. Feature Selection Methods

Feature selection is a critical step in using a machine learning model, particularly when dealing with datasets containing a large number of features. This process involves identifying and selecting the most relevant and informative features from the original dataset for training a machine learning model. The primary objectives of feature selection are to improve model performance, reduce overfitting, speed up training, and often provide better model interpretability [69,70].

Feature selection methods can be broadly categorized into four groups: Hybrid, Embedded, Wrapper, and Filter, with each method suitable for feature extraction in different domains [71]. The present study employs Filter and Embedded categories. Methods such

as Var, Kb, and Chi2 fall under the Filter category, while methods like LGB, Per, and Xg belong to the Embedded group.

In Embedded methods, tuning the hyperparameters of the machine learning model is essential. The selection of the optimal hyperparameter configuration directly impacts model performance [72,73]. In this study, the Grid search method is used for hyperparameter tuning, which is a theoretical decision-making approach that involves a comprehensive search for a fixed range of hyperparameter values [74]. The Grid search algorithm determines a predefined range for each key hyperparameter, establishing a grid of potential combinations that are systematically assessed. Evaluation is carried out with cross-validation, then the dataset is partitioned into training and validation subsets so we can evaluate each model on both settings. The metric of comparison is computed for each configuration, and the best average performance across fold combinations is selected as optimal. We performed this process on each embedded model existing in the study (e.g., LGB, Xg, and Per models) so as to guarantee that each model is being operated under the best configuration it can provide, and hence the consistency and generalization of results.

In the following, the detailed explanations of all six feature selection methods used in this study are given.

1. **Chi2**

This statistical test is specifically used to examine the dependency between two variables [75]. In feature selection, the chi2 method selects non-negative features demonstrating the highest statistical dependency on the target variable [76]. In this method, the chi2 value is calculated for each feature in relation to the target variable, with a higher chi2 value indicating a stronger dependency between the feature and the target. Accordingly, features with larger chi2 values are selected as important features. This method is also well-suited for categorical data, and understanding the concept of variable dependency is relatively straightforward. However, its main limitation is limited applicability to non-negative features and the target variable.

2. **Var**

In this simple and fast method, features that show minimal variation, meaning those with low variance, are removed from the dataset [77]. The central concept is that features that are almost constant tend not to provide valuable information for the machine-learning model [78]. A variance threshold is determined for applying this method, removing features with variances lower than this value from the feature set. Due to its simplicity and high speed, this method is often used as a preprocessing stage for data dimension reduction. However, it is important to note that this method examines features individually while ignoring potential interactions between them. Additionally, selecting an appropriate value for the variance threshold can be somewhat arbitrary and dependent on the data.

1. **Kb**

This method aims to select the K most relevant features to the target variable [79]. For this purpose, univariate statistical tests evaluate the relationship between each feature and the target variable. The functions in this method assign a score to each feature based on statistical criteria. Subsequently, the K features that have obtained the highest scores are selected as the optimal features. Furthermore, the chi2 test can also serve as a scoring function for non-negative features. This method is relatively fast and efficient, and it can effectively identify features related to the target. However, similar to the variance threshold method, the Kb method does not consider the interactions between features. It assumes that the relationship of each feature with the target can be evaluated independently.

4. **LGB**

LGB is a robust gradient-boosting framework that inherently calculates and delivers feature significance scores [80,81]. This score indicates the impact of each feature on the building of the decision trees in the boosting model. During model training, LGB calculates metrics such as the number of times a feature is used to split nodes in trees, known as "split," and the reduction in node impurity due to using that feature, referred to as "gain". These values are indicators of feature significance. This approach has the advantage of directly integrating feature selection into the model training process while accounting for the interactions between features. The key hyperparameters of this method, tuned before the training process using Grid search, include n_estimators, num_leaves, max_depth, and learning_rate.

5. **Per**

This method is applied to evaluate the relative significance of features after training a machine learning model [82]. The model is initially employed to predict the importance of any feature. Next, the feature values in the validation set are randomly shuffled. After this alteration, the model's performance on the altered data are evaluated. A significant drop in performance after randomizing feature values indicates that the feature is highly significant to the model, as disturbance of its values considerably impacts the model's predictive ability. The advantage of this approach is that it can be used for any trained model, and its conceptual basis is relatively easy to grasp. However, it can be computationally costly for large datasets with many features, as it would require re-evaluating the model performance for each feature. As the model employed in this process is LightGBM, hyperparameters from the previous section are employed.

6. **Xg**

Like LGB, Xg is a popular gradient-boosting algorithm that offers feature significance calculation [83,84]. Xg, while training the model, assigns feature importance scores based on how frequently a feature is used for splitting nodes, the contribution of the split criterion from the feature-induced split, and the number of samples covered by splits of the feature, or "coverage". Similar to LGB feature importance, this approach comes with model training inherently and considers interaction among features. It must be noted that the calculated feature significance is specific to the Xg model and may produce different results for other models. The tuned hyperparameters for the current research study are n_estimators, eta, gamma, and max_depth.

2.6. Machine Learning Models

Machine learning is a branch of artificial intelligence that enables computers to learn from data without explicit programming. In other words, rather than giving computers step-by-step instructions to complete a task, large volumes of data are provided, with specific algorithms used to help the computer discern patterns, relationships, and rules within this data and to make predictions or decisions based on this knowledge [85]. The primary goal of machine learning is to develop systems that can improve their performance over time as they receive additional data. This improvement could involve various areas, such as prediction accuracy, processing speed, or the ability to recognize more complex patterns.

2.6.1. Regression in Machine Learning

Regression is one of the most critical and widely used aspects of supervised machine learning. Regression problems aim to establish a relationship between input and output

variables. In this context, a relationship is developed to predict a continuous objective variable based on one or more predictor variables [86]. In the present study, four machine learning models, namely RF, SVM, BAG, and LGB, are used for regression problems, which will be outlined in detail in the following sections.

1. **Random Forest (RF)**

The initial idea of the random forest was first introduced in 1972 by Messenger and Mandell [87]. This concept was later developed by Cutler [88]. The random forest model is among the most widely used algorithms in machine learning for classification and regression [89]. This model uses combined decision trees to increase prediction accuracy and stability. The main concept here is that each tree is trained independently, and each tree makes different decisions regarding the data. The final result is then obtained through voting (for classification problems) or averaging (for regression problems) among the trees. The advantages of random forest include stability and high accuracy. By minimizing overfitting and enhancing diversity in predictions, this model attains high accuracy in complex problems. Another advantage of the random forest model is its resistance to noise. Specifically, this model is less sensitive to noise and incorrect data due to the utilization of multiple trees. The adjusted hyperparameters of this method in the present study include n_estimators, min_samples_split, and max_depth.

2. **SVM**

SVM is one of the most powerful and widely used algorithms in supervised machine learning [90]. This algorithm is specifically used in classification and regression problems. The main concept behind SVM is locating an optimal hyperplane that separates the data in the best possible way. The "optimal hyperplane" refers to finding a hyperplane that maximizes the margin. The margin refers to the distance between the hyperplane and the nearest data points from the objective function value. These close points are called "support vectors" and play a key role in determining the hyperplane position [91]. In other words, only these points affect the hyperplane's location, while other data points have no impact. SVM offers several advantages. This algorithm performs particularly well in high-dimensional spaces and is memory-efficient due to its focus on support vectors. Furthermore, SVMs are still recognized as valuable tools in the machine learning toolkit due to their high accuracy and decent generalization capabilities. Thus, they are widely used in various fields, including machine vision, natural language processing, and bioinformatics [92,93]. The adjusted hyperparameters of this method in the present study include the regularization parameter (C), kernel, and gamma.

3. **BAG**

This idea was first used by Breiman [94] to predict classification and regression models, in which they evaluated different models by varying the number of bags. The results ultimately demonstrated enhanced accuracy with the combined BAG model (Breiman [94]). The BAG model approach is an ensemble learning process that generates multiple instances of a learner, specifically a classifier, resulting in several predictions [95]. The final model output is obtained by applying a combination rule (i.e., majority voting) to the outputs from each created subspace. Multiple samples are generated by creating self-initiated iterations from the learning set, where samples are randomly drawn from the entire training data with replacement, with the same number of samples in each subset [96]. The adjusted hyperparameters in this method in the present study include n_estimators, max_samples, and max_features.

4. **LGB**

The initial concept of boosting learning methods was presented by Schapire [97]. In this learning model, the goal is to boost performance. The performance of this method involves implementing a weak learner on the data, which is subsequently enhanced into a strong learner in later stages [98]. The boosting learning method consists of various types, including the Gradient Boosting model, which converts a weak learner into a strong learner. The LGB model is an optimized version of the Gradient Boosting framework, designed for efficient regression and classification, particularly for high-dimensional data.

The risk of overfitting increased in previous models as tree depth increased. This was due to the Level-Wise logic, which incrementally raised tree depth during training to enhance model accuracy. However, under the new logic of the LGB algorithm, the enhancement and training process is Leaf-Wise, meaning that the best branching between leaves (features) is selected at each stage of the decision tree. This process is quite effective in increasing computational speed and reducing overfitting risk. The fundamental hyperparameters of this method were previously described in earlier sections.

In all the above machine learning models, the k-fold cross-validation technique is employed to mitigate overfitting. It enhances the model's generalization ability and minimizes the possibility of overfitting when applied to new datasets.

2.6.2. Model Evaluation

Three criteria, R^2, MAE and RMSE, are used to evaluate machine learning models. These criteria demonstrate the effectiveness and suitability of machine learning models for the dataset. The R^2 criterion indicates how much of the variance in the objective variable is explained by the model [99]. Furthermore, the MAE and RMSE criteria show how far the predicted values are from the actual values. The relationships between these two criteria are as follows:

$$R^2 = 1 - \frac{\sum_{i=1}^{n}(y_i - \hat{y}_i)^2}{\sum_{i=1}^{n}(y_i - \overline{y})^2} \tag{4}$$

$$RMSE = \sqrt{\sum_{i=1}^{n} \frac{(y_i - \hat{y}_i)^2}{n}} \tag{5}$$

$$MAE = \frac{1}{n}\sum_{i=1}^{n}|y_i - \hat{y}_i| \tag{6}$$

The values y_i, $\hat{y}_i$, $\overline{y}$, and n are outlined below:
y_i: The real value of the objective variable.
$\hat{y}_i$: The predicted value of objective variable.
$\overline{y}$: The mean value of objective variable.
n: The total number of samples.

2.6.3. Hanoi WDN

The most effective machine learning model, as determined by the comparative analysis, is selected for application to the Hanoi WDN. The Hanoi WDN, initially introduced by Fujiwara and Khang [100], is a benchmark case study in optimizing WDNs. This network consists of 32 nodes, 34 pipes, 3 loops, and 1 reservoir with a water elevation of 100 m.

Key hydraulic parameters of the Hanoi WDN include:

- Minimum pressure head at demand nodes: 30 m
- Hazen-Williams coefficient for all pipes: 130

Figure 2 provides a visual representation of the Hanoi WDN layout, illustrating the network's topological structure and component relationships.

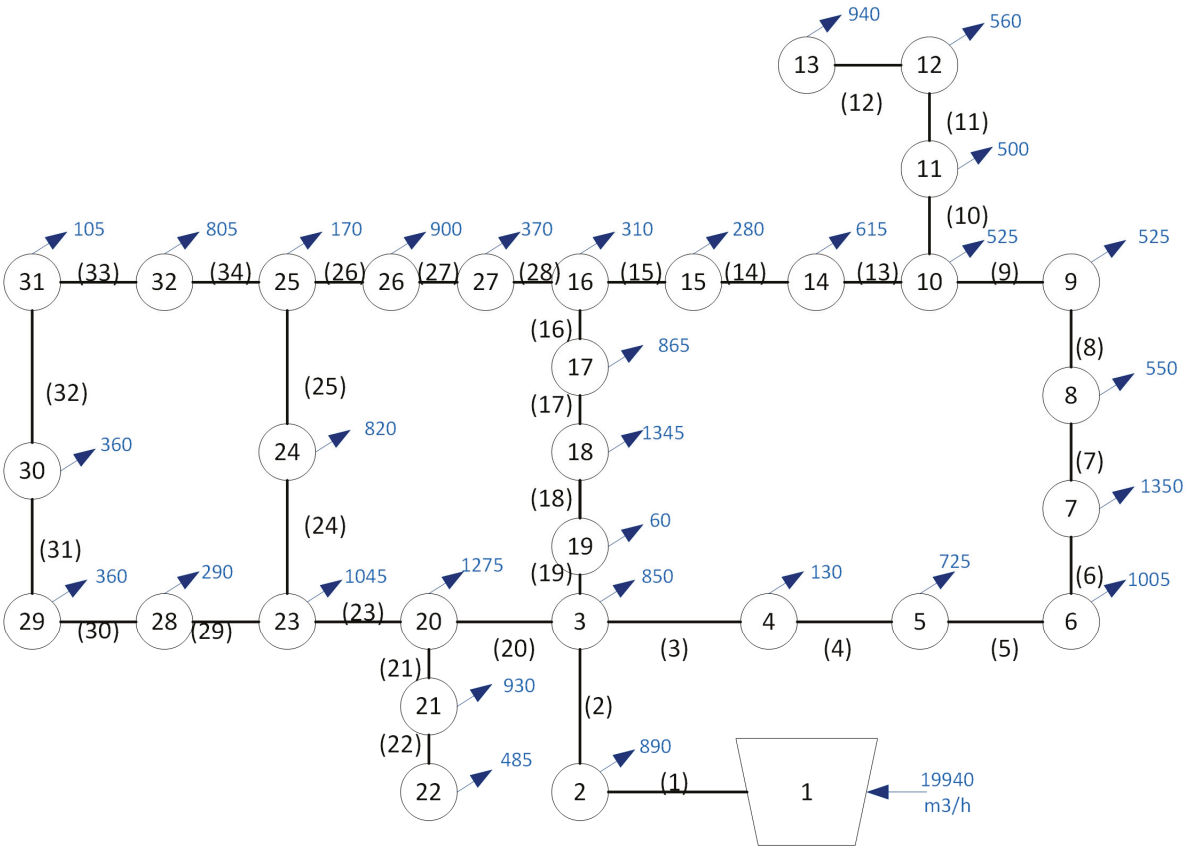

Figure 2. Hanoi WDN.

Figure 2 presents the demand at each node. Additionally, the pipe lengths in order of their respective numbers are: {100, 1350, 900, 1150, 1450, 450, 850, 850, 800, 950, 1200, 3500, 800, 500, 550, 2730, 1750, 800, 400, 2200, 1500, 500, 2650, 1230, 1300, 850, 300, 750, 1500, 2000, 1600, 150, 860, 950}. Five commercial pipe diameters are utilized in the design of the Hanoi WDN: 12, 16, 20, 24, 30, and 40 inches.

3. Results and Discussion

The first stage in the developed model involves the generation of synthetic WDNs. This process utilizes a developed algorithm that includes the graph mining library in Python (NetworkX), the EPANET Toolkit in Python (EPyT), and the genetic algorithm optimizer (geneticalgorithm2). Figure 3 shows the output of three synthetic WDNs. As is evident from these WDNs, all components of the generated networks are interconnected, without any pipes interfering with one another. The minimum and maximum number of pipes connected to each node are 1 and 4, respectively. Finally, appropriate random values are assigned to each component of the generated networks to enable the hydraulic design process. For instance, as previously mentioned, pipe lengths are assigned values between 20 and 100 m, or the Hazen-Williams coefficient in pipes is assigned values between 80 and 130. Following the generation of 600 synthetic networks, the design process for the optimal WDN diameters begins. The number of genetic algorithm iterations is 400 iterations on average. Additionally, population size, mutation probability, and crossover probability are set to 12 times the WDN pipes, 0.06, and 0.85, respectively. It is worth noting that the parameters of the GA are tuned through trial-and-error runs. The ranges and optimal values of the hyperparameters utilized in the GA algorithm are presented in Table 4.

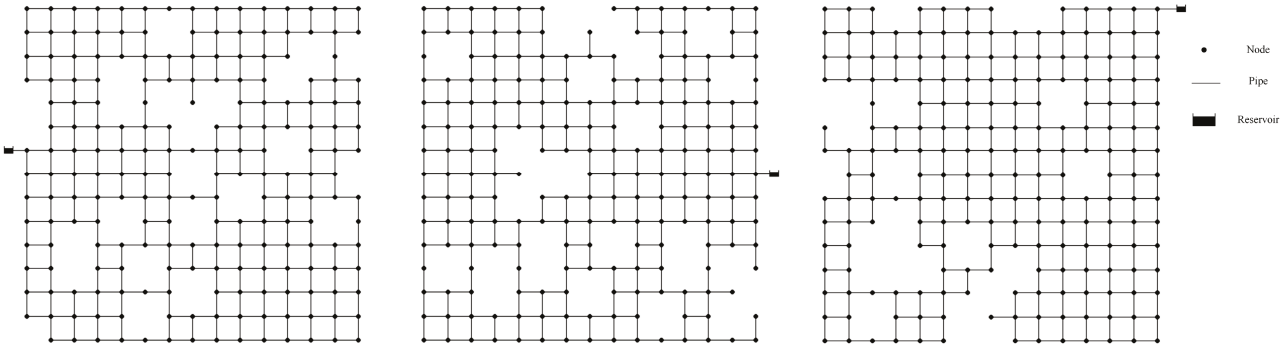

Figure 3. Generated synthetic WDNs.

Table 4. The ranges and optimal values of the hyperparameters used in GA.

Optimization Algorithm	Hyperparameter	Tuning Range of Hyperparameter Values	Optimal Hyperparameter Values
GA	Population Size	[5–20] × Number Of Pipes	12 × Number Of Pipes
	Mutation Probability	0.01–0.015	0.06
	Crossover Probability	0.6–0.95	0.85
	Number of Iterations	100–600	400

In this study, Equation (1) is utilized as a performance indicator to evaluate the effectiveness of the network design cost optimization process. Furthermore, the convergence monitoring process is implemented for responses to ensure optimal solutions. This process involved determining the number of optimization algorithm iterations for each WDN based on network dimensions through a trial-and-error process, with an average of 400 iterations. Moreover, the convergence criterion for the objective function is defined as a less than 1% improvement in cost over a predetermined number of iterations. In order to investigate hydraulic constraints, each optimal solution is simulated using EPANET software to ensure that the minimum pressure at all nodes is met as presented in Equation (2). Notably, nodal mass continuity and loop energy conservation are implicitly satisfied by solving the governing equations of WDNs.

The topological and hydraulic features are extracted from the WDNs during the next stage. These features generally pertain to the topological and hydraulic properties of nodes, pipes, and the overall network graph, totaling 80 characteristics, with the target feature being the optimal pipe diameters. The features that are attained in this stage are displayed in Table 5. This dataset contains 80 columns, and each column is a specific feature. The features are hydraulic and topological features relating to nodes, pipes, and the overall network graph. The dataset includes 85,745 rows, which are the attributes of nodes, pipes, and the overall network graph assigned to the pipes. The features identified for nodes are allocated to the corresponding connected pipes. This is done by calculating the arithmetic mean of the features of the nodes that are on either side of each pipe and subsequently calculating this as the respective feature of the pipe. Regarding the features obtained for the overall network graph, each extracted feature is applied to all pipes in that WDN. For instance, the network efficiency feature (G7) illustrated in Table 5 is repeated for all pipes in the WDN with the same G7 value. The dataset constructed at this stage has been uploaded to the GitHub site (https://github.com/bahrami-i/WDNs-Dataset; accessed on 24 May 2025), where readers can conveniently download it for use in their research. Table A1 in the article's Appendix A provides a detailed overview of the features analyzed in this study.

Table 5. First and last rows of extracted features from WDNs.

Index	Graph Features				Node Features				Edge Features				Diameters (mm)
	G1	G2	…	G44	N1	N2	…	N27	E1	E3	…	E9	
0	379	407	…	3749	2.50	0.50	…	11.80	87	31	…	0.01	200
1	379	407	…	3749	2.50	1.00	…	11.90	108	71	…	0.00	600
2	379	407	…	3749	3.50	1.50	…	13.70	112	94	…	0.04	125
3	379	407	…	3749	3.00	1.00	…	11.90	112	22	…	0.00	500
4	379	407	…	3749	3.50	1.50	…	14.20	111	23	…	0.20	200
5	379	407	…	3749	2.50	1.00	…	15.20	114	29	…	0.22	50
6	379	407	…	3749	3.00	1.50	…	18.70	111	21	…	0.03	160
7	379	407	…	3749	3.00	1.50	…	18.90	111	22	…	0.00	800
8	379	407	…	3749	2.50	1.50	…	18.70	96	92	…	0.00	400
9	379	407	…	3749	3.50	2.00	…	18.50	96	78	…	0.00	315
…	…	…	…	…	…	…	…	…	…	…	…	…	…
85,735	484	507	…	3672	3.00	0.50	…	28.80	120	46	…	0.00	250
85,736	484	507	…	3672	3.00	1.50	…	36.50	118	54	…	0.30	40
85,737	484	507	…	3672	3.00	1.50	…	45.00	106	63	…	0.03	250
85,738	484	507	…	3672	3.00	1.00	…	46.30	87	38	…	0.02	315
85,739	484	507	…	3672	3.00	1.50	…	52.20	88	49	…	0.22	90
85,740	484	507	…	3672	3.00	1.50	…	58.80	91	40	…	0.06	315
85,741	484	507	…	3672	3.00	1.50	…	63.80	92	89	…	0.08	315
85,742	484	507	…	3672	3.00	2.00	…	68.20	83	45	…	0.03	1,000
85,743	484	507	…	3672	3.00	2.00	…	70.20	90	35	…	0.01	800
85,744	484	507	…	3672	2.00	1.50	…	35.80	89	63	…	0.09	800

In the next step, outliers are identified and removed from the dataset after obtaining topographical and hydraulic features. To this end, all features are examined, and values exceeding four times the standard deviation from the data mean are identified according to the Z-score criterion. The row related to that specific feature known as outlier, along with all other features, is removed from the dataset. Following the outlier removal process, the number of rows in the dataset decreases from 85,745 to 67,226 rows. Figure 4 compares the frequency histogram of the N4 feature before and after outlier removal. As illustrated, removing outliers has led to variations within the range of the N4 feature. The other step taken in this stage is forming the Spearman correlation matrix to evaluate multicollinearity among 80 features with the aim of gaining an initial understanding of the relationship between features. The features with high correlation coefficients (more than 90 percent correlation) are examined, removed, or merged. The high correlation between features G33 and G20 can serve as an example in this regard. Because of this, these two features are omitted in the output of the six feature selection methods.

The dataset is then normalized using the min-max normalization method to scale the features within the range of 0 to 1. This data normalization improves machine learning model performance, increases convergence speed in gradient-based algorithms, and prevents characteristics with larger scales from dominating. Table 6 displays the results of the features from Table 5 after outlier removal and data normalization.

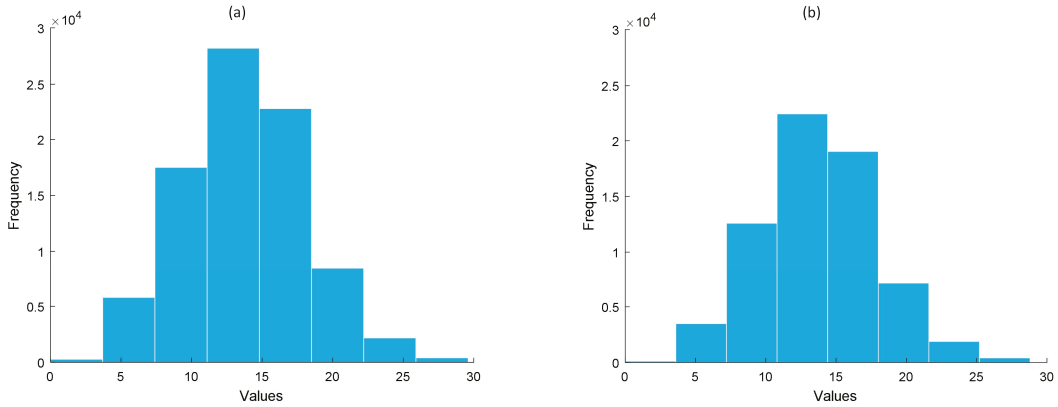

Figure 4. Histogram of the N4 feature before (**a**) and after (**b**) outlier removal.

Table 6. First and last rows of extracted features following outlier removal and normalization.

Index	Graph Features				Node Features				Edge Features				Diameters (mm)
	G1	G2	…	G44	N1	N2	…	N27	E1	E3	…	E9	
0	0.23	0.04	…	0.41	0.25	0.00	…	0.13	0.17	0.14	…	0.01	0.19
1	0.23	0.04	…	0.41	0.25	0.20	…	0.14	0.70	0.64	…	0.00	0.59
2	0.23	0.04	…	0.41	0.75	0.40	…	0.16	0.80	0.92	…	0.07	0.11
3	0.23	0.04	…	0.41	0.50	0.20	…	0.14	0.80	0.02	…	0.00	0.49
4	0.23	0.04	…	0.41	0.75	0.40	…	0.16	0.77	0.04	…	0.38	0.19
5	0.23	0.04	…	0.41	0.25	0.20	…	0.17	0.85	0.11	…	0.44	0.03
6	0.23	0.04	…	0.41	0.50	0.40	…	0.22	0.77	0.01	…	0.06	0.15
7	0.23	0.04	…	0.41	0.50	0.40	…	0.22	0.77	0.02	…	0.00	0.80
8	0.23	0.04	…	0.41	0.25	0.40	…	0.22	0.40	0.90	…	0.01	0.39
9	0.23	0.04	…	0.41	0.75	0.60	…	0.21	0.40	0.73	…	0.00	0.30
…	…	…	…	…	…	…	…	…	…	…	…	…	…
85736	0.55	0.05	…	0.39	0.50	0.40	…	0.42	0.95	0.42	…	0.56	0.02
85737	0.55	0.05	…	0.39	0.50	0.40	…	0.52	0.65	0.54	…	0.06	0.24
85738	0.55	0.05	…	0.39	0.50	0.20	…	0.54	0.17	0.22	…	0.04	0.30
85739	0.55	0.05	…	0.39	0.50	0.40	…	0.61	0.20	0.36	…	0.44	0.07
85740	0.55	0.05	…	0.39	0.50	0.40	…	0.68	0.27	0.25	…	0.12	0.30
85741	0.55	0.05	…	0.39	0.50	0.40	…	0.74	0.30	0.86	…	0.17	0.30
85743	0.55	0.05	…	0.39	0.50	0.60	…	0.82	0.25	0.19	…	0.15	0.80
85744	0.55	0.05	…	0.39	0.00	0.40	…	0.41	0.22	0.54	…	0.17	0.80

A visual comparison of Tables 5 and 6 reveals that the row corresponding to index 85,742 in Table 5 has been removed from Table 6, which, as previously explained, occurred due to outlier removal. Additionally, Table 6 clearly shows that the data have been normalized between 0 and 1 following the data normalization process. In the following step, the dataset is shuffled and split into training and test sets. A total of 70 percent of the data are assigned to the training set, while 30 percent is reserved for the test set. The reason behind this splitting is that allocating 70% of the data for training allows the model to learn underlying patterns with sufficient variety and volume, which is especially important in complex problems such as those involving WDNs. Meanwhile, reserving 30% for testing ensures an adequate and representative portion of unseen data to evaluate the generalization ability of the trained model.

The next stage involves extracting essential features from the 80 existing features in the dataset. To this end, as previously mentioned, six models, namely Var, Kb, Chi2, LGB, Per, and Xg, are utilized. The Var, Chi2, and Kb models belong to the Filter model category, while the LGB, Xg, and Per models belong to the Embedded category. The hyperparameter tuning in Embedded models is carried out using the Grid search algorithm. Table 7 depicts the hyperparameter values of the Embedded models tuned using the Grid search algorithm. The adjustment of these hyperparameters presented in Table 7 is conducted in a manner that prevents overfitting while maintaining a balance between exploitation and exploration in embedded methods. Additionally, Table 8 illustrates the top 20 features provided by the feature selection methods.

Table 7. Hyperparameter Values of Embedded Methods.

Hyperparameter Tuning with Grid Search	**Embedded Methods**		
	Xg	**LGB**	**Per**
n-estimators	1350	1500	1500
eta	0.250	-	-
gamma	0.002	-	-
Max-depth	15	12	12
Num-leaves	-	45	45
Learning-rate	-	0.011	0.011

Table 8. Selection of top 20 features based on feature selection methods.

Methods	**Kb**	**Chi2**	**Var**	**LGB**	**Per**	**Xg**
Selected Features	N5	N5	E1	E9	N5	E9
	N7	N7	E3	E8	N7	N5
	E5	E5	G43	N5	E3	E8
	N8	N8	G44	N7	E9	N7
	E9	N17	G7	E3	E1	E1
	E3	E9	G20	E1	E5	E3
	E1	N15	G21	N8	E8	N8
	G42	N19	G23	E5	N8	N10
	N23	E8	G30	N10	N10	E5
	G12	N18	G31	N6	N6	N6
	G8	N2	G32	N4	N3	N26
	G4	N10	G35	N17	N17	N4
	G17	N3	G36	N26	N1	E6
	G13	N13	G39	E4	N23	E7
	G10	N6	G41	N19	N25	N17
	G41	E3	N1	N9	N4	N20
	G6	N4	N2	E6	G25	N15
	G18	N14	N5	N18	G3	E4
	G27	N22	N7	E7	G2	N9
	G2	E1	N23	N20	G10	N19
Node features percentage	20	75	25	60	55	60
Pipe features percentage	20	25	10	40	25	40
Over all graph features percentage	60	0.0	65	0.0	20	0.0

The analysis of the results of feature selection methods in Table 8 reveals several key insights:

Feature importance by category:

- Node-related features dominate in four methods (Xg, Per, LGB, and Chi2)
- Overall network graph properties are most prominent in two methods (Kb and Var)

Significance of specific features:

- N5 and N7 (weighted node centrality degrees) consistently rank in the top quartile for most methods, except Var
- Features that use pipe resistance (R) as a weighted criterion show greater importance than those based on pipe length.

Distribution of top features:

- Node features: 50% on average
- Pipe features: 26% on average
- Graph features: 24% on average

Method-specific observations:

- Filter methods (e.g., Kb and Var) tend to select more overall network graph features.
- Embedded methods (e.g., Xg, Per, LGB) primarily select node and pipe features.

Application to machine learning:

- Top features from each selection method are paired with corresponding optimal diameters.
- These feature sets are used as inputs for four machine learning models.

Hyperparameters for each model are optimized using the Grid search algorithm (detailed in Table 9).

Table 9. Hyperparameter values of machine learning models.

Hyperparameter Tuning with Grid Search	Ensemble Model			
	RF	**SVM**	**BAG**	**LGB**
n-estimators	250	-	140	1500
Max-depth	30	-	-	-
Min-samples-split	10	-	-	12
Max-samples	-	-	0.7000	-
Max-features	-	-	0.7500	-
C	-	1.0000	-	-
kernel	-	‘rbf’	-	-
gamma	-	-	0.0001	-
Num-leaves	-	-	-	45
Learning-rate	-	-	-	0.0110

Figure 5 illustrates the Jaccard similarity matrix. According to this figure, the Embedded methods (Xg, LGB) present nearly identical feature selection (similarity = 0.90), confirming a core set of hydraulic-topological features such as E8, N8, N5, and E9 for diameter prediction. Additionally, Filter methods (Var, Kb) are highly divergent (similarity ≤ 0.18), as they prioritize overall network graph criteria that are overlooked by Embedded methods. The Jaccard indices of the Chi2 method with Embedded methods (Xg, LGxamB) and the Filter method (Kb) are 0.54 and 0.21, respectively. This means the Kb method shows a more substantial alignment with Embedded methods while preserving some Filter method behaviors, effectively acting as a connecting bridge between Embedded and Filter methods.

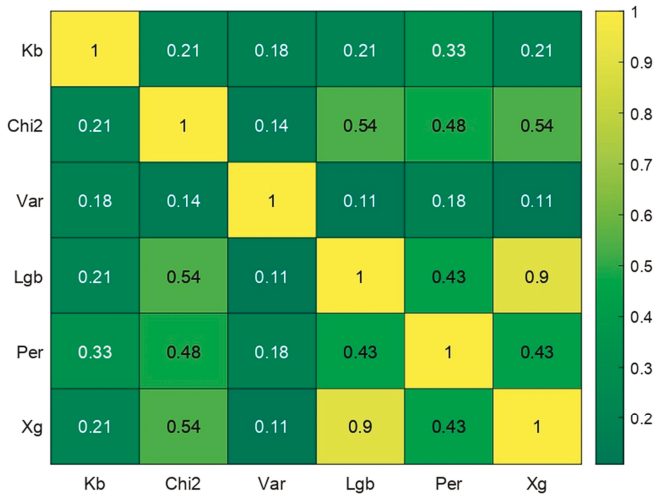

Figure 5. The Jaccard similarity between feature selection methods.

The 24 combined machine learning models are trained and evaluated using test data. The evaluation metrics used are R^2, MAE, and RMSE. Figure 6 shows the output of 24 coupled machine learning models. As observed in this figure, the strongest model based on three evaluation metrics is the Xg-LGB model, which implements the best features of the Xg method on the LGB regressor, with R^2, MAE, and RMSE values at 0.98, 0.017, and 0.02, respectively. The weakest model is Var-SVM, with R^2, MAE, and RMSE values at 0.41, 0.146, and 0.21, respectively. The critical point inferred from the XG-LGB model output is that the developed model is highly accurate in hydraulic simulations, even without utilizing governing hydraulic equations. Although the current study employs a data-driven approach, it indirectly and inherently considers hydraulic equations during the learning stages. This is made possible by designing all WDNs optimally through connecting the hydraulic simulation to the optimization algorithm. It is evident that hydraulic equations and components, such as pressure head loss, flow constraints, and pressure requirements, are applied during the simulation-optimization step. Thus, the objective function (optimal diameter) constitutes a function of the hydraulic behavior in the mentioned simulations.

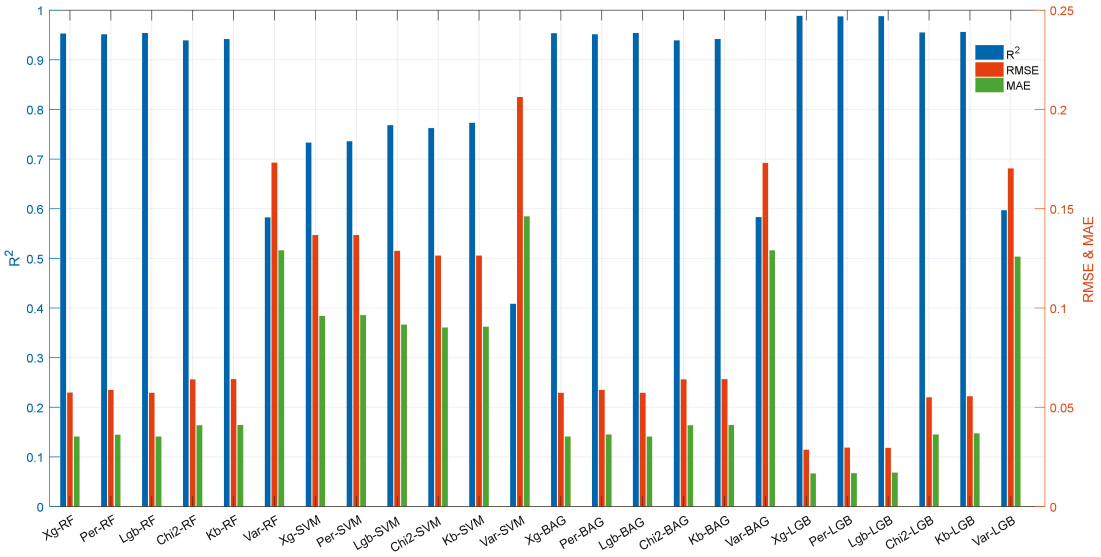

Figure 6. The output of 24 coupled machine learning models.

After selecting the best machine learning method, the Xg-LGB model is used to find the optimal diameters in the Hanoi WDN. The results show that R^2 is 0.94, indicating a high percentage of variance in the objective values (optimal diameters presented by Kadu [101]) identified by the Xg-LGB model. Furthermore, the MAE and RMSE values are 0.054 and 0.06, respectively, indicating that a small percentage of variance in the objective values remains unidentified by the model due to various factors: a shortage of features, measurement errors, incidental noise, model limitations, and data limitations. The model's efficiency could be enhanced by improving each of the mentioned factors. In this study, overfitting in machine learning models is controlled simultaneously using K-fold cross-validation (K = 5) and ensemble models, which are inherently resistant to overfitting. The similarity in performance criteria (R^2, MAE, and RMSE) between test and validation data provides evidence of the generalizability of the developed model. Table 10 presents the diameters calculated by the Xg-LGB model for the Hanoi WDN, along with the diameters of this network presented by Kadu. As per Table 10, the output diameters predicted by the Xg-LGB model are within a continuous range that should be mapped to standard commercial ranges. To this end, three mapping cases have been performed for diameters: (1) Mapping to the nearest diameter that may be a larger or smaller commercial diameter, (2) Mapping to the nearest upper diameter that produces a larger commercial diameter, and (3) Mapping to the nearest lower diameter that produces a smaller commercial diameter. Subsequently, the three mapping cases are simulated in EPANET. The mapping case that is the least expensive and meets the minimum pressure constraint of 30 m at nodes while avoiding over-design is selected. By comparing the commercial diameters of the developed method with the Kadu method, it becomes clear that in approximately 65% of cases, the forecasted diameters of the Xg-LGB model are equal to Kadu's outputs, while in the remaining 35%, these diameters are one size larger than Kadu's results. Considering the strong similarity between the results predicted by the Xg-LGB model and the Kadu model, along with the performance criteria of the Xg-LGB model, it can be concluded that the Xg-LGB model is suitable and applicable for use in other real-world WDNs for the following reasons: first, the original synthetic database presented in Table 5 is suitable for generating the optimal diameters for a given number of random WDNs; second, the Xg feature selection method in Table 8 has effectively identified the efficient features corresponding to the objective function; and third, the Xg-LGB model has been well trained on the original synthetic database and then applied to the Hanoi benchmark network. All the reasons mentioned earlier can somehow lead to the appropriate model generalization.

Additionally, using the predicted diameter results from the Xg-LGB model on the Hanoi WDN and conducting the hydraulic simulation with Epanet software yields the nodal pressure heads displayed in the last column of Table 10. Except for node 2, which has a pressure of 97.14 m (due to its nearness to the reservoir), the pressures at other nodes range from 35 to 65 m. This enhances the minimum pressure derived from the Kadu model while meeting the maximum pressure requirements, which is essential for ensuring adequate pressure in consumer nodes.

Figure 7 illustrates diameters obtained from the Xg-LGB machine learning method and the Kadu method, along with nodal pressure distributions. As is evident from this figure, 14 different diameters are present between the two methods. On average, solutions by the suggested method choose higher diameters, raising nodal pressure in comparison to the Kadu method. This higher pressure enhances system reliability and resiliency during a failure state. The comparison of execution times for determining optimal pipe diameters reveals that the developed method achieves the optimal pipe diameters in just 0.004 s. In

contrast, the Kadu method and the methods presented in [101] take significantly longer, requiring 7.8 min and 158 min, respectively.

Table 10. The pipe diameters from Kadu and Xg-LGB models and pressure head in each node of Hanoi WDN.

Pipe Number	Predicted Diameters			Node Number	Pressure Head from [101] (m)	Pressure Head from Xg-LGB Model (m)
	Pipe Diameters from [101] (in)	Continuous Pipe Diameters from Xg-LGB Model (in)	Commercial Pipe Diameters from Xg-LGB Model (in)			
1	40	38.9	40	1	100.00	100.00
2	40	36.9	40	2	97.08	97.14
3	40	40.7	40	3	60.82	61.67
4	40	40.3	40	4	56.38	57.39
5	40	39.9	40	5	50.88	52.09
6	40	39.5	40	6	45.13	46.56
7	40	39.1	40	7	43.81	45.29
8	40	40.0	40	8	42.28	43.83
9	30	33.7	30	9	41.09	42.69
10	30	35.4	40	10	37.61	39.40
11	30	34.9	30	11	36.01	39.01
12	24	27.4	30	12	34.83	37.85
13	16	18.2	20	13	30.53	36.44
14	12	14.0	16	14	32.06	37.81
15	12	13.0	12	15	30.96	37.66
16	16	18.4	20	16	31.13	38.17
17	20	22.1	24	17	39.28	45.01
18	24	24.4	24	18	50.04	51.52
19	24	28.2	30	19	57.13	60.16
20	40	40.0	40	20	49.59	51.41
21	20	23.4	24	21	40.04	47.56
22	12	13.1	12	22	34.76	42.40
23	40	39.2	40	23	43.42	45.98
24	30	34.6	30	24	37.73	41.44
25	30	34.4	30	25	34.07	38.72
26	20	21.4	20	26	30.51	36.67
27	12	14.1	16	27	30.32	36.69
28	12	14.6	16	28	38.05	39.30
29	16	17.6	16	29	30.08	36.26
30	12	14.5	16	30	30.58	36.26
31	12	13.0	12	31	30.90	36.47
32	16	17.6	16	32	31.81	36.74
33	20	23.9	24			
34	24	26.8	24			

In this research, only one real WDN (the Hanoi WDN) is utilized for validation and to prepare this ability for other researchers to compare their results with the results obtained in this study. However, it is important to note that this study generates 600 synthetic WDNs to simulate the characteristics and hydraulic behavior of real-world WDNs closely.

So, using this wide range of synthetic WDNs that are hydraulically similar to real WDNs makes the proposed method a strong method that has generalization and can reliably be applied to other new real WDNs.

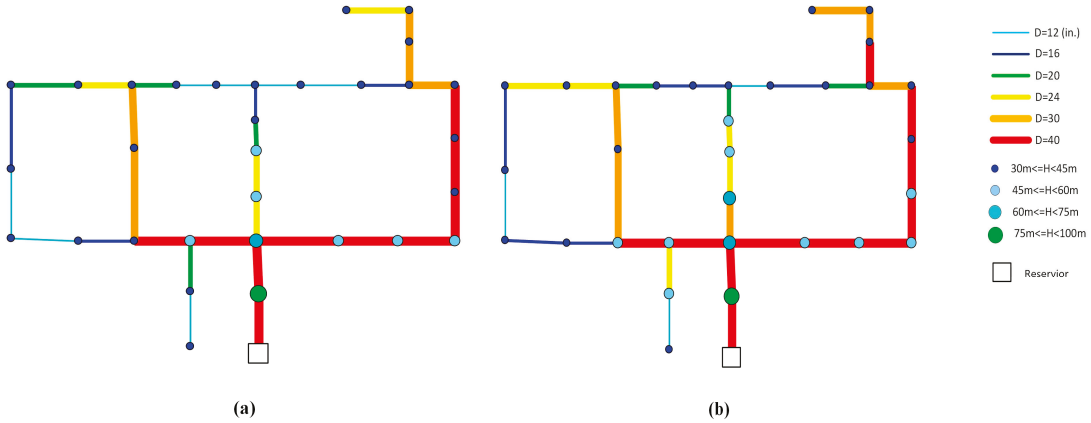

Figure 7. WDN design solution and pressure distribution for Hanoi network: (**a**) Kadue method; (**b**) Developed method.

This study assumed that the elevation of nodes is zero, but since inside the developed model, the piezometric head is utilized, and the piezometric head is equal to the sum of elevation and pressure head, this assumption does not affect the performance of the developed model.

A critical and valuable advantage of utilizing the developed method in this study is the significant reduction in computational time for the method relative to traditional optimization-based design methods. Conventional WDN design methods, i.e., simulation-optimization methods, involve performing several hydraulic simulations on every iteration. So, the time that it requires for these models can range from a few minutes to several hours, depending on the complexity of the WDN and how large the WDN is, so with traditional methods, it could take a considerable time to design a WDN. In contrast, the developed method uses data-driven models following training and pre-processing to obtain the optimal network diameters for new WDNs in seconds, based on the network size. One of the issues with traditional WDN design methods is the need to perform hydraulic simulations and the interaction with the optimization algorithm. The reasoning behind this problem is that, with optimization methods, hydraulic simulations are required to be performed on all of the designs being evaluated at every iteration. Therefore, this is time-consuming and increases the computational costs of the design. The developed method eliminates the need for hydraulic simulations, effectively addressing the issue and significantly reducing computational costs.

According to the information presented in Table 10 and Figure 7, it can be inferred that the diameters extracted using the Xg-LGB machine learning model are larger than the diameters obtained in the Kadu method. Although a complete match between the results of these two methods is observed for all large diameters (40-inch diameter), the diameters resulting from the developed method are equal to or larger than the values from the Kadu method for other pipes, which leads to increased design costs. It is important to note that the method proposed by Kadu [101] employs a single-objective genetic algorithm to minimize design costs. However, the developed model in the current study determines diameters based on the patterns extracted from data. In practice, the developed model is trained using data that implicitly encompasses multiple objectives such as pressure, network reliability, and design cost. In contrast, the proposed model demonstrates considerably higher generalizability compared to traditional

methods, in addition to favorable performance related to computational time. The model considers hydraulic reliability and prediction accuracy and can lead to more conservative pipe diameters to ensure minimum pressure. Among the proposed strategies for minimizing design costs in the developed model are directly integrating design cost in the learning process through a loss function or adopting a hybrid approach that combines data-driven models with optimization algorithms. Additionally, in the feature engineering section, there is potential to add a new characteristic related to pipe costs to the feature set, enabling cost component training in the machine learning model.

4. Conclusions

The optimal design of WDNs is one of the most critical engineering challenges, directly impacting service quality, economic costs, and water resource sustainability. Given urban population growth and increasing water demand, there is an increasingly urgent need for efficient methods to design these networks. Traditional WDN design methods are often time-consuming and have significant limitations when facing complex networks. Thus, developing novel and intelligent methods that can perform optimal design with high speed and accuracy seems essential.

A novel machine learning-based approach for optimal water distribution network design was presented in this study. To this end, 600 synthetic WDNs were generated and optimized. Then, 80 topological and hydraulic features concerning nodes, pipes, and the overall network graph were extracted from the optimized WDNs. Following data preprocessing, including outlier detection and normalization, six feature selection methods, namely Chi2, Var, Kb, LGB, Per, and Xg, were employed. Subsequently, four machine learning algorithms, including RF, SVM, LGB, and BAG, were utilized in combination with feature selection methods. Results showed that the Xg-LGB method had the best performance based on R^2, MAE, and RMSE in optimal WDN design. This combination method not only demonstrated higher accuracy compared to other methods but also showed significant capability in generalizability and predicting optimal pipe diameters. Finally, the LGB-Xg method is applied to a real-world WDN, the Hanoi WDN, demonstrating that this model can predict the optimal pipe diameters with R^2, MAE, and RMSE values of 0.94, 0.054, and 0.06, respectively. Based on the comparison between the traditional and developed methods, it is noticed that the developed method leads to selecting larger diameters. This larger selection of diameters makes a safety margin of nodal heads, making the WDN much more reliable than the traditional method. Also, because the proposed method is based on training the data and there is no need to run the hydraulic simulation model, this results in much less computational time in comparison to the traditional method that couples an optimization algorithm to the hydraulic simulation model and runs lots of hydraulic simulations in each iteration. Another benefit inferred from the performance criteria (R^2, MAE, and RMSE) is that the developed method has generalization since it involves a variety of samples in the dataset, extracting suitable features by feature selection methods, and optimal training. The research results indicated that among node, pipe, and overall network graph features, topological and hydraulic node features are of very high importance. This study demonstrates that using machine learning approaches can significantly improve water WDN design processes. Moreover, the study results can serve as a guideline for engineers and designers in the selection of appropriate pipe diameters in WDNs.

It is recommended that future studies investigate and explore the feasibility of using graph neural networks as an alternative to coupled machine learning models. Additionally, other factors such as reliability and uncertainty could be considered when developing machine learning methods for designing WDNs that achieve optimal diameters and enhance reliability. Also, to further reduce design costs in data-driven models, future studies

can incorporate a loss function sensitive to design costs during model training or utilize engineering knowledge to attempt to include cost-related features inside machine learning model training. Finally, since machine learning models resemble black boxes without providing insight into decision-making processes, future studies are recommended to utilize tools that improve model transparency, such as SHAP or LIME.

Author Contributions: Conceptualization, M.M.R.; Methodology, I.B.C., M.M.R., A.E.B. and A.H.; Validation, M.M.R.; Investigation, I.B.C.; Writing – original draft, I.B.C.; Writing – review & editing, M.M.R., A.E.B., M.A. and A.H.; Visualization, I.B.C.; Supervision, A.E.B. and A.H. All authors have read and agreed to the published version of the manuscript.

Funding: This project is partially funded by the Deutsche Forschungsgemeinschaft (DFG) under Project number 544048327.

Data Availability Statement: The data presented in this study are openly available in https://github.com/bahrami-i/WDNs-Dataset.

Conflicts of Interest: The authors declare no conflict of interest.

Appendix A

Table A1. Complete List of Features Used in this Study.

		Index		Features Name
Node Features	*Topological Features*	*N*1	$Node_{DC}$	Node Centrality Degree
		*N*2	$Node_{D-Out}$	Output Degree of Directed Graph Nodes
		*N*3	$Node_{D-In}$	Input Degree of Directed Graph Nodes
		*N*4	$Node_{DC-InL}$	Internal Weighted Centrality Degree for Weighted Multiplication of Input Edge Lengths by Input Degree in the Directed Graph
		*N*5	$Node_{DC-InRHW}$	Internal Weighted Centrality Degree for Weighted Multiplication of Resistance Index (R) of Input Edges by Input Degree in the Directed Graph
		*N*6	$Node_{DC-OutL}$	External Weighted Centrality Degree for Weighted Multiplication of Input Edge Lengths by Input Degree in the Directed Graph
		*N*7	$Node_{DC-OutR}$	External Weighted Centrality Degree for Weighted Multiplication of Resistance Index (R) of Input Edges by Input Degree in the Directed Graph
		*N*8	$Node_{Ave.Dim}$	Average Diameter of Tubes Connected to Node
		*N*9	$Node_{Min.Path.Length}$	Minimum Weighted Length Distance from Reservoir to Node in the Directed Graph
		*N*10	$Node_{Min.Path.RHW}$	Minimum Weighted Resistance Distance from Reservoir to Node in the Directed Graph
		*N*11	$Node_{SCC}$	Node Clustering Coefficient in the Undirected Graph
		*N*12	$Node_{CC-Undir-L}$	Weighted Length Closeness Centrality Index in the Undirected Graph
		*N*13	$Node_{CC-Undir-R}$	Weighted Resistance Closeness Centrality Index in the Undirected Graph
		*N*14	$Node_{CC-dir-L}$	Weighted Length Closeness Centrality Index in the Directed Graph
		*N*15	$Node_{CC-dir-R}$	Weighted Resistance Closeness Centrality Index in the Directed Graph
		*N*16	$Node_{BC-Undir-L}$	Weighted Length Betweenness Centrality Index in the Undirected Graph
		*N*17	$Node_{BC-Undir-R}$	Weighted Resistance Betweenness Centrality Index in the Undirected Graph

Table A1. *Cont.*

		Index		Features Name
Node Features	*Topological Features*	*N*18	$Node_{BC-dir-L}$	Weighted Length Betweenness Centrality Index in the Directed Graph
		*N*19	$Node_{BC-dir-R}$	Weighted Resistance Betweenness Centrality Index in the Directed Graph
		*N*20	$Node_{EC-Undir-L}$	Weighted Length Eigenvector Centrality Index in the Undirected Graph
		*N*21	$Node_{EC-dir-L}$	Weighted Length Eigenvector Centrality Index in the Directed Graph
		*N*22	$Node_{EC-dir-R}$	Weighted Resistance Eigenvector Centrality Index in the Directed Graph
		*N*23	$Node_{SC-Undir}$	Subgraph Centrality Index in the Undirected Graph
		*N*24	$Node_{EcC-Undir-L}$	Weighted Length Node Eccentricity Index in the Undirected Graph
		*N*25	$Node_{EcC-Undir-R}$	Weighted Resistance Node Eccentricity Index in the Undirected Graph
	Hydraulic Features	*N*26	$Node_{Demand}$	Consumption Flow Rates at Nodes
		*N*27	$Node_{Pressure}$	Pressure at Nodes
Edge Features	*Topological Features*	*E*1	$Edge_{Friction}$	Pipe Roughness Index
		*E*2	$Edge_{Diameter}$	Pipe Diameter Index
		*E*3	$Edge_{Length}$	Pipe Length Index
		*E*4	$Edge_{BC-Undir-L}$	Weighted Length Edge Betweenness Centrality Index in the Undirected Graph
		*E*5	$Edge_{BC-Undir-R}$	Weighted Resistance Edge Betweenness Centrality Index in the Undirected Graph
		*E*6	$Edge_{BC-dir-L}$	Weighted Length Edge Betweenness Centrality Index in the Directed Graph
		*E*7	$Edge_{BC-dir-R}$	Weighted Resistance Edge Betweenness Centrality Index in the Directed Graph
	Hydraulic Features	*E*8	$Edge_{Velocity}$	Flow Velocity Index in Pipe
		*E*9	$Edge_{HeadLoss}$	Energy Loss Index per Pipe Length
Graph Features	*Topological Features*	*G*1	$Graph_{Ave.Min.Path.L}$	Average Minimum Weighted Length Distance from Reservoir to Node in the Overall Directed Graph
		*G*2	$Graph_{Ave.Min.Path.R}$	Average Minimum Weighted Resistance Distance from Reservoir to Node in the Overall Directed Graph
		*G*3	$Graph_{Dia-Undir-L}$	Graph Diameter of Weighted Length Type in Overall Undirected Graph
		*G*4	$Graph_{Dia-Undir-R}$	Graph Diameter of Weighted Resistance Type in the Overall Undirected Graph
		*G*5	$Graph_{Rad-Undir-L}$	Graph Radius of Weighted Length Type in the Overall Undirected Graph
		*G*6	$Graph_{Rad-Undir-R}$	Graph Radius of Weighted Resistance Type in the Overall Undirected Graph
		*G*7	$Graph_{Effi-Undir}$	Graph Efficiency in the Overall Undirected Graph
		*G*8	$Graph_{Ave.CC-Undir-L}$	Average Closeness Centrality Index of Weighted Length Type in the Overall Undirected Graph
		*G*9	$Graph_{Ave.CC-Undir-R}$	Average Closeness Centrality Index of Weighted Resistance Type in the Overall Undirected Graph
		*G*10	$Graph_{Ave.CC-dir-L}$	Average Closeness Centrality Index of Weighted Length Type in the Overall Directed Graph
		*G*11	$Graph_{Ave.CC-dir-R}$	Average Closeness Centrality Index of Weighted Resistance Type in the Overall Directed Graph
		*G*12	$Graph_{Ave.BC-Undir-L}$	Average Betweenness Centrality Index of Weighted Length Type in the Overall Undirected Graph

Table A1. *Cont.*

		Index		Features Name
Graph Features	*Topological Features*	*G*13	$Graph_{Ave.BC-Undir-R}$	Average Betweenness Centrality Index of Weighted Resistance Type in the Overall Undirected Graph
		*G*14	$Graph_{Ave.BC-dir-L}$	Average Betweenness Centrality Index of Weighted Length Type in the Overall Directed Graph
		*G*15	$Graph_{Ave.BC-dir-R}$	Average Betweenness Centrality Index of Weighted Resistance Type in the Overall Directed Graph
		*G*16	$Graph_{CD-Undir-L}$	Dominance of Central Point of Weighted Length Type in the Overall Undirected Graph
		*G*17	$Graph_{CD-Undir-R}$	Dominance of Central Point of Weighted Resistance Type in the Overall Undirected Graph
		*G*18	$Graph_{CD-dir-L}$	Dominance of Central Point of Weighted Length Type in Overall Directed Graph
		*G*19	$Graph_{CD-dir-R}$	Dominance of Central Point of Weighted Resistance Type in the Overall Directed Graph
		*G*20	$Graph_{Ave.Deg-Undir}$	Average Graph Degree in the Overall Undirected Graph
		*G*21	$Graph_{Ave.OutDeg-dir}$	Average Output Degree in the Overall Directed Graph
		*G*22	$Graph_{\mathrm{Max}.Deg-Undir}$	Maximum Degree in the Overall Undirected Graph
		*G*23	$Graph_{\mathrm{Max}.InDeg-dir}$	Maximum Input Degree in the Overall Directed Graph
		*G*24	$Graph_{\mathrm{Max}.OutDeg-dir}$	Maximum Output Degree in the Overall Directed Graph
		*G*25	$Graph_{\mathrm{Ave}.LCC}$	Average Node Square Clustering Coefficient in the Overall Undirected Graph
		*G*26	$Graph_{\mathrm{FV}-Undir}$	Algebraic Connectivity Index in the Overall Undirected Graph
		*G*27	$Graph_{\mathrm{FV}-Undir-L}$	Algebraic Connectivity Index of Weighted Length Type in the Overall Undirected Graph
		*G*28	$Graph_{\mathrm{FV}-Undir-R}$	Algebraic Connectivity Index of Weighted Resistance Type in the Overall Undirected Graph
		*G*29	$Graph_{\mathrm{SD}-Undir}$	Spectral Difference of the Overall Undirected Graph
		*G*30	$Graph_{\mathrm{SD}-dir}$	Number of Edges in the Overall Undirected Graph
		*G*31	$Graph_{\mathrm{Density-Undir}}$	Density of the Overall Undirected Graph
		*G*32	$Graph_{\mathrm{Density-dir}}$	Density of the Overall Directed Graph
		*G*33	$Graph_{\mathrm{Mesh-Undir}}$	Mesh Coefficient of Overall Undirected Graph
		*G*34	$Graph_{\mathrm{DeadEnd-dir}}$	Sum of Input Degrees of Dead-End Nodes in the Overall Directed Graph
		*G*35	$Graph_{\mathrm{NC-Undir-Res}}$	Normalized Minimum Cut between Reservoir and First Node with Other Nodes in the Overall Undirected Graph
		*G*36	$Graph_{\mathrm{NC-Undir-Res}-L}$	Normalized Minimum Cut of Weighted Length Type between Reservoir and First Node with Other Nodes in the Overall Undirected Graph
		*G*37	$Graph_{NC-Undir-Res-R}$	Normalized Minimum Cut of Weighted Resistance Type between Reservoir and First Node with Other Nodes in Overall Undirected Graph
		*G*38	$Graph_{\mathrm{NC-Undir-End}}$	Normalized Minimum Cut between Terminal Node and Other Nodes in the Overall Undirected Graph
		*G*39	$Graph_{\mathrm{NC-Undir-End}-L}$	Normalized Minimum Cut of Weighted Length Type between Terminal Node and Other Nodes in the Overall Undirected Graph
		*G*40	$Graph_{\mathrm{NC-Undir-End}-R}$	Normalized Minimum Cut of Weighted Resistance Type between Terminal Node and Other Nodes in the Overall Undirected Graph
		*G*41	$Graph_{\mathrm{TotalLength}}$	Total Network Length in the Overall Graph
		*G*42	$Graph_{R_{HW}}$	Overall Network Resistance Index in the Overall Undirected Graph
	Hydraulic Features	*G*43	$Graph_{ResElv}$	Water Level in Reservoir in the Overall Graph
		*G*44	$Graph_{TotalDemand}$	Total Input Flow to Network in the Overall Graph

Appendix B

The synthetic water distribution networks (WDNs) are generated in the first step of the current study. Then, topological and hydraulic features are extracted from the synthetic WDNs using graph theory, and the initial database is formed. Next, machine learning models are used to extract the most influential features in the database, and then, they are employed to design pipe diameters in WDNs. Finally, the LGB-XG machine learning model, implemented on the Hanoi network, presented the best results for predicting pipe diameters based on the evaluation metrics (R^2, MAE, and RMSE are 0.94, 0.054, and 0.06, respectively). In this section, the compound WOA-ANN model is implemented on the best features obtained from the XgBoost method to allow other researchers to reproduce the results. For this purpose, a brief explanation of the mentioned model components is provided, and then, its implementation on the Hanoi network is executed. The implementation code and documentation file for the ANN-WOA model have been uploaded to GitHub (https://github.com/bahrami-i/WDNs-Dataset; accessed on 24 May 2025), allowing readers to download them for their research and reuse conveniently.

Appendix B.1. Whale Optimization Algorithm (WOA)

The initial idea of using the WOA algorithm was introduced by Mirjalili and Lewis in 2016 [102]. The mentioned algorithm, imitating the hunting behavior of whales, optimizes the complex and nonlinear problems. Furthermore, the WOA algorithm is a population-based algorithm and classified as a swarm intelligence algorithm. In this algorithm, whales are solution vectors, and the target prey is the best possible answer (global optimum). The general steps of the WOA algorithm include the following:

(1) Prey Encircling (Exploitation Phase)

In this step, whales identify the target prey and encircle it. In fact, the algorithm moves toward the best candidate solution among all available options, restricting the search area.

(2) Bubble-Net Attacking (Local Search Phase)

Since whales surround their prey by creating bubbles, they use spiral bubbles to hunt the prey. In this phase, the solutions move in a spiral path toward the best solution, leading to an accurate search near the best solution.

(3) Searching for Prey (Exploration Phase)

When there is no suitable prey near the whale, the whales randomly search for better prey. In fact, the algorithm explores new solutions through random whale movements and does not stop in non-optimal regions.

The primary parameters of the WOA algorithm in the current study are selected based on trial and error. The ranges and optimal values of the hyperparameters used in the WOA algorithm are shown in Table A2. They include Number of Whales = 30, which is used for the population size; Number of Iterations = 100, which indicates the number of algorithm iterations until achieving convergence and finding the best solution; and Coefficient A, which decreases in descending order from 2 to 0 and is used to control exploration and exploitation spaces.

Table A2. The ranges and optimal values of the hyperparameters used in WOA.

Optimization Algorithm	Hyperparameter	Tuning Range of Hyperparameter Values	Optimal Hyperparameter Values
WOA	Number of Whales	20–50	30
	Number of Iterations	50–200	100

Appendix B.2. Artificial Neural Networks (ANNs)

The initial idea of using Artificial Neural Networks (ANNs) was introduced by McCulloch and Pitts in 1943 [103]. An ANN network consists of several layers. These layers include an input layer, hidden layers (for feature transformation), and an output layer (for predicting results). The training process in the mentioned network is implemented by adjusting the weights to minimize prediction errors. The current study uses the Multilayer Perceptron (MLP) model (as a sub-collection of ANN networks) to predict the designed pipe diameters.

The WOA algorithm is used to achieve the best parameters for the MLP model. The compound WOA-ANN model is created, and the WOA algorithm extracts the best parameters for the ANN model by multiple iterations. The parameters obtained are, in fact, the most suitable ones for training the ANN to predict the designed pipe diameters in WDNs. In the current study, the parameters for the two-layer ANN model include hidden_n = 24, which indicates the number of neurons in each layer; Alpha = 2.14×10^{-7}, which is the regularization parameter, preventing overfitting by implementing a penalty to the loss function; Lr = 1.37×10^{-2}, which is the learning rate and is used to create balance between exploration and exploitation spaces; and max_iter = 2500, which defines the maximum number of iterations during the MLP model training.

Next, the implementation and training of the compound WOA-ANN model are executed using the best features obtained from the XgBoost method. It is done in a way that the model outputs (optimal pipe diameters) are a continuous value. Then, the Hanoi network's data are used to assess the WOA-ANN model, and the evaluation metrics R^2, MAE, and RMSE are obtained as 0.93, 0.056, and 0.069, respectively. Moreover, Table A3 illustrates the results of predicted pipe diameters for the Hanoi network using the compound WOA-ANN model.

After extracting the predicted pipe diameters through the WOA-ANN model, considering that the pipe diameters are within a continuous range, the mapping process is applied to them, controlling hydraulic pressure constraints at the nodes of the Hanoi network. This leads to the settlement of the predicted diameters within the range of the commercial pipe diameters. Table A3 presents the predicted diameters by the WOA-ANN model. Comparing these pipe diameters with the results obtained from the LGB-XG model, a complete overlap of approximately 68% among predicted results is observed. Since this overlap was achieved after the post-processing and pipe diameter mapping to commercial parameters, it is a suitable criterion for the reproducibility of results obtained using Xg-LGB. Furthermore, comparing the results obtained from R^2, MAE, and RMSE evaluation metrics for both Xg-LGB and WOA-ANN models indicates the reproducibility in all the study's executed phases, from initial database creation to implementing the learning model and pipe diameter prediction in WDNs.

Table A3. Results of diameter predictions for Kadu, Xg-LGB, and ANN-WOA methods in the Hanoi WDN.

Pipe Number	Predicted Diameters		
	Pipe Diameters from [101] (In)	Commercial Pipe Diameters from Xg-LGB Model (In)	Commercial Pipe Diameters from ANN-WOA Model (In)
1	40	40	40
2	40	40	40
3	40	40	40
4	40	40	40
5	40	40	40
6	40	40	40
7	40	40	40
8	40	40	40

Table A3. *Cont.*

Pipe Number	Predicted Diameters		
	Pipe Diameters from [101] (In)	Commercial Pipe Diameters from Xg-LGB Model (In)	Commercial Pipe Diameters from ANN-WOA Model (In)
9	30	30	40
10	30	40	30
11	30	30	30
12	24	30	20
13	16	20	20
14	12	16	16
15	12	12	16
16	16	20	20
17	20	24	24
18	24	24	30
19	24	30	30
20	40	40	40
21	20	24	24
22	12	12	16
23	40	40	40
24	30	30	40
25	30	30	30
26	20	20	24
27	12	16	16
28	12	16	12
29	16	16	20
30	12	16	16
31	12	12	12
32	16	16	16
33	20	24	20
34	24	24	24

References

1. Swamee, P.K.; Sharma, A.K. *Design of Water Supply Pipe Networks*; John Wiley & Sons: Hoboken, NJ, USA, 2008.
2. Gupta, I. Linear programming analysis of a water supply system. *AIIE Trans.* **1969**, *1*, 56–61. [CrossRef]
3. Karmeli, D.; Gadish, Y.; Meyers, S. Design of optimal water distribution networks. *J. Pipeline Div.* **1968**, *94*, 1–10. [CrossRef]
4. Schaake, J.C., Jr.; Lai, D. *Linear Programming and Dynamic Programming Application to Water Distribution Network Design*; M.I.T. Hydrodynamics Laboratory: Cambridge, MA, USA, 1969.
5. Su, Y.-C.; Mays, L.W.; Duan, N.; Lansey, K.E. Reliability-based optimization model for water distribution systems. *J. Hydraul. Eng.* **1987**, *113*, 1539–1556. [CrossRef]
6. Duan, N.; Mays, L.W.; Lansey, K.E. Optimal reliability-based design of pumping and distribution systems. *J. Hydraul. Eng.* **1990**, *116*, 249–268. [CrossRef]
7. Samani, H.M.; Taghi Naeeni, S. Optimization of water distribution networks. *J. Hydraul. Res.* **1996**, *34*, 623–632. [CrossRef]
8. Murphy, L.; Simpson, A. Pipe optimization using genetic algorithms. *Res. Rep.* **1992**, *93*, 95.
9. Savic, D.A.; Walters, G.A. Genetic algorithms for least-cost design of water distribution networks. *J. Water Resour. Plan. Manag.* **1997**, *123*, 67–77. [CrossRef]
10. Simpson, A.R.; Dandy, G.C.; Murphy, L.J. Genetic algorithms compared to other techniques for pipe optimization. *J. Water Resour. Plan. Manag.* **1994**, *120*, 423–443. [CrossRef]
11. Creaco, E.; Franchini, M. Low level hybrid procedure for the multi-objective design of water distribution networks. *Procedia Eng.* **2014**, *70*, 369–378. [CrossRef]
12. Farmani, R.; Walters, G.A.; Savic, D.A. Trade-off between total cost and reliability for Anytown water distribution network. *J. Water Resour. Plan. Manag.* **2005**, *131*, 161–171. [CrossRef]
13. Farmani, R.; Walters, G.; Savic, D. Evolutionary multi-objective optimization of the design and operation of water distribution network: Total cost vs. reliability vs. water quality. *J. Hydroinform.* **2006**, *8*, 165–179. [CrossRef]
14. Prasad, T.D.; Park, N.-S. Multiobjective genetic algorithms for design of water distribution networks. *J. Water Resour. Plan. Manag.* **2004**, *130*, 73–82. [CrossRef]
15. Riyahi, M.M.; Bakhshipour, A.E.; Haghighi, A. Probabilistic warm solutions-based multi-objective optimization algorithm, application in optimal design of water distribution networks. *Sustain. Cities Soc.* **2023**, *91*, 104424. [CrossRef]

16. Todini, E. Looped water distribution networks design using a resilience index based heuristic approach. *Urban Water* **2000**, *2*, 115–122. [CrossRef]
17. Elshaboury, N.; Marzouk, M. Prioritizing water distribution pipelines rehabilitation using machine learning algorithms. *Soft Comput.* **2022**, *26*, 5179–5193. [CrossRef]
18. Jafari, S.M.; Nikoo, M.R.; Bozorg-Haddad, O.; Alamdari, N.; Farmani, R.; Gandomi, A.H. A robust clustering-based multi-objective model for optimal instruction of pipes replacement in urban WDN based on machine learning approaches. *Urban Water J.* **2023**, *20*, 689–706. [CrossRef]
19. Maußner, C.; Oberascher, M.; Autengruber, A.; Kahl, A.; Sitzenfrei, R. Explainable artificial intelligence for reliable water demand forecasting to increase trust in predictions. *Water Res.* **2025**, *268*, 122779. [CrossRef]
20. Namdari, H.; Haghighi, A.; Ashrafi, S.M. Short-term urban water demand forecasting; application of 1D convolutional neural network (1D CNN) in comparison with different deep learning schemes. *Stoch. Environ. Res. Risk Assess.* **2023**, 1–16. [CrossRef]
21. Baziar, M.; Behnami, A.; Jafari, N.; Mohammadi, A.; Abdolahnejad, A. Machine learning-based Monte Carlo hyperparameter optimization for THMs prediction in urban water distribution networks. *J. Water Process Eng.* **2025**, *73*, 107683. [CrossRef]
22. Magini, R.; Moretti, M.; Boniforti, M.A.; Guercio, R. A machine-learning approach for monitoring water distribution networks (WDNS). *Sustainability* **2023**, *15*, 2981. [CrossRef]
23. Pandian, C.; Alphonse, P. Evaluating water pipe leak detection and localization with various machine learning and deep learning models. *Int. J. Syst. Assur. Eng. Manag.* **2025**, 1–13. [CrossRef]
24. Ayati, A.H.; Haghighi, A. Multiobjective wrapper sampling design for leak detection of pipe networks based on machine learning and transient methods. *J. Water Resour. Plan. Manag.* **2023**, *149*, 04022076. [CrossRef]
25. Pei, S.; Hoang, L.; Fu, G.; Butler, D. Real-time multi-objective optimization of pump scheduling in water distribution networks using neuro-evolution. *J. Water Process Eng.* **2024**, *68*, 106315. [CrossRef]
26. Bondy, J.A.; Murty, U.S.R. *Graph Theory with Applications*; Macmillan London: London, UK, 1976; Volume 290.
27. Hamam, Y.; Brameller, A. Hybrid method for the solution of piping networks. *Proc. Inst. Electr. Eng.* **1971**, *118*, 1607–1612. [CrossRef]
28. Kesavan, H.K.; Chandrashekar, M. Graph-theoretic models for pipe network analysis. *J. Hydraul. Div.* **1972**, *98*, 345–364. [CrossRef]
29. Riyahi, M.M.; Bakhshipour, A.E.; Giudicianni, C.; Dittmer, U.; Haghighi, A.; Creaco, E. An Analytical Solution for the Hydraulics of Looped Pipe Networks. *Eng. Proc.* **2024**, *69*, 4.
30. Sitzenfrei, R. A graph-based optimization framework for large water distribution networks. *Water* **2023**, *15*, 2896. [CrossRef]
31. Jung, D.; Yoo, D.G.; Kang, D.; Kim, J.H. Linear model for estimating water distribution system reliability. *J. Water Resour. Plan. Manag.* **2016**, *142*, 04016022. [CrossRef]
32. Alzamora, F.M.; Ulanicki, B.; Zehnpfund. Simplification of Water Distribution Network Models. In Proceedings of the 2nd International Conference on Hydroinformatic, Zurich, Switzerland, 9–13 September 1996.
33. Giudicianni, C.; di Nardo, A.; Oliva, G.; Scala, A.; Herrera, M. A dimensionality-reduction strategy to compute shortest paths in urban water networks. *arXiv* **2019**, arXiv:1903.11710.
34. Satish, R.; Hajibabaei, M.; Dastgir, A.; Oberascher, M.; Sitzenfrei, R. A graph-based method for identifying critical pipe failure combinations in water distribution networks. *Water Supply* **2024**, *24*, 2353–2366. [CrossRef]
35. Ostfeld, A. Water distribution systems connectivity analysis. *J. Water Resour. Plan. Manag.* **2005**, *131*, 58–66. [CrossRef]
36. Yazdani, A.; Jeffrey, P. Robustness and vulnerability analysis of water distribution networks using graph theoretic and complex network principles. In *Water Distribution Systems Analysis 2010*; American Society of Civil Engineers: Reston, VA, USA, 2010; pp. 933–945.
37. Yazdani, A.; Otoo, R.A.; Jeffrey, P. Resilience enhancing expansion strategies for water distribution systems: A network theory approach. *Environ. Model. Softw.* **2011**, *26*, 1574–1582. [CrossRef]
38. Ulusoy, A.-J.; Stoianov, I.; Chazerain, A. Hydraulically informed graph theoretic measure of link criticality for the resilience analysis of water distribution networks. *Appl. Netw. Sci.* **2018**, *3*, 1–22. [CrossRef]
39. Oberascher, M.; Minaei, A.; Sitzenfrei, R. Graph-Based Genetic Algorithm for Localization of Multiple Existing Leakages in Water Distribution Networks. *J. Water Resour. Plan. Manag.* **2025**, *151*, 04024059. [CrossRef]
40. Rajeswaran, A.; Narasimhan, S.; Narasimhan, S. A graph partitioning algorithm for leak detection in water distribution networks. *Comput. Chem. Eng.* **2018**, *108*, 11–23. [CrossRef]
41. Di Nardo, A.; Giudicianni, C.; Greco, R.; Herrera, M.; Santonastaso, G.F. Applications of graph spectral techniques to water distribution network management. *Water* **2018**, *10*, 45. [CrossRef]

42. Sitzenfrei, R.; Satish, R.; Rajabi, M.; Hajibabaei, M.; Oberascher, M. Graph-Based Methodology for Segment Criticality Assessment and Optimal Valve Placements in Water Networks. In Proceedings of the EGU General Assembly 2025, Vienna, Austria, 27 April–2 May 2025.
43. Riyahi, M.M.; Giudicianni, C.; Haghighi, A.; Creaco, E. Coupled multi-objective optimization of water distribution network design and partitioning: A spectral graph-theory approach. *Urban Water J.* **2024**, *21*, 745–756. [CrossRef]
44. Tzatchkov, V.G.; Alcocer-Yamanaka, V.H.; Bourguett Ortíz, V. Graph theory based algorithms for water distribution network sectorization projects. In Proceedings of the Water Distribution Systems Analysis Symposium 2006, Cincinnati, OH, USA, 27–30 August 2006; pp. 1–15.
45. Deuerlein, J.W. Decomposition model of a general water supply network graph. *J. Hydraul. Eng.* **2008**, *134*, 822–832. [CrossRef]
46. Price, E.; Ostfeld, A. Graph theory modeling approach for optimal operation of water distribution systems. *J. Hydraul. Eng.* **2016**, *142*, 04015061. [CrossRef]
47. Price, E.; Ostfeld, A. Optimal pump scheduling in water distribution systems using graph theory under hydraulic and chlorine constraints. *J. Water Resour. Plan. Manag.* **2016**, *142*, 04016037. [CrossRef]
48. Marini, G.; Fontana, N.; Maio, M.; Di Menna, F.; Giugni, M. A novel approach to avoiding technically unfeasible solutions in the pump scheduling problem. *Water* **2023**, *15*, 286. [CrossRef]
49. Ahmed, A.A.; Sayed, S.; Abdoulhalik, A.; Moutari, S.; Oyedele, L. Applications of machine learning to water resources management: A review of present status and future opportunities. *J. Clean. Prod.* **2024**, *441*, 140715. [CrossRef]
50. Zhou, X.; Guo, S.; Xin, K.; Tang, Z.; Chu, X.; Fu, G. Network embedding: The bridge between water distribution network hydraulics and machine learning. *Water Res.* **2025**, *273*, 123011. [CrossRef] [PubMed]
51. Coelho, M.; Austin, M.A.; Mishra, S.; Blackburn, M. Teaching Machines to Understand Urban Networks: A Graph Autoencoder Approach. *Int. J. Adv. Netw. Serv.* **2020**, *13*, 70–81.
52. Arsene, C.; Al-Dabass, D.; Hartley, J. Decision support system for water distribution systems based on neural networks and graphs. In Proceedings of the 2012 UKSim 14th International Conference on Computer Modelling and Simulation, Cambridge, UK, 28–30 March 2012; pp. 315–323.
53. Kang, J.; Park, Y.-J.; Lee, J.; Wang, S.-H.; Eom, D.-S. Novel leakage detection by ensemble CNN-SVM and graph-based localization in water distribution systems. *IEEE Trans. Ind. Electron.* **2017**, *65*, 4279–4289. [CrossRef]
54. Barros, D.; Zanfei, A.; Menapace, A.; Meirelles, G.; Herrera, M.; Brentan, B. Leak detection and localization in water distribution systems via multilayer networks. *Water Res. X* **2025**, *26*, 100280. [CrossRef]
55. Komba, G. A Novel Leak Detection Algorithm Based on SVM-CNN-GT for Water Distribution Networks. *Indones. J. Comput. Sci.* **2025**, *14*. [CrossRef]
56. Amali, S.; Faddouli, N.-e.E.; Boutoulout, A. Machine learning and graph theory to optimize drinking water. *Procedia Comput. Sci.* **2018**, *127*, 310–319. [CrossRef]
57. Li, Z.; Liu, H.; Zhang, C.; Fu, G. Real-time water quality prediction in water distribution networks using graph neural networks with sparse monitoring data. *Water Res.* **2024**, *250*, 121018. [CrossRef]
58. Liy-González, P.-A.; Santos-Ruiz, I.; Delgado-Aguiñaga, J.-A.; Navarro-Díaz, A.; López-Estrada, F.-R.; Gómez-Peñate, S. Pressure Interpolation in Water Distribution Networks by Using Gaussian Processes: Application to Leak Diagnosis. *Processes* **2024**, *12*, 1147. [CrossRef]
59. Cheng, M.; Li, J. Optimal sensor placement for leak location in water distribution networks: A feature selection method combined with graph signal processing. *Water Res.* **2023**, *242*, 120313. [CrossRef] [PubMed]
60. Di Nardo, A.; Di Natale, M.; Giudicianni, C.; Musmarra, D.; Santonastaso, G.F.; Simone, A. Water distribution system clustering and partitioning based on social network algorithms. *Procedia Eng.* **2015**, *119*, 196–205. [CrossRef]
61. Han, R.; Liu, J. Spectral clustering and genetic algorithm for design of district metered areas in water distribution systems. *Procedia Eng.* **2017**, *186*, 152–159. [CrossRef]
62. Chen, T.Y.-J.; Guikema, S.D. Prediction of water main failures with the spatial clustering of breaks. *Reliab. Eng. Syst. Saf.* **2020**, *203*, 107108. [CrossRef]
63. Grammatopoulou, M.; Kanellopoulos, A.; Vamvoudakis, K.G.; Lau, N. A Multi-step and Resilient Predictive Q-learning Algorithm for IoT with Human Operators in the Loop: A Case Study in Water Supply Networks. *arXiv* **2020**, arXiv:2006.03899.
64. Xia, W.; Wang, S.; Shi, M.; Xia, Q.; Jin, W. Research on partition strategy of an urban water supply network based on optimized hierarchical clustering algorithm. *Water Supply* **2022**, *22*, 4387–4399. [CrossRef]
65. Chen, R.; Wang, Q.; Javanmardi, A. A Review of the Application of Machine Learning for Pipeline Integrity Predictive Analysis in Water Distribution Networks. *Arch. Comput. Methods Eng.* **2025**, 1–29. [CrossRef]
66. Rossman, L.A.; Woo, H.; Tryby, M.; Shang, F.; Janke, R.; Haxton, T. *EPANET 2.2 User Manual*; Water Infrastructure Division, Center for Environmental Solutions and Emergency Response, U.S. Environmental Protection Agency: Cincinnati, OH, USA, 2020.

67. Kyriakou, M.S.; Demetriades, M.; Vrachimis, S.G.; Eliades, D.G.; Polycarpou, M.M. Epyt: An epanet-python toolkit for smart water network simulations. *J. Open Source Softw.* **2023**, *8*, 5947. [CrossRef]
68. Makaremi, Y.; Haghighi, A.; Ghafouri, H.R. Optimization of pump scheduling program in water supply systems using a self-adaptive NSGA-II; a review of theory to real application. *Water Resour. Manag.* **2017**, *31*, 1283–1304. [CrossRef]
69. Zheng, A.; Casari, A. *Feature Engineering for Machine Learning: Principles and Techniques for Data Scientists*; O'Reilly Media, Inc.: Sebastopol, CA, USA, 2018.
70. Venkatesh, B.; Anuradha, J. A review of feature selection and its methods. *Cybern. Inf. Technol* **2019**, *19*, 3–26. [CrossRef]
71. Chandrashekar, G.; Sahin, F. A survey on feature selection methods. *Comput. Electr. Eng.* **2014**, *40*, 16–28. [CrossRef]
72. Yang, L.; Shami, A. On hyperparameter optimization of machine learning algorithms: Theory and practice. *Neurocomputing* **2020**, *415*, 295–316. [CrossRef]
73. Probst, P.; Boulesteix, A.-L.; Bischl, B. Tunability: Importance of hyperparameters of machine learning algorithms. *J. Mach. Learn. Res.* **2019**, *20*, 1–32.
74. Injadat, M.; Moubayed, A.; Nassif, A.B.; Shami, A. Systematic ensemble model selection approach for educational data mining. *Knowl.-Based Syst.* **2020**, *200*, 105992. [CrossRef]
75. Liu, H.; Setiono, R. Chi2: Feature selection and discretization of numeric attributes. In Proceedings of the 7th IEEE International Conference on Tools with Artificial Intelligence, Herndon, VA, USA, 5–8 November 1995; pp. 388–391.
76. Khomytska, I.; Bazylevych, I.; Teslyuk, V.; Karamysheva, I. The chi-square test and data clustering combined for author identification. In Proceedings of the 2023 IEEE 18th International Conference on Computer Science and Information Technologies (CSIT), Lviv, Ukraine, 19–21 October 2023; pp. 1–5.
77. Guyon, I.; Elisseeff, A. An introduction to variable and feature selection. *J. Mach. Learn. Res.* **2003**, *3*, 1157–1182.
78. Fida, M.A.F.A.; Ahmad, T.; Ntahobari, M. Variance threshold as early screening to Boruta feature selection for intrusion detection system. In Proceedings of the 2021 13th International Conference on Information & Communication Technology and System (ICTS), Surabaya, Indonesia, 20–21 October 2021; pp. 46–50.
79. Desyani, T.; Saifudin, A.; Yulianti, Y. Feature selection based on naive bayes for caesarean section prediction. *IOP Conf. Ser. Mater. Sci. Eng.* **2020**, *879*, 012091. [CrossRef]
80. Ye, Y.; Liu, C.; Zemiti, N.; Yang, C. Optimal feature selection for EMG-based finger force estimation using LightGBM model. In Proceedings of the 2019 28th IEEE International Conference on Robot and Human Interactive Communication (RO-MAN), New Delhi, India, 14–18 October 2019; pp. 1–7.
81. Hua, Y. An efficient traffic classification scheme using embedded feature selection and lightgbm. In Proceedings of the 2020 Information Communication Technologies Conference (ICTC), Nanjing, China, 29–31 May 2020; pp. 125–130.
82. Altmann, A.; Toloşi, L.; Sander, O.; Lengauer, T. Permutation importance: A corrected feature importance measure. *Bioinformatics* **2010**, *26*, 1340–1347. [CrossRef]
83. Hsieh, C.-P.; Chen, Y.-T.; Beh, W.-K.; Wu, A.-Y.A. Feature selection framework for XGBoost based on electrodermal activity in stress detection. In Proceedings of the 2019 IEEE International Workshop on Signal Processing Systems (SiPS), Nanjing, China, 20–23 October 2019; pp. 330–335.
84. Alsahaf, A.; Petkov, N.; Shenoy, V.; Azzopardi, G. A framework for feature selection through boosting. *Expert Syst. Appl.* **2022**, *187*, 115895. [CrossRef]
85. Riyahi, M.M.; Rahmanshahi, M.; Ranginkaman, M.H. Frequency domain analysis of transient flow in pipelines; application of the genetic programming to reduce the linearization errors. *J. Hydraul. Struct.* **2018**, *4*, 75–90.
86. Han, J.; Pei, J.; Tong, H. *Data Mining: Concepts and Techniques*; Morgan Kaufmann: Burlington, MA, USA, 2022.
87. Messenger, R.; Mandell, L. A modal search technique for predictive nominal scale multivariate analysis. *J. Am. Stat. Assoc.* **1972**, *67*, 768–772. [CrossRef]
88. Cutler, A.; Cutler, D.R.; Stevens, J.R. Random forests. In *Ensemble Machine Learning: Methods and Applications*; Springer: New York, NY, USA, 2012; pp. 157–175.
89. Breiman, L. Random forests. *Mach. Learn.* **2001**, *45*, 5–32. [CrossRef]
90. Cortes, C.; Vapnik, V. Support-vector networks. *Mach. Learn.* **1995**, *20*, 273–297. [CrossRef]
91. Vapnik, V. *The Nature of Statistical Learning Theory*; Springer Science & Business Media: New York, NY, USA, 2013.
92. Scholkopf, B.; Smola, A.J. *Learning with Kernels: Support Vector Machines, Regularization, Optimization, and Beyond*; MIT Press: Cambridge, MA, USA, 2018.
93. Ben-Hur, A.; Weston, J. A user's guide to support vector machines. In *Data Mining Techniques for the Life Sciences*; Springer: New York, NY, USA, 2009; pp. 223–239.
94. Breiman, L. Bagging predictors. *Mach. Learn.* **1996**, *24*, 123–140. [CrossRef]

95. Gaikwad, D.P.; Thool, R.C. Intrusion detection system using bagging ensemble method of machine learning. In Proceedings of the 2015 International Conference on Computing Communication Control and Automation, Pune, India, 26–27 February 2015; pp. 291–295.
96. Tüysüzoğlu, G.; Birant, D. Enhanced bagging (eBagging): A novel approach for ensemble learning. *Int. Arab J. Inf. Technol.* **2020**, *17*, 515–528.
97. Schapire, R.E. The strength of weak learnability. *Mach. Learn.* **1990**, *5*, 197–227. [CrossRef]
98. Ke, G.; Meng, Q.; Finley, T.; Wang, T.; Chen, W.; Ma, W.; Ye, Q.; Liu, T.-Y. Lightgbm: A highly efficient gradient boosting decision tree. In Proceedings of the 31st Conference on Neural Information Processing Systems (NIPS 2017), Long Beach, CA, USA, 4–9 December 2017.
99. Kutner, M.H.; Nachtsheim, C.J.; Neter, J.; Li, W. *Applied Linear Statistical Models*; McGraw-Hill: New York, NY, USA, 2005.
100. Fujiwara, O.; Khang, D.B. A two-phase decomposition method for optimal design of looped water distribution networks. *Water Resour. Res.* **1990**, *26*, 539–549. [CrossRef]
101. Kadu, M.S.; Gupta, R.; Bhave, P.R. Optimal design of water networks using a modified genetic algorithm with reduction in search space. *J. Water Resour. Plan. Manag.* **2008**, *134*, 147–160. [CrossRef]
102. Mirjalili, S.; Lewis, A. The whale optimization algorithm. *Adv. Eng. Softw.* **2016**, *95*, 51–67. [CrossRef]
103. McCulloch, W.S.; Pitts, W. A logical calculus of the ideas immanent in nervous activity. *Bull. Math. Biophys.* **1943**, *5*, 115–133. [CrossRef]

Disclaimer/Publisher's Note: The statements, opinions and data contained in all publications are solely those of the individual author(s) and contributor(s) and not of MDPI and/or the editor(s). MDPI and/or the editor(s) disclaim responsibility for any injury to people or property resulting from any ideas, methods, instructions or products referred to in the content.

water

MDPI

Article

Fractal-Based Approach to Simultaneous Layout Routing and Pipe Sizing of Water Supply Networks

Paweł Suchorab *, Dariusz Kowalski and Małgorzata Iwanek

Department of Water Supply and Wastewater Disposal, Faculty of Environmental Engineering and Energy, Lublin University of Technology, Nadbystrzycka 40B, 20-618 Nadbystrzycka 40B, 20-618 Lublin, Poland; d.kowalski@pollub.pl (D.K.); m.iwanek@pollub.pl (M.I.)
* Correspondence: p.suchorab@pollub.pl

Abstract: The process of designing water distribution networks is divided into two main stages: network layout routing and pipe sizing. However, routing and sizing are not separate tasks—the shape of the network affects the diameters of the pipes, and vice versa. This paper presents an innovative fractal-based method, which enables the simultaneous layout routing and pipe sizing of water supply networks. The developed pipe routes and diameters selected according to the method are mathematically justified; the selection considers the total length of the pipes, the number of rotation angles of the base section, the cost of the water supply system construction and the priority of water supply to individual customers. The novelty of the method lies in the possibility of carrying out the processes of routing and sizing of the network in a recursive manner by the adoption of the principles of fractal geometry and Murray's law. The method was tested under the conditions of a synthetic settlement. The obtained results enable us to conclude that the method is universal and suitable for shaping water supply networks, while determining the pipes' diameters, both under the conditions of a single- and multi-sided water supply source.

Keywords: routing; sizing; water supply network; fractals; WDN; SRS method

1. Introduction

One of the first steps in designing a water distribution network (WDN) is pipeline routing, defined as giving the water supply network a geometric shape [1]. The shape of the geometric structure depends on many factors, including the spatial arrangement of the settlement, topography, the presence of natural and artificial obstacles in pipe routing, the location of the water demand centers or the layout of communication routes [2]. Therefore, the routing of the water supply network is subject to various rules and restrictions, depending on both external factors and the type of water supply pipelines being designed. The routing process has an impact on further design steps, such as hydraulic calculations, investment costs, and subsequent operation of the water supply system. That is why developing an effective and profitable way of designing water supply networks, including the search for the optimal method of routing and sizing, is still a current issue.

Water supply network structures are generally classified in terms of topology, distinguishing networks into branched, looped, or mixed structures [1,3,4]. To find the correlations between geometrical properties and design or operational aspects of WDN, the complex network theory (CNT), graph theory (GT), and fractal geometry (FG) are applied [5–9]. All the above-mentioned approaches provide the tools (indicators) for a precise

description of network structures, comparison of the networks [10], and application to analyses of WDNs [11], including analyses of their optimization [12] and reliability [13,14]. Advanced methods of describing and classifying WDNs are still relevant due to the fact that accurate network management also involves socioeconomic and environmental issues [15]. In the context of the routing of water supply networks, presenting networks in the form of graphs makes it possible to use least cost path algorithms (LCPA) or path of least resistance (PLR) algorithms, combined with geographic information systems (GIS) [16], to determine the connection route between water nodes. The CNT optimization approach has been used by researchers to formulate different design methodologies [5,17–19]. In accordance with the application of FG, routing of a WDN can be achieved by reproducing dendric (tree) structures by copying and rotating the initial section (axiom) [20–23]. However, despite many approaches observed, none of the routing methods are fully universal, mainly with regard to extensive looped networks with multiple sources. The search for new methods is still ongoing; as the benefits of the optimal geometric layout of the network may be greater than the savings obtained from the pipe sizing [24].

Sizing of water networks is a complex combinatorial problem (NP-hard problem NPH) [25] and should be treated as an optimization task. It includes the selection of diameters from a predefined pipe type series in order to find the minimum total cost while meeting hydraulic requirements [26] as well as assuming constant geometric shape and nodal demands [27]. As the shape of the network influences the dimensioning process, both tasks should be solved simultaneously. Numerous different approaches have been implemented, including mathematical programming [28–31], heuristic [32,33], metaheuristic [34–43], and multi-objective optimization approaches [44–49]. However, there is still no automated network design method under the conditions of a complex, real settlement.

Considering the premises above, it is reasonable to search for and develop new methods supporting the process of designing water supply networks, including the routing and sizing processes. The aim of this paper is to present and evaluate a novel fractal-based approach of simultaneous routing and sizing (SRS) of water network structures. The main objectives of the paper are testing the developed method in different initial conditions, the verification of the possibility of obtaining repeatable results and evaluation of the hydraulic operation parameters of the designed water supply networks.

2. Materials and Methods

The analyses and results presented in this paper are a part of a larger scope of research, the aim of which is the development and implementation of a new method of designing WDNs. The full scope of research is presented in Figure 1. After developing the rules of the method, the solution was tested in various conditions, including artificial settlements plans, quasi-real networks (virtual cities) and real condition networks. Finally, the proposed sizing method was evaluated in comparison to the genetic algorithm method. In this section of the manuscript we present the scientific background of the original method, a description and novelty of the proposed SRS method, and exemplary calculations as well as the method and results evaluation methodology under the conditions of artificial settlements created randomly for the purpose of this research.

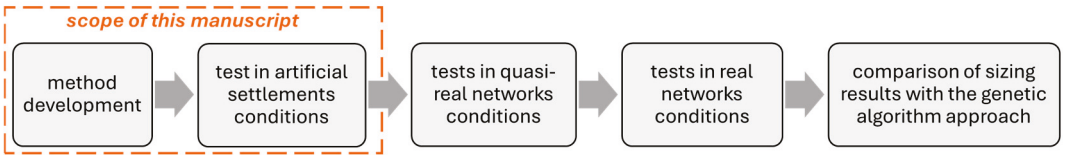

Figure 1. Research workflow diagram.

2.1. Scientific Background of the Original Method

The SRS method [50] is a modification to the original approach proposed by Kowalski [20]. In his original method, Kowalski proved that after considering certain assumptions, branched, looped, and mixed water supply networks can be reflected and described using dendritic (tree-shaped) structures. Such structures are common in nature; for example, in the architecture of trees, river basins, water transport in plants, or the circulatory system of living organisms [51–54]. Moreover, Kowalski verified that tree-shaped WDNs can be treated as fractal sets which are difficult to describe using classical geometry because of their high irregularity [55]. Fractals are characterized by such main features as: fine structure at arbitrarily small scales, recursive procedures of construction, intricate detailed structures, self-similarity, and size not quantified by the usual measures, e.g., length [56]. In fractal geometry, a basic property of a fractal is its dimension, which describes how fractals fill space and how irregular that arrangement is [7]. Fractal dimension often refers to the so-called box counting method (Formula (1)) [56]. Its application in WDNs is wide, including reliability, connectivity, redundancy, and operational aspects [7,8,57].

$$D_b(F) = \lim_{\delta \to 0} \frac{logN_\delta(F)}{-log\delta}, \tag{1}$$

where F—a non-empty bounded subset of a finite-dimensional Euclidean space, $D_b(F)$—the box-counting dimension of the set F, $N_\delta(F)$—the smallest number of sets of diameters δ covering F.

Tree-like structures found in nature (e.g., blood vessels) are "optimized" in some way through evolutionary processes. Researchers often observe the solutions found in nature and then, by analogy, apply them to technical solutions. In the 1920s, Murray postulated one of the fundamental principles that the organization of vessels in the circulatory system of living organisms is based on minimizing the energy required to ensure adequate blood flow [58,59]. According to Murray's theory, the process of increasing vascular composition is based on the relationship between the volumetric flow rate Q and the vessel diameter d (Formula (2)). In his works, Murray claimed that the total energy expenditure of the flow is minimized when $x = 3$, while the relationship between the diameters of the vessels of subsequent generations of the optimal vascular tree are given by Formula (3).

$$Q = b \cdot d^x, \tag{2}$$

$$d_0^x = d_1^x + d_2^x, \tag{3}$$

where Q—volumetric flow, b—a certain constant, the same before and after the division of vessels, d—vessel diameter, x—positive exponent, d_0—parent vessel diameter, d_1, d_2—child vessel diameter.

Using the self-similarity properties of a geometric set representing a water supply network, based on tree structures, allows for the application of Murray's law, which states that each branching of a base pipe leads to a reduction in the diameters of the child pipes. In the case of water supply networks, due to technical constraints, this law can be modified [20]. The diameters of the child pipes should be reduced by one value in the pipe series, relative to the base pipe. This represents a divergence from Formula (3) while retaining the very idea of Murray's law.

2.2. Description and Novelty of the Proposed SRS Method

The main novelty of the proposed SRS method refers to the simultaneous performance of the routing and sizing process, while in the method [20] these processes were conducted

independently. In accordance with the fractal-based nature of the method, the routing process involves copying and rotating (affine transformations) the base section of the water pipeline (the first link of the network directly connected to the water source) and conducting a mathematical analysis of the potential connection routes. The sizing process, depending on the iteration, involves determination of diameters in accordance with the modified Murray's law [58,59] or selecting diameters from an adopted pipe type series. The application of the proposed method is performed in a recursive manner—the processes of routing and sizing are carried out cyclically within subsequent groups (classes) of demand nodes. Each subsequent iteration leads to a more detailed structure of the designed water supply network. Successive transformations of the base section are called bifurcations of a given iteration. The routing process is carried out by copying and rotating the base segment L_i. Creating a new segment L_{i+1} is performed by copying the base segment L_i and rotating it by an angle α. The length of the segment L_{i+1} is the product of the length of the base segment L_i and the length parameter a of the newly constructed section (Formula (4)). The example of routing symmetrical and asymmetrical water supply structure through successive transformations of the base section L_0 is presented in Figure 2a,b [20].

$$L_{i+1} \rightarrow \begin{cases} a \cdot L_i, \alpha' \\ b \cdot L_i, \alpha'' \\ c \cdot L_i, \alpha''' \end{cases} \tag{4}$$

where L_i—length of the segment in i-th bifurcation, L_{i+1}—length of the next section, a, b, c—parameters of the length of the newly constructed sections, α', α'', α'''—angles describing the position of the newly created sections in relation to the preceding section.

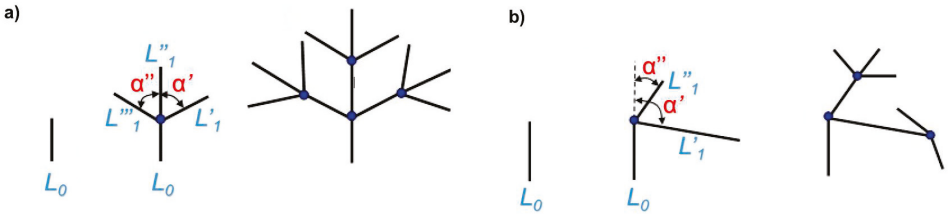

Figure 2. Process of routing (**a**) symmetric and (**b**) asymmetric water supply structure [20].

Using the Formula (4), it is also possible to create looped structures. Figure 3 shows a single-loop network. Additionally, a diagram of the hierarchical dependence of the segments forming this network is presented. Considering Figure 3a, it can be noticed that the loop cannot be closed, regardless of whether segment 5 is created from segment 2 or 4. As a solution to this problem, an additional connecting node (Figure 3b) was proposed, which allows for loop closure. This means that when creating looped structures using the tree structures procedure, it may be necessary to introduce additional connection nodes [20].

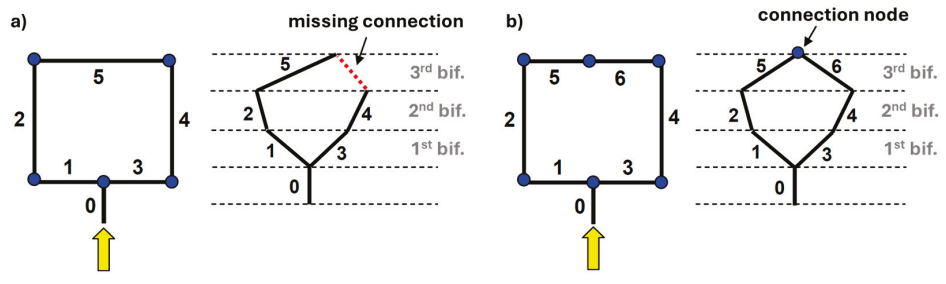

Figure 3. A single-loop, symmetrical structure with highlighted nodes and schemes of hierarchical connections of subsequent network sections, (**a**) no additional connection node, (**b**) with an additional connection node (yellow arrows—water sources) [20].

The SRS method introduces additional modifications [50] to the original approach:

- Water demand nodes are classified in a ranking considering the quantity of water demand and priority of water supply delivery.
- In the first two iterations (to the two first classes of demand nodes), the network is routed from the water source to the nodes of a given class. In subsequent iterations, the direction of routing is reversed.
- If a lower-class node is located on the water pipeline route developed as a result of previous iterations, it is assumed that the consumers represented by this node have already been supplied with water, which excludes it from further routing process.
- The application of the proposed method requires the following: (i) determining the plan of a settlement, including street grids, number, capacity, and location of water sources; (ii) determining the spatial distribution of water demand nodes; (iii) estimating the unit costs of constructing a water supply pipeline.

The connection routes created in the routing process between two given water nodes should have the characteristics of minimum paths in terms of two basic criteria: the sum of the lengths (ΣL) and the sum of the rotation angles ($\Sigma\alpha$) of the base section. While the ΣL criterion refers to finding the shortest route, the $\Sigma\alpha$ criterion allows determining which of the identical minimal paths should be selected during the routing process. Additionally, a third criterion for selecting the most favorable (economically) route is proposed: the cost (ΣK) of making a given connection, in case where criteria ΣL and $\Sigma\alpha$ are insufficient. This approach makes it possible to assess which path is more financially profitable. Detailed definitions of minimum routing paths are presented through Formulas (5)–(7).

$$\sum L = \min\left(L_1 = \sum_{j=1}^{p}\sum_{i=1}^{r} L_{ji}, \ldots,\ L_k = \sum_{j=1}^{p}\sum_{i=1}^{t} L_{ji}\right) \tag{5}$$

$$\sum \propto = min\left(\alpha_1 = \sum_{j=1}^{p}\sum_{i=1}^{r}\left|\alpha_{ji}\right|, \ldots,\ \alpha_z = \sum_{j=1}^{p}\sum_{i=1}^{t}\left|\alpha_{ji}\right|\right) \tag{6}$$

$$\sum K = min(K_1 = K_{L1} + K_{\alpha 1},\ \ldots, K_w = K_{Lw} + K_{\alpha w}) \tag{7}$$

where ΣL—total length of water supply sections, k—number of alternative water supply paths to nodes of a given class, p—number of nodes of a given class, r,t—the number of bifurcations necessary to connect the base section with a given node, z—number of alternative paths satisfying Formula (2), $\Sigma\alpha$—total sum of the rotation angles of the base sections in subsequent bifurcations, ΣK—total cost of construction of a given section, w—number of alternative paths satisfying Formulas (2) and (3), K_{Lw}—cost of constructing a straight pipe in the w-th section, $K_{\alpha w}$—cost of constructing the pipe elbows in the w-th section.

To assess the connection route in terms of construction costs, knowledge of the diameters of individual pipelines is required. This means that the routing and sizing processes should be carried out in parallel because they determine each other. This requires a recursive procedure within the developed method. The dimensioning process is based on the application of modified Murray's law [58,59] but is also dependent on the available range of pipe type series and the required minimum diameter approved by water utility. Initially, a smaller diameter value from the pipe type series is assigned to each subsequent branch of the network. Next, the pipe diameter values are assigned to specific dimensioning stages (last iteration—the smallest permissible value from the pipe type series). A detailed description of the routing and sizing processes in individual iterations is presented in Table 1, while the block diagram of the consecutive steps in developed method is shown in Figure 4. In the presented diagram, the occurrence of double loops can be noticed—these

are the interactions between the routing and sizing processes in subsequent iterations. The application of the method for networks with single and multiple water sources differs in one step: establishing a connection between the sources.

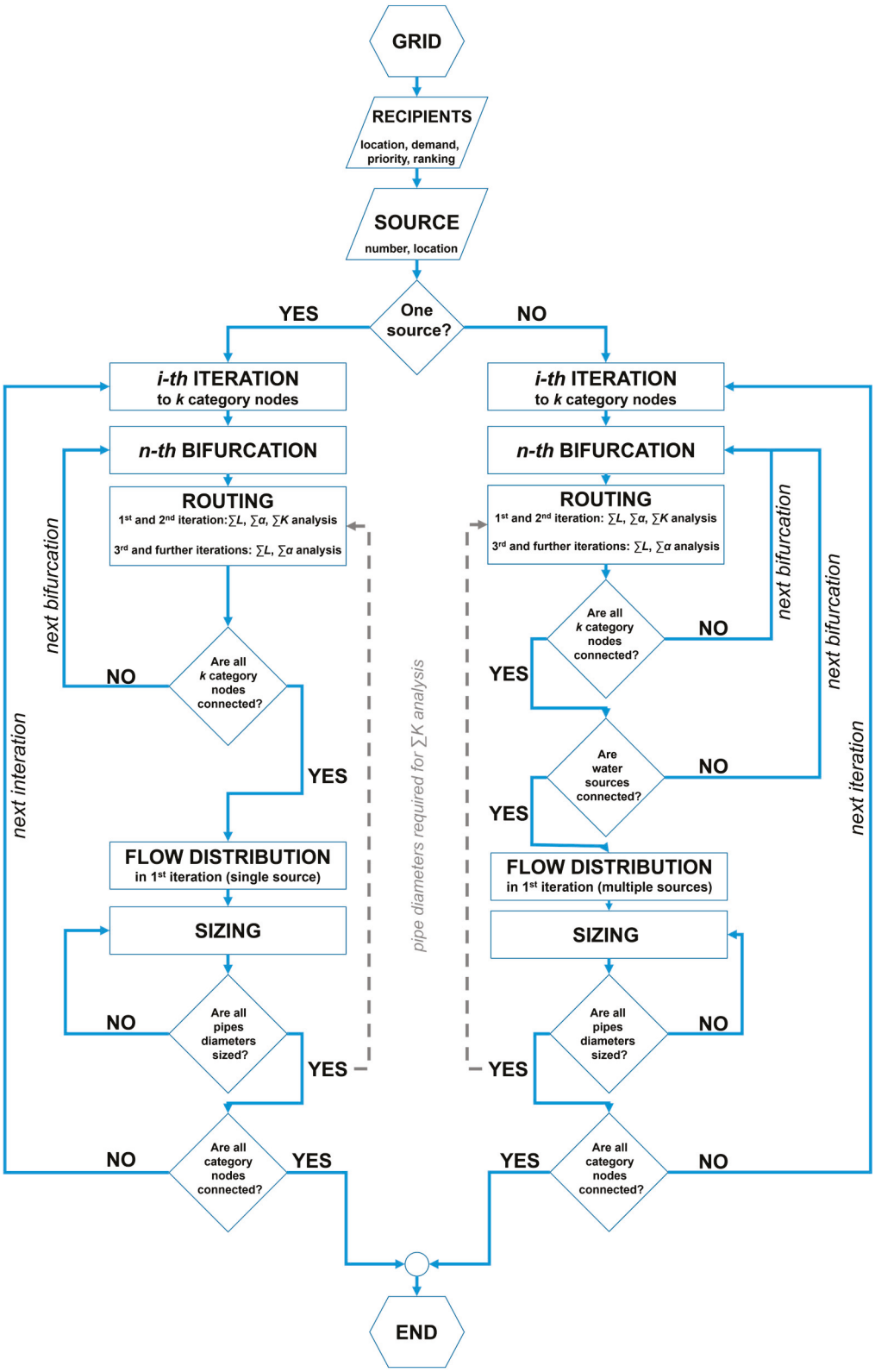

Figure 4. Block diagram of the developed SRS method.

Table 1. The routing and sizing process divided into iterations.

Iteration	Routing	Sizing
1st and 2nd	• Direction: from supply points to class I and II nodes • End: when connected to all class I and II nodes • If there are 2 or more water sources—establish connection between sources • Analysis of minimal efficiency paths—ΣL, $\Sigma \alpha$ • When alternative paths exist—analysis of ΣK • When equivalent routes exist—all are maintained	• Continuity equation and assumed flow velocity (e.g., 1 m/s) for determining the main water pipe diameter • If 2 or more water sources—establish percentage share between sources • Diameter sizing—via modified Murphy's law • When identical routes—larger diameter is used
3rd and further	• Direction: from class III nodes and further to the network routed in 1st and 2nd iteration • End: when connected to all nodes of a given class • No minimal efficiency paths analysis—all pipes from the bifurcation that provide a connection to the demand node are maintained	• Each iteration is assigned with specific diam-eter: • Last iteration—smallest diameter (e.g., DN80) • Penultimate iteration—second smallest di-ameter in the type series (e.g., DN100) • The third last iteration—next smallest diam-eter in the type series (e.g., DN125)

The individual steps of routing and dimensioning water supply networks according to the developed SRS method are listed below:

1. Preparing the settlement grid, potential connection, and demand nodes.
2. Determining the location, demand, and priority of water supply to individual demand nodes. Classification of demand nodes in the ranking.
3. Determining the number and location of water sources. Possible definition of the percentage share of individual water sources.
4. 1st iteration of pipe routing to class I nodes. Analysis of connection paths in terms of ΣL, $\Sigma\alpha$, and ΣK. In the case of networks with two or more water sources, the routing process should be carried out between the connecting individual sources.
5. Determining the distribution of flows in the routed network based on the water consumption of class I demand nodes.
6. Conducting the pipe sizing process. The dimensioning process is linked back to step 4—routing of water pipes.
7. Carrying out the 2nd iteration routing and sizing processes to class II nodes.
8. Routing and sizing processes of subsequent iterations to the remaining node classes.
9. The process of routing and sizing of the water supply network is complete when demand nodes of all classes are connected with the water source.

2.3. Calculation Example

The process of implementing the SRS method is presented in an example calculation for a simple settlement (Figure 5a), containing 9 water demand nodes located in a development area plan (in the form of a grid of 5 × 5 squares with a side length of 150 m) with streets (30 m wide) between them. The location of the demand nodes is random, specifying the so called "centers of water consumption". The water source is marked as a Z node and the total water demand of the settlement is assumed to be 75 dm^3/s. Demand nodes are divided into 3 classes: one node (A) is assigned to class I, three nodes are classified as class II (B, C, D), and 5 nodes are placed in class III (E–I).

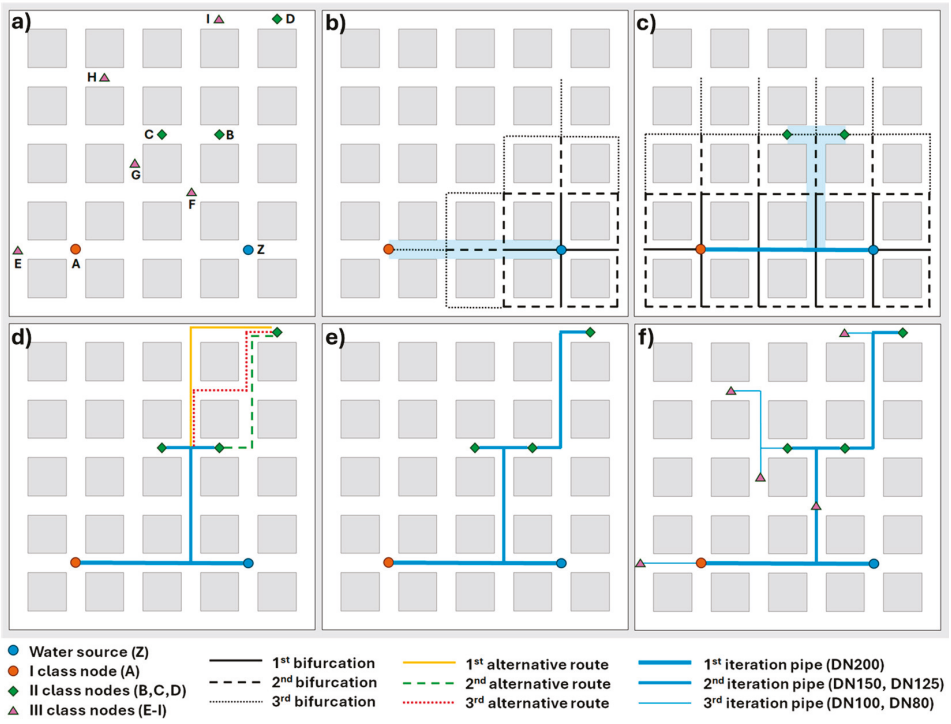

Figure 5. Steps of routing and sizing exemplary water supply network: (**a**) location of water source and demand nodes, (**b**) 1st iteration routing, (**c**) 2nd iteration routing, (**d**) alternative routes to node D, (**e**) result of 2nd iteration, (**f**) result of 3rd iteration.

The subsequent stages (bifurcations) of the routing process in the 1st iteration are presented in Figure 5b. The process of the rotation of the base section started from the water source Z. From the source node, potential connections are routed in all possible directions to the nearest intersections (continuous line). Next, from all the ends of the continuous lines, further potential connections are made to further intersections (dashed lines). In this way, through subsequent bifurcations, routing is carried out until a connection with a node of a given category is reached. The assumed goal was to connect the source to the class I node (A) which was achieved in the 3rd bifurcation. The connecting route was 540 m long and had a rotation angle of the base section of 0° (marked in light blue in Figure 5b). After the routing process, the diameter of the Z–A pipe had to be determined. For this purpose, the continuity equation was used, assuming total water consumption to be 75 dm^3/s and the water flow velocity to be v = 1 m/s. The calculated diameter of the Z–A pipe was 0.309 m, so the DN300 pipe was selected from the DN/ID type series line of ductile iron pipes. This completed the 1st iteration of the SRS process. The assumed velocity of 1 m/s refers only to the selection of the pipe diameter routed in the first iteration. This may correspond to the pipes originating from the water supply stations. Due to the water flow in further directions and the minimum diameters that can be used in the WDNs, it is expected that the velocities in the further parts of the network (farther from the source) will be lower. Due to the dimensioning process being carried out in accordance with the modified Murray's law, no pressure constraints were introduced—according to the applied law, the appropriate selection of diameters should guarantee the minimization of flow energy.

The routing process of the 2nd iteration was carried out from the water pipeline route obtained in the previous iteration to class II nodes (nodes B, C, D). As a result of the routing, a connection with nodes B and C in the 3rd bifurcation was achieved. The resulting routes to nodes B and C provided a simultaneous connection to the nodes and were equivalent—they had an identical length (450 m) and an identical sum of the rotation angles of the base

section required to obtain the connection (90°). A visualization of the routing process of the 3rd bifurcation of the 2nd iteration is shown in Figure 5c. In subsequent bifurcations, attempts were made to obtain a connection with node D. As a result of the routing, three potential paths were distinguished (Figure 5d).

- 1st alternative route: $\sum L = 630$ m $\quad \sum \alpha = 90°$
- 2nd alternative route: $\sum L = 540$ m $\quad \sum \alpha = 180°$
- 3rd alternative route: $\sum L = 630$ m $\quad \sum \alpha = 270°$

To determine the final connection route, it was necessary to analyze the sum of the lengths of the sections ($\sum L$), the sum of the rotation angles ($\sum \alpha$) and the total cost ($\sum K$) of making a given connection. To determine the cost of implementing individual routes, it was necessary to know the pipe diameters. For this purpose, sizing was carried out according to the modified Murray's law. The sections created in the 3rd bifurcation of the 2nd iteration (the connections with nodes B and C) were assigned a diameter of DN250, and the connection with node D was made with a diameter of DN200 mm. For the purposes of this example, the unit costs of constructing 1 m of DN200 water supply pipe (600.00 PLN/m) and a 90° pipe elbow (4000.00 PLN) were calculated, which were used to analyze the costs of constructing three potential connection routes to node D. The calculation results of the total cost of implementing the given connection routes are presented in Table 2. The lowest cost was estimated to be route 2 (Figure 5d), with a length of 540 m and a sum of the rotation angles of the base section equal to 180° (double rotation of the base section required to connect to node D). The resulting network, ensuring the connection to all class II nodes with the existing water supply, is presented in Figure 5e.

Table 2. Total cost of alternative routes to node D.

Route	Length	Unit Cost of DN200 Pipe	Pipeline Cost	Number of 90° Elbow	Unit Cost of 90° Elbows	∑K
	m	PLN/m	PLN	-	PLN	PLN
1	630	600	378,000	1	4000	382,000
2	540		324,000	2	8000	332,000
3	630		378,000	3	12,000	390,000

In the 3rd iteration, in accordance with the assumptions of the SRS method, there was a change in the routing direction: from class III nodes towards the existing water supply pipelines. Additionally, the method of sizing the pipes was also changed—specific values from the DN/ID type series were assigned to specific iterations. Due to the fact that in the 2nd iteration, the smallest specified diameter was DN200, specific diameter values were also used for individual bifurcations (1st bifurcation of the 3rd iteration—DN150, 2nd bifurcation of the 3rd iteration—DN125, etc.). Connections to all class III nodes were achieved in the 2nd bifurcation of the 3rd iteration. Therefore, the selected pipe diameters were DN150 and DN125. Because the minimum diameter DN80 was not achieved, in accordance with the principles of the SRS method, all selected diameters were reduced by 2 positions from the DN/ID type series. The final diameter range of the routed network is DN80-DN200. During the routing process, it turned out that one of the class III nodes (F) was located in a place where the WDN had already been routed, and it was excluded from the further routing process. The final routing results are shown in Figure 5f.

During the routing and sizing of the exemplary water supply network, it can be observed that the assumptions of the SRS method were met; the pipes were sized with

descending diameter gradation and consideration of the permissible minimum diameter; thus, there was no need to perform tedious hydraulic calculations of the looped system.

2.4. Methodology of the SRS Method Evaluation

The application of the presented SRS method was carried out as a multi-stage study and numerical research. After the implementation of preliminary tasks (assessment of unit costs of constructing water pipes and defining general principles for creating a node ranking), the method was tested under the conditions of a virtual settlement.

2.4.1. Description of the Synthetic Settlement Plan

The goal of the model tests was to evaluate the applicability of the SRS method in terms of (i) the hydraulic conditions of the designed networks, (ii) the absence of any blockages when using the presented method (iii) repeatability of the obtained results. The synthetic settlement plan was represented by a grid map consisting of development areas and streets. The structure of the model grid is presented in Figure 6. The area of the synthetic settlement plan was mapped as a 10-row and 10-column grid of squares (green color—development areas), each with a side of 150 m. It was assumed that there were 30 m wide streets (white color) between the development areas and a flat terrain. The total area was 380.25 ha, and the estimated number of inhabitants of the model unit was 85,556 people. The average daily water demand was 21,769.26 m^3/d (≈252 dm^3/s). During the model test studies, the irregular location of consumers as well as single- and multi-sided water supply cases were taken into account. Potential connection points for the water supply network located at street intersections (with a total number of 100) are marked with red points in Figure 6. Potential water demand nodes (total: 220 nodes) are marked with gray points. The model studies included the routing and sizing of 7 different WDNs:

- 3 single-side supplied water networks (A, B, C)—one water source,
- 3 multi-side supplied water networks (D, E, F)—two water sources,
- 1 multi-side supplied water network, G, with a top-down water source capacity (source no. 1—capacity equal to 70% of total demand; source no. 2–30%).

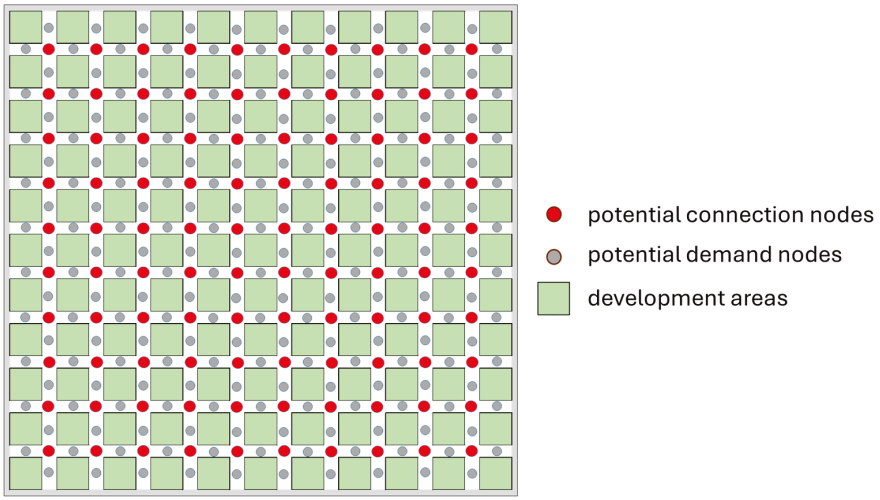

Figure 6. Structure of the synthetic settlement grid with the location of potential connection nodes (red points) and potential demand nodes (gray points), development areas (green), streets (white).

In each test, different locations of the water sources and demand nodes were assigned randomly for each of the A–G networks. Each of the water demand nodes in the analyzed networks was classified into one of the subtypes in the water consumption volume category

(KQ1-KQ3) and the water delivery priority category (KP1-KP3). Subsequently, the demand nodes were ranked based on the sum of points obtained based on the assigned weights. In this way, 5 classes of nodes were distinguished, listed in Table 3. The nodes with the largest demand were classified as class I (KQ1, weight: 3) with high priority for water delivery (KP1, weight: 3). In turn, class V included the nodes with the smallest demand (KQ3, weight: 1) with low priority for water delivery (KP3, weight: 1). The number of classes of water demand nodes directly determines the number of iterations during the process of network routing and sizing according to the SRS method. With the proposed division of nodes into 5 classes, there were 5 iterations. Each iteration corresponds to the connection of nodes from a given class with a water source or existing water network.

Table 3. Ranking of demand nodes divided into classes.

Class	Total Weight	Water Demand KQ		Delivery Priority KP	
		Subtype	Weight	Subtype	Weight
I	6	KQ1	3	KP1	3
II	5	KQ1 KQ2	3 2	KP2 KP1	2 3
III	4	KQ1 KQ2 KQ3	3 2 1	KP3 KP2 KP1	1 2 3
IV	3	KQ2 KQ3	2 1	KP3 KP2	1 2
V	2	KQ3	1	KP3	1

According to the classification of the nodal demands carried out in [60], it was assumed that out of the 220 potential demand nodes, water was demanded by 42% (92 consumer nodes) and the largest consumer had a base water demand equal to 5% of the total demand (13 dm^3/s). The structure of the demand nodes was determined as follows:

- the largest consumers: 23 nodes (25% of the 92) with base demand 4–13 dm^3/s,
- the medium consumers: 9 nodes (10% of the 92) with base demand 2–3 dm^3/s,
- the smallest consumers: 60 nodes (65% of the 92) with base demand equal to 1 dm^3/s.

On average, there were 7 nodes in the A–G networks in class I and 20 nodes in class V, respectively. The largest group was class III, in which, on average, 32 out of 92 nodes were qualified. A maximum of 38 nodes were qualified in each class (in networks C and E). A detailed summary of the number of nodes in networks A–G is presented in Table 4. The synthetic settlement plans with the locations of water sources and the division of demand nodes into individual classes in networks A–G are shown in Figure 7.

Table 4. Number of nodes in individual classes in networks A–G.

Class	Network							Average	
	A	B	C	D	E	F	G		
I	9	7	5	10	4	7	5	7	7.30%
II	11	9	7	7	5	9	12	9	9.32%
III	24	29	38	31	38	35	31	32	35.09%
IV	30	22	23	23	28	22	25	25	26.86%
V	18	25	19	21	17	19	19	20	21.43%
Total	92	92	92	92	92	92	92	92	100%

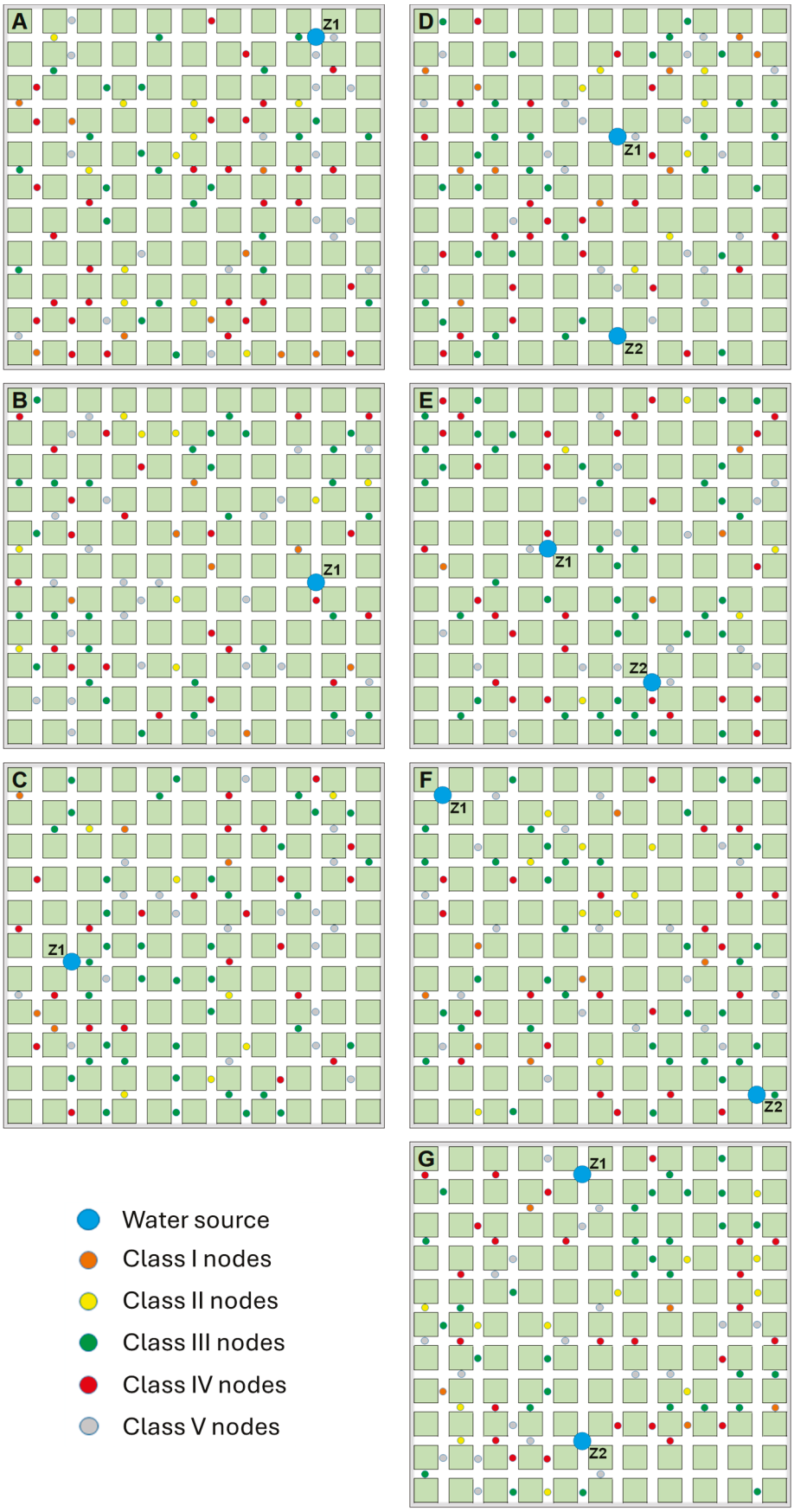

Figure 7. Location of water sources and demand nodes in networks A–G.

2.4.2. Results, Analysis, and Methodology

Networks A–G, routed and sized via the SRS method, were further compared to each other in order to determine the repeatability of the method. The assessment of the results was performed with regard to two major aspects: the geometric characteristics of the networks and the operating hydraulic conditions. The assessment of the geometric structures was carried out by determining the sum of the lengths (ΣL) of water pipes constituting the routed network, by specifying the number of iterations and bifurcations needed to route the network, and by determining the sum of the rotation angles ($\Sigma\alpha$) of the base section in the first two iterations. Additionally, the geometric structure was characterized by a fractal dimension (Formula (1)), calculated via Fractalyze 3.0 software [61]. The developed networks were also analyzed in terms of the diameter range and the existence of branched endings.

The operating hydraulic conditions were analyzed in accordance with numerical steady state models of each of the designed networks. Simulations were performed in the EPANET 2.2 software [62]. The basic settings of the model were as follows: LPS flow units, Darcy–Wiesbach head loss formula, and 1.5 mm pipe roughness. When analyzing the flow velocity in the model networks, a unified scale was adopted. The pressure and the water age in the networks were analyzed with regard to the occurrence of minimum, maximum, and average values. In order to compare the A–G networks, it was assumed that the minimum required pressure in the network was 40 m H_2O and the characteristics of individual pumping stations were developed with this in mind. The single-point pump curves were defined by the head (H) and flow (Q). The pump heads were determined using a trial and error approach, so that the minimum pressure in the network was reached. Additionally, for each of the networks, pump energy consumption was evaluated assuming 75% pump efficiency. To determine the water age, it was necessary to change the type of simulation to an Extended Period Simulation (EPS) and define the simulation time, which had to be longer than the time of water inflow from the source to its most distant nodes.

3. Results

3.1. Networks A, B, and C

As the result of applying the SRS method on the model grid, the following networks with a single water source were created:

- network A: total pipe length ΣL = 23,670 m, diameter range DN80-DN600, total number of iterations: 5, total number of bifurcations in all iterations: 46, total rotation of the base sections in the first two iterations: $\Sigma\alpha = 1800^\circ$,
- network B: ΣL = 23,940 m, DN80-DN500, 5 iterations, 21 bifurcations, $\Sigma\alpha = 1260^\circ$,
- network C: ΣL = 25,110 m, DN80-DN350, 5 iterations, 20 bifurcations, $\Sigma\alpha = 1080^\circ$.

The geometric structures of the designed water supply networks A, B, and C with the pipe diameters are shown in Figure 8. In the designed networks, source nodes are located in different places: for network A it is the upper right corner of the area, for network B it is the right side of the area, and for network C it is the left side of the synthetic settlement plan area. The location of water sources has a direct impact on the number of bifurcations needed to route the network to class I nodes. When analyzing the geometric structures of the designed water supply networks A, B and C, it can be noticed that the routed structures cover the area of the entire synthetic settlement. In all three networks, the smallest selected diameter is DN80, which is achieved during the dimensioning process in the fifth iteration (up to class V nodes). However, the maximum diameters differ between networks, from DN600 in network A, to DN500 in network B, to DN350 in network C. This is a consequence of the randomly selected locations of water sources and demand nodes. In each of the

analyzed networks A, B and C, there were visible "end branches" of the networks with significant diameters. Such situations should be treated as unfavorable, because they would require structural protection of the water pipe ends against the resulting stress forces.

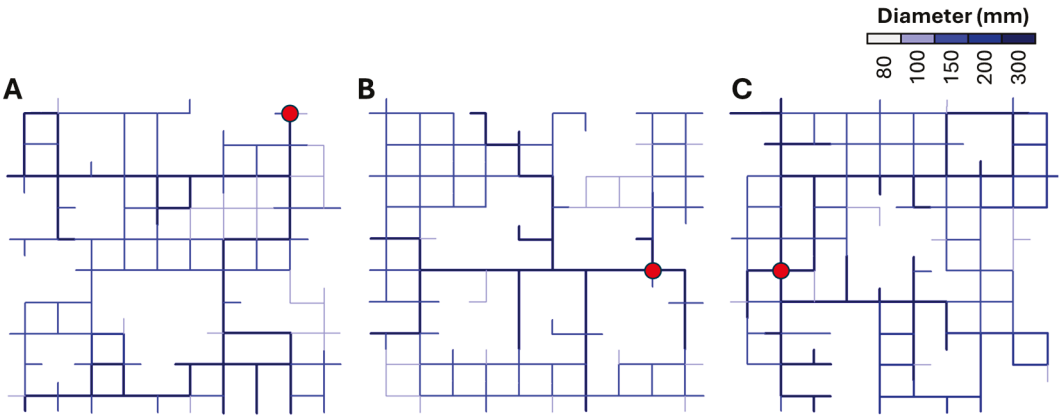

Figure 8. Single-sourced (red dots) networks A, B and C designed via the SRS method.

A detailed list of water velocities in the analyzed networks A, B, and C is presented in Table 5. When analyzing the distribution of water flow velocities in the pipes, it can be noticed that the pipes in which the water flow velocities range from 0 to 0.29 m/s predominate. They constitute 71.10% of all sections in network A, 57.89% in B and 58.06% in C. Although this velocity is unsatisfactory in terms of the hydraulic operating conditions of the network, it is also typical for real water supply networks operating under standard water flow conditions due to the minimum required diameter DN80. The average value of water flow velocity in network A was 0.26 m/s, in network B 0.32 m/s, and in network C 0.31 m/s.

Table 5. Velocities in water pipes in networks A, B, and C.

Velocity	Network A		Network B		Network C	
	Length					
m/s	m	%	m	%	m	%
≥1.5	0	0	0	0	0	0
1.0–1.49	0	0	990	4.14	720	2.87
0.7–0.99	540	2.28	1260	5.26	1530	6.09
0.3–0.69	6300	26.62	7830	32.71	8280	32.98
0.0–0.29	16,830	71.10	13,860	57.89	14,580	58.06
Σ*L*	23,670	100	23,940	100	25,110	100
Average Velocity (m/s)	0.26		0.32		0.31	

The contour maps of pressures in networks A, B, and C are shown in Figure 9. In all A, B, and C networks, there are very small differences in pressure within the designed networks. The maximum pressure can be observed in network B (44.62 m H_2O), while the lowest average pressure occurs in network A (40.94 m H_2O). The water age in networks A, B and C is presented in the form of contour maps in Figure 10. In network A, the maximum value of water age is 3 h 39 min, with an average of 70.2 min. In network B, the maximum and average values are 4 h 37 min and 67.8 min, respectively. In turn, in network C, one can notice the relatively highest maximum value of water age (4 h 55 min) with the lowest average value (54.6 min). The estimated electricity consumption by pumps in networks A, B, and C was 138.33, 148.51, and 142.88 kW, respectively.

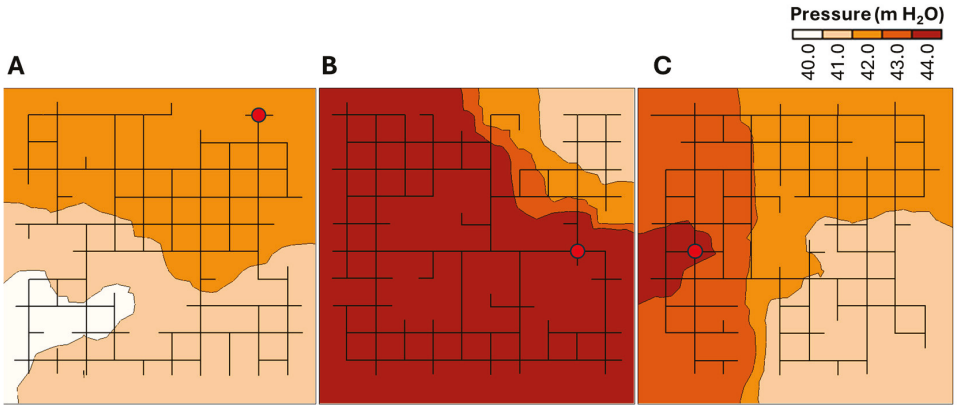

Figure 9. Contour maps of pressure in networks A, B and C (red dots—water sources).

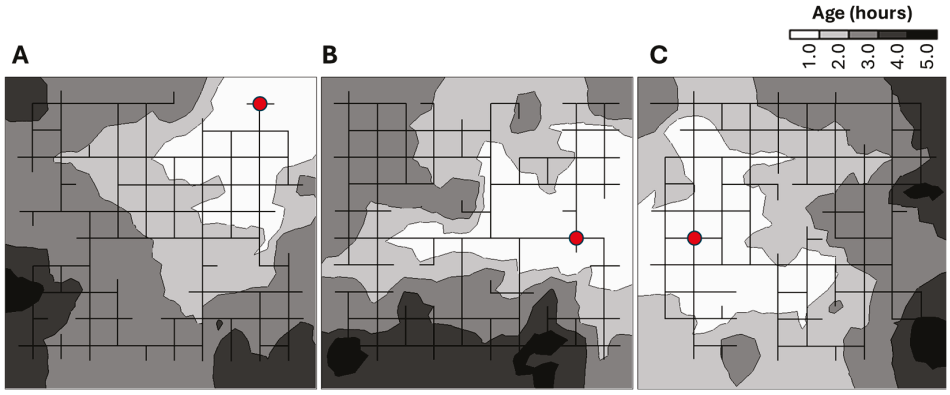

Figure 10. Contour maps of water age in networks A, B and C (red dots—water sources).

3.2. Networks D, E, and F

As the result of applying the SRS method to the model grid, the following networks with a double water source were created:

- Network D: ΣL = 23,400 m, DN80-DN450, 5 iterations, 16 bifurcations, Σα = 1440°,
- Network E: ΣL = 22,500 m, DN80-DN400, 5 iterations, 21 bifurcations, Σα = 720°,
- Network F: ΣL = 22,770 m, DN80-DN400, 5 iterations, 19 bifurcations, Σα = 1170°.

The geometric structures of the designed water supply networks D, E, and F, along with the pipe diameters, are shown in Figure 11.

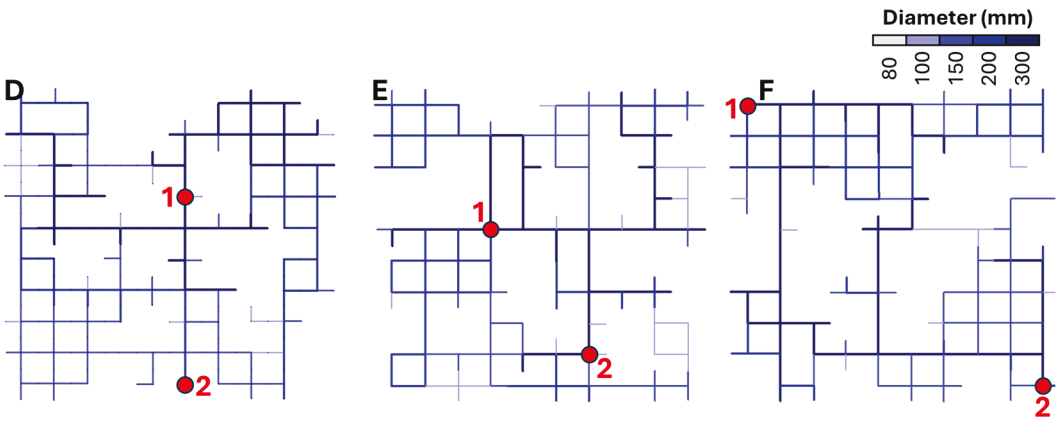

Figure 11. Multi-sourced (red dots 1 and 2) networks D, E and F designed via the SRS method.

Similarly to the case of the networks supplied from one side, networks D–F also cover the entire area of the synthetic settlement. In all three cases, the minimum diameter in the networks is DN80, while the maximum diameter is DN400 or DN450. As in the case of networks supplied from one side, in each of them there are "end branches" of the water pipeline with significant diameters.

When analyzing the distribution of water velocities in networks D, E, and F, it can be observed that the pipes with the lowest flow velocities dominate (0–0.29 m/s). In the case of the D network, they constitute 63.85% of the pipe length of the entire network, in the E network, 58.40%, and in the F network, 68.38%. The average value of water flow velocity in network D was 0.28 m/s, in network E, 0.34 m/s, and in network F, 0.25 m/s (Table 6).

Table 6. Velocities in water pipes in networks D, E, and F.

Velocity	Network D		Network E		Network F	
	Length					
m/s	m	%	m	%	m	%
≥1.5	0	0	0	0	0	0
1.0–1.49	90	0.38	720	3.20	0	0
0.7–0.99	900	3.85	1620	7.20	1080	4.74
0.3–0.69	7470	31.92	7020	31.20	6120	26.88
0.0–0.29	14,940	63.85	13,140	58.40	15,570	68.38
ΣL	23,400	100	22,500	100	22,700	100
Average Velocity (m/s)	0.28		0.34		0.25	

The contour maps of pressure in networks D, E, and F are shown in Figure 12. The maximum pressure can be observed in the E network (46.87 m H_2O), while the lowest average pressure occurs in the D network (40.94 m H_2O). The designed networks are characterized by an overall low water age—a maximum time of approximately 3 h (Figure 13). The total electricity consumption necessary for the operation of the pumps was 138.06 kW in the D network, 153.97 kW in the E network, and 139.30 kW in the F network.

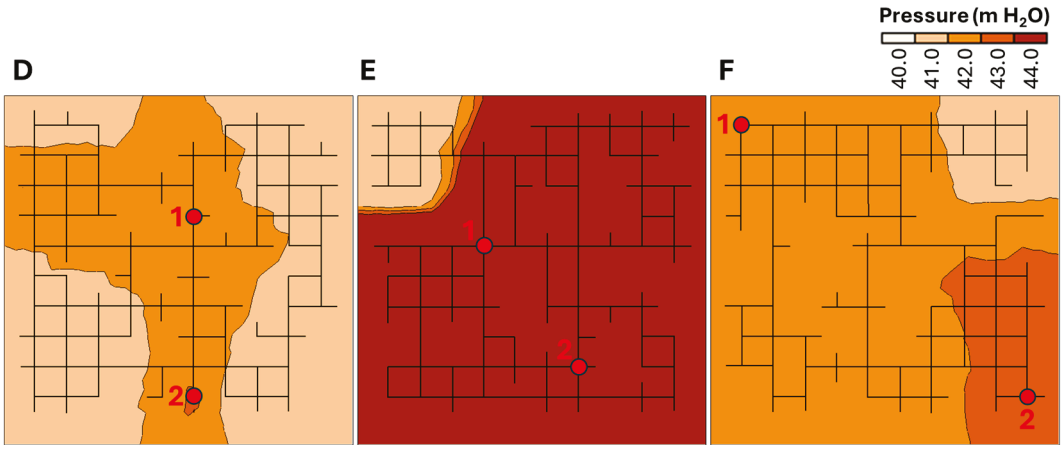

Figure 12. Contour maps of pressure in networks D, E and F (red dots 1 and 2—water sources).

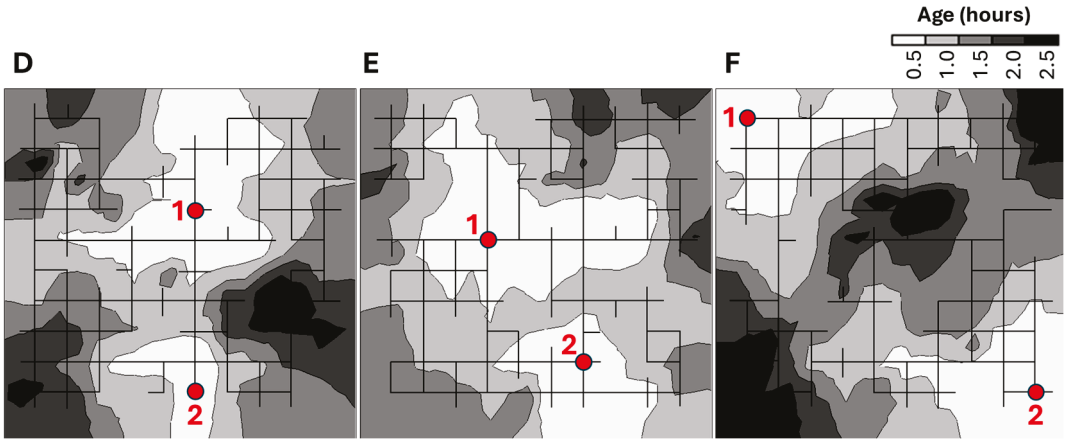

Figure 13. Contour maps of water age in networks D, E and F (red dots 1 and 2—water sources).

3.3. Network G

As the final part of the model studies, the SRS method was applied under the conditions of a top-down assumed water source capacity. In the case of the G network, the capacity of the first water source was 70% of the total demand. Application of the proposed method resulted in the designing of a network ∑L equal to 23,130 m and the diameter range of DN80-DN450. As in the previous cases, the network was routed in five iterations with a total number of bifurcations equal to twenty. The sum of the rotation angles of the base section ∑α in the first two iterations was 1170°. The geometric structure of the G network along with the specification of the selected diameters of water pipes is shown in Figure 14. Red markers, numbered 1 and 2, indicate the location of water sources. The G network covered the entire settlement. As in all previously considered cases, the resulting network includes "end branches" of the network with significant diameters (DN350-DN400).

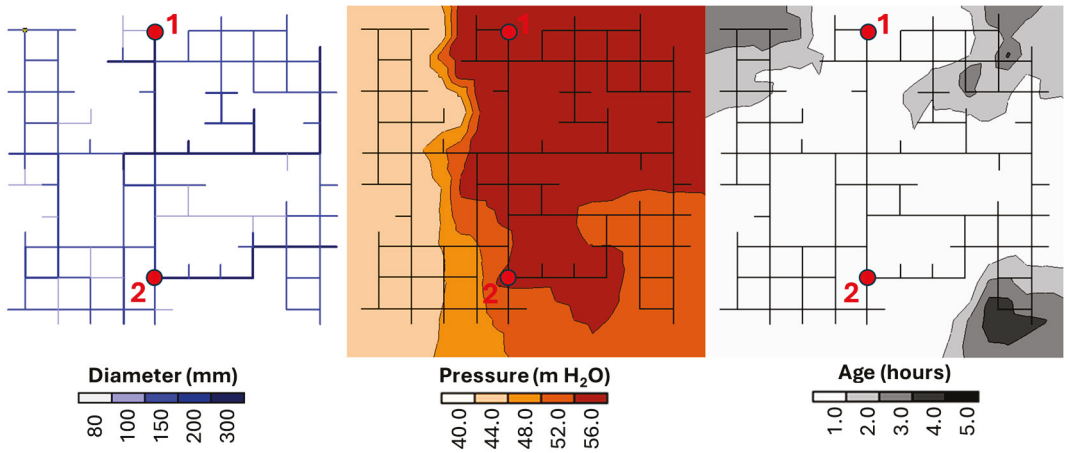

Figure 14. Graphs of multi sourced (red dots 1 and 2) network G designed via the SRS method, together with contour maps of pressure and water age.

Network G is characterized by the share of pipes with the lowest water velocities equal to 46.3%. Additionally, this network includes sections with velocities ranging from 1.0 to 1.49 m/s (8.95% of all), as well as single sections with velocities above 1.5 m/s and even 2 m/s. Velocities above 1 m/s are the consequence of the capacities of the top-down water sources and occur in the pipes located far from the pumping station. The maximum pressure in the network was 55.28 m H_2O, while the average was 49.07 m H_2O.

The maximum water age was 4 h 5 min, with the average equal to 45.6 min. Electricity consumption amounted to a total of 180.05 kW.

4. Discussion

A detailed list of the parameters of A–G networks designed using the SRS method is presented in Table 7. When comparing the networks with a single water source (A, B, and C) with the networks with two water sources (D, E, and F), one can notice an increased value of the total length of water pipes (on average 24,240 m in networks A, B, and C, and 22,890 m in networks D, E, and F—an increase of 5.5%). Double-side supplied networks are additionally characterized by lower sums of rotation angles of the base section, calculated in the first two iterations. In all analyzed cases, the minimum diameter in the networks is DN80, while the maximum diameter is DN350, DN500 and DN600 in networks A, B, and C, respectively, and DN400 and DN450 in networks D, E, and F. In each network, the existence of "branch ends" with significant diameters (DN300–DN400) can be noticed. In all analyzed networks, the fractal dimension is defined as a non-integer number. This confirms that the geometric structures created by the SRS method possess the properties of fractal figures.

Table 7. Characteristics of networks A–G.

Network	No. of Water Sources	ΣL	Σα	D_b	DN	Velocity (Average)	Pressure (Average)	Water Age		Energy
								Max	Average	
		m	°	-	mm	m/s	m H_2O	h:min	min	kW
A	1	23,670	1800	1.109	80–600	0.26	40.94	3:39	70.2	138.33
B	1	23,940	1260	1.108	80–500	0.32	43.54	4:37	67.8	148.51
C	1	25,110	1080	1.162	80–350	0.31	41.62	4:55	54.6	142.88
D	2	23,400	1440	1.105	80–450	0.28	40.94	2:43	57.6	138.06
E	2	22,500	720	1.101	80–400	0.34	45.12	2:43	43.8	153.97
F	2	22,770	1170	1.144	80–400	0.25	41.49	3:16	60.0	139.30
G	2	23,130	1170	1.111	80–450	0.49	49.07	4:05	45.6	180.05

Average flow velocities and pressure heads in the networks did not show significant differences depending on the number of water sources. In networks A, B, and C, the average velocity in the pipes was 0.30 m/s, while in networks D, E, and F it was 0.29 m/s. The average water pressure was 42.03 m H_2O in networks A, B, and C and 42.51 m H_2O in networks D, E, and F. The water age in all analyzed networks was relatively small. Additionally, there was a tendency for the water age to decrease as the number of water sources increases. The maximum water age was 2 h 43 min (network B), up to 4 h 55 min in network C. In networks D, E, and F the average water age was 53.8 min, while in networks A, B, C it was 62.4 min. Regardless of the number of water sources, all networks showed very similar electricity consumption necessary to supply water at the appropriate pressure. There was an average of 143.24 kW in networks A–C and 143.77 kW in D–F.

Compared to the networks in which the source capacities were defined in accordance with the SRS Method (A–F), the G network clearly stands out, in which the source capacity ratio was assigned top-down. Comparing the percentage of pipe length with specific flow velocities, a clear decrease in the share of the pipes with the lowest velocities can be noticed: 46.3% in the G network to an average of 62.95% in the A-F networks. In network G, the highest average water flow velocity can also be observed (0.49 m/s), as well as water flow velocities above 1.5 m/s. Such high velocities under standard flow conditions may

indicate the limited capacity of the selected pipes, as well as high water losses during water flow under fire flow conditions. The pressure amplitude in the G network was over 15 m H_2O. Additionally, in the G network there were nodes with water age more than 4 h. High pressure losses were also confirmed by the high electrical power consumption—the highest value, 180.05 kW, was approx. 25% higher compared to the A-F networks.

5. Conclusions and Future Directions of Research

Considering the results obtained from these model tests, it can be concluded that the main research objectives set in this article have been met. The proposed method of simultaneous routing and sizing allows us to obtain repeatable results with various numbers as well as locations of water sources and recipients. Similar features characterizing the geometric systems were obtained, as well as similar hydraulic parameters of the operation of individual networks. The SRS method is characterized by the following: (1) the method allows for simultaneous routing and sizing processes, (2) the method includes a benchmarking mechanism for classifying demand nodes in terms of water consumption and water supply priority, (3) a new criterion for selecting water path is proposed—the cost of constructing the water pipeline, (4) the selection of pipe diameters is carried out according to the modified Murray's law, (5) the method is applicable to systems with single and multiple water sources, (6) the SRS method enables routing a network in which the capacities of water sources are pre-defined.

However, the developed method has certain limitations, which opens the possibility of further research. The proposed research directions include: testing the method under the conditions of a quasi-real and real settlement, verifying the sizing process by comparison with an existing recognized method (e.g., the genetic algorithm approach), checking the impact of different demand node weights and priorities on the shape of the developed water supply networks, determining other ranking categories, modification of the SRS method so that network ends with significant diameters are not created during the routing process, and development of a computer software for network routing and sizing with the implemented SRS method. To comprehensively assess the potential application of the developed method, a comparison with other design methods is also planned, both traditional (e.g., the Hardy–Cross method) as well as those using advanced heuristic and metaheuristic methods.

Supplementary Materials: The following supporting information can be downloaded at: https://www.mdpi.com/article/10.3390/w17182745/s1, Supplementary Materials contain a detailed presentation of the individual iterations and bifurcations performed during the routing and sizing of A–G networks.

Author Contributions: Conceptualization, P.S. and D.K.; methodology, P.S.; validation, P.S.; formal analysis, P.S.; investigation, P.S. and M.I.; data curation, P.S.; writing—original draft preparation, P.S.; writing—review and editing, P.S., D.K. and M.I.; visualization, P.S.; supervision, D.K.; project administration, P.S.; funding acquisition, P.S., D.K. and M.I. All authors have read and agreed to the published version of the manuscript.

Funding: This research was funded by internal projects of Lublin University of Technology, Poland (numbers FD-20/IS-6/034, FD-20/IS-6/017 and FD-20/IS-6/015).

Data Availability Statement: The original contributions presented in this study are included in the article/Supplementary Materials. Further inquiries can be directed to the corresponding author.

Conflicts of Interest: The authors declare no conflicts of interest.

Abbreviations

The following abbreviations are used in this manuscript:

CNT	Complex network theory
EPS	Extended period simulation
FG	Fractal geometry
GIS	Geographic information system
GT	Graph theory
LCPA	Least cost path algorithm
NPH	NP-hard problem
PLR	Path of least resistance
SRS	Simultaneous routing and sizing method
WDN	Water distribution network

References

1. Mays, L.W. *Water Distribution System Handbook*, 1st ed; McGraw-Hill: New York, NY, USA, 2000.
2. Washington State Department of Health. Water System Design Manual December, DOH Pub 331-123. 2020. Available online: https://doh.wa.gov/sites/default/files/2022-02/331-123.pdf (accessed on 26 April 2025).
3. Grigg, N.S. *Water, Wastewater and Stormwater Infrastructure Management*, 2nd ed; CRC Press Company: Boca Raton, FL, USA, 2012. [CrossRef]
4. Walski, T.M.; Chase, D.V.; Savic, D.A.; Grayman, W.; Beckwith, S.; Koelle, E. *Advanced Water Distribution Modeling and Management*, 1st ed; Haestad Press: Waterbury, CT, USA, 2003.
5. Sitzenfrei, R.; Wang, Q.; Kapelan, Z.; Savić, D. Using Complex Network Analysis for Optimization of Water Distribution Networks. *Water Resour. Res.* **2020**, *56*, e2020WR027929. [CrossRef]
6. Ferrari, G.; Savic, D.; Becciu, G. Graph-Theoretic Approach and Sound Engineering Principles for Design of District Metered Areas. *J. Water Resour. Plan. Manag.* **2014**, *140*, 04014036. [CrossRef]
7. Diao, K.; Butler, D.; Ulanicki, B. Fractality in Water Distribution Networks: Application to Criticality Analysis and Optimal Rehabilitation. *Urban Water J.* **2021**, *18*, 885–895. [CrossRef]
8. Di Nardo, A.; Di Natale, M.; Giudicianni, C.; Greco, R.; Santonastaso, G.F. Complex Network and Fractal Theory for the Assessment of Water Distribution Network Resilience to Pipe Failures. *Water Supply* **2018**, *18*, 767–777. [CrossRef]
9. Vargas, K.; Saldarriaga, J. Analysis of Fractality in Water Distribution Networks Using Hydraulic Criteria. In *World Environmental and Water Resources Congress 2019: Hydraulics, Waterways, and Water Distribution Systems Analysis*; American Society of Civil Engineers: Reston, VA, USA, 2019; pp. 564–572. [CrossRef]
10. Hwang, H.; Lansey, K. Water distribution system classification using system characteristics and graph-theory metrics. *J. Water Resour. Plan. Manag.* **2017**, *143*, 04017071. [CrossRef]
11. Ostfeld, A. Water distribution systems connectivity analysis. *J. Water Resour. Plan. Manag.* **2005**, *131*, 58–66. [CrossRef]
12. Jacobs, P.; Goulter, I.C. Optimization of redundancy in water distribution networks using graph theoretical principles. *Eng. Optim.* **1989**, *15*, 71–82. [CrossRef]
13. Walski, T.M. Water distribution valve topology for reliability analysis. *Reliab. Eng. Syst. Saf.* **1993**, *42*, 21–27. [CrossRef]
14. Yazdani, A.; Jeffrey, P. Water distribution system vulnerability analysis using weighted and directed network models. *Water Resour. Res.* **2012**, *48*, W06517. [CrossRef]
15. Giustolisi, O.; Simone, A.; Ridolfi, L. Network structure classification and features of water distribution systems. *Water Resour. Res.* **2017**, *53*, 3407–3423. [CrossRef]
16. Herrera, M.; Abraham, E.; Stoianov, I. A graph-theoretic framework for assessing the resilience of sectorized water distribution networks. *Water Resour. Manag.* **2016**, *30*, 1685–1699. [CrossRef]
17. Möderl, M.R.; Sitzenfrei, T.F.; Fleischhacker, E.; Rauch, W. Systematic generation of virtual networks for water supply. *Water Resour. Res.* **2011**, *47*, W02502. [CrossRef]
18. Zheng, F.; Simpson, A.R.; Zecchin, A.C.; Deuerlein, J.W. A Graph Decomposition-based Approach for Water Distribution Network Optimization. *Water Resour. Res.* **2013**, *49*, 2093–2109. [CrossRef]
19. Diao, K.; Fu, G.; Farmani, R.; Guidolin, M.; Butler, D. Twin-Hierarchy Decomposition for Optimal Design of Water Distribution Systems. *J. Water Resour. Plan. Manag.* **2016**, *142*, C4015008. [CrossRef]

20. Kowalski, D.; Kowalska, B.; Suchorab, P. A proposal for the application of fractal geometry in describing the geometrical structures of water supply networks. In *Urban Water*; Mambretti, S., Brebbia, C.A., Eds.; WIT Press: London, UK, 2014; pp. 75–90. Available online: https://www.witpress.com/Secure/elibrary/papers/UW14/UW14007FU1.pdf (accessed on 13 May 2025).
21. Beaza, D.; Ihle, C.; Ortiz, J. A comparison between ACO and Dijkstra algorithms for optimal ore concentrate pipeline routing. *J. Clean. Prod.* **2017**, *144*, 149–160. [CrossRef]
22. Costa, L.H.M.; Rodrigues, G.P.W. Automatic Generation of Water Distribution Networks from Streets Layout. *Water Resour. Manag.* **2021**, *35*, 1299–1319. [CrossRef]
23. Frota, A.F.; Costa, L.H.M.; de Abreu Costa, J.N.; Castro, M.A.H. Automatic Generation of Water Distribution Networks Using Central Street Lines. *Water Resour. Manag.* **2024**, *38*, 1225–1240. [CrossRef]
24. Razei, G.; Afshar, M.H.; Rohani, M. Layout optimization of looped networks by constrained ant colony optimization algorithm. *Adv. Eng. Softw.* **2014**, *70*, 123–133. [CrossRef]
25. Gupta, I.; Bassin, J.K.; Gupta, A.; Khanna, P. Optimization of water distribution system. *Environ. Softw.* **1993**, *8*, 101–113. [CrossRef]
26. Bragalli, C.; D'Ambrosio, C.; Lee, J.; Lodi, A.; Toth, P. An MINLP Solution Method for a Water Network Problem. In *Algorithms–ESA 2006 (ESA 2006)*; Azar, Y., Erlebach, T., Eds.; Lecture Notes in Computer Science; Springer: Berlin, Heidelberg, Germany, 2006; Volume 4168. [CrossRef]
27. Reca, J.; Martinez, J. Genetic algorithms for the design of looped irrigation water distribution networks. *Water Resour. Res.* **2006**, *42*, W05416. [CrossRef]
28. Alperovits, E.; Shamir, U. Design of Optimal Water Distribution Systems. *Water Resour. Res.* **1977**, *13*, 885–900. [CrossRef]
29. Fujiwara, O.; Jenchaimahakoon, B.; Edrisinghe, N.C.P. A modified linear programming gradient method for optimal design of looped water distribution networks. *Water Resour. Res.* **1987**, *23*, 977–982. [CrossRef]
30. Uma, R. Optimal Design of Water Distribution Network Using Differential Evolution. *Int. J. Sci. Res.* **2016**, *5*, 1515–1520. Available online: https://www.ijsr.net/archive/v5i11/ART20163145.pdf (accessed on 25 April 2025).
31. Gakpo, E.; Tsephe, J.; Nwonwu, F.; Viljoen, M. Application of stochastic dynamic programming (SDP) for the optimal allocation of irrigation water under capacity sharing arrangements. *Agrekon* **2005**, *44*, 436–451. [CrossRef]
32. Land, A.H.; Doig, A.G. An automatic method of solving discrete programming problems. *Econometrica* **1960**, *28*, 497–520. [CrossRef]
33. Sherali, H.D.; Smith, E.P. A global optimization approach to a water distribution network design problem. *J. Glob. Optim.* **1997**, *11*, 107–132. [CrossRef]
34. Kirkpatrick, S.; Gelatt, C.D.; Vecchi, M.P. Optimization by simulated annealing. *Science* **1983**, *220*, 671–680. [CrossRef] [PubMed]
35. Cisty, M. Hybrid Genetic Algorithm and Linear Programming Method for Least-Cost Design of Water Distribution Systems. *Water Resour. Manag.* **2010**, *24*, 1–24. [CrossRef]
36. Geem, Z.W.; Kim, J.H.; Loganathan, G.V. A new heuristic optimization algorithm: Harmony search. *Simulation* **2001**, *76*, 60–68. [CrossRef]
37. Fanni, A.; Liberatore, S.; Sechi, G.M.; Soro, M.; Zuddas, P. Optimization of water distribution systems by a Tabu Search metaheuristic. In *Computing Tools for Modeling, Optimization and Simulation*; Laguna, M., Velarde, J.L.G., Eds.; Operations Research/Computer Science Interfaces Series; Springer: Boston, MA, USA, 2000; Volume 12, pp. 279–298. [CrossRef]
38. Simpson, A.R.; Maier, H.R.; Foong, W.K.; Phang, K.Y.; Seah, H.Y.; Tan, C.L. Selection of parameters for ant colony optimization applied to the optimal design of water distribution systems. In Proceedings of the International Congress on Modelling and Simulation, Modelling and Simulation Society of Australia, Canberra, Australia, 10–13 December 2001.
39. Montalvo, I.; Izaquierdo, J.; Perez, R.; Tung, M.M. Particle Swarm Optimization applied to the design of water supply systems. *Comput. Math. Appl.* **2008**, *56*, 769–776. [CrossRef]
40. Abdel-Gawad, H. Modified Jaya Algorithm for Optimal Design of Water Distribution Network. *Mansoura Eng. J.* **2021**, *46*, 41–57. [CrossRef]
41. Djebedjian, B.; Abdel-Gawad, H.A.A.; Ezzeldin, R.M. Global performance of metaheuristic optimization tools for water distribution networks. *Ain Shams Eng. J.* **2021**, *12*, 223–239. [CrossRef]
42. Najarzadegan, M.R.; Moeini, R. Optimal Design of Water Distribution Network Using Improved Artificial Bee Colony Algorithm. *Iran. J. Sci. Technol. Trans. Civ. Eng.* **2023**, *47*, 3123–3136. [CrossRef]
43. Salto, C.; Minetti, G.; Alfonso, H.; Zurita, E.; Hernandez, J.; Carnero, M. Optimal Design of Water Distribution Network Using Two Different Metaheuristics. *Chem. Eng. Trans.* **2023**, *100*, 691–696. [CrossRef]
44. Sirsant, S.; Reddy, M.J. Improved MOSADE Algorithm Incorporating Sobol Sequences for Multi-Objective Design of Water Distribution Networks. *Appl. Soft Comput.* **2022**, *120*, 108682. [CrossRef]

45. Hajibabaei, M.; Hesarkazzazi, S.; Minaei, A.; Savić, D.; Sitzenfrei, R. Pareto-optimal design of water distribution networks: An improved graph theory-based approach. *J. Hydroinformatics* **2023**, *25*, 1909–1926. [CrossRef]
46. Ramani, K.; Rudraswamy, G.K.; Umamahesh, N.V. Optimal Design of Intermittent Water Distribution Network Considering Network Resilience and Equity in Water Supply. *Water* **2023**, *15*, 3265. [CrossRef]
47. Riyahi, M.M.; Bakhshipour, A.E.; Haghighi, A. Probabilistic warm solutions-based multi-objective optimization algorithm, application in optimal design of water distribution networks. *Sustain. Cities Soc.* **2023**, *91*, 104424. [CrossRef]
48. Shmaya, T.; Ostfeld, A. Conjunctive optimal design of water and power networks. *J. Hydrol.* **2024**, *643*, 131932. [CrossRef]
49. Bahrami Chegeni, I.; Riyahi, M.M.; Bakhshipour, A.E.; Azizipour, M.; Haghighi, A. Developing Machine Learning Models for Optimal Design of Water Distribution Networks Using Graph Theory-Based Features. *Water* **2025**, *17*, 1654. [CrossRef]
50. Suchorab, P. Metoda Jednoczesnego Trasowania i Wymiarowania Wodociągowych Struktur Sieciowych (The Method of Simultaneous Routing and Sizing of Water Supply Network's Structures). Ph.D. Thesis, Lublin University of Technology, Lublin, Poland, 2023. Available online: https://rock.pollub.pl/entities/publication/42fe04ac-2b09-43b8-88d8-9421fd4d5338 (accessed on 22 April 2025). (In Polish).
51. Perttunen, J.; Sievanen, R. Incorporating Lindenmayer systems for architectural development in a functional-structural tree model. *Ecol. Model.* **2005**, *181*, 479–491. [CrossRef]
52. Strahler, A.N. Quantitative analysis of watershed geomorphology. *Trans. Am. Geophys. Union* **1957**, *8*, 913–920. [CrossRef]
53. Ubertosi, F.; Delay, F.; Bodin, J.; Porel, G. A new method for generating a pipe network to handle channelled flow in fractured rocks. *Comptes Rendus. Géosci.* **2007**, *339*, 682–691. [CrossRef]
54. Gabryś, E.; Rybaczek, M.; Kędzia, A. Blood flow simulation through fractal models of circulatory system. *Chaos Solitons Fractals* **2006**, *27*, 1–7. [CrossRef]
55. Mandelbrot, B.B. Stochastic models for the earth's relief, the shape and fractal dimension of coastlines, and the number area rule for islands. *Proc. Natl. Acad. Sci. USA* **1975**, *72*, 2825–2828. [CrossRef]
56. Falconer, K. *Fractal Geometry: Mathematical Foundations and Applications*, 3rd ed.; John Wiley & Sons: Chichester, UK, 2014.
57. Gómez, S.; Salcedo, C.; González, L.; Saldarriaga, J. Fractal Dimension as a Criterion for the Optimal Design and Operation of Water Distribution Systems. *Water* **2025**, *17*, 1318. [CrossRef]
58. Murray, C.D. The physiological principle of minimum work: I. The vascular system and the cost of blood volume. *Proc. Natl. Acad. Sci. USA* **1926**, *12*, 207–214. [CrossRef]
59. Murray, C.D. The physiological principle of minimum work applied to the angle of branching of arteries. *J. Gen. Physiol.* **1926**, *9*, 835–841. [CrossRef]
60. Suchorab, P.; Kowalski, D. Classification of the nodal demands in 3 case study water supply networks. In Proceedings of the Water-Excellent Science and Industrial Development 3'rd Polish YWP Conference, Poznań, Poland, 15–17 November 2023; Available online: https://chmura.put.poznan.pl/s/6PkCVry4P6B8gGb (accessed on 25 April 2025).
61. Fractalyse 3.0, Gilles Vuidel at Th'eMA Laboratory (CNRS–University of FrancheComt'e, Besançon, France). Available online: https://thema.univ-fcomte.fr/productions/software/fractalyse/ (accessed on 17 January 2022).
62. Rossman, L.; Woo, H.; Tryby, M.; Shang, F.; Janke, R.; Haxton, T. *EPANET 2.2 User Manual*; EPA/600/R-20/133; U.S. Environmental Protection Agency: Washington, DC, USA, 2020. Available online: www.epa.gov/water-research/epanet (accessed on 14 March 2022).

Disclaimer/Publisher's Note: The statements, opinions and data contained in all publications are solely those of the individual author(s) and contributor(s) and not of MDPI and/or the editor(s). MDPI and/or the editor(s) disclaim responsibility for any injury to people or property resulting from any ideas, methods, instructions or products referred to in the content.

water

MDPI

Article

Water Networks Management: Assessment of Heuristic and Exact Approaches for Optimal Valve Location and Operation Settings Schedule

Maria Cunha [1,*], João Marques [1] and Enrico Creaco [2]

[1] Department of Civil Engineering, CEMMPRE, University of Coimbra, 3030-788 Coimbra, Portugal; jmarques@dec.uc.pt
[2] Dipartimento di Ingegneria Civile e Architettura, Università degli Studi di Pavia, 27100 Pavia, Italy; enrico.creaco@unipv.it
* Correspondence: mccunha@dec.uc.pt

Abstract: This paper deals with the optimal design-for-control of water distribution networks (WDNs) with the objectives of minimizing pressure-induced background leakage and maximizing resilience. This problem entails defining locations for installing valves and/or pipes and for simultaneously determining valve settings and belongs to the class of non-convex mixed-integer nonlinear problems. Solving highly complex infrastructure problems, such as WDNs, raises a fundamental question about the accuracy of the solutions to be implemented for sound water management. Therefore, two kinds of optimization methods are applied and assessed on two case studies. While the first is an exact global optimization method, the second is the metaheuristic based on the concept of simulated annealing. This paper proposes an innovative methodological analysis to interpret and discuss the results provided by both methods, as well as to identify their impact on the performance of the WDN. This type of analysis may help in highlight how the integration of the best features of both solution methods can promote a step forward in solving WDN problems.

Keywords: water distribution networks (WDNs); design; pressure control; leakage; deterministic global optimization; meta heuristic optimization

1. Introduction

Water distribution networks (WDNs) are a critical infrastructure for the wellbeing of societies. Therefore, it is very important to accurately design and operate them. The optimization of WDNs has been extensively studied in the water engineering area in recent decades [1]. WDN design was formulated as a single-objective optimization problem, with cost minimization as the objective function to determine the diameters to be assigned to each pipe. In early attempts, many simplifications were used, such as considering the diameters as continuous variables or linearizing objective functions and constraints (see reviews by [2–4] for early approaches to solving water distribution systems optimization problems). The limitations of these approaches led to the use of heuristic methods in the 1990s by several authors [4–7]. Pipe diameters began to be selected from the set of commercial sizes available for networks with a known topology, and suitable formulations of physical laws governing flow and pressure issues began to be applied. Subsequently, the need for considering other types of objectives (mainly related to network performance) gave rise to multi-objective

formulations. The multi-objective design of WDNs is a highly complex optimization problem. It is a non-convex mixed integer nonlinear problem (with nonlinear objective functions and constraints) including discrete decision variables and a large solution space of admissible solutions, even for small WDN case studies [8]. Metaheuristic methods have been proposed to solve these problems in several previous studies, including the following: Non-dominated Sorting Genetic Algorithm II (NSGAII) by [9–11]; ParEGO and LEMMO hybrid algorithms by [12]; five different evolutionary algorithms (AMALGAM, Borg, ε-NSGA-II, ε-MOEA and NSGA-II) by [13]; the Self-Adaptive Multi-Objective Harmony Search by [14]; the Multi-objective Simulated Annealing by [15], enhanced in [16] with new Generation and Reannealing procedures (MOSA-GR); the Multi-objective Particle Swarm Optimization (MOPSO) by [17]; and the Multi-Objective Self Adaptive Differential Evolution (S-MOSADE) by [8]. These are just a few salient methods, and many others can be found in the literature of WDN multi-objective design (including many objective formulations). Most of the references cited above involve solving a bi-objective problem to minimize cost and maximize resilience, as it will happen in this paper (recent examples are [1,18,19]).

In recent years, exact global optimization methods [20,21] have been proposed to deal with problems in water network management, particularly for leakage control. Some criticisms of the implications of using metaheuristics are part of the reasons for moving on to such applications. Besides being considered very time-consuming, according to [22], heuristic methods such as evolutionary algorithms can be implemented to solve multi-objective problems, though they show some disadvantages: they do not guarantee the optimality of solutions, not even local optimality, and they neither explicitly nor accurately handle nonlinear constraints. More recently, simulated annealing (SA) was also added to the methods that present disadvantages [23]. According to [23], heuristics do not deal with optimal pressure control, and the computation time increases drastically with WDN size. These concerns are explicit in relation to the design-for-control of WDNs. Thus, an exact optimization method is specifically proposed, mainly to resolve the problem of optimal valve placement and operation. The multi-objective problem solved by [22] aims to minimize average zone pressure (AZP), a concept proposed by [24], and pressure variability index. Ulusoy et al. [23] presents a bi-objective global optimization approach to resolve the problem of design-for-control of WDNs (to minimize pressure-induced background leakage, also represented by the average zone pressure, and to maximize the resilience), noting that this is a non-convex bi-objective mixed-integer nonlinear problem (BOMINLP). A spatial branch-and-bound (sBB) algorithm, specially tailored to solve this model, as well as a scalarization technique to implement the ε-constraint method, was proposed. They have developed a novel approach that outperforms other existing well-known mathematical programming algorithms from the literature (see details in [23]). There is much controversy and competition over the use of exact optimization methods and metaheuristics. This has raised a crucial discussion in the engineering field, namely, the meaning of the solutions obtained by various optimization methods—mathematical optimum versus engineering optimum. This is part of a long story that started many years ago when the first attempts were made to find the best decisions for water resources and water infrastructure decision problems through operations research methods. Still today, the question of how accurately real-world problems are represented, including all physical, technological, environmental, and economic aspects that characterize their essence, is of fundamental importance when it comes to engineering problems.

In this paper, the authors aim to participate in the scientific debate about this topic while developing knowledge about the optimized design-for-control of water distribution

networks problem. This problem entails defining locations for the installation of valves and/or pipes and simultaneously determining valve operating settings in existing networks that optimize two conflicting objectives—the minimization of pressure-induced background leakage and the maximization of network resilience [23]. It is recognized nowadays as a fundamental problem because utilities must both cope with the management of water losses and prevent the disruption of WDN services [25]. The success of controlling WDN water leakages is an important issue contributing to a more sustainable management of natural resources that impacts on economics and society.

While two kinds of optimization approaches are present in the scientific literature, e.g., metaheuristic and exact approaches, very few papers have so far been dedicated to their comparison and to the identification of pros and cons of either approach in the context of design-for-control of WDNs. To bridge this research gap, a metaheuristic based on the concept of simulated annealing [16] is applied in the present paper to the problems resolved in [23] by means of a deterministic global optimization algorithm. This is instrumental to apply the innovative methodological analysis developed in this paper that will serve to dissect the solutions obtained by both methods in the light of their mathematical structure. Linking these mathematical characteristics to the results in terms of hydraulic functioning of the networks is also a fundamental step in this paper and will allow for an in-depth interpretation of any cross-effects, thus contributing to the flow of knowledge in WDNs. Furthermore, a comprehensive understanding of the underlying mechanics of these methods can promote more promising research directions for accurately solving real-world problems.

This paper is organized as follows. In the Section 2, the problem in question is analyzed, and additional details about the main motivation for this paper are provided. The Section 3, on materials and methods, presents the instrumental part of the methodology developed for the analysis (models and methods are introduced and commented on), as well as some important theoretical concepts to characterize the resolution approaches. Case studies are also described in this section. Then, Section 4 contains a detailed comparison of the solutions provided by the sBB algorithm presented in [23] and the metaheuristic approach based on the concept of simulated annealing, emphasizing the hydraulic impact of their use in terms of pressure and resilience management. This is followed by the Section 5, where the results are thoroughly discussed, further developing on the methodological concepts already introduced in the Section 3. The main takeaways from this work are summarized in the conclusions, highlighting how the integration of the best features of each approach can contribute to promoting a step forward in resolving WDN problems.

2. The Design-for-Control Problem

The subdivision of a WDN into sectors or district metered areas (DMAs) is common practice for pressure control and leakage reduction [24]. DMAs began to be implemented in the nineteen-eighties by water utilities around the world. Lambert [26] argues that high nodal pressure needs to be controlled to reduce water loss through leaks and to reduce burst pipes. Daily pressure control can prevent these problems. To minimize pressure, some utilities have subdivided the WDNs into small DMAs for pressure control and demand metering. The divisions are made by closing boundary valves to form network sections supplied from a single point for flow measurement and downstream pressure control. DMAs have been studied from different perspectives, for example, Ref. [27] to partition real Mexican WDNs; Ref. [28] to detect and remove leakages; Ref. [29] to simultaneously optimize leakage reduction and WDN partitioning; Ref. [30] to quantify leak volumes; Ref. [31] to transform intermittent water supply into a constant supply WDNs; and Ref. [32] for water quality control.

Wright et al. [33] and Wright et al. [34] made progress in this area by proposing DMAs with a dynamic topology. Wright et al. [34] argue that segregating DMAs is very useful for reducing and locating leakages, but it also has a severe impact on reducing the network resilience. The proposed dynamic DMAs combine the benefits of static DMAs for leakage reduction with improvements in the resilience of WDNs. This is achieved by sectoring the network at night (low volume demand conditions) to reduce pressure and decrease leakage, and during the day, some of the DMAs are aggregated to respond to extra demand conditions, which improves the WDN's resilience by supplying water to consumers at the appropriate pressure. This can be performed in practice by remotely controlling flow and pressure via pressure control valves.

Giudicianni et al. [35] also prefer dynamic DMAs to respond to disruption scenarios such as burst pipes, sudden changes in water demand, or changes in network topology. Another problem is related to water age issues; these can arise in low consumption areas with water stagnation if traditional DMA segregation is used. These problems can be prevented by using dynamic DMAs, where previous small-sized DMAs are aggregated into larger sets.

The single objective problem of optimizing WDN control by pressure control valves to minimize the AZP was solved by [24] with a method based on sequential convex programming. Pecci et al. [36] take it a step further when solving DMA design and operation problems by optimal placement and operation of pressure control valves with the objective of minimizing AZP. For this, they propose a penalty and relaxation method to solve a problem combining binary variables for valve placement with continuous variables for valve control (representing operational settings that define the outlet pressure in valves). The minimization of the average zone pressure (AZP) objective was recently considered by Refs. [37,38] in a single objective problem of minimizing AZP for localizing and operating pressure-reducing valves and chlorine booster stations in WDNs. Heuristic methods have instead been used for valve placement and control by [39], with a multi-objective genetic algorithm designed to minimize the number of valves and reduce the total leakage. Creaco and Pezzinga [40,41] embedded mathematical programming for valve control into genetic algorithm-based optimization aimed at the optimal location of control valves. Furthermore, Ref. [42] also used such methods with a sequential addition algorithm and NSGA-II for maximizing the equity and the impact on the supply at each node of the network.

Recently, the bi-objective problem of controlling water losses by minimizing the pressure-induced background leakage, addressed by [23], has created a new area of research by developing an innovative global optimization tailored method to approximate the Pareto front. Decreasing the background leakage in WDNs is associated with reducing average zone pressure (AZP). A conflicting objective is to maximize the resilience of the network, given by the index proposed by [43]. This index increases with rising nodal pressure. This resilience index has often been used as a measure of reliability in the literature on the optimization of WDNs [1].

It is clear that the literature still lacks the application of metaheuristics methods to solve a multi-objective problem like the one proposed by [23] with AZP and resilience as objectives. As previous comparisons of metaheuristic algorithms and mathematical programming suggested that none of the methods should be discarded, the results obtained by the use of a metaheuristic will allow comparisons to be promoted with regard to the results from [23]. Therefore, the Multi-objective Simulated Annealing with new Generation and Reannealing procedures (MOSA-GR) algorithm proposed by [16] will be updated to deal with the innovative sequence of intertwined calculations developed in this paper to simultaneously address the choice of locations for installing new valves and the definition of their control settings, as well as the locations of new pipes and their sizes. As mentioned above, MOSA-GR will play an instrumental role in performing calculations and determining solutions to the problem at hand. This is fundamental

for the implementation of the new methodological approach developed to evaluate the results of the sBB method and of the metaheuristic method.

3. Materials and Methods

3.1. Multi-Objective Model

The problem of the optimal design-for-control takes into account two objectives: one is to minimize the average zone pressure (AZP) as a surrogate measure of pressure-induced background leakage, and the other is to maximize the resilience index (Ir), a surrogate measure for resilience, to maintain proper conditions for delivering customer demand [23]. The average zone pressure [24] minimization is computed by Equations (1)–(3) and the resilience index proposed by Todini [43] is formulated in Equation (4).

$$\text{minAZP} = \frac{1}{W}\sum_{j=1}^{NN} w_j\left(H_j - E_j\right) \tag{1}$$

$$w_j = \sum_{m=1}^{NPI_j} \frac{L_m}{2} \tag{2}$$

$$W = \sum_{j=1}^{NN} w_j \tag{3}$$

$$\max Ir = \frac{\sum_{j=1}^{NN} QC_j\left(H_j - Hmin_j\right)}{\sum_{r=1}^{NR} Q_r H_r - \sum_{j=0}^{NN} QC_j Hmin_j} \tag{4}$$

where AZP—average zone pressure; W—AZP Normalization factor; NN—number of nodes; w_j—weight of node j; H_j—head of node j; E_j—elevation of node j; NPI_j—number of pipes incident to node j; L_m—length of pipe m; Ir—resilience index; QC_j—demand at node j; $Hmin_j$—minimum head at node j; NR—number of reservoirs; Q_r—discharge from reservoir r; Hr—head at reservoir r.

The aim is to simultaneously optimize the design and operating conditions of a WDN by minimizing the AZP and maximizing the resilience index. The AZP is a weighted sum of nodal pressure, with the node weights defined according to the length of pipes connected to each node, and it is used in [23]. AZP reduction is achieved by decreasing network pressure, and these low-pressure values help reduce pipe damage and leaks [44]. The resilience index is an indirect measure of reliability expressing the surplus of power delivered to WDN nodes, compared to the minimum power surplus meeting users' satisfaction. As the pursued increase in resilience is achieved by increasing service pressure, which is, however, accompanied by the undesirable growth of leakage, the two objectives are clearly conflicting. However, this surplus of pressure can be used in critical operational scenarios such as those related to segment isolations or hydrant activations.

Conversely, the minimization of AZP and leakage causes service pressure reduction and, therefore, the lowering of Ir. Optimization runs aimed at simultaneously maximizing Ir and minimizing AZP will yield Pareto fronts of optimal solutions in the trade-off between these two objectives. In this context, it must be stressed that the use of Equation (4) is motivated by the need to obtain results that can be compared with those of [23]. In fact, as the original resilience in Equation (4) was proposed by [43] for WDNs with demand-driven nodal outflows, with no account of leakage and pressure-driven outflow to users, a generalized resilience failure index was later proposed by [11] to overcome this assumption. This aspect will be analyzed in more detail later.

The optimization model includes sets of constraints (1) to ensure the satisfaction of energy and mass conservation laws for pipe flows and associated head losses'; (2) to ensure minimum and maximum values for node heads and pipe flow rates; (3) to limit the diameters to be chosen from a set of commercially available ones when there is an option to include new pipes; (4) to embody binary variables to model the status of candidate valves and links or to prevent the installation of specific combinations of valves and links (see [23]) for details of the formulation of all the constraints.

3.2. Multi-Objective Optimization Approaches

3.2.1. Multi-Objective Simulated Annealing Algorithm

In this paper, the multi-objective simulated annealing with new generation and reannealing procedures, MOSA-GR, developed in [16] is instrumental to solve the bi-objective optimization problem presented above, to produce results to be compared with those of [23]. It is based on the concept of simulated annealing, which was first introduced by [45] and later widely applied to solve single-objective optimization problems. MOSA-GR has been used in the area of WDNs, and in [16] it is compared to other metaheuristics. It was able to handle very difficult problems and find good quality solutions in reasonable computational time, outperforming a large spectrum of metaheuristics and procedures commented on [13]. Additional features were added to MOSA-GR in this paper to deal with design-for-control problems. The various steps followed by the innovative sequence of intertwined calculations developed in this paper to simultaneously embrace the specific choice of locations for installing new valves, new pipes, and their sizing, and the definition of valve control settings are presented in the pseudocode inserted further (pseudocode). After performing an initial group of iterations to generate new solutions based on the classic procedure for SA, the new MOSA-GR procedure to generate candidate solutions (possible valve locations or new pipes or possible settings proposed to be evaluated throughout the iterative optimization procedure) is applied. It explores the neighborhood of other solutions chosen from different areas of the Pareto front (extreme solutions, uncrowded areas, mean value solutions of both objectives, and knee area solutions), as explained in [16]. The generation procedures are cast into the upper red rectangle indicated for the generation of new solutions of the general simulated annealing flowchart of Figure 1. The pseudocode below is used for each specific generation of a candidate solution based on a current solution of the front. Therefore, an inner loop to define the settings of pressure reduction valves (PRVs) and status (open/closed) of boundary valves (BVs) is embedded into an outer loop for the intertwined design (for sizing new pipes and defining the insertion of PRVs and BVs among their possible locations).

Each time a solution is generated, the algorithm calls upon a hydraulic simulator to verify the constraints (orange rectangle on the right in the flowchart in Figure 1). When the stopping criteria are met, a reannealing procedure (lower red rectangle of the flowchart) is accomplished using a local search procedure (see [16]).

3.2.2. Characterization of the Bi-Objective Global Optimization Approach

An overview of the spatial branch-and-bound algorithm, sBB, is briefly described below (see [23] for details) so that its results can be interpreted and compared with those obtained by MOSA-GR. Ulusoy et al. [23] develop a novel tailored method to approximate the Pareto front, i.e., (using quotation marks) "a set of potentially non-dominated solutions as well as global non-dominance bounds, in the form of a superset of the Pareto front". The "potentially non-dominated solutions with global non-dominance bounds" are determined following an iterative procedure that implements the sBB algorithm. After applying a scalarization method

to define a sequence of single-objective mixed-integer nonlinear problems (MINLP) based on an ε-constraint method [46], sBB is applied to compute upper and lower bounds on the optimal values of the MINLP sequence of parametrized single-objective problems. A quadratic version of the Hazen–Williams equation is proposed to evaluate the friction head losses associated with pipe flows [47]. Lower bounds are determined using a mixed-integer linear approach (MILP) after performing a linear outer approximation to relax the non-convex head loss equality constraints (limitations on the application of this method in such circumstances are mentioned in [48]). A polyhedral envelope method is implemented for this purpose. A linear reformulation of the resilience index is also executed. Upper bounds correspond to "locally optimal solutions" determined by the sBB after fixing the values of the binary variables "corresponding to the lower bounding MILP relaxations". This will allow the use of an NLP solver to conclude the calculations. The iterative process continues until "the relative optimality gap between upper bound and lower bound is smaller than a specified tolerance". After showing how to combine the results obtained by implementing this procedure and using the Pareto filter algorithm to eliminate the dominated solutions, Ref. [23] define a "tighter superset of the Pareto front" of BOMINLP. This is a novel approach that outperforms other existing well-known mathematical optimization algorithms from the literature, such as SCIP and BARON (see details in [23]).

3.2.3. Synthesis of Solving Approaches

The main limitations specified in [22,23,49] with regard to heuristic methods should be put in the context of the main concerns about finding the best options for solving engineering problems. Real-world engineering problems are complex and challenging operations research problems; they are often nonlinear and include discrete variables [50]. In fact, these are Non-deterministic Polynomial time hard problems with difficult resolution, since algorithms that solve them in polynomial time are not available when large instances of such problems are at stake [51].

The literature shows that after spending a long time on various efforts to solve mixed integer nonlinear engineering problems and understanding the main difficulties that persist in this endeavor, new methods emerged, these being the so-called heuristic and metaheuristic methods. Firstly, they were tailored to tackle specific problems, and later, the so-called "modern heuristics" [52] made an attempt to create general heuristic methods.

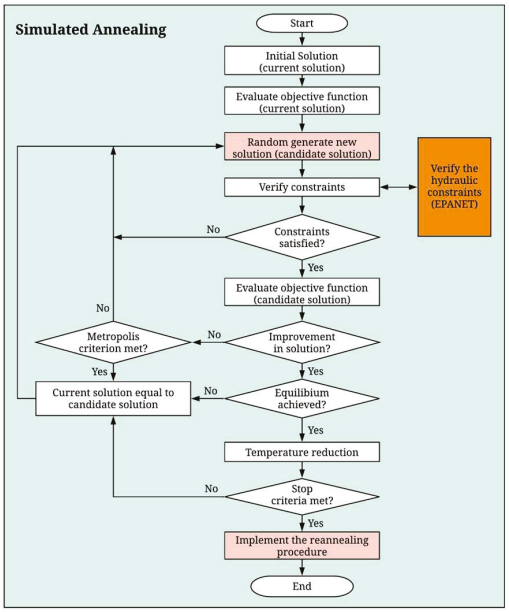

Figure 1. Simulated annealing flowchart.

Pseudocode: Generation process of new candidate solutions

Input: current solution, counter of inner loop generations
IF counter = number inner loop generations **THEN**
    Generation of candidate solutions by a design change (Outer loop)
        Choose *at random a network link. The link may correspond to a location for a new pipe installation or the location of valve links such as BVs or PRVs*
        IF *link = new pipe location* ***THEN***
            Generate candidate solution by altering the diameter of the new pipe
        ELSE IF *link = BV location* ***THEN***
        Generate candidate solution by altering the status of the valve (BV):
            IF *valve status = Open* ***THEN***
                Close valve
            ELSE
                Open valve
            END IF
        ELSE IF *link = valve PRV* ***THEN***
        Generate candidate solution by altering the status of the valve (PRV):
            IF *valve status = Active* ***THEN***
                Open valve
            ELSE
                Active valve
            END IF
        END IF
        counter = 0
ELSE
    Generation of candidate solutions by an operation change (inner loop)
        Generate candidate solution by altering the valve settings of BVs or PRVs:
        Choose *at random an active BV or PRV*
        Choose *at random an hour from the operation set*
        Change *the value of the valve setting between maximum and minimum allowed values*
        IF *Setting = Max* ***THEN***
            Decrease *valve setting*
        ELSE IF*Setting = Min* ***THEN***
            Increase *valve setting*
        ELSE
            Randomly *increase or decrease the valve setting*
        END IF
        counter = counter + 1
END IF
Output: *candidate* solution

The accuracy of the representation of the real-world problem, in terms of incorporating all the crucial aspects to fully characterize the essence of the problem analyzed, is an issue when dealing with engineering problems. This is a complex but worthwhile task, as its potential accomplishment will provide decision makers with powerful tools to be used in real-world engineering problems. A great deal of work has been developed on this topic, and the literature presents systematized ways to categorize types of models by taking into account the level of accuracy accomplished in the representation of a problem [53].

In Table 1, the main characteristics of the metaheuristic algorithm (MOSA-GR) used in this paper are outlined with the sBB approach of [23], in terms of resolution method characteristics and how objective functions and constraints are handled.

Table 1. Characteristics of the approach used by MOSA-GR in this paper and the approach proposed in [23].

	MOSA-GR	**Mathematical Optimization (sBB)**
Resolution Method	Metaheuristic based on simulated annealing concept, including innovative forms for generation of solutions and intertwined calculations of design and operation of the hydraulic infrastructure.	Application of a scalarization method (e-constraints method), together with global optimization methods, to approximate the Pareto front. Use of a spatial branch-and-bound algorithm to compute upper and lower bounds on the optimal values of the resulting sequence of parametrized single-objective problems in an iterative fashion till stopping criteria are met. Then a Pareto filter algorithm is used to define a "tighter superset of the Pareto front".
Objective functions	The resolution method is applied to both objective functions as they are presented in the bi-objective optimization model.	Non-linear resilience objective function is linearized
Constraints	The original constraints included in the bi-objective model are assessed in each iteration of the metaheuristic. No simplification or relaxation is used.	(1) The head losses equation is replaced by its quadratic version. (2) Lower bounds are determined using a MILP formulation, after relaxing the non-convex head-loss equality constraints through a linear outer approximation, by means of a polyhedral envelope method. (3) Upper bounds are obtained by an NLP solver after fixing the values of the binary variables according to the results of the MILP formulation.
Stopping criteria	Stopping criteria is based on the evaluation of the quality of the solution found so far. It is based on the number of temperature reductions that are made without the optimum value of current configuration showing any improvement. The temperature parameter is used to control the optimization process by accepting a large number of worse candidate solutions at the beginning of the optimization process and a small number at the end of the process. Furthermore, the minimum value that can be reached by the percentage of solutions accepted can also be used. This procedure is applied to each of the two phases of the SA algorithm [16].	Iterative process stops when a specified tolerance gap is reached, before the maximum iteration time. The maximum iteration time plays the role of stopping criteria otherwise.

3.3. Case Studies

Since the aim of this work is to compare and analyze the performance of the novel global optimization method (software not commercially available) developed by Ref. [23] and the MOSA-GR metaheuristic developed by Ref. [16] and enhanced in this paper by a novel sequence of intertwined calculations, the same case studies must be used by both methods simultaneously. Furthermore, systematizing the information required to implement the methodological analysis proposed in this paper requires a clear protocol to promote a fair comparison of the methods under evaluation. Therefore, the same optimization models (objectives and constraints) and the data used to feed them must be the same. This is the reason to adopt the optimization model (a multiobjective one) presented in [23]. The mass of results provided by the application of such an optimization model is of fundamental importance for the evaluation of the solution methods at stake.

The case studies (and corresponding results) used are the Pescara network, a medium-sized real-world case study (from Italy), and Net 25, a small academic case study, included in [23]. The size of the case studies has the advantage of allowing an exhaustive analysis of their hydraulic functioning for a closer and deeper understanding of detailed aspects. This will make it easier to identify cause and effect relationships and interpret any cross-effects that may arise. In the following section, the MOSA-GR algorithm is applied to solve these two case studies. Therefore, the solutions available in [23] will be compared with the results thus obtained. They will serve to deeply explore the features of both methods based on the myriad of results examined using a wide range of analytical perspectives.

The Supplementary material of [23] includes detailed information about these networks. It is directly available in https://link.springer.com/article/10.1007/s11081-021-09598-z#Sec29 (accessed on 17 September 2025).

3.3.1. Pescara Network

The first case study is a modified version of the Pescara WDN (of the medium-sized city in Italy), initially proposed by Ref. [54], and here including the possible location for valve placement and a few additional pipes. This WDN has 3 reservoirs, 71 nodes, and 99 links simulated for a single time step. Hazen–Williams equations are used to compute pipe head losses. The constraints are a minimum pressure head of 10 m required at nodes with water demand and 0 m at nodes without demand, while a maximum speed of 3 m/s is permitted for pipes, and the use of a single pipe diameter per new installation link is required. The Pescara layout is shown in Figure 2, and the data corresponding to this network for implementing the EPANET2.0 hydraulic simulator [55] can be found in [23]. New pipe links (NP) can be installed in 11 predefined possible locations, as shown in Figure 2. Three pipe diameters (100, 150, and 200 mm) can be used in these links when a new pipe is installed. Furthermore, three new PRVs can be installed at the network points marked in the same figure. If they are installed, their settings have to be defined.

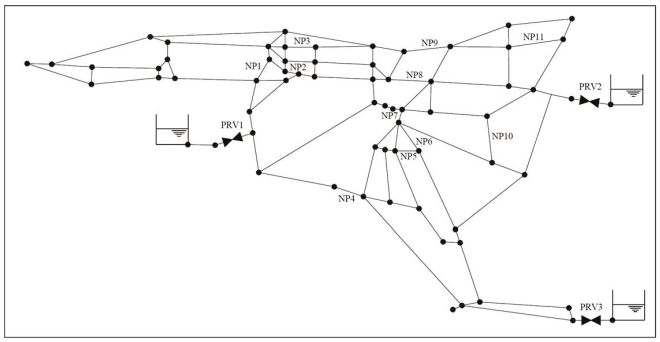

Figure 2. Pescara network.

3.3.2. Net 25

The second case study (Figure 3) is the modified Net25 network proposed by [49]. This consists of a WDN with 3 reservoirs, 17 nodes, and 26 links. Of the 26 links, 3 correspond to existing PRVs, 8 to BVs, and 15 to pipes. The network is simulated for 24 h with a one-hour time step. For this problem, the formulation of AZP and *Ir* objectives and constraints is extended to consider all time steps. Hazen–Williams equations are used to compute the pipe head losses. In terms of constraints, minimum pressure heads of 10 m and 0 m are required at the nine nodes with consumption and at the eight nodes without water consumption, respectively. Other specific constraints are that a maximum velocity of 2 m/s is allowed for pipes and the consideration of the DMAs' pairing limits according to [49]. Pairing of

two DMAs excludes pairing opportunities with other neighboring DMAs. This network characterization for implementing the EPANET hydraulic simulator [55] can also be found in [23], and the layout is in Figure 3. Ulusoy et al. [49] also assume, for this problem, that "all nodes with positive demand represent DMAs". The boundary valves (possible location of BVs in Figure 3) can be used to open or close links. If these valves are closed, isolated network nodes can be defined (the DMAs), but the redundancy to supply these nodes is reduced. The problem is to define the status of these BVs in 8 possible locations (the same for each valve for 24 h) and to define the control of the existing 3 PRVs for the 24 h of daily operation.

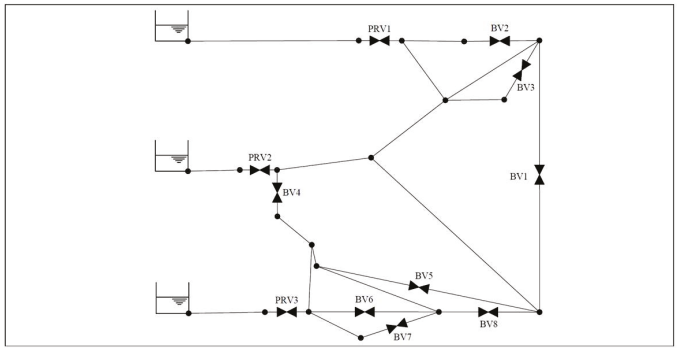

Figure 3. Net 25 network.

4. Results

4.1. Pescara Results

4.1.1. Characterization of the Pescara Pareto Front

The decision variables of the Pescara case study imply the possibility of installing 11 new pipes with three possible diameter sizes, installing three PRVs downstream of the reservoirs, and defining the PRV control settings if these valves are installed.

The MOSA-GR results for four runs are presented in Table 2 in terms of the computation time and the number of (non-dominated) solutions obtained for different numbers of function evaluations (NFEs). This is a parameter normally used to compare the computational effort of different optimization methods [13].

Table 2. Computation time and number of solutions for different NFEs for the Pescara network.

NFEs	Computation Time (s)	Number of Solutions
75,493	287	3309
172,078	806	4851
769,891	3303	6055
1,553,890	6406	6420

The number of solutions found for four MOSA-GR runs with NFEs varying between 75,493 and 1,553,890 ranges from 3309 to 6420 solutions. The computer used to achieve these results is an Intel Core i-8700k 3.70 GHz, 16.0 GB RAM and with a 64-bit operating system.

It can be stated that a small number of NFEs is enough to determine a large number of solutions (3309). Another conclusion is that, in terms of the number of solutions, it is not necessary to extend the process to too many NFEs. In fact, the number of solutions obtained for 1,553,890 NFEs is just 6% higher than the number of solutions obtained for less than

half of these NFEs (769,891). There is no need for such a high number of solutions to draw a Pareto front to understand the trade-off between the two objectives. The computation times range between 287 s and 6406 s for these four MOSA-GR runs.

Additional details about MOSA-GR results are given in Figure 4, as well as about solutions defined by sBB [23]. Figure 4a displays the printed solutions corresponding to 769,891 NFEs compared to sBB solutions.

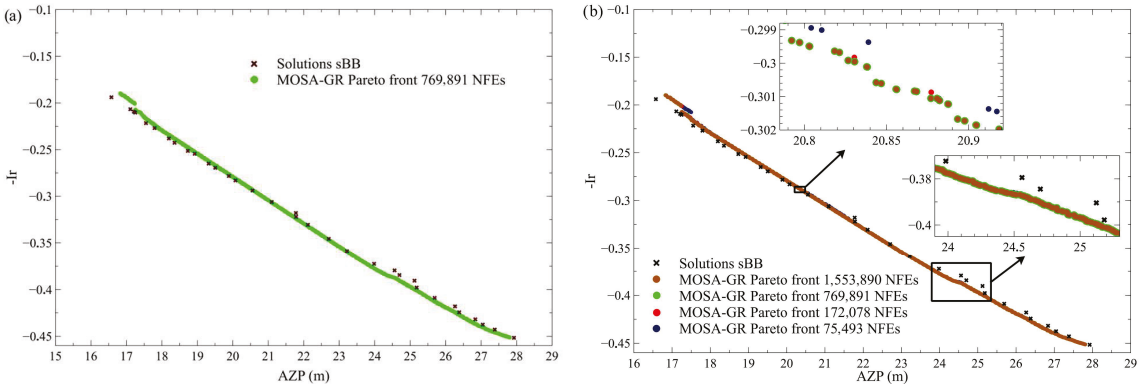

Figure 4. (**a**) MOSA-GR solutions for Pescara from 769,891 NFEs compared to sBB solutions for the AZP-*Ir* and *Ir*-AZP problems; (**b**) Fronts for different numbers of NFEs.

Supplementary material displays fronts in Figure S1 (available in [56]) for all NFEs (from Table 2) separately used to draw Figure 4b. This figure includes sets of non-dominated solutions obtained by four MOSA-GR runs with different computational efforts that are then compared with the solutions found using the sBB algorithm proposed by [23]. The increase in NFEs tends to densify the Pareto front with more non-dominated sets of solutions. These improvements cannot be observed easily because there are very slight variations in the density and in the values of the front points. The zoomed areas in Figure 4b show the improvement in solutions related to the number of NFES performed, and the overlapping of the fronts obtained with 1,553,890 and 769,891 NFEs. The upper zoomed area shows that there are no sBB solutions included there.

The results of [23] were obtained after using the ε-constraints scalarization method, allowing the Pareto front to be defined by solving single objective problems. They solved a sequence of single objective optimization problems by first minimizing AZP and introducing different ε-constraint levels on the second objective *Ir* (this is the AZP-*Ir* problem), and then, a second sequence of single objective optimization problems is solved in order to minimize *Ir* and introducing different ε-constraint levels on the other objective AZP (this is the *Ir*-AZP problem). The solutions obtained after converting sBB results using the original Hazen–Williams head loss equation are available in the [23] Supplementary material (in fact, sBB used an approximate formulation for the Hazen–Williams equation to be mentioned and discussed later on in this paper). Twenty solutions were obtained sequentially for each of these scalarized problems. The computational time was 5 min to determine each solution, and as 40 solutions were obtained, this amounted to 12,000 s. Assuming realistically a similar computational performance, the computational time to obtain each of the solutions presented in [23] is approximately the same as the time taken by MOSA-GR to obtain 3309 solutions. This challenges the statements of [22,23,49] about metaheuristics being much more time-consuming than global optimization methods. It is important to note that these assertions were made based on the same or similar case studies.

Supplementary material (Table S1 available in [56]) reports the values of the objectives of the non-dominated solutions from AZP-*Ir* and *Ir*-AZP problems (33 of the 40 are non-dominated) from sBB algorithm available at [23], as well as the values obtained by MOSA-GR (for different NFEs) that are closest to the sBB solutions. Regarding objective values, the results of MOSA-GR are quite similar to those of sBB, except for the low AZP area of the front where the MOSA-GR values are above the sBB values, particularly the single minimum AZP extreme solution of the AZP-*Ir* (see Figure 3). However, even slight differences should be taken into account when comparing the solutions of the two optimization methods. In fact, the values of the objectives are calculated with equations aggregating simultaneously a large spectrum of information. Therefore, the meaning of such solutions should be clarified in terms of the hydraulic functioning of the network. This issue merits a closer analysis later in this paper. Table 3 presents just the extreme values of the Pareto front displayed in Figure 4 that can be found in Table S1 (available in [56]).

Table 3. Comparison of objective values of the two approaches for the Pescara network.

sBB		**MOSA-GR**							
		75,493 NFEs		**172,078 NFEs**		**769,891 NFEs**		**1,553,890 NFEs**	
AZP (m)	***Ir***	**AZP (m)**	***Ir***	**AZP (m)**	***Ir***	**AZP (m)**	***Ir***	**AZP (m)**	***Ir***
27.926	−0.452	27.809	−0.451	27.809	−0.451	27.809	−0.451	27.809	−0.451
16.577	−0.194	16.827	−0.190	16.827	−0.190	16.827	−0.190	16.827	−0.190

4.1.2. Comparison of Specific Network Designs

The difference in objective values between MOSA-GR and sBB algorithms is first analyzed for a particular pair of design solutions. The maximum value of the resilience index is obtained in the situation of the maximum nodal pressure rates across the whole network. This is achieved for the Pescara case study if no pressure is reduced by PRVs and if the maximum diameter is given to the 11 new pipes. The values of the objectives for this network design are: AZP = 27.809 m and *Ir* = 0.451 by MOSA-GR (Table 3). This is the extreme point of the MOSA-GR front corresponding to the highest *Ir*. However, the extreme sBB solution of the front (Figure 4) is a solution defined without PRVs but with 10 new pipes: 2 of 100 mm, 3 of 150 mm and 5 of 200 mm. The objective values for this sBB solution are mentioned in Table 3: AZP = 27.926 m and *Ir* = 0.452. If the EPANET hydraulic simulator [55] directly determines the values of the objectives for this solution, then AZP = 27.66 m and *Ir* = 0.449 are obtained (using the original Hazen–Williams head loss equation and not its quadratic approximation). This means that sBB failed to determine the extreme point of the front for the highest *Ir*. These objective values are functions of the nodal pressure rates (Equations (1) and (4)).

4.1.3. Detailed Comparison of Solutions for Pescara

The values of the objectives of the non-dominated solutions from AZP-*Ir* and *Ir*-AZP problems (33 of the 40 are non-dominated) from sBB algorithm, and the values obtained by MOSA-GR that are closest to the sBB solutions are compared with regard to the number of new pipes used to reinforce the Pescara network for a given specific diameter (see Table S2 in Supplementary material available in [56], including diameter sizing, for these comparisons). It can be seen that all 33 pairs of design solutions of sBB are different from those of MOSA-GR. The number of new pipes for sBB tends to be higher than for MOSA-GR (for 21 solutions out of 33), but in terms of diameter size, the trend is for MOSA-GR to use larger pipe diameters than sBB; sBB results show 53 pipes with 100 mm, 40 with

150 mm, and 58 with 200 mm, while MOSA-GR uses 27 with 100 mm, 9 with 150 mm and 100 with 200 mm. Another trend is that MOSA-GR uses more PRVs than sBB; for the 33 solutions, these valves are used 70 times in MOSA-GR and 51 times in sBB (see Table S3a,b available in [56]).

The solutions of the optimization problem with a high *Ir* value, obtained by means of MOSA-GR, tend to use a large number of new pipes with large diameter sizes and to avoid installing PRVs. These configurations are used to increase the nodal pressure as much as possible throughout the network. The opposite occurs with solutions to minimize AZP values. These tend to use all three PRVs downstream of the reservoirs, and to reduce the network pressure as much as possible and use a few new pipes with small diameters. The solutions from sBB for high *Ir* value and to minimize AZP values follow the same trend as in MOSA-GR; however, the number of pipes is lower for both extreme solutions as well as diameters assigned to these few pipes (see Table S3a,b).

Additional comparisons of MOSA-GR and sBB solutions are carried out, taking into account four different areas of the Pareto front shown in Figure 5 (6 solutions between AZPs Max–26.0 m; 9 solutions between AZPs 26.0 m–22.1 m; 12 solutions between AZPs 22.1 m–18.2 m; and 6 solutions between AZPs 18.2 m–Min). To promote this analysis, it is important to emphasize that the original Pescara network [54] does not consider the installation of reinforcements involving the 11 new pipes that can be used in the present case study. The hydraulic information characteristics of the original network comprise nodes located in some areas where pressure is lower than in other areas (if the present nodal demands are used to simulate the existing network). These nodes are in the vicinity of some of the possible locations for installing new pipes, NP1, NP2, NP3, NP4, NP7, NP8, and NP9 (Figure 1). These are the areas of the network where it is most difficult to ensure the minimum pressure required. The nodes in these zones are, therefore, regarded as critical nodes for further discussion. It must also be mentioned that [23] do not provide the values of valve settings.

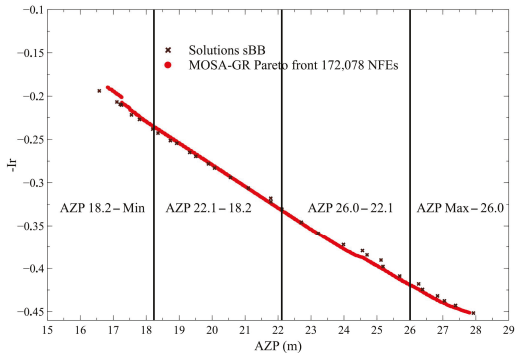

Figure 5. Pescara network Pareto front divided into four parts.

Based again on the information included in the supplementary material (Tables S1, S2 and S3a,b available in [56]) and on Figure 5, the following can be observed:

- In general, the differences between the designs of the MOSA-GR and sBB tend to increase when we move to solutions with lower AZP. Among AZP Max-26.0 m solutions, two pipes, NP7 and NP11, sized with a diameter of 200 mm, are those that show the greatest differences. In the six solutions for this part of the front, MOSA-GR does it in all of them, and sBB only twice. Between AZPs 26.0 m–22.1 m, additional differences are noticed for these two pipes: the diameter 200 mm appears nine times in MOSA-GR solutions for pipe NP7 and NP11, and only once in SBB for pipe NP7, and it is not used for NP11; the diameter 150 mm is used four times for NP7 for sBB, and it is not

used by MOSA-GR. NP10 is also sized differently by both methods: a diameter of 200 mm appears eight times in sBB and zero times in MOSA-GR solutions.

- For the intervals with low AZP values (22.1 m–18.2 m and 18.2 m–Min), the differences are even higher; there are seven pipes with significant differences: the NP7 200 mm, NP11 200 mm, NP7 150 mm, and NP10 200 mm are joined by NP3, NP5, and NP9 sized with a diameter of 100 mm. In the 18 solutions for these parts of the front, the relation (/) between MOSA-GR and sBB, in terms of number of pipes sized with a given diameter, is as follows: for NP7, 200 mm—18/2; for NP11, 200 mm—17/0; for NP7, 150 mm—0/14; for NP10, 200 mm—0/16; for NP3, 100 mm—3/14; for NP5, 100 mm—2/17; and for NP9, 100 mm—2/6. These low AZP areas of the Pareto font are the ones where we find the largest number of PRVs. In the 18 solutions for these parts of the front, MOSA-GR uses PRVs 49 times and sBB 33 times.

There are two pipes, NP7 and NP11, that deserve further attention:

- MOSA-GR uses the 200 mm diameter to reinforce the NP7 pipe many times more (33) than sBB (5). NP7 is very important because it allows an additional connection of two parts of the network that in the original network are unconnected. It is through this reinforcement that MOSA-GR solutions make it possible to supply water while complying with minimum pressure levels at critical nodes in the central area close to the NP7 pipe. This reinforcement is used by MOSA-GR in all four parts of the front. The use of a smaller diameter by sBB in solutions with lower AZPs may compromise the compliance with minimum pressure values at the nodes in the vicinity of this reinforcement. sBB also uses a 200 mm diameter in NP10 (30 times), which also allows an additional connection of two parts of the network, but this reinforcement is not so relevant because the nodes in the neighborhood of this pipe are not as critical as those close to the NP7 pipe.
- In all four parts of the front, MOSA-GR reinforces NP11 with a diameter of 200 mm in almost all solutions (32 out of 33). The NP11 with a 200 mm diameter is used by MOSA-GR because it reinforces an area of the network where there are pipes that have high flow velocities and, therefore, significant pressure losses in the original network. The use of this pipe with the largest possible diameter allows velocities to be reduced in pipes and pressure to increase in critical network nodes close to NP9. The NP11 pipe is essential to prevent pressure violations, especially in solutions in the AZP 18.2 m–Min interval. The sBB only uses this reinforcement twice, in the part of the front with the highest AZPs, but no reinforcements are considered in low AZP solutions, and then the fulfilment of minimum nodal pressure requirements could be hampered.

It is clear that the area corresponding to lower AZP values (where the MOSA-GR values are above the sBB) presents the most divergent results (see Figure 4 and data from Tables S1, S2 and S3a,b in the supplementary material available in [56]). For a full interpretation of these results, the reflection below is necessary.

4.1.4. Comments on the *Ir* Resilience Index and Solutions with Low AZP Values for Pescara

Resilience, as defined by Ref. [43] to evaluate WDNs, together with maximum pressure constraints, will lead to results ranging from zero to one for this index. Therefore, taking into account Equation (4) (also mentioned in [23]), node pressure should never violate the minimum pressure requirements. The results presented in Table 2, detailed in the Supplementary Materials (Tables S1 and S2 available in [56]) for MOSA-GR, were obtained while ensuring that all the constraints during the iterative procedure are met, and any relaxation or approximation of constraints is not considered in the MOSA-GR algorithm (as is clear in the flowchart in Figure 1 and in Table 1).

As already mentioned, in the front area of low AZP values, the MOSA-GR solutions are above the sBB solution. This is the front area where the network design solution tries to minimize the nodal pressure so as to reduce the AZP objective as much as possible. In Ref. [23], it is stated that "*For the AZP minimizing configurations more than 90% of all simulated pressures violate minimum pressure requirements by less than 0.04 m in Net 25, while all simulated pressure violations are below 0.02 m in Pescara*". Therefore, in this area of the front it seems that minimum pressure requirements are not fully satisfied by sBB, and this could be the reason for the difference between solutions in this part of the front (resilience in [23] is actually determined by summing up negative and positive terms, due to the presence of some pressure violations).

In Section 4.1.3., the design differences between MOSA-GR and sBB are clear, particularly for low values of AZPs, which helps to understand why MOSA-GR solutions meet all the minimum pressure requirements, even at the most critical nodes in the network.

Another comment that should be made is that dropping pressure below the threshold value would cause nodal outflow to users to fall below demand, according to the pressure-driven modelling of outflows.

As already mentioned in the methodology section, in the presence of leakage and other pressure-dependent outflows, the generalized resilience failure (*GRF*) index proposed by [11] should replace Todini's resilience index [43]. *GRF* is based on the original resilience index proposed by [43] and presented earlier in Equation (4). The *GRF* (Equation (5)) is the sum of the resilience (Equation (6)) and the failure index (Equation (7)). The *GRF* value is a measure of the power surplus/deficit of WDNs and is equal to the resilience index when it is greater than 0, or it is equal to the failure index if it is less than 0. Details about this *GRF* index can be found in [11].

$$maxGRF = Ir_{GRF} + If_{GRF} \tag{5}$$

$$Ir_{GRF} = \frac{\max\left(\sum_{j=1}^{NN}\left(Cn_jH_j - QC_jHmin_j\right), 0\right)}{\sum_{r=1}^{NR} Q_rH_r - \sum_{i=0}^{NN} QC_jHmin_j} \tag{6}$$

$$If_{GRF} = \frac{\min\left(\sum_{j=1}^{NN}\left(Cn_jH_j - QC_jHmin_j\right), 0\right)}{\sum_{i=0}^{NN} QC_jHmin_j} \tag{7}$$

where *GRF*—generalized resilience/failure index; Ir_{GRF}—resilience index for *GRF*; If_{GRF}—failure index for *GRF*; Cn_j—outflow delivered in node *j*.

The consideration of this *GRF* index requires the use of a pressure driven hydraulic simulator as the demand is not fully delivered if pressure values are lower than the minimum required. The pressure-driven simulator used to implement the multiobjective simulated annealing in these new conditions is the EPANETpdd [57], an upgrade of the original EPANET [55]. Resolving the problem of minimizing AZP (Equation (1)) and maximizing the *GRF* (Equation (5)), the solutions obtained are given in Figure 6. In Figure 6a results from sBB should be read in the left axis (*Ir*) and results from MOSA-GR are displayed in the right axis (*GRF*). In Figure 6b, the *GRF* results are converted into *Ir* values to clarify the comparisons. In the green part, all the MOSA-GR pressure constraints are met, while the blue part includes solutions that do not meet the pressure constraints (see Table S4 in the Supporting information available in [56]).

MOSA-GR solutions considering *GRF* maximization and AZP minimization are similar to the sBB solutions across the whole front. In the minimum AZP area of the front, the use of *GRF* enables MOSA-GR solutions to approach the sBB solution if the minimum pressure

requirements are not fully met. Solutions with low AZPs are characterized by the use of the three new PRVs installed downstream of the reservoirs that decrease nodal pressure throughout network, and new pipe diameters in more or less half of the possible locations (pipes with diameters of 100 mm, 150 mm, and 200 mm) that are used to try to keep the resilience at a relatively acceptable value and, with that, keep nodal pressure close to the required minimum of 10 m. In all the solutions obtained considering *GRF*, 98.2% of all simulated pressure values either satisfy minimum pressure limits or violate them by less than 0.02 m.

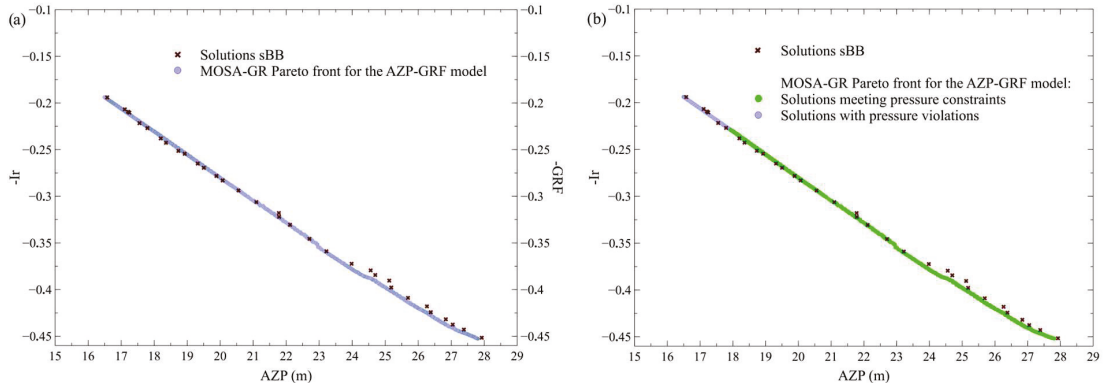

Figure 6. (**a**) MOSA-GR Pescara solutions considering the objective *GRF* and the sBB solutions obtained from the AZP-*Ir* and *Ir*-AZP problems; (**b**) The same results with *GRF* solutions converted into *Ir* solutions.

A Lagrangian relaxation method was also implemented (Figure S2 and Table S5 in the Supplementary material of [56]) and similar results were obtained.

4.1.5. Effects of Compliance or Non-Compliance with Constraints

The results presented in Sections 4.1.1–4.1.4 show some limitations of the sBB optimization method. In fact, there are parts of the front where constraints are not verified, particularly in the low AZPs area, and even the extreme point in the high *Ir* area is not found. The effects of compliance or non-compliance with the constraints merit further analysis in order to understand the impacts on the hydraulic functioning of the network. There is not enough data from [23] to make comparisons between sBB and MOSA-GR along the entire front. A more in-depth analysis is, therefore, carried out, including 28 MOSA-GR solutions selected for Min AZP-Max *Ir* compared to 28 MOSA-GR solutions selected for Min AZP-Max *GRF*, with very similar AZP values and in the low AZP front zone. This means comparing the fronts obtained with the same algorithm, either satisfying all the constraints (Min AZP-Max *Ir*) or allowing them to be violated (Min AZP-Max *GRF*). Table S6 in the Supplementary Materials is available in [56] and reports the target values of the objectives for these 28 solutions (for solutions with AZP values greater than 18.174 all minimum pressure requirements are met). Table 4 presents just the extreme values of Table S6 (available in [56]).

Table 4. Comparison of results using resilience index Ir or *GRF* as objectives.

Min AZP-Max *Ir* MOSA-GR Solutions		**Min AZP-Max *GRF* MOSA-GR Solutions**	
AZP (m)	***Ir***	**AZP (m)**	***GRF***
18.174	0.234	18.170	0.235
16.828	0.190	16.8249	0.203

These solutions are compared in terms of the number of new pipes used to reinforce the Pescara network from a specific diameter and the PRVs installed (see Figure 7):

- AZP-*Ir* sizes NP3 with a diameter of 100 mm several times (cast-off in 10 of the 28 solutions). AZP-*GRF* solutions do not include NP3 with a pipe size of 100 mm. Similar situations occur in NP5-150 mm and 200 mm, NP8-100 and 150 mm, NP10-100 mm, NP11-150 mm, and NP2-200 mm.
- In some other cases, the AZP-*GRF* solutions include more pipes in the 28 solutions than AZP-*Ir* solutions, as is the case with NP7-100 mm, NP7-150 mm, and NP6-200 mm.
- The number of pipes used in the 28 AZP-*Ir* solutions is 133, and in the 28 AZP-*GRF* solutions, it is 94. In terms of PRVs, the AZP-*Ir* uses almost all three PRVs in the 28 solutions, and in AZP-*GRF*, PRV2 and PRV3 are used in the 28 solutions, but PRV1 is used in just 10 solutions.
- For the solutions of the same level, AZP-*Ir* solutions tend to use more diameters and control the pressure with more PRVs than AZP-*GRF* solutions do.

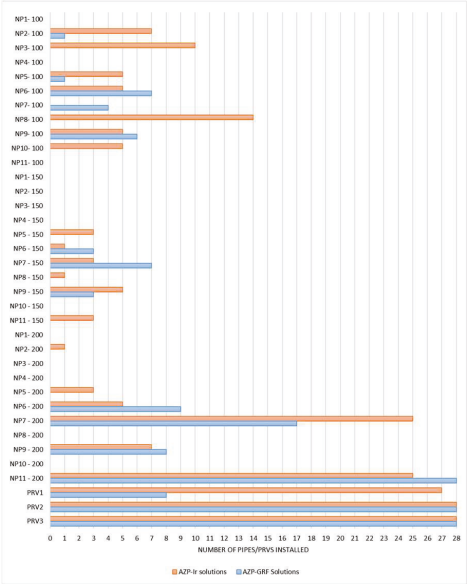

Figure 7. Characteristics of the hydraulic design for solutions considering or not the violation of constraints.

The comparison of pressure rates from some solutions of the Table S6 (solutions a–e, available in [56]) in Figure 8a–e demonstrates that complying with constraints (left side of Figure 8) or not complying (right side of Figure 8) impacts the hydraulic characteristics of the network. The orange circles on the right side underline nodal pressure deficits. The objective values analyzed are (grey values of Table S6 available in [56]): AZP(*Ir*) = 18.1744 m and AZP(*GRF*) = 18.1698 m (also in Table 4—first row); AZP(*Ir*) = 17.8583 m and AZP(*GRF*) = 17.8507 m; AZP(*Ir*) = 17.5087 m and AZP(*GRF*) = 17.5041 m; AZP(*Ir*) = 17.1501 m and AZP(*GRF*) = 17.1543 m; AZP(*Ir*) = 16.8275 m and AZP(*GRF*) = 16.8249 m (also in Table 4—last row).

The analysis of networks in Figure 8 shows that as we move down in Table S6 (available in [56]) (from higher to lower AZP values), the effect of fulfilling or not fulfilling the constraints becomes evident. When the constraints are not satisfied (right side of Figure 8), lowering the AZP leads to more and more nodes experiencing pressure deficits associated with pipes 3, 7, 8, 9, and 11. Moving to the lower value of AZPs' additional areas (right and left of those pipes and to NP4) also leads to lower pressure. The orange circles in this

figure correspond to the critical nodes identified earlier and show that these are the areas of the network most susceptible to pressure deficit problems.

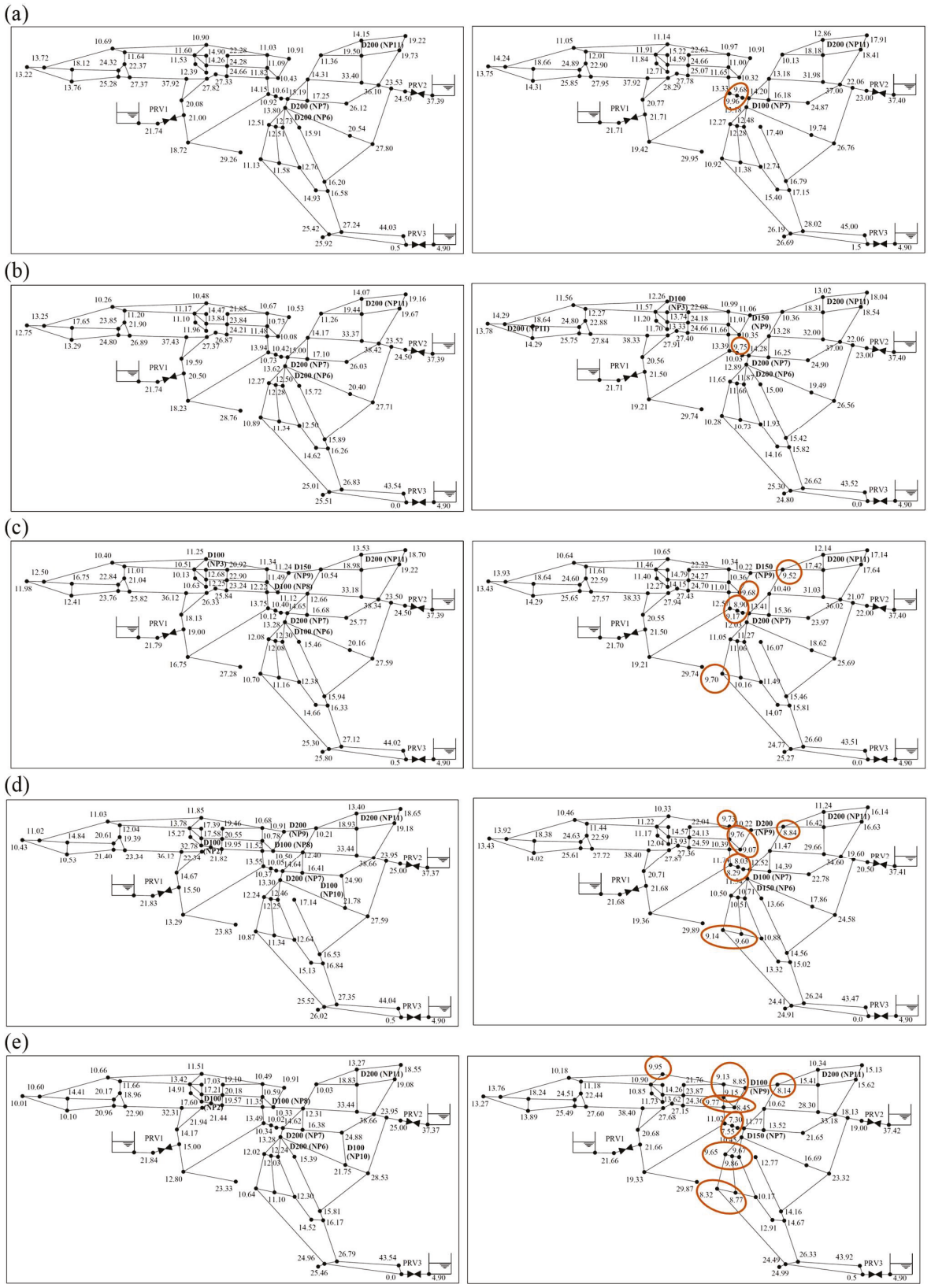

Figure 8. (**a**–**e**) Characteristics of solutions determined by resolving the Min AZP-Max *Ir* and Min AZP-Max *GRF* problems using MOSA-GR.

The reason for the discrepancies between sBB and MOSA-GR results, mainly linked to constraint violations, can result from the stopping criterion used by the two approaches, respectively, computing time (sBB) and solution quality evolution (MOSA-GR) (see Table 1). For MOSA-GR solutions, it can also be seen that if the algorithm is stopped inappropriately, the solutions obtained compared with the optimal solutions confirm some pressure problems corresponding to different pipe reinforcements and valve settings (supplementary material Tables S7 and S8 available in [56]). Taking from these tables, for example, the solutions with AZP = 18.605 m and *Ir* = 0.245 (satisfying pressure constraints) and the solution with AZP = 18.598 m and *Ir* = 0.240 (not meeting pressure constraints), node pressures are displayed in Figure 9. New-sized pipes can be noted for both networks, as well as their results in terms of pressure deficits. For AZP = 18.605 m no pressure deficits are observed; for AZP = 18.598 m, the results obtained by early stopping of the running procedure (just 111 s earlier), constraints are not met in some nodes (red nodes flagged in Figure 9). It is important to note that a solution not fulfilling the constraints would never be accepted by MOSA-GR, as confirmed in the flowchart of Figure 1 and in Table 1. For very similar values of the objectives, the differences between the pressure distribution for both situations are also relevant.

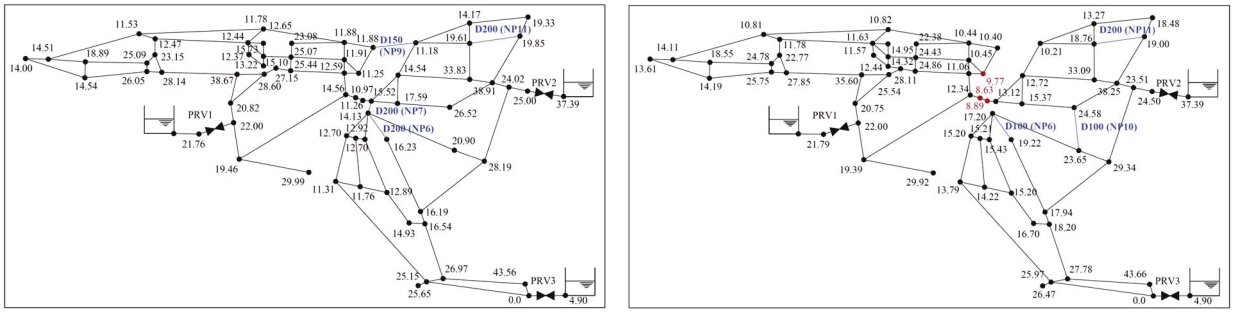

Figure 9. Solution with AZP = 18.605 m satisfying pressure constraints (**left**); Solution with AZP = 18.598 m not meeting pressure constraints (**right**).

4.2. Net25 Results

4.2.1. Characterization of the Net25 Pareto Front

The Net25 problem is different from the Pescara case study. The decision variables are related to the status of 8 boundary valves (BVs) and the control of the 3 existing pressure reducing valves (PRVs) across the 24 hourly time steps. In this case, comparisons are also made with sBB solutions.

The MOSA-GR results for 4 MOSA-GR runs with different numbers of NFEs are presented in Table 5. It shows the number of solutions obtained and the computation time using an Intel Core i-8700k 3.70 GHz, 16.0 GB RAM, with a 64-bit operating system computer.

Table 5. Computation time and number of solutions for different NFEs for Net25.

NFEs	Computation Time (s)	Number of Solutions
122,095	1242	2943
262,073	2661	4414
514,879	5087	5973
1,023,681	13,131	7984

As in the previous case study, a small number of NFEs is enough to provide a large number of solutions (2943). The Pareto front obtained for 514,876 NFEs is presented in Figure 10a, and all the fronts corresponding to different numbers of NFEs from Table 5 are displayed in Figure 10b. Supplementary material (Figure S3 available in [56]) includes fronts for all NFEs used separately to draw Figure 10b.

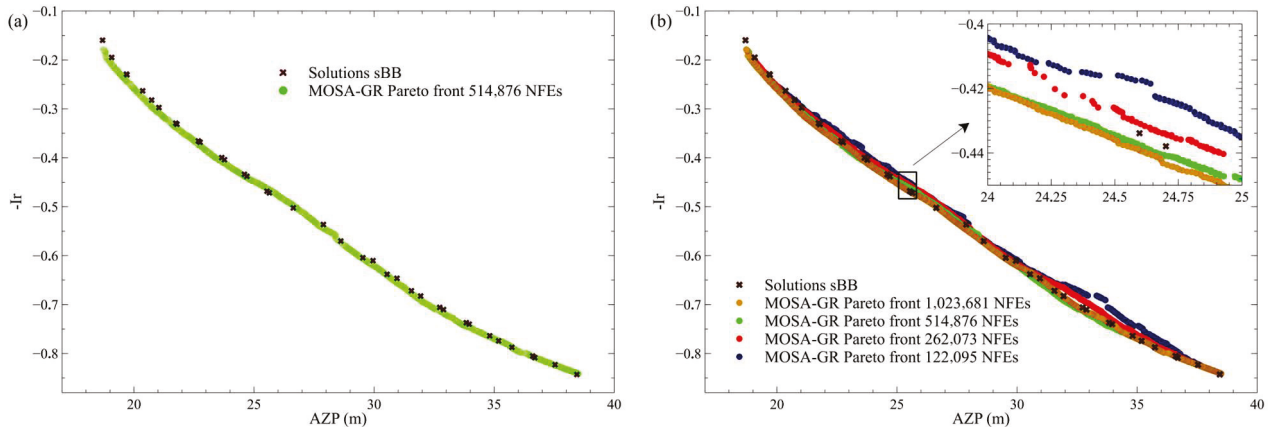

Figure 10. (**a**) MOSA-GR solutions for Net25 from 514,876 NFEs compared to sBB solutions for the AZP-*Ir* and *Ir*-AZP problems; (**b**) Fronts for different numbers of NFEs.

The MOSA-GR solutions obtained for 514,879 NFEs with a computation time equal to 1.4 h compare well with the [23] solutions (Figure 10a). The number of solutions found is 5973. Net25 has a smaller number of links and nodes than Pescara (PES), but Net25's resolution takes longer (for a similar number of NFEs) because the network operation has to be optimized for a set of 24 time steps, and PES is optimized just for a single step, 24 h long. Even so, 1.4 h (Table 5) is less than the computational time taken to obtain the 40 solutions by sBB, which is 3.3 h (5 min for each solution).

Supplementary material (Table S9 available in [56]) reports the values of the objectives of the non-dominated solutions from AZP-*Ir* and *Ir*-AZP problems (37 of the 40 are non-dominated) from the sBB algorithm and the values obtained by MOSA-GR (for different NFEs) that are closest to the sBB solutions (Table 6 presents just the extreme points of the fronts). From this information, it is also concluded that there is no need to extend the optimization process beyond 1.4 h because the solutions obtained for 1,023,681 NFEs (Figure 10) are similar to those obtained with 514,876 NFEs.

Table 6. Comparison of objective values of the two approaches for the Net25 network.

sBB		**MOSA-GR**							
		122,095 NFEs		**262,073 NFEs**		**514,876 NFEs**		**1,023,681 NFEs**	
AZP (m)	***Ir***	**AZP (m)**	***Ir***	**AZP (m)**	***Ir***	**AZP (m)**	***Ir***	**AZP (m)**	***Ir***
38.443	−0.8434	38.499	−0.842	38.499	−0.841	38.499	−0.841	38.499	−0.841232
18.689	−0.1604	18.721	−0.1788	18.721	−0.179	18.721	−0.179	18.721	−0.179

In general, the results show that for solutions with higher *Ir*, more BVs are open to define a more redundant network and to reduce pressure loss in the pipes. More open BVs mean more aggregation of DMAs, which leads to increasing the resilience and the capacity of the network to supply consumers, even in pipe failure conditions. AZP also increases with increasing open BVs. MOSA-GR adopts network configurations that open three or

four BVs in solutions with higher *Ir* and one to two open BVs in solutions with lower AZPs to define more sectorized networks and reduce the pressure delivered to consumer nodes.

In the part of the front where the highest values for the resilience index are observed (Figure 10), the sBB solution with the highest *Ir* considers all BVs closed except for BVs 3, 4, and 8. The corresponding objective values for this solution are AZP = 38.443 m and *Ir* = 0.843 (solution in the lowest region of the front with a bottom brown cross in Figure 10). The MOSA-GR yields a solution with the same hydraulic characteristics with regard to the status of BVs and PRVs for the entire 24 h of operation. However, the objective values determined by MOSA-GR are slightly different: AZP = 38.499 m and Ir = 0.841. The AZP value is 0.06 m higher, and the *Ir* is 0.002 lower. Nevertheless, if sBB values are converted using the EPANET hydraulic simulator [55], the same values as those found by MOSA-GR are obtained. At any rate, it is clear that the MOSA-GR results are similar to those of sBB across the entire front, except for the lowest value of AZP (Figure 10). In fact, it is important to note that the solution from the sBB algorithm with the lowest value for AZP (AZP = 18.689 m and *Ir* = 0.1597), top brown cross of Figure 10, considers only one BV open (BV2, see Figure 3). The MOSA-GR solution is slightly different from these objective values in that the minimum AZP solution yielded by MOSA-GR is AZP = 18.721 m with *Ir* = 0.1788 and considers two BVs open, BVs 2 and 7 (see Figure 2), a situation that deserves further analysis. The settings for the three PRVs vary between 16 and 40 m. BV status is presented in Table S10 (available in [56]).

4.2.2. Detailed Comparison of Solutions for Net25

The 37 non-dominated sBB solutions obtained for the AZP-*Ir* and *Ir*-AZP problems are compared with MOSA-GR solutions with the most similar AZP values for the NET25 case study. Supplementary material Table S9 is available in [56]. In the supplementary material of [23], the designs for these 37 solutions are offered in terms of the status (open or closed) of 8 boundary valves (BVs). The settings of the three existing PRVs are not included. In the 37 pairs of solutions compared, there are many equal solutions in terms of BV status; specifically, there are 19 pairs of solutions with the same BV status. Pairs of solutions with the same BV status are mainly obtained for solutions with high AZP values. In these solutions, BV3, BV4, and BV8 (Figure 3) are open, and the remaining 5 valves are closed. Furthermore, additional assertions can be made: in the 37 pairs of compared solutions, BV1 is always closed; BV2 is only open for a single pair, that is, the one with the lowest value for AZP (solution pair with AZP = 18.689 m from sBB and AZP = 18.721 m from MOSA-GR). In the 37 pairs of solutions compared, the major differences are found in solutions with the low AZP values. In this area of the front, MOSA-GR finds solutions with BV3 and BV7 open, and sBB solutions tend to just open BV3. By opening an extra BV, MOSA-GR provides additional redundancy to the network and makes it possible to supply the demand and simultaneously satisfy the minimum pressure levels in all network nodes. Opening more BVs tends to increase nodal pressure and so makes it easier to verify minimum pressures.

4.2.3. Comments on the *Ir* Resilience Index and Solutions with Low AZP Values for NET25

The same considerations raised for Pescara about the values expected for the resilience index can be repeated here. Also, in the Net25 case study, pressure requirements are not fully met in [23]. In fact, according to [23], for Net25, "*more than 90% of all simulated pressures violate minimum pressure requirements by less than 0.04 m*".

Net25 was also tested with the MOSA-GR using the *GRF* objective (Equation (5)) to allow nodal pressures smaller than 10 m. As such, the minimum allowable pressures may

be lower than the minimum required. The solutions found by the MOSA-GR, using the objective of maximizing *GRF* and a pressure-driven simulator, are shown in Figure 11. This allows MOSA-GR to extend the front and reach the minimum AZP value of 18.488 m, which is lower than AZP = 18.689 m from sBB. Comparing the lowest AZP hydraulic solution obtained by sBB with the one from MOSA-GR, it is observed that the sBB includes a single open BV (BV2), and the MOSA-GR solution considers two open BVs (BV2 and BV7). The MOSA-GR solution includes a larger value for *Ir* (0.1719) than the sBB case (0.1597), and this could be a consequence of the additional open BV (see Table S11 available in [56]).

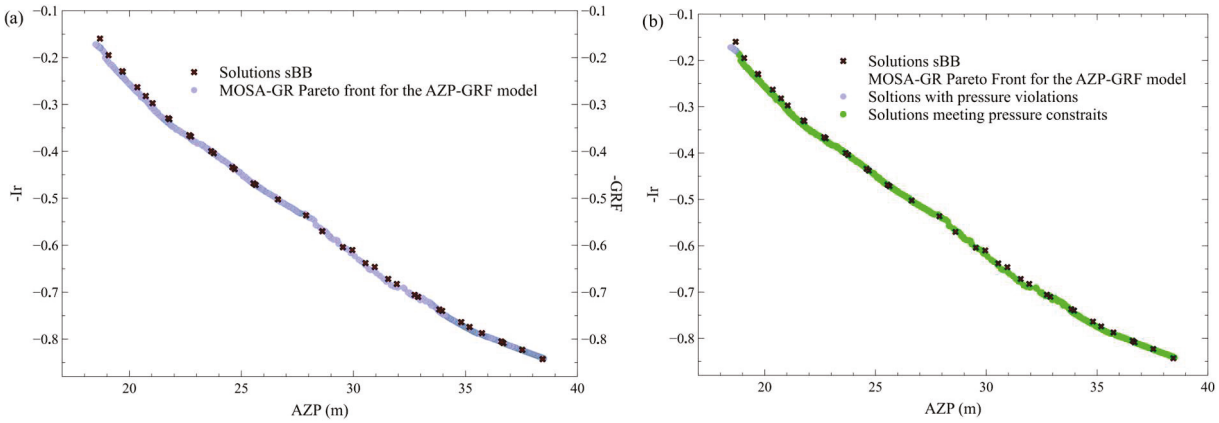

Figure 11. (**a**) MOSA-GR NET 25 solutions considering the objective *GRF* and the sBB solutions obtained from the AZP-*Ir* and *Ir*-AZP problems; (**b**) The same results with *GRF* solutions converted into *Ir* solutions.

A Lagrangian relaxation method was also implemented (Figure S4 and Table S12 in the Supplementary material of [56]) and similar results were obtained.

4.2.4. Comparison of Specific Network Designs in Terms of Pressure Requirements

By comparing three solutions (with similar values) in the lowest AZP part of the front obtained in different ways (just described) it can be noticed that: the solution found by the MOSA-GR using the *Ir* as objective (Table 6: AZP = 18.721 m and *Ir* = 0.1788) fulfills all nodal pressure values during the 24 h of the day; the solution found by the MOSA-GR considering a Lagrangian relaxation of the minimum nodal pressure rates (Table S12 available in [56]: AZP = 18.686 m and *Ir* = 0.1777), finds that minimum pressure is not fully satisfied at hours 4 and 6 in two different nodes of the network; and for the solution provided by MOSA-GR using as objective *GRF* (Table S11 available in [56]: AZP = 18.687 m and *Ir* = 0.1787) pressures are also partially unmet at hours 4, 7, and 23 at three different nodes of the network. This shows that meeting or not the pressure constraints has an impact on the operation of the distribution network.

5. Discussion

Real-world design engineering problems are usually nonlinear and often include discrete variables. These are generally very challenging Non-deterministic Polynomial time hard MINLP operations research problems [51,58]. Mathematical programming techniques were developed to tackle such problems as early as the 1960s and 1970s; however, they could not be successfully applied to real-world problems due to limitations of the computational facilities and optimization algorithms available then. The focus was, therefore, placed on simplified versions or approximations of the real-world problems [59]. In fact, the literature includes works about aquifers, drainage systems at urban or regional level,

or water distribution system sizing and operation, where even the representation of the physical systems themselves was simplified so that they could be handled through optimization models (for aquifer management, see [60]; for wastewater drainage and treatment, see [61]; for WDNs, see [62]). The resolution of real-world problems using exact methods at the expense of significant simplifications created many unpleasant situations due to the reluctance of practitioners to accept them [50] and raised the discussion about the meaning of the solutions obtained—mathematical optimum versus engineering optimum. Although decision-making in the area of water use problems has been a concern in the past, even in the most ancient civilizations [63], it was only after the Second World War that decision problems relating to the use of resources were recognized as a "respectable and defined body of knowledge" [53]. Thus, a long path of application and analysis of various possible methods to solve problems with the aforementioned mathematical characteristics was embarked upon. Along this path, the important efforts made to develop trustworthy simulation models deserve to be emphasized [64].

Lately, numerous mathematical programming methods use "a divide and conquer strategy to the partition of the solution space into subproblems and then optimizing individually each subproblem" [65], integrating their solutions in an iterative fashion, such as the approach used by [23]. This type of approach has turned out to be very time-consuming to be functional for large-scale problems or to solve very complex ones [51,66,67]. In fact, theoretically, exact global optimization methods are expected to deliver the optimal solution for real-world engineering problems. However, the literature shows that MINLP formulations can often rely on non-rigorous versions of the problems at stake by implementing linearizations, quadratic forms of highly nonlinear functions, relaxation of constraints, etc. As in the past, when rough representations of the physical aspects of the problem were made, the solutions obtained in this way, although theoretically constituting mathematical optima, might not be useful from a practical point of view [59], particularly for large instances of the problems. More recently, it has been shown that some metaheuristics can deal with problems including all the characteristics of real-world problems; however, with some issues related to convergence requiring careful evaluation. Even today, the detail with which real-world problems are embodied, incorporating all physical, technological, environmental, and economic issues that describe their essence, is of primary importance when it comes to engineering problems.

In this section, the results delivered in the previous section are analyzed, taking into account the mathematical structure of both approaches used to obtain them, highlighting their physical/hydraulic features and several aspects related to the approximations or simplifications introduced into the optimization process. Only the simultaneous analysis of case studies used by both methods allows fair conclusions to be drawn. Issues deserving a closer examination and interpretation will also be addressed in the next paragraphs. For this purpose, in some cases, sentences or paragraphs from [23] will be cited, being referenced using quotation marks. Table 1 is also used to structure the analysis.

Running times, constraints, and convergence issues

- First, Ref. [23] starts by claiming the superiority of global optimization methods based on the difficulties of metaheuristics regarding running times, convergence to optimal solutions, and handling constraints in general, and on the difficulties in dealing with valves for design-for-control problems in particular. In both case studies, the opposite has happened: MOSA-GR (Multi-Objective Simulated Annealing with new Generation and Reannealing procedures) was less time-consuming than sBB (spatial branch-and-bound) and led to a denser Pareto front, including high-quality

solutions. It is important to emphasize that Ref. [23] comments were produced based on the results of their case studies that were used for the assessment developed in the present paper.

- Additionally, the MOSA-GR approach solved the model established to represent the real engineering problem without the approximations or simplifications required by sBB (Table 1) and the Section 4. Constraints were fully met by MOSA-GR, as expected given its mathematical structure, and sBB showed some drawbacks with regard to this issue.
- The simulated annealing algorithm is based on a solid mathematical background, and its convergence in probability to the global optimum has been proven. The conditions for obtaining a global optimal solution are described in [68]. However, in practical terms, they would imply a very high number of iterations to be carried out. The number of iterations will critically affect the computing time and convergence rate [69,70].
- The theoretical structure of the global optimization method is expected to provide global optimal solutions. However, the approximations or simplifications introduced into the original problem/model to make it possible to apply it to real-world problems represent a limitation to finding the global optimum.

Scalarization issues

- A scalarization procedure, "together with global optimization methods, to approximate the Pareto front of BOMINLP," is implemented by [23]. The ε-constraints scalarization allows the "use of a spatial branch-and-bound to compute upper and lower bounds on the optimal values of the resulting sequence of parametrized single-objective problems", or in other words, "to compute feasible solutions of the single-objective MINLPs with certified global optimality bounds".
- It is important to stress the following sentence from [23]: "The approximation of the Pareto front depends on the order of objective functions and choice of scalarization parameters". With regard to this, the literature mentions that "The disadvantages of ε-constraint method are difficulty in choice of perfect value for epsilon vector, no equality-spaced Pareto solutions and demand of a large number of iterations like weighting method" [71].

Lower and upper bounds

- Following [23], "The use of the ε-constraint scalarization method has two main benefits. First we show ... that relaxing the potential-flow coupled constraints in MINLP ... produces a problem which can be equivalently reformulated into a mixed-integer linear program (MILP). This provides a convenient mean to compute tight lower bounds throughout the sBB procedure." (relying also on an "equivalent" linear reformulation of the nonlinear resilience index). The concept of a polyhedral envelope is applied to obtain a linear relaxation of non-convex flow coupling constraints, i.e., the non-convex head loss equality constraints (limitations on the application of this method to non-convex functions is commented in [48]). In fact, the polyhedral envelope of the non-convex head loss equality constraints is computed to relax the MINLP. The potential coupling constraints are replaced by linear constraints after a number of linearizations to find the linear approximation of the convex envelope. This means that lower bounds "are obtained by solving mixed-integer linear relaxations".
- The Hazen–Williams head loss equation used by [23] is mentioned "as neither equation is smooth, it is convenient to use a quadratic approximation of the formulae over the

operational range of flows in each link." The cumulative effect of this approximation in large-sized networks can give rise to defining inappropriate node pressures.

- Upper bounds [23] "are computed throughout the sBB search by fixing the values of the binary variables ... to the solution of the corresponding lower bounding MILP relaxations" and "computing a locally optimal solution to the resulting non-convex NLPs. This is performed directly using an NLP solver". These are local solutions completely dependent on the quality of those already determined by the MILP solver referred to above.
- With regard to lower and upper bounds, it is important to stress the following statement from [23]: "We show that, using this approach, we can compute a superset of the Pareto front of BOMINLP, i.e., potentially non-dominated solutions as well as guarantees of their global non-dominance".

Gap of optimality

- After defining the procedure to obtain lower and upper bounds, there is a conclusion in [23] that: "Global optimality is then certifiably reached when the relative optimality gap between upper bound and lower bound is smaller than a specified tolerance". According to the literature [72], that gap defines "how close from the optimal objective function value a solution can be to stop the optimization process". The tolerance (δ) is set to 10^{-2} for the resolution of the case studies used in the paper. However, Algorithm 1 presented in [23] includes an instruction where it is clear that the termination criterion may be the maximum iteration time. Therefore, the gap of optimality found reported in [23] may be due to a premature termination of the algorithm. That is, convergence guarantees are sacrificed to ensure low running times.
- The early termination of the procedure may be one of the reasons why the solutions presented do not satisfy constraints. One of the criticisms made by [23] when dismissing metaheuristics is that they have difficulties in handling constraints. A question may also be posed for the same work: how much time would be needed to prevent constraints from not being met? The results obtained by MOSA-GR show the differences in the hydraulic characteristics of the solutions when the algorithm is prematurely interrupted.
- Additionally, it may happen that the premature termination of the algorithm occurs with too many branches still open in the tree of the sBB. The corresponding results can then show unbalanced hydraulic situations characterized by WDN areas that include many pressure binding constraints, while in others, pressure presents low values. WDNs that include many nodes where the pressure values are the minimum possible are much more vulnerable to not being able to cope with changes in demand.

Results

After the analysis of the transformations of the original problem mentioned above, and the results commented on in the Section 4, it is clear that there are some drawbacks in the results obtained by [23]. As we mentioned in that section, slight differences in the objective values can correspond to solutions with very different hydraulic characteristics. The results obtained clearly show that the nodal pressure constraints are not fully met. This raises additional comments:

- The resilience index originally conceived for demand-driven modelling was used in the pressure-driven context as mentioned in Section 4.1.4. Therefore, the generalized resilience/failure index (*GRF*) should be adopted, and an appropriate hydraulic simulator used (a pressure-driven one). In fact, satisfying the demand in each node is highly dependent on satisfying the pressure requirements.

- Nodal pressure constraints are not fully met. There could be several reasons for this, such as the application of the concept of a polyhedral envelope to deal with nonlinear non-convex constraints [48], and the early termination of the optimization procedure.

The use of optimization techniques is aimed at finding high-quality hydraulic solutions full of practical meaning (based on truthful simulation models). The issues just commented on raise questions about the accuracy in representing the real engineering problem by the reformulation and optimization approach followed by [23]. The results show the impact on the hydraulic characteristics of the results, whether constraints are fulfilled or not. To confirm this assertion, MOSA-GR determined solutions for both situations (see Section 4). It is important to emphasize that Pescara is a medium-sized network and Net25 is a small network. Therefore, one should reflect on these issues for large real-world problems. The present paper aims to contribute to the debate on "mathematical optimum vs. engineering optimum". In fact, when any author proposes a formulation of an optimization model, it is to be expected that solution methods will be applied to the proposed optimization model. The issue is that, in the case of the global optimization method used for application in WDNs, the initial problem may be "masked" by different types of approximations. For this reason, a novel methodology has been developed so that these aspects can be analyzed in a fair and structured way. The point is that, in the case of a global optimization-based algorithm, sBB, it is possible to see the wide range of approximations used for the real problem to be solved and their effects on the hydraulic design and management of the network.

Statements from [23] about the application of metaheuristic methods to complex engineering problems can be questioned, and the same applies to comments such as "they sacrifice optimality and accuracy to deliver a solution in a relatively short time", "no guarantee that the solution will be optimal", and "it is very difficult to detect infeasibility of optimization problems with a heuristic" [72]. In fact, metaheuristics can play an important role in incorporating all the issues of real-world engineering problems. Ref. [67] recognizes this and proposes decoupling the problem of design for control into two problems solved in sequence: first, the design and valve settings are obtained through the use of a metaheuristic, and then, in a refinement stage, a gradient-based mathematical programming method "is used to solve continuous optimal control problems corresponding to design solutions returned by an initial (metaheuristic) search".

The results obtained through the two approaches compared in the present paper show the opportunity to solve design-for-control problems using a metaheuristic method. However, we are not claiming that metaheuristics, particularly the one proposed by the authors (MOSA-GR [16]), is the ultimate approach to solving real-world engineering problems. In fact, stimulating controversies around the competition between heuristics and global optimization methods have a negative impact on the advancement of knowledge [73]. At this point, it is important to discuss how to tackle WDN problems in order to confidently provide quality solutions for practical application.

The characterization of the core behavior of metaheuristics and global optimization approaches may contribute to a move towards the coupling of both types of optimization methods [74,75]. In water systems analysis, where complex physical issues give rise to tricky simulation models embedded into optimization models, we believe that analytical investigations to understand the behavior of metaheuristics and global optimization algorithms could help to outline their strengths and weaknesses and promote new frameworks. Both approaches could then play an important role in the progress in this area.

The comprehensive mechanics underlying metaheuristics must be dissected, and this could lead to concentrating on more promising research directions. Part of this can include

picking up ideas conventionally used by global optimization to solve subproblems after a smart breakdown of the overall problem. The deep analysis of the combinatorial properties of the problem can help to deconstruct the most complex aspects and focus on those components that truly help to enhance the performance of the algorithms. As mentioned by Ref. [65], "hybrid methods involving heuristic approaches in order to consider cooperative schemes between exact methods and metaheuristics" can be of great interest.

6. Conclusions

Sustainable management of water resources is nowadays of fundamental importance, and, therefore, water utilities must control water losses and meet consumer expectations by avoiding interruption of WDN services. This paper develops an innovative methodology for analyzing the solutions provided by the optimization of a design-for-control of water distribution networks problem using an exact global optimization method and a metaheuristic method. This problem entails identifying locations for the installation of valves and/or pipes and outlining valve operating settings that optimize two conflicting objectives, the minimization of pressure-induced background leakage and the maximization of network resilience. The global optimization method relies on a specially tailored spatial branch and bound algorithm to solve the aforementioned problem. This algorithm is described and applied to two case studies (one based on a real-world case study and the other on an academic study) available in [23]. A metaheuristic based on the concept of simulated annealing (MOSA-GR) is used to resolve the same optimization problem and case studies. This is instrumental for applying the methodological analysis, serving to dissect the solutions obtained by both methods. MOSA-GR has been upgraded with new features to make it possible to simultaneously solve the two intertwined problems of water distribution system—design and operation. To the best of our knowledge, this is the first time a heuristic method has been used to solve the problem at stake.

The assessment of the results provided by both solution methods was made available because a detailed methodology was developed for their analysis. It was quite challenging to build it, as it needs to be comprehensive and, more importantly, link the hydraulic behavior of water distribution networks to the theoretical aspects that characterize each approach used. It addresses a sequence of topics related to their mathematical characteristics, as well as their integration and conclusive discussion. This creates the opportunity to examine the role of metaheuristics and global optimization to solve real-world engineering problems, and further scrutinize their impacts on the solutions achieved (presented in the Section 5). The link between these mathematical characteristics of the solution methods and the results in terms of the hydraulic functioning of the networks is a fundamental component of this work.

The results provided by the sBB algorithm, analyzed in this paper, show that constraints are sometimes not fulfilled. The analysis performed on solutions by MOSA-GR shows that meeting or not meeting the constraints impacts the characteristics of the hydraulic solutions obtained, and this situation becomes important when dealing with low Average Zone Pressure (AZP) values. If properly built, metaheuristics can find solutions of quality in a shorter time (there is no need for simplifications of the optimization model proposed). The comparison of those results with the ones delivered by applying a global optimization method shows how the metaheuristic based on the simulated annealing concept is able to successfully address the challenges posed by real-world engineering problems. A denser Pareto front is obtained in less time, and all the constraints are always met. The methodology of analysis used also reveals the impacts produced on the functioning of the WDNs as a result of the myriad of approximations or simplifications to the representation

of real-world engineering problems implemented by the global optimization method. After all the modifications required to make it possible to solve the problem by means of a specially tailored global optimization method, it is necessary to perform a deep analysis of the pros and cons of such an approach. This is a broad subject, which involves many issues, as can be seen from this paper, and which must be approached with care. Convergence issues should be addressed in larger problems. In fact, the Net 25 network, a smaller case study, shows better results when compared to the Pescara case study, a medium-sized case study, using the sBB method. Furthermore, it is important to detect which mechanisms may give rise to inappropriate hydraulic solutions as well as how this situation can be avoided. The accuracy of the solutions to be implemented is key to the successful control of WDN water leakages, making a significant contribution towards sustainable management of natural resources with an impact on the economy and society. We are not claiming that the metaheuristics approach is the ultimate one. Both approaches can contribute to the flow of knowledge in this field. We believe there is a real opportunity to thoughtfully address the challenges posed by complex real-world problems. In fact, the decision on which approach to use (metaheuristics or global optimization) should not be dichotomous. On the contrary, the two approaches should be complementary to create a hybrid approach by leveraging what is most attractive in each of them (see Sections 4 and 5). Even if there are other issues, such as uncertainty, relating to the efficient management of water distribution networks, the debate on the mathematical optimum versus the engineering optimum raises questions of great interest to professionals and utility companies in general.

Author Contributions: Conceptualization, M.C.; methodology, M.C.; software, J.M.; validation, M.C. and E.C.; formal analysis, M.C. and E.C.; investigation, M.C. and J.M.; resources, M.C. and E.C.; data curation, J.M.; writing—original draft preparation, M.C. and J.M.; writing—review and editing, M.C. and E.C.; visualization, J.M.; supervision, M.C. All authors have read and agreed to the published version of the manuscript.

Funding: This research was funded by the support of national funds through FCT—Fundação para a Ciência e a Tecnologia, under projects UID/00285—Centre for Mechanical Engineering, Materials and Processes and LA/P/0112/2020.

Data Availability Statement: The original data presented in the study are openly available. The hydraulic model of the PES and NET25 networks can be accessed in Ulusoy et al. (2022) [23]: https://doi.org/10.1007/s11081-021-09598-z. Relevant information for the analysis of case studies is openly available in Cunha et al. (2025) [56]: https://doi.org/10.17632/yzcrddzkfn.3.

Conflicts of Interest: The authors declare no conflicts of interest.

References

1. Boindala, S.P.; Ostfeld, A. Robust Multi-Objective Design Optimization of Water Distribution System under Uncertainty. *Water* **2022**, *14*, 2199. [CrossRef]
2. Walski, T.M. State-of-the-Art Pipe Network Optimization. In Proceedings of the Computer Applications in Water Resources, Buffalo, NY, USA, 10–12 June 1985; ASCE: Reston, VA, USA, 1985; pp. 559–568.
3. Lansey, K.E.; Mays, L.W. Optimization Model for Water Distribution System Design. *J. Hydraul. Eng.* **1989**, *115*, 1401–1418. [CrossRef]
4. Simpson, A.R.; Dandy, G.C.; Murphy, L.J. Genetic Algorithms Compared to Other Techniques for Pipe Optimization. *J. Water Resour. Plan. Manag.* **1994**, *120*, 423–443. [CrossRef]
5. Walski, T.M.; Brill, E.D.; Gessler, J.; Goulter, I.C.; Jeppson, R.M.; Lansey, K.; Lee, H.-L.; Liebman, J.C.; Mays, L.; Morgan, D.R.; et al. Battle of the Network Models: Epilogue. *J. Water Resour. Plan. Manag.* **1987**, *113*, 191–203. [CrossRef]
6. Savic, D.A.; Walters, G.A. Genetic Algorithms for Least-Cost Design of Water Distribution Networks. *J. Water Resour. Plan. Manag.* **1997**, *123*, 67–77. [CrossRef]

7. Cunha, M.C.; Sousa, J. Water Distribution Network Design Optimization: Simulated Annealing Approach. *J. Water Resour. Plan. Manag.* **1999**, *125*, 215–221. [CrossRef]
8. Sirsant, S.; Reddy, M.J. Improved MOSADE Algorithm Incorporating Sobol Sequences for Multi-Objective Design of Water Distribution Networks. *Appl. Soft Comput.* **2022**, *120*, 108682. [CrossRef]
9. Farmani, R.; Savic, D.A.; Walters, G.A. Evolutionary Multi-Objective Optimization in Water Distribution Network Design. *Eng. Optim.* **2005**, *37*, 167–183. [CrossRef]
10. Creaco, E.; Franchini, M. Fast Network Multi-Objective Design Algorithm Combined with an a Posteriori Procedure for Reliability Evaluation under Various Operational Scenarios. *Urban Water J.* **2012**, *9*, 385–399. [CrossRef]
11. Creaco, E.; Franchini, M.; Todini, E. Generalized Resilience and Failure Indices for Use with Pressure-Driven Modeling and Leakage. *J. Water Resour. Plan. Manag.* **2016**, *142*, 04016019. [CrossRef]
12. di Pierro, F.; Khu, S.-T.; Savić, D.; Berardi, L.; Dipierro, F.; Khu, S.-T.; Savic, D.; Berardi, L. Efficient Multi-Objective Optimal Design of Water Distribution Networks on a Budget of Simulations Using Hybrid Algorithms. *Environ. Model. Softw.* **2009**, *24*, 202–213. [CrossRef]
13. Wang, Q.; Guidolin, M.; Savic, D.; Kapelan, Z. Two-Objective Design of Benchmark Problems of a Water Distribution System via MOEAs: Towards the Best-Known Approximation of the True Pareto Front. *J. Water Resour. Plan. Manag.* **2015**, *141*, 04014060. [CrossRef]
14. Choi, Y.H.; Lee, H.M.; Yoo, D.G.; Kim, J.H. Self-Adaptive Multi-Objective Harmony Search for Optimal Design of Water Distribution Networks. *Eng. Optim.* **2017**, *49*, 1957–1977. [CrossRef]
15. Marques, J.; Cunha, M.; Savić, D.A. Multi-Objective Optimization of Water Distribution Systems Based on a Real Options Approach. *Environ. Model. Softw.* **2015**, *63*, 1–13. [CrossRef]
16. Cunha, M.; Marques, J. A New Multiobjective Simulated Annealing Algorithm—MOSA-GR: Application to the Optimal Design of Water Distribution Networks. *Water Resour. Res.* **2020**, *56*, e2019WR025852. [CrossRef]
17. Torkomany, M.R.; Hassan, H.S.; Shoukry, A.; Abdelrazek, A.M.; Elkholy, M. An Enhanced Multi-Objective Particle Swarm Optimization in Water Distribution Systems Design. *Water* **2021**, *13*, 1334. [CrossRef]
18. Jain, P.; Khare, R. Multi-Objective Rao Algorithm in Resilience-Based Optimal Design of Water Distribution Networks. *Water Supply* **2022**, *22*, 4346–4360. [CrossRef]
19. Kidanu, R.A.; Cunha, M.; Salomons, E.; Ostfeld, A. Improving Multi-Objective Optimization Methods of Water Distribution Networks. *Water* **2023**, *15*, 2561. [CrossRef]
20. Locatelli, M.; Schoen, F. (Global) Optimization: Historical Notes and Recent Developments. *EURO J. Comput. Optim.* **2021**, *9*, 100012. [CrossRef]
21. Csendes, T.; G.-Tóth, B.; Locatelli, M. Special Issue: Global Optimization. *Math. Program.* **2025**, *211*, 1–3. [CrossRef]
22. Pecci, F.; Abraham, E.; Stoianov, I. Scalable Pareto Set Generation for Multiobjective Co-Design Problems in Water Distribution Networks: A Continuous Relaxation Approach. *Struct. Multidiscip. Optim.* **2017**, *55*, 857–869. [CrossRef]
23. Ulusoy, A.J.; Pecci, F.; Stoianov, I. Bi-Objective Design-for-Control of Water Distribution Networks with Global Bounds. *Optim. Eng.* **2022**, *23*, 527–577. [CrossRef]
24. Wright, R.; Abraham, E.; Parpas, P.; Stoianov, I. Control of Water Distribution Networks with Dynamic DMA Topology Using Strictly Feasible Sequential Convex Programming. *Water Resour. Res.* **2015**, *51*, 9925–9941. [CrossRef]
25. Mottahedin, A.; Giudicianni, C.; Di Nunno, F.; Granata, F.; Cunha, M.; Walski, T.; Creaco, E. Analysis, Design, and Maintenance of Isolation Valves in Water Distribution Networks: State of the Art Review, Insights from Field Experiences and Future Directions. *Water Res.* **2024**, *262*, 122088. [CrossRef]
26. Lambert, A. What Do We Know About Pressure: Leakage Relationships in Distribution Systems? In Proceedings of the IWA Conference on Systems Approach to Leakage Control and Water Distribution SystemManagement, Brno, Czech Rebublic, 16–18 May 2001; pp. 1–8.
27. di Nardo, A.; di Natale, M.; Giudicianni, C.; Santonastaso, G.F.; Tzatchkov, V.; Varela, J.M.R. Economic and Energy Criteria for District Meter Areas Design of Water Distribution Networks. *Water* **2017**, *9*, 463. [CrossRef]
28. Kowalska, B.; Suchorab, P.; Kowalski, D. Division of District Metered Areas (DMAs) in a Part of Water Supply Network Using WaterGEMS (Bentley) Software: A Case Study. *Appl. Water Sci.* **2022**, *12*, 166. [CrossRef]
29. Creaco, E.; Haidar, H. Multiobjective Optimization of Control Valve Installation and DMA Creation for Reducing Leakage in Water Distribution Networks. *J. Water Resour. Plan. Manag.* **2019**, *145*, 04019046. [CrossRef]
30. van Thienen, P. Direct Assessment of Background Leakage Levels for Individual District Metered Areas (DMAs) Using Correspondence of Demand Characteristics between DMAs. *Water Supply* **2022**, *22*, 6370–6388. [CrossRef]
31. Sánchez, D.H.; Navarro-Gómez, C.J.; Rentería, M.; Sánchez-Navarro, J.R. Saving Water by Returning to a Constant Water Supply in Chihuahua. *Water Int.* **2022**, *48*, 87–97. [CrossRef]

32. Kim, T.; Oh, Y.; Koo, J.; Yoo, D. Evaluation of Priority Control District Metered Area for Water Distribution Networks Using Water Quality-Related Big Data. *Sustainability* **2022**, *14*, 7282. [CrossRef]
33. Wright, R.; Stoianov, I.; Parpas, P. Dynamic Topology in Water Distribution Networks. *Procedia Eng.* **2014**, *70*, 1735–1744. [CrossRef]
34. Wright, R.; Stoianov, I.; Parpas, P.; Henderson, K.; King, J. Adaptive Water Distribution Networks with Dynamically Reconfigurable Topology. *J. Hydroinform.* **2014**, *16*, 1280–1301. [CrossRef]
35. Giudicianni, C.; Herrera, M.; di Nardo, A.; Adeyeye, K. Automatic Multiscale Approach for Water Networks Partitioning into Dynamic District Metered Areas. *Water Resour. Manag.* **2020**, *34*, 835–848. [CrossRef]
36. Pecci, F.; Abraham, E.; Stoianov, I. Penalty and Relaxation Methods for the Optimal Placement and Operation of Control Valves in Water Supply Networks. *Comput. Optim. Appl.* **2017**, *67*, 201–223. [CrossRef]
37. Pecci, F.; Stoianov, I.; Ostfeld, A. Relax-Tighten-Round Algorithm for Optimal Placement and Control of Valves and Chlorine Boosters in Water Networks. *Eur. J. Oper. Res.* **2021**, *295*, 690–698. [CrossRef]
38. Pecci, F.; Stoianov, I.; Ostfeld, A. Convex Heuristics for Optimal Placement and Operation of Valves and Chlorine Boosters in Water Networks. *J. Water Resour. Plan. Manag.* **2022**, *148*, 04021098. [CrossRef]
39. Nicolini, M.; Zovatto, L. Optimal Location and Control of Pressure Reducing Valves in Water Networks. *J. Water Resour. Plan. Manag.* **2009**, *135*, 178–187. [CrossRef]
40. Creaco, E.; Pezzinga, G. Multiobjective Optimization of Pipe Replacements and Control Valve Installations for Leakage Attenuation in Water Distribution Networks. *J. Water Resour. Plan. Manag.* **2015**, *141*, 04014059. [CrossRef]
41. Creaco, E.; Pezzinga, G. Embedding Linear Programming in Multi Objective Genetic Algorithms for Reducing the Size of the Search Space with Application to Leakage Minimization in Water Distribution Networks. *Environ. Model. Softw.* **2015**, *69*, 308–318. [CrossRef]
42. Gullotta, A.; Campisano, A.; Creaco, E.; Modica, C. A Simplified Methodology for Optimal Location and Setting of Valves to Improve Equity in Intermittent Water Distribution Systems. *Water Resour. Manag.* **2021**, *35*, 4477–4494. [CrossRef]
43. Todini, E. Looped Water Distribution Networks Design Using a Resilience Index Based Heuristic Approach. *Urban Water* **2000**, *2*, 115–122. [CrossRef]
44. Nerantzis, D.; Pecci, F.; Stoianov, I. Optimal Control of Water Distribution Networks without Storage. *Eur. J. Oper. Res.* **2020**, *284*, 345–354. [CrossRef]
45. Kirkpatrick, S.; Gelatt, C.D.; Vecchi, M.P. Optimization by Simulated Annealing. *Science* **1983**, *220*, 671–680. [CrossRef]
46. Ehrgott, M. A Discussion of Scalarization Techniques for Multiple Objective Integer Programming. *Ann. Oper. Res.* **2006**, *147*, 343–360. [CrossRef]
47. Pecci, F.; Abraham, E.; Stoianov, I. Quadratic Head Loss Approximations for Optimisation Problems in Water Supply Networks. *J. Hydroinform.* **2017**, *19*, 493–506. [CrossRef]
48. Lundell, A.; Kronqvist, J. Polyhedral Approximation Strategies for Nonconvex Mixed-Integer Nonlinear Programming in SHOT. *J. Glob. Optim.* **2021**, *82*, 863–896. [CrossRef]
49. Ulusoy, A.J.; Pecci, F.; Stoianov, I. An MINLP-Based Approach for the Design-for-Control of Resilient Water Supply Systems. *IEEE Syst. J.* **2020**, *14*, 4579–4590. [CrossRef]
50. Cunha, M.D.C. Water Systems Planning: The Optimization Perspective. *Eng. Optim.* **2003**, *35*, 255–266. [CrossRef]
51. Petropoulos, F.; Laporte, G.; Aktas, E.; Alumur, S.A.; Archetti, C.; Ayhan, H.; Battarra, M.; Bennell, J.A.; Bourjolly, J.-M.; Boylan, J.E.; et al. Operational Research: Methods and Applications. *J. Oper. Res. Soc.* **2023**, *75*, 423–617. [CrossRef]
52. Reeves, C. *Modern Heuristic Techniques for Combinatorial Problems*; John Wiley & Sons: Hoboken, NJ, USA, 1990; ISBN 9780470220795.
53. Bradley, H.; Magnanti. *Applied Mathematical Programming*; Addison-Wesley: Boston, MA, USA, 1977; Volume 1.
54. Bragalli, C.; D'Ambrosio, C.; Lee, J.; Lodi, A.; Toth, P. *Water Network Design by MINLP*; IBM: Armonk, NY, USA, 2008.
55. Rossman, L. *A EPANET 2: Users Manual*; United States Environmental Protection Agency National Risk Management Research Laboratory: Cincinnati, OH, USA, 2000; Volume 38, p. 200.
56. Cunha, M.; Marques, J.; Creaco, E. Data_Water Networks Management: Assessment of Heuristic and Exact Approaches for Optimal Valve Location and Operation Settings Schedule. Mendeley Data V3. 2025. [CrossRef]
57. Morley, M.S.; Tricarico, C. *Pressure Driven Demand Extension for EPANET (EPANETpdd)*; Technical Report 2008/02; Centre of Water Systems, University of Exeter: Exeter, UK, 2008.
58. Giovanni, L.D. Methods and Models for Combinatorial Optimization Heuristics for Combinatorial Optimization. *Comput. Sci. Math.* **2017**.
59. Bachelet, B.; Yon, L. Model Enhancement: Improving Theoretical Optimization with Simulation. *Simul. Model. Pract. Theory* **2007**, *15*, 703–715. [CrossRef]

60. Cunha, M. On Solving Aquifer Management Problems with Simulated Annealing Algorithms. *Water Resour. Manag.* **1999**, *13*, 153–170. [CrossRef]
61. Cunha, M.C.; Pinheiro, L.; Zeferino, J.; Antunes, A.; Afonso, P. Optimization Model for Integrated Regional Wastewater Systems Planning. *J. Water Resour. Plan. Manag.* **2009**, *135*, 23–33. [CrossRef]
62. Cunha, M.d.C.; Sousa, J. Hydraulic Infrastructures Design Using Simulated Annealing. *J. Infrastruct. Syst.* **2001**, *7*, 32–39. [CrossRef]
63. Cunha, M.d.C. Optimization Techniques for Groundwater and Water Distribution Systems. *Water Int.* **2000**, *25*, 394–402. [CrossRef]
64. Amaran, S.; Sahinidis, N.V.; Sharda, B.; Bury, S.J. Simulation Optimization: A Review of Algorithms and Applications. *Ann. Oper. Res.* **2016**, *240*, 351–380. [CrossRef]
65. Jourdan, L.; Basseur, M.; Talbi, E.G. Hybridizing Exact Methods and Metaheuristics: A Taxonomy. *Eur. J. Oper. Res.* **2009**, *199*, 620–629. [CrossRef]
66. Kheiri, A.; Ahmed, L.; Boyacı, B.; Gromicho, J.; Mumford, C.; Özcan, E.; Dirikoç, A.S. Exact and Hyper-Heuristic Solutions for the Distribution-Installation Problem from the VeRoLog 2019 Challenge. *Networks* **2020**, *76*, 294–319. [CrossRef]
67. Ulusoy, A.J.; Mahmoud, H.A.; Pecci, F.; Keedwell, E.C.; Stoianov, I. Bi-Objective Design-for-Control for Improving the Pressure Management and Resilience of Water Distribution Networks. *Water Res.* **2022**, *222*, 118914. [CrossRef]
68. Aarts, E.H.L.; Van Laarhoven, P.J.M. Statistical Cooling: A General Approach to Combinatorial Optimization Problems. *Phillips J. Res.* **1985**, *40*, 193–226.
69. Cunha, M.; Antunes, A. Simulated Annealing Algorithms for Water Systems Optimization. In *Hydrology, Hydraulics and Water Resources Management—A Heuristic Optimization Approach*; WIT Press: Southampton, UK, 2012; pp. 57–73.
70. Feller, W. *An Introduction to Probability Theory and Its Applications*; Wiley: Hoboken, NJ, USA, 1968; ISBN 9780471257080.
71. Mesquita-Cunha, M.; Figueira, J.R.; Barbosa-Póvoa, A.P. New E−constraint Methods for Multi-Objective Integer Linear Programming: A Pareto Front Representation Approach. *Eur. J. Oper. Res.* **2023**, *306*, 286–307. [CrossRef]
72. Gurobi Optimization. Mathematical Optimization Heuristics. Available online: https://cdn.gurobi.com/wp-content/uploads/2022/08/ManagementPaper-4KeyAdvantagesOfMoVsHeuristics.pdf?x17923 (accessed on 17 September 2025).
73. Liu, M.L.; Sahinidis, N.V. Bridging the Gap between Heuristics and Optimization: Capacity Expansion Case. *AIChE J.* **1997**, *43*, 2289–2299. [CrossRef]
74. Sörensen, K. Metaheuristics—The Metaphor Exposed. *Int. Trans. Oper. Res.* **2015**, *22*, 3–18. [CrossRef]
75. Hooker, J.N. Toward Unification of Exact and Heuristic Optimization Methods. *Int. Trans. Oper. Res.* **2015**, *22*, 19–48. [CrossRef]

Disclaimer/Publisher's Note: The statements, opinions and data contained in all publications are solely those of the individual author(s) and contributor(s) and not of MDPI and/or the editor(s). MDPI and/or the editor(s) disclaim responsibility for any injury to people or property resulting from any ideas, methods, instructions or products referred to in the content.

water

MDPI

Article

Comparative Analysis of Machine Learning Techniques in Enhancing Acoustic Noise Loggers' Leak Detection

Samer El-Zahab [1,*], Eslam Mohammed Abdelkader [2], Ali Fares [3] and Tarek Zayed [3]

[1] College of Engineering and Technology, American University of the Middle East, Egaila 54200, Kuwait
[2] Structural Engineering Department, Faculty of Engineering, Cairo University, Giza 12613, Egypt; eslam_ahmed1990@cu.edu.eg
[3] Department of Building and Real Estate, Faculty of Construction and Environment, The Hong Kong Polytechnic University, Kowloon, Hong Kong 999077, China; ali-i.fares@connect.polyu.hk (A.F.); tarek.zayed@polyu.edu.hk (T.Z.)
* Correspondence: samer.el-zahab@aum.edu.kw

Abstract: Urban areas face a significant challenge with water pipeline leaks, resulting in resource wastage and economic consequences. The application of noise logger sensors, integrated with ensemble machine learning, emerges as a promising real-time monitoring solution, enhancing efficiency in Water Distribution Networks (WDNs) and mitigating environmental impacts. The paper investigates the integrated use of Noise Loggers with machine learning models, including Support Vector Machines (SVMs), Random Forest (RF), Naïve Bayes (NB), K-Nearest Neighbors (KNN), Decision Tree (DT), Logistic Regression (LogR), Multi-Layer Perceptron (MLP), and YamNet, along with ensemble models, for effective leak detection. The study utilizes a dataset comprising 2110 sound signals collected from various locations in Hong Kong through wireless acoustic Noise Loggers. RF model stands out with 93.68% accuracy, followed closely by KNN at 93.40%, and MLP with 92.15%, demonstrating machine learning's potential in scrutinizing acoustic signals. The ensemble model, combining these diverse models, achieves an impressive 94.40% accuracy, surpassing individual models and YamNet. The comparison of various machine learning models provides researchers with valuable insights into the use of machine learning for leak detection applications. Additionally, this paper introduces a novel method to develop a robust ensemble leak detection model by selecting the most performing machine learning models.

Keywords: leak detection; machine learning; ensemble models; acoustic noise loggers; acoustics; water distribution networks

1. Introduction

Water Distribution Networks (WDNs) constitute a critical infrastructure in the ever-increasingly urbanized world. They comprise massive systems of pressurized pipelines to transport portable water to millions of households across the globe. However, a considerable amount of the transmitted water is lost, mainly due to leakages. Indeed, the deteriorating state of aging water infrastructure presents a significant challenge that exacerbates the leakage problem in WDNS. Leakages in pressurized water pipelines lead to considerable economic losses, environmental degradation, and potential health hazards [1]. The situation is particularly alarming as leaks can remain undetected for extended periods, resulting in the wastage of valuable potable water, which is becoming increasingly scarce.

A concrete example of this problem can be seen in Hong Kong, one of the most urbanized places globally. Between 2004 and 2015, the cost of non-revenue water losses was estimated at HKD 17 billion (around USD 2.2 billion) [2]. In 2015, approximately 321 million m^3 of transported potable water (33% of the supplied freshwater) was lost, and leaks in pressurized water pipelines were identified as the primary cause of water loss [2]. This marks a substantial rise from the water loss rates of 26.5% in 2010 and 31.6% in 2013. Recent assessments highlight that Hong Kong's water loss situation remains a critical concern. More specifically, coverage from the Centre for Water Research and Resource Management (CWRRR) indicates that in 2023–2024, metered water loss rates in Hong Kong reached a record high of 38.3%, surpassing the earlier cited 33% benchmark from 2015 [3]. Notably, almost half of the annual water loss was attributed to leaks and bursts in government mains alone, with a leakage rate estimated at about 15% in 2018 [2,4]. These trends underscore a persistent or even worsening challenge, contradicting earlier improvements and indicating that, despite infrastructure upgrades, water loss remains a major issue. Hence, starting in 2008, the Water Supplies Department of Hong Kong established a goal under the total water management strategy to save 85 million m^3 of water per year by 2030. As of 2024, the Water Supplies Department (WSD) reports a 13.4% leakage rate in government mains, with ongoing rollout influencing a projected decline below 10% by 2030 [5]. Estimated fresh-water leakage volumes for government mains were approximately 121 million m^3 in 2024, increasing gradually from 97 million m^3 in 2020 [6]. With that said, early and effective leak detection is vital to prevent water waste, minimize economic impact, and ensure a continuous supply of clean water to communities. Hence, robust detection methods are vital to identify leaks of varying magnitudes in WDNs [1,7]. The conventional methods for leak detection in water pipelines primarily rely on periodic visual inspections or pressure measurements, which are labor-intensive, time-consuming, and often prone to errors [8]. Moreover, these methods may not effectively detect small or intermittent leaks, which can gradually exacerbate into larger ones [9]. To overcome these limitations, researchers have increasingly turned to a variety of sensing technologies, such as acoustic [9], vibration [10], ultrasonic [11], infrared thermography [12], fiber optic sensor [13], and ground penetration radar [14]. Acoustic-based techniques have emerged as an outstanding means for leak detection in WDNs, as leakage involves the generation of flow-induced acoustic signals that manifest as trans-tube stress waves [15,16].

Recently, acoustic-based techniques for leak management have been gaining increasing attention. However, most studies were based on small databases from laboratories and testbed facilities [17]. Multiple studies have investigated the effects of various factors on leak-induced acoustic signals, including leak flow rate [18], pipe flow pressure [19], pipe diameter [20,21], pipe material [22], pipe surrounding media [17], and leak shape and size [18]. These studies are essential to advance the understanding of acoustic signal phenomena in leaking pipes. However, they do not constitute a good resemblance to real WDNs that are complex and manifold. Thus, laboratory and testbed experiment results are insufficient to develop robust leak detection and pinpointing models. Notably, an increasing number of studies have been investigating the use of acoustic sensing technologies for leak detection in WDNs in recent years. The investigated technologies include Noise Loggers [15], accelerometers MEMS (Micro-Electro-Mechanical Sensors) [10], and hydrophones [23]. Among these, Noise Logger-based monitoring systems have emerged as a promising solution due to their simplicity of deployment, cost-effectiveness, and ability to capture subtle changes in pipeline behavior [15]. The use of such technologies is often coupled with the employment of machine learning algorithms.

Machine learning, a subfield of artificial intelligence, has revolutionized various industries by enabling computers to learn from data and make predictions or decisions without explicit programming [24,25]. In the context of leak detection, machine-learning models can analyze large datasets of acoustic signals and identify patterns associated with leak conditions [15]. ML models can automatically learn from vast acoustic datasets, extracting subtle features that traditional rule-based analyses might miss. For example, by learning complex patterns in noisy data, ML can detect small leaks or adapt to varying background noise levels without manual tuning. Thus, ML offers a powerful approach that overcomes the limitations of static threshold or manual signal analysis. A variety of machine learning techniques have been used to advance leak detection, such as Support Vector Machines (SVMs), K-Nearest Neighbors (KNN), and Decision Tree (DT) [26]. The use of machine learning models offers several advantages over traditional methods, including the ability to process complex data, adapt to changing conditions, and detect anomalies more effectively [27]. Another group of research studies adopted deep learning models in their work. Ullah et al. [28] deployed an integrated model of a 1D convolutional neural network and long short-term memory (LSTM) network for pipe leak detection. The Savitzky–Golay filter was adopted to minimize noise and retain features of the original signals. In another attempt, Siddique et al. [29] adopted convolutional autoencoders and a convolutional neural network to retrieve features from leak-augmented scalograms. The obtained feature map was then passed to an artificial neural network (ANN) with one hidden layer to diagnose the health status of pipelines. Thirdly, Ullah et al. [27] leveraged the use of continuous wavelet transform alongside enhanced short-time Fourier transform to identify the temporal and spatial characteristics of acoustic emission signals. ANN was then applied to classify the retrieved feature vector into leak and normal states. Fourthly, Ullah et al. [30] presented a time series-based deep learning framework for leak detection. They experimented with the use of gated recurrent units (GRUs), LSTM, and bi-directional LSTM to differentiate between the acoustic emission signals. It was found that bi-LSTM was able to provide superior prediction performance in terms of precision and recall. In response to the discussed challenges, this study proposes a real-time monitoring system that harnesses the potential of wireless Noise Loggers and machine learning models for efficient leak detection in water pipelines. This study investigated multiple machine-learning models, including KNN, SVM, DT, Random Forest (RF), Naïve Bayes (NB), Logistic Regression (LogR), and Multi-Layer Perceptron (MLP), to evaluate their suitability in detecting leaks in water pipelines. Knowing that each model has unique strengths and weaknesses, including bias, variance, and overfitting problems, this study employed an ensemble approach. Ensemble methods have shown considerable success across various domains by capitalizing on the diversity of individual models and aggregating their predictions to make more reliable decisions, notably in the context of leak detection [31,32]. Therefore, this article proposes an ensemble approach to achieve high detection accuracy by selecting the most accurate and robust combination of models to further improve leak detection accuracy [33].

The significance of our study lies in its potential impact on water infrastructure management and conservation efforts. The successful implementation of a real-time leak detection system utilizing wireless Noise Loggers and machine learning models can empower municipalities to promptly detect leaks, enabling faster intervention and reduced water loss. This not only preserves valuable resources but also fosters sustainable water management practices and environmental preservation. This article aims to develop robust machine learning models that can effectively detect leaks in real WDNs, to contribute a step towards improving and automating leak management in WDNs.

2. Materials and Methods

This section details the methodology employed for the analysis of acoustic signals and the development of machine learning-based leak detection models. As illustrated in Figure 1, the methodology encompasses multiple phases of data collection, data preprocessing, feature extraction, data visualization, statistical analysis, and development of machine learning models. The subsequent presentation covers the results obtained, followed by a discussion of limitations and potential avenues for future research.

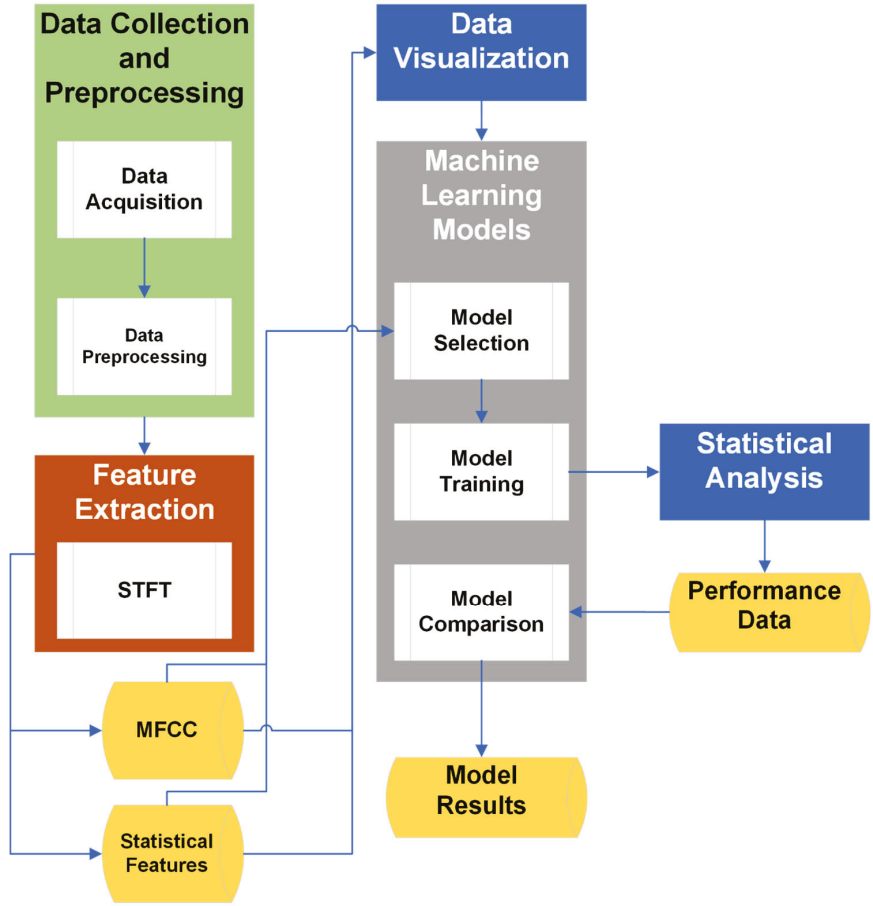

Figure 1. Research methodology of the developed leak detection model.

The adopted experimental setup involved the deployment of wireless Noise Loggers on the exterior of valves connecting water pipelines throughout the city of Hong Kong. The acoustic signals captured by these Noise Loggers were processed to extract relevant features. Subsequently, several machine learning models were employed, including SVM, RF, NB, KNN, DT, LogR, and MLP, to classify the acoustic signals and identify leak states by means of a supervised learning approach, trained on manually labeled leak and non-leak signal data, with ground truth established via inspection or hydrophone confirmation. The classifiers (SVM, RF, etc.) were trained to discriminate between the two predefined classes. The ensemble model was constructed to leverage the diverse strengths of individual classifiers, leading to superior leak detection accuracy. The illustrated methodology in Figure 1 is further expanded upon in the following subsections.

2.1. Data Collection and Preprocessing

The data collection process involved the acquisition of acoustic signals using high-quality recording devices. Efforts were made to ensure consistent sampling rates and formats across all

collected signals. First, the raw audio signals were captured using condenser microphones with a 44.1 kHz sampling rate and saved in WAV (WAVeform Audio File) format. Data were collected at multiple valve locations in Hong Kong. Leak signals were identified by acoustic noise loggers and verified manually using inspections or hydrophones, and non-leak signals were recorded from similar pipes under normal operation. The dataset includes 992 leak samples and 1118 no-leak samples (a slightly unbalanced but representative set). Each signal is labeled by confirming the presence/absence of a leak via inspection. To avoid geographic bias, leak and non-leak recordings were obtained from similar sites and times. Also, both classes included signals from all regions of the study area.

The adopted data collection system is depicted in Figure 2. As shown in Figure 2, the system includes a Noise logger deployed on-site, accompanied by a cloud service responsible for receiving and storing data. These data can be accessed remotely from an office desk. The experiment involved the use of PermaNET+ Noise Loggers. The sensors were deployed in the chamber, where the gate valve was located, to collect vibration signals. The PermaNET+ device (manufactured by HWM—Water Ltd., Ty Coch House, United Kingdom, model PermaNET+) features a built-in Hydrophone 2 acoustic sensor paired with a leak-noise logger, offering effective monitoring from approximately 20 Hz up to 5 kHz. Its sensitivity is around −50 dB re 1 Pa, typical for high-performance leak detectors designed for trunk mains and plastic pipelines. The Hydrophone 2 excels at capturing low-frequency leak noise over large or non-metallic pipes. The used Noise Loggers are equipped with an integral modem equipped with GPRS/2G and 4G technologies, enabling data transmission to the cloud. The collected acoustic signals have a length of 10 s. Four readings were collected at deployment with 15 min lag. The sampling frequency was set at 4096 Hz.

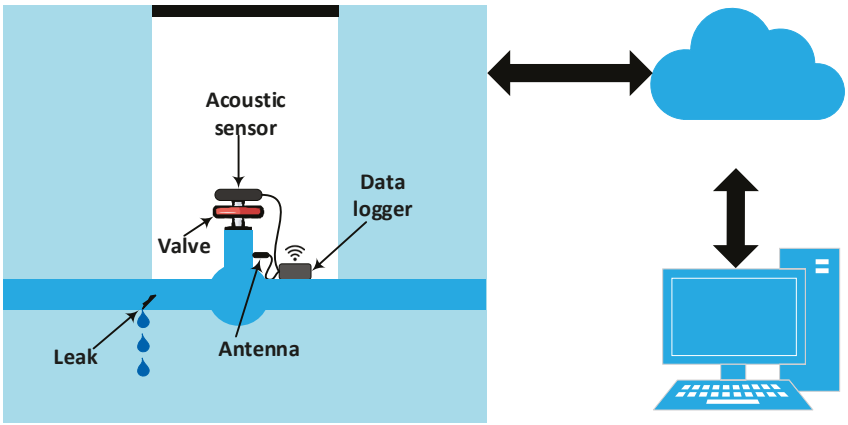

Figure 2. Visual representation of the developed data collection system.

Subsequently, the collected data were preprocessed for noise reduction, which was applied through spectral subtraction, and resampling was conducted to ensure uniformity in sampling rates. Librosa library [34] was utilized to load audio signals. The acquired signals in this study were collected from metallic pipes (such as steel, stainless steel, cast iron, and ductile iron) and non-metallic pipes (such as polyethylene and unplasticized polyvinyl chloride). In addition, the pipe diameters varied between 40 and 300 mm. Figure 3 illustrates a common deployment location for noise loggers within water distribution networks of Hong Kong. The red arrow present in Figure 3a indicate the positions of the noise loggers mounted on the pipe valves to capture leakage noise signals. Moreover, Figure 3b a real-world leak site where water is observed within the access chamber.



(**a**) (**b**)

Figure 3. (**a**) Typical installation points for noise loggers in real water distribution pipeline, and (**b**) typical leak location.

2.2. Feature Extraction

Mixed time domain and frequency domain features are highly efficacious in deriving actual information about leaks and diminishing false alarms [35]. In addition, another group of studies implemented statistical features of acoustic signals in leakage diagnosis [36,37]. With that said, multiple techniques were employed to extract meaningful features from the acoustic signals. Short-Time Fourier Transform (STFT) was computed to convert signals into spectrograms, providing insights into time-frequency representations. Mel-frequency cepstral coefficients (MFCCs) were calculated, along with spectral contrast and chroma features. Statistical features encompassed mean, variance, skewness, and kurtosis. Additionally, time-domain features like zero-crossing rate and root mean square energy were extracted.

2.3. Data Visualization

Multiple visualization techniques were employed to present the characteristics of the acoustic signals. Spectrograms were generated using STFT to visualize signal energy over time and frequency. Waveform plots depicted the raw signal's amplitude variations. MFCCs were displayed as heatmaps to convey audio feature nuances. Scatter plots were utilized to showcase the distributions of extracted features. The analysis of STFT-based derived features (MFCC, spectral contrast, etc.) showed clear separability between leak and non-leak signals via clustering and visualization. Accordingly, MFCC-based envelopes captured distinct spectral energy patterns in leak signals, justifying their use. Quantitative metrics (e.g., higher average energy in leak MFCC bands) supported this decision and motivated further modeling using time–frequency features.

2.4. Machine Learning Models

The proposed model is an innovative approach that leverages wireless Noise Loggers to detect leaks in pressurized water pipelines. The Noise Loggers capture acoustic signals from the pipelines, which are then processed as input features for machine learning models. This study evaluates several machine-learning algorithms, including SVM, RF, NB, KNN, DT, LogR, and MLP. Each algorithm analyzes the acoustic signals and classifies them into leak or non-leak states. The models were trained using the extracted features on training sets. Hyperparameter tuning was performed via grid search. Performance was evaluated using accuracy, precision, recall, F1-score, and confusion matrices. Ultimately, the models were compared based on their evaluation metrics, allowing for an understanding of their

capabilities in varying scenarios. The hyperparameters used for the selected models are found in Table A1 of the Appendix A.

A significant differentiator of this study is the development of ensemble machine learning using the best-performing individual machine learning models. The ensemble approach combines the predictions of multiple machine learning models to achieve enhanced accuracy and robustness. By leveraging the diversity of individual classifiers, the ensemble model can capture various aspects of the acoustic signals, leading to improved detection performance.

Also, a newly developed deep learning model known as YamNet was used to develop a leak detection model based on the acoustic data. YamNet analyzes sound patterns to identify leaks in water pipelines. It operates by capturing acoustic signals from the pipelines and processing them using pre-trained deep learning models [38]. The system uses a large-scale convolutional neural network (CNN) to classify the acoustic signals into leak and non-leak categories. While YamNet offers promise in detecting leaks based on acoustic signatures, it faces certain challenges. Acoustic-based methods may be susceptible to environmental noise interference, which can affect the accuracy of leak detection. Additionally, accurately distinguishing leak-related sounds from other sources of noise can be challenging, especially in noisy urban environments. It is critical to note that the publicly available YamNet model (pre-trained on AudioSet) was used without further fine-tuning on the collected data. Furthermore, the YamNet model was assessed using the same dataset; no separate field data were used in this experiment. In future work, it is recommended to fine-tune YamNet on the noise-logger dataset for improved performance. The current results thus reflect the baseline performance of YamNet's general sound classification on leak data.

2.5. Results and Interpretation

Finally, the results were presented and compared. Classification accuracy and evaluation metrics were provided for each model. Confusion matrices were used to evaluate accuracy, recall, precision, and *F1 score* for the initial models. Receiver Operating Characteristic (ROC) curves were plotted, Area Under the Curve (AUC), and Jaccard Cross-Validation values were calculated for binary classification tasks. The obtained results were interpreted with respect to the research objectives. Insights into classification performance and potential real-world applications were discussed.

The accuracy was computed as $(TP + TN)/(TP + TN + FP + FN)$, as illustrated in Equation (1), where TP, TN, FP, and FN are the true positive, true negative, false positive, and false negative counts. This measures overall classification correctness. Additionally, Equations (2)–(5) provide the equations for the remaining performance metrics.

$$Acc = \frac{TP + TN}{TP + TN + FP + FN} \tag{1}$$

Measures the overall proportion of correct predictions.

- *Sensitivity* (*Recall* or True Positive Rate):

$$Sensitivity = \frac{TP}{TP + FN} \tag{2}$$

Indicates the model's ability to correctly detect actual leak events.

- *Specificity* (True Negative Rate):

$$Specificity = \frac{TN}{TN + FP} \tag{3}$$

Reflects the ability to correctly identify non-leak conditions.

- *Precision* (Positive Predictive Value):

$$Precision = \frac{TP}{TP + FP} \tag{4}$$

Indicates the proportion of predicted leak cases that were actually leaks.

- *F1 Score* (harmonic mean of precision and recall):

$$F1\ \ Score = \frac{2 \cdot Precision \cdot Recall}{Precision + Recall} \tag{5}$$

Balances precision and recall, giving an overall sense of model reliability.

These metrics were calculated for each classifier to ensure a comprehensive evaluation of leak detection capability. In addition to quantitative metrics, SHAP (SHapley Additive Explanations) analysis (shown in the following Figures) was used to interpret model behavior by identifying the most influential acoustic features driving predictions. Together, these metrics and explainability tools provide both performance and transparency for the proposed models.

3. Model Implementation

This section presents the results of the performance evaluation of different machine learning models in accurately detecting leak states and non-leak states. The results comparison is useful to provide valuable insights into the performance of various machine learning models for leak detection in water pipelines. Table 1 compares the performance of seven machine learning models across four performance metrics. Also, Table 1 presents the ranking of the machine learning models based on their performance. The accuracy of the model was used as the main metric for ranking. From Table 1, it is evident that the RF model achieved the highest accuracy of 93.68%, making it the top-performing model among all the tested machine learning algorithms. RF's ensemble nature and ability to effectively handle large and highly dimensional datasets and feature interactions contributed to its superior performance. Furthermore, RF is distinguished by its robustness against noise and outliers. The KNN model closely followed RF with an accuracy of 93.40%. KNN's adaptability to local patterns and its capability to perform well on non-linear data distributions made it a strong candidate for leak detection. The MLP achieved an accuracy of 92.15%, demonstrating the efficacy of deep learning approaches in analyzing acoustic signals and detecting leaks in water pipelines. These results highlight the significance of ensemble methods like Random Forest and the potential of deep learning models like Multi-Layer Perceptron.

Table 1. Results of machine learning models for leak detection.

Model	Accuracy (%)	Precision (%)	Recall (%)	F1 Score * (%)	Rank	Used in Ensemble
Support Vector Machines (SVMs)	88.97	90.00	89.00	89.00	4	-
Random Forest (RF)	93.68	93.00	93.00	93.00	1	Yes
Naïve Bayes (NB)	68.38	70.00	70.00	70.00	7	-
K-Nearest Neighbors (KNN)	93.40	93.00	93.00	93.00	2	Yes
Decision Tree (DT)	77.95	77.00	75.00	76.00	5	-
Logistic Regression (LogR)	72.05	70.00	69.00	69.00	6	-
Multi-Layer Perceptron (MLP)	92.15	91.00	91.00	91.00	3	Yes

* F1 score: harmonic mean of precision and recall.

The three best-performing models were selected to develop the ensemble model. Table 2 presents the results of the ensemble model, which combined the predictions of multiple machine learning models. The ensemble model outperformed individual models and reinforced the value of combining different perspectives to improve detection accuracy. These findings underscore the importance of leveraging modern techniques such as ensemble models to enhance leak detection capabilities, contributing to sustainable water management practices.

Table 2. Performance analysis of the results of the Ensemble and YamNet models.

Ensemble Model	Accuracy (%)	Precision (%)	Recall (%)	F1 Score (%)	AUC (%)	Jaccard (%)
Ensemble	94.40	89.78	92.66	91.00	96.00	89.31
YamNet	52.63	41.7	8.77	14.49	49.45	23.53

The results of the proposed model and YamNet are significantly different, as seen from the accuracy metrics obtained in their respective experiments. The proposed model outperformed YamNet, which achieved only 52.63% accuracy. This substantial difference in accuracy demonstrates the superiority of the proposed model in identifying leaks in water pipelines. In addition, the low performance of YamNet can be attributed to its struggle in the detection of subtle and small leaks due to their weak acoustic signatures [39]. Furthermore, YamNet was trained based on controlled audio environments; thus, it lacks the adaptability to deal with real-world variabilities in pipe materials, pressure fluctuations, and background noise, leading to inconsistent performance [40]. As such, YamNet requires specialized training and fine-tuning to optimize its architecture so that it can be adopted in a domain-specific application like leak detection of water pipes.

The precision values for the Ensemble Model and YamNet were 89.78% and 41.7%, respectively. This discrepancy emphasizes the heightened ability of the Ensemble Model to accurately identify positive instances, showcasing a more refined and precise discrimination in comparison to YamNet.

In terms of recall, the Ensemble Model exhibited a notably higher value of 92.66% compared to YamNet's 8.77%. This distinction underscores the Ensemble Model's proficiency in capturing a substantial proportion of actual positive instances, reinforcing its efficacy in the identification of leaks within water pipelines. The exceptionally low recall of YamNet (8.77%) suggests it missed most actual leak cases, whereas the ensemble model achieved a high recall (92.66%). This indicates that ensemble training captured leak-specific frequency patterns, while YamNet likely misinterpreted them. MFCCs (Mel–Frequency Cepstral Coefficients) quantify the slow-changing spectral envelope of an audio signal in the mel-scaled frequency domain. MFCCs reflect harmonic and resonance characteristics of sound, making them ideal for detecting structured acoustic leak signatures. High MFCC coefficients (especially $MFCC_{1–10}$) correspond to strong harmonic energy typical of pressurized leak flows.

The F1 Score, a harmonic mean of precision and recall, further accentuates the Ensemble Model's superiority. With an F1 Score of 91.00%, the Ensemble Model achieves a more balanced trade-off between precision and recall, indicative of a more robust and reliable predictive model. In contrast, YamNet's F1 Score of 14.49% suggests a less harmonized performance in balancing precision and recall.

Figure 4 depicts the Receiver Operating Characteristic (ROC) curve of the developed ensemble model. The ROC curve graphically exemplifies the trade-off between true

positive rate and false positive rate. In addition, Area Under the Curve (AUC) signifies an aggregated measurement of the performance of the classification model. The AUC for the ROC curve is notably higher for the Ensemble Model (98.00%) in comparison to YamNet (49.45%). This substantial difference signifies the Ensemble Model's superior discriminatory ability, crucial for distinguishing between positive and negative instances in the context of leak detection.

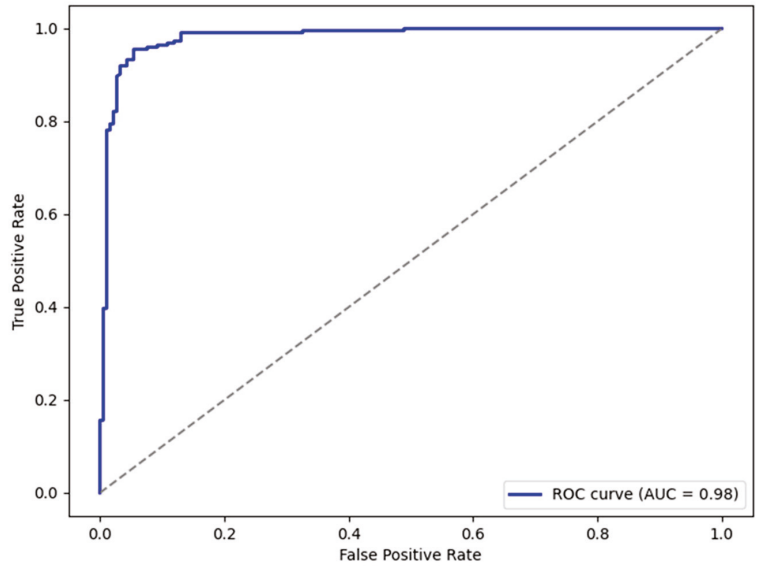

Figure 4. Receiver Operating Characteristic (ROC) curve of the developed ensemble model.

Examining the Jaccard index, the Ensemble Model once again outshines YamNet with a value of 89.31% compared to 23.53%. This emphasizes the Ensemble Model's capacity for an enhanced intersection over union, indicative of a more substantial overlap between predicted and actual positive instances.

The key difference between the proposed model and YamNet lies in their underlying analysis mechanisms. While the ensembled machine learning models utilize the extracted and selected features to classify acoustic signals captured by Noise Loggers, YamNet relies directly on the acoustic signals for leak detection. The use of Noise Loggers in the proposed model offers advantages in terms of ease of deployment, cost-effectiveness, and sensitivity to subtle changes in pipeline behavior. It also reduces susceptibility to environmental noise, leading to more accurate leak detection in various environments. SHAP (shapely additive explanations) is applied to identify the significant factors influencing leak detection (see Figure 5).

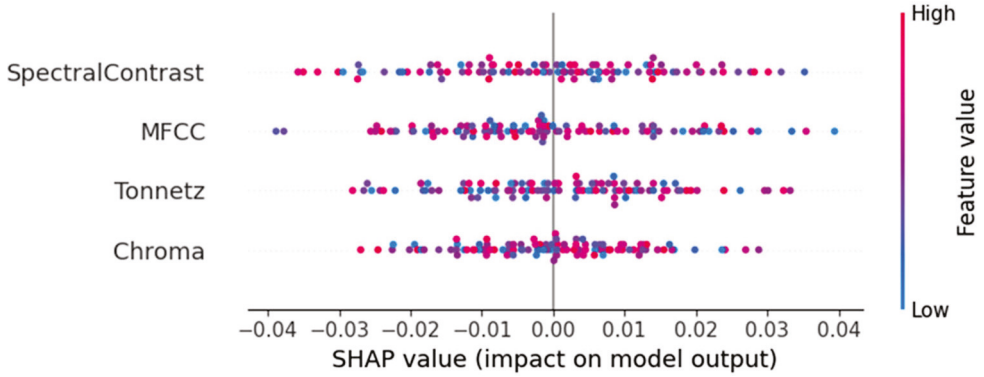

Figure 5. SHAP values for leak detection.

Figure 5 displays grouped SHAP values for the ensemble model, highlighting the relative importance of the four main acoustic feature types: MFCC, Spectral Contrast, Tonnetz, and Chroma. The MFCC group shows the widest range of SHAP values, approximately from −0.04 to +0.04, indicating that these features exert the strongest influence on the model's predictions. In contrast, Spectral Contrast ranges from −0.035 to +0.035, Tonnetz from −0.03 to +0.035, and Chroma has the smallest impact, ranging between −0.028 and +0.03. The color coding (from blue to red) represents the original feature values, and for MFCCs in particular, higher values (red dots) tend to correspond with positive SHAP values, meaning they push the prediction toward the leak class. This aligns with known acoustic leak signatures, where elevated MFCC components reflect the structured harmonic patterns of leak-induced flow. Overall, Figure 5 confirms that the ensemble model relies most heavily on MFCC-derived time–frequency features, reinforcing their diagnostic value in distinguishing leak events from normal pipeline conditions. Unlike YamNet—used without fine-tuning on audio data dominated by general ambient sounds—the developed model focuses specifically on leak acoustic signatures. It extracts domain-specific features (e.g., MFCCs capturing low-frequency harmonics of leaks), trained on labeled leak and non-leak samples—even under conditions with environmental noise. As SHAP analysis confirms, leak-specific components like $MFCC_{1–10}$ heavily influence the model's decisions, while ambient noise-related features carry low SHAP influence. This targeted feature selection and supervised training explain the superior performance and robustness of this article's model compared to YamNet.

The confusion matrix of the developed ensemble model is given in Figure 6. It is indicated that the developed model managed to detect leak and non-leak events with nearly equal efficiency. In this respect, it is conceived that 166 actual leaks and 207 actual non-leaks are accurately predicted by the developed model. In the same vein, 17 non-leak cases are identified as leak cases, besides 18 leak cases that are wrongly determined as non-leak cases.

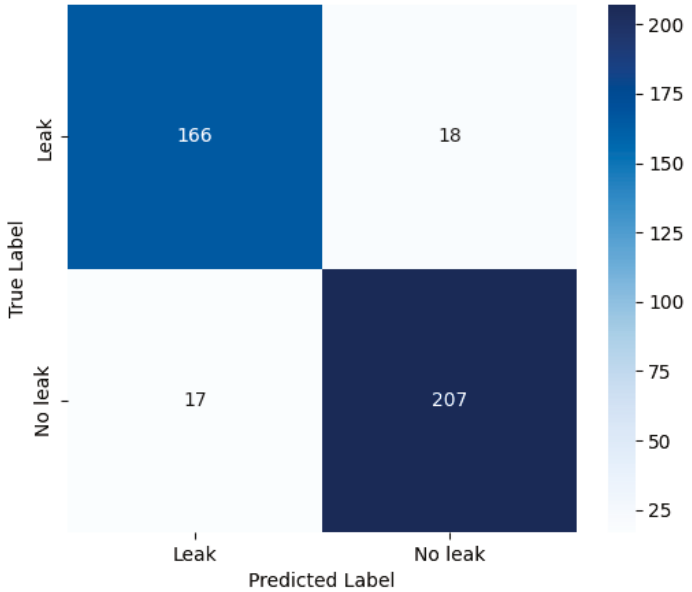

Figure 6. Confusion matrix of the developed ensemble model (voting classifier).

4. Analysis and Discussion

The results of the experiments conducted on various machine learning models for leak detection in water pipelines provide valuable insights into the performance and significance of each approach. This segment analyzes the results obtained for each tested machine

learning model and highlights their individual strengths and implications for real-world leak detection applications.

The Random Forest model gave the best results among all the tested models and achieved a high accuracy of 93.68%. The superior performance of RF can be attributed to its ensemble nature, which combines multiple decision trees and aggregates their predictions. This approach helps reduce overfitting and enhances the model's robustness. RF's ability to handle large datasets and feature interactions makes it particularly well-suited for detecting leaks in water pipelines. Its high accuracy and efficiency make it a strong candidate for real-time monitoring and early detection of leaks.

KNN performed remarkably well, achieving an accuracy of 93.40%. KNN's effectiveness lies in its ability to classify data based on the majority class of its neighboring data points in the feature space. This approach allows KNN to adapt to local patterns and perform well on non-linear data distributions. Its simplicity and ease of implementation make it an attractive choice for leak detection, particularly when spatial relationships between data points are crucial. However, KNN's performance may be sensitive to the choice of the number of neighbors (K) and the distance metric used.

MLP achieved a high accuracy of 92.15% in leak detection. As a deep learning model, MLP can capture complex patterns in the data through multiple layers of interconnected neurons. Its ability to learn hierarchical representations makes it well-suited for leak detection tasks involving large datasets and non-linear relationships. Fine-tuning and hyperparameter optimization can further enhance MLP's performance in leak detection.

Decision Tree obtained an accuracy of 77.95% in leak detection. Decision Trees are interpretable and easy to visualize, providing valuable insights into the decision-making process. However, they may suffer from overfitting and lack the complexity to capture intricate relationships within the data. To improve DT's accuracy, pruning techniques and ensemble methods, such as Random Forest, can be explored to enhance generalization capability and robustness.

SVM demonstrated a respectable accuracy of 88.97% in distinguishing between leak states and non-leak states. This model's high accuracy suggests that SVM can effectively capture patterns and features in the acoustic signals associated with leaks. SVM's ability to identify intricate boundaries between classes makes it suitable for handling complex datasets, making it a promising choice for leak detection in water pipelines. While SVM's accuracy is impressive, further optimization and tuning may be required to enhance its performance and reduce false positives or negatives.

Logistic Regression achieved an accuracy of 72.05% in leak detection. Logistic Regression is a simple and interpretable model that provides probability estimates for binary classification tasks. While it may not be as powerful as other complex models, LogR's interpretability can aid in understanding the importance of individual features in leak detection. To improve LogR's performance, feature engineering and regularization techniques can be employed to handle complex datasets more effectively.

NB, a probabilistic classifier, achieved an accuracy of 68.38% in leak detection. While the accuracy is relatively lower compared to other models, NB's simplicity and computational efficiency make it a suitable option for certain applications. NB assumes independence between features, which may not always hold in real-world scenarios, but it remains effective in certain situations with limited computational resources or when the dataset conforms to its assumptions. Further improvements in leak detection accuracy could be achieved by exploring more sophisticated feature engineering techniques that align with NB's assumptions.

The results of the experiments demonstrate the significance of each tested machine learning model for leak detection in water pipelines. By understanding the implications

of each model's performance, researchers and practitioners can make informed decisions in selecting the most suitable models for their specific leak detection needs. The results of this study show that RF stands out as the top-performing model, showcasing its potential for real-time monitoring and accurate leak detection. However, other models, such as KNN and MLP, also demonstrate promising performance, each with unique strengths and applicability. The combination of the three best-performing models in the ensemble approach further enhances the accuracy of leak detection. The ensemble model surpassed the performance of individual models, thus emphasizing the efficacy of integrating diverse perspectives to enhance detection accuracy.

The results of this study confirm the efficacy of Noise Logger-based monitoring and the potential of ensemble machine learning models for accurate leak detection in water pipelines. The ensemble model's success can be attributed to its ability to combine the strengths of different classifiers, leading to improved performance. In contrast, YamNet's lower accuracy suggests limitations in handling the complexities of the data and highlights the benefits of the proposed approach.

In conclusion, the proposed model for Noise Logger-based leak detection with ensemble machine learning offers a novel and efficient approach for real-time monitoring of water pipelines. Leveraging wireless Noise Loggers and ensemble machine learning, the proposed model achieves a high accuracy in detecting leaks, outperforming the YamNet approach. The superiority of the proposed model lies in its robustness, sensitivity to subtle pipeline changes, and reduced susceptibility to environmental noise. By utilizing acoustic signals and ensemble machine learning, the proposed model presents a promising solution for accurate and efficient leak detection, contributing to sustainable water management practices.

On the level of computational costs, the computational requirements of the ensemble model and individual machine learning models were assessed to provide insights into their practicality for deployment in resource-constrained environments. The ensemble model combines predictions from three top-performing individual models—Random Forest (RF), K-Nearest Neighbors (KNN), and Multi-Layer Perceptron (MLP). Each model has unique computational demands:

- Random Forest (RF) is relatively computationally efficient during inference but requires substantial memory for storing multiple decision trees.
- K-Nearest Neighbors (KNN) has minimal training costs but incurs significant computational overhead during inference due to the need to calculate distances from all training data points.
- Multi-Layer Perceptron (MLP) involves higher computational costs during both training and inference due to its deep learning architecture.

In comparison, the ensemble model aggregates the outputs of these individual models, which increases inference time and resource usage. For example, combining predictions requires running all three models in parallel or sequentially, depending on system design, leading to higher latency and energy consumption. However, the ensemble model's increased computational cost is justified in scenarios where high detection accuracy is critical, such as monitoring high-value infrastructure or environments prone to frequent leaks.

In the common test split, the Voting Ensemble achieved an accuracy of 94.40%, while the best single model (Random Forest) achieved 93.68%. Precision was slightly higher for the ensemble (89.78%) compared with RF (93.00%, rounded to whole percentages in Table 1). Recall was almost the same for both models, and the F1 score for the ensemble (91.00%) was slightly lower than for RF (93.00%).

To check if this small accuracy difference was real or due to chance, McNemar's test was applied to paired predictions from both models. The result was $p = 0.0987$, which is not below the significance level of 0.05. This means there is no strong statistical proof that one model is better than the other on this specific test set. However, a one-way ANOVA on cross-validated accuracies for all models gave $F \approx 496.8$, $p < 0.0001$, showing that model choice does have a big impact when results are averaged over many data splits.

The ensemble was chosen over RF not because it won in every single metric, but because it is more robust. By combining three different types of models—tree-based, instance-based, and neural—it reduces random variation in results and works more reliably across different data samples and conditions. This is especially useful when each model makes different types of detection mistakes, because the ensemble can correct them.

In practice, the extra computation for using the ensemble is very small. The three models are all fast to run, and the total prediction time per signal is less than 10 ms on a standard laptop CPU. If resources are very limited, RF alone can still be used, with only a small drop in performance.

Although the ensemble model achieved high accuracy on the Hong Kong dataset, some caution is warranted. The model may be partially tailored to the specific noise characteristics of Hong Kong urban pipelines; its performance on data from other regions or environments could be lower. Even with noise reduction, ambient noise (traffic, construction, etc.) may still affect detections in some cases. Additionally, the machine learning models (especially with multiple features) risk overfitting the training set; future work should validate the approach on independent datasets. To ensure robust generalization, it is planned to collect more diverse data (as suggested in Section 5) and to explore regularization or data augmentation. These steps would mitigate the above limitations. Additionally, while the studied dataset includes signals from multiple districts within Hong Kong, this study does not conduct a formal region-wise significance analysis. In future work, geographic stratification will be explored, and statistical tests will be applied (e.g., Chi-square or stratified ANOVA) to evaluate whether leak detection performance significantly varies by district or pipeline characteristics.

5. Conclusions

Water pipeline leaks present a critical challenge, with significant economic, environmental, and resource implications. Existing detection methods are either limited in scope or inefficient for real-world applications, necessitating innovative approaches. This study presents a pioneering approach by integrating wireless acoustic noise loggers with ensemble machine learning models to achieve real-time leak detection in water pipelines. Unlike previous studies, which often rely on laboratory datasets, this work utilizes a comprehensive dataset collected from real-world urban environments, ensuring robust and practical applicability. Accordingly, this study analyzes water pipeline leak detection using machine learning with 2110 sound signals from Hong Kong. Using acoustic noise loggers, the dataset had 992 leak signals and 1118 non-leak signals. The goal was to evaluate different machine learning algorithms for effective leak detection and sustainable water management. Results show RF as the top-performing algorithm with 93.68% accuracy. KNN and MLP also demonstrated significant accuracy, providing diverse leak detection approaches. The ensemble model, combining Random Forest, K-Nearest Neighbors, and Multi-Layer Perceptron, significantly surpassed existing approaches, including YamNet. One of the primary challenges faced by YamNet was its sensitivity to environmental noise. Unlike the proposed ensemble model, which uses carefully extracted features and noise reduction techniques, YamNet processes raw acoustic signals directly. This approach made it more susceptible to interference from urban background noise, such as traffic, construction, and other environmental sounds. These noise sources likely obscured the subtle acoustic patterns

associated with leaks, leading to reduced classification accuracy. Another limitation of YamNet is its reliance on general-purpose sound classification. YamNet was pre-trained on the AudioSet dataset, which encompasses a wide range of audio events but does not specifically target leak-induced acoustic signals in pressurized water pipelines. As a result, the model may have struggled to identify domain-specific features critical for leak detection. Furthermore, the fixed architecture of YamNet, while efficient for general-purpose tasks, lacked the flexibility to adapt to the nuances of this specialized dataset. Additionally, YamNet's reliance on a single deep-learning architecture contrasts with the ensemble approach's ability to combine the strengths of multiple models. This highlights the importance of tailoring machine learning models to specific applications, particularly when dealing with specialized datasets and challenging environmental conditions. Future work could explore domain-specific training for deep learning models or the integration of noise reduction preprocessing pipelines to mitigate these limitations.

Beyond academia, efficient leak detection has broad implications, minimizing water losses, reducing economic burdens, and preserving water resources. Real-time monitoring allows for early detection and repairs, contributing to sustainable water management. While promising, future research should explore additional features and data preprocessing. Expanding the dataset will enhance model generalizability. In conclusion, leveraging wireless noise loggers and machine learning is crucial for effective water pipeline leak detection, with the potential to revolutionize practices for sustainable water management. This study contributes to sustainable water management by providing municipalities with a cost-effective, accurate, and scalable solution for detecting water pipeline leaks. The proposed approach sets a foundation for future research and development in leveraging machine learning for real-world infrastructure challenges. By integrating real-world datasets with innovative ensemble machine learning models, this study offers a significant leap toward practical and reliable water leak detection, paving the way for smarter and more sustainable urban water management systems. On the level of future advancements, one avenue would be the integration of real-time data streams to enhance model performance in dynamic environments. Adaptive learning methods, such as online learning or reinforcement learning, could be employed to continuously update the models as new data become available, improving their accuracy and robustness over time. Additionally, expanding the dataset to include diverse geographical regions and pipeline materials would enhance the model's generalizability. These advancements would not only refine leak detection capabilities but also support the development of fully autonomous and scalable monitoring solutions for water distribution networks. One challenge is the increased computational demand when analyzing signals from extensive networks with a high density of noise loggers. The ensemble model, while accurate, requires more computational resources compared to individual models, which may limit its feasibility in resource-constrained environments. Accordingly, for city-wide implementation, the model can be integrated with an IoT-based monitoring system, where acoustic noise loggers are deployed in key junctions and transmit data to a centralized processing unit. The trained ensemble model can then be used in real time to analyze signals and flag potential leaks. Region-specific retraining or transfer learning could be applied to finetune the model to new environments, accounting for different pipe materials, ambient noise profiles, or leak typologies.

Future research should focus on addressing these scalability concerns by developing lightweight, energy-efficient models and refining data collection strategies to balance performance with practical deployment needs. Furthermore, one challenge that may arise is the increased computational demand when analyzing signals from extensive networks with a high density of noise loggers. The ensemble model, while accurate, requires more computational resources compared to individual models, which may limit its feasibility in resource-constrained environments.

Additionally, the deployment of noise loggers across large-scale systems introduces logistical challenges, including the initial investment cost, sensor maintenance, and data transmission infrastructure. Addressing these concerns may require optimizing the model for edge computing, exploring cost-effective sensor solutions to enable widespread adoption, or optimizing the model for cloud-based computing.

This research work can be expanded in the future to include a comparison of the developed ensemble model against the combined model of a convolutional neural network and a long short-term memory network. Furthermore, more experimental cases from disparate geographic locations need to be considered to test the robustness of the developed ensemble model against various noise levels and ambient conditions. From a dataset standpoint, while the dataset comprises 992 leak and 1118 non-leak samples from similar valves and pipe types across multiple regions in Hong Kong, it is critical to acknowledge that leak acoustic signatures can vary with pipe material, diameter, and pressure. As part of future work, it is paramount to conduct statistical tests or sampling stratification to confirm representativeness in more heterogeneous network sections.

Author Contributions: S.E.-Z. and E.M.A. contributed to the data analysis and manuscript writing. A.F. was responsible for data collection and writing. T.Z. provided supervision, proofreading, and critical revisions of the manuscript. All authors have read and agreed to the published version of the manuscript.

Funding: The authors gratefully acknowledge the support from the Innovation and Technology Fund (ITF), Hong Kong Special Administrative Region, under the Innovation and Technology Support Programme (ITSP), grant number ITS/067/19FP. The APC was not funded.

Data Availability Statement: The datasets generated and/or analyzed during the current study are not publicly available due to them being owned by the municipality of Hong Kong, but a sample could be made available from the corresponding author on reasonable request.

Conflicts of Interest: The authors declare no conflicts of interest.

Abbreviations

The following abbreviations are used in this manuscript:

ANN	Artificial Neural Network
AUC	Area Under the Curve
CNN	Convolutional Neural Network
DT	Decision Tree
IEEE	Institute of Electrical and Electronics Engineers
ITS	Innovation and Technology Support
ITSP	Innovation and Technology Support Programme
KNN	k-Nearest Neighbors
LSTM	Long Short-Term Memory
MEMS	Micro-Electro-Mechanical Systems
MLP	Multilayer Perceptron
NB	Naive Bayes
RF	Random Forest
ROC	Receiver Operating Characteristic
SHAP	SHapley Additive exPlanations
STFT	Short-Time Fourier Transform
SVM	Support Vector Machine
TIE	Transactions on Industrial Electronics
WSD	Water Supplies Department

Appendix A

Table A1. Hyperparameters used.

Model	Hyperparameter	Value
MLPClassifier	hidden_layer_sizes	(64, 32, 16)
	max_iter	1000
SVM	kernel	"rbf"
	C	1
	random_state	42
RandomForestClassifier	n_estimators	100
	random_state	42
VotingClassifier	estimators	MLP, SVC, RF
	voting	"hard"
KFold Cross-Validation	n_splits	2
	shuffle	True
	random_state	42
train_test_split	test_size	0.2

References

1. Chan, T.K.; Chin, C.S.; Zhong, X. Review of Current Technologies and Proposed Intelligent Methodologies for Water Distributed Network Leakage Detection. *IEEE Access* **2019**, *6*, 78846–78867. [CrossRef]
2. ADM Capital Foundation. *The Illusion of Plenty: Hong Kong's Water Security, Working Towards Regional Water Harmony*; The MIT Press: Cambridge, MA, USA, 2017.
3. Centre for Water Risk and Resilience (CWRRR). *International Lessons to Manage Hong Kong's 7 Billion Dollar Water Loss Problem*; CWRRR: Hong Kong SAR, China, 2025.
4. Water Supplies Department (WSD). *Total Water Management Strategy: Strategy for Sustainable Water Supply in Hong Kong*; WSD: Hong Kong SAR, China, 2019.
5. Water Supplies Department. *Leakage Rate of Government Mains*; Water Supplies Department: Hong Kong SAR, China, 2025.
6. Government of the Hong Kong Special Administrative Region. *LCQ14: Handling Water Mains Leakage*; Government of the Hong Kong: Hong Kong SAR, China, 2025.
7. Cody, R.; Harmouche, J.; Narasimhan, S. Leak Detection in Water Distribution Pipes Using Singular Spectrum Analysis. *Urban Water J.* **2018**, *15*, 636–644. [CrossRef]
8. Water Supplies Department (WSD). *Guideline on Leak Detection on Underground Communal Service of Housing Estates*; WSD: Hong Kong SAR, China, 2017.
9. El-Zahab, S.; Zayed, T. Leak Detection in Water Distribution Networks: An Introductory Overview. *Smart Water* **2019**, *4*, 5. [CrossRef]
10. El-Zahab, S.; Abdelkader, E.M.; Zayed, T. An Accelerometer-Based Leak Detection System. *Mech. Syst. Signal Process.* **2018**, *108*, 276–291. [CrossRef]
11. Awwad, A.; Yahyia, M.; Albasha, L.; Mortula, M.M.; Ali, T. Communication Network for Ultrasonic Acoustic Water Leakage Detectors. *IEEE Access* **2020**, *8*, 29954–29964. [CrossRef]
12. Yahia, M.; Gawai, R.; Ali, T.; Mortula, M.M.; Albasha, L.; Landolsi, T. Non-Destructive Water Leak Detection Using Multitemporal Infrared Thermography. *IEEE Access* **2021**, *9*, 72556–72567. [CrossRef]
13. Wang, C.; Olson, M.; Doijkhand, N.; Singh, S. A Novel DdTS Technology Based on Fiber Optics for Early Leak Detection in Pipelines. In Proceedings of the International Carnahan Conference on Security Technology, Orlando, FL, USA, 24–27 October 2016.
14. Atef, A.; Zayed, T.; Hawari, A.; Khader, M.; Moselhi, O. Multi-Tier Method Using Infrared Photography and GPR to Detect and Locate Water Leaks. *Autom. Constr.* **2016**, *61*, 162–170. [CrossRef]
15. Li, S.; Song, Y.; Zhou, G. Leak Detection of Water Distribution Pipeline Subject to Failure of Socket Joint Based on Acoustic Emission and Pattern Recognition. *Measurement* **2018**, *115*, 39–44. [CrossRef]
16. Martini, A.; Troncossi, M.; Rivola, A. Leak Detection in Water-Filled Small-Diameter Polyethylene Pipes by Means of Acoustic Emission Measurements. *Appl. Sci.* **2017**, *7*, 2. [CrossRef]
17. Shukla, H.; Piratla, K.R.; Atamturktur, S. Influence of Soil Backfill on Vibration-Based Pipeline Leakage Detection. *J. Pipeline Syst. Eng. Pract.* **2020**, *11*, 04019055. [CrossRef]
18. Butterfield, J.D.; Meruane, V.; Collins, R.P.; Meyers, G.; Beck, S.B. Prediction of Leak Flow Rate in Plastic Water Distribution Pipes Using Vibro-Acoustic Measurements. *Struct. Heal. Monit.* **2018**, *17*, 959–970. [CrossRef]

19. Brennan, M.J.; Karimi, M.; Almeida, F.C.L.; De Lima, F.K.; Ayala, P.C.; Obata, D.; Paschoalini, A.T.; Kessissoglou, N. On the Role of Vibro-Acoustics in Leak Detection for Plastic Water Distribution Pipes. *Procedia Eng.* **2017**, *199*, 1350–1355. [CrossRef]
20. Long, R.; Cawley, P.; Lowe, M. Acoustic Wave Propagation in Buried Iron Water Pipes. *Proc. R. Soc. A Math. Phys. Eng. Sci.* **2003**, *459*, 2749–2770. [CrossRef]
21. Khalifa, A.E.; Chatzigeorgiou, D.M.; Youcef-Toumi, K.; Khulief, Y.A.; Ben-Mansour, R. Quantifying Acoustic and Pressure Sensing for In-Pipe Leak Detection. In Proceedings of the ASME 2010 International Mechanical Engineering Congress and Exposition, Vancouver, BC, Canada, 12–18 November 2010; Volume 13: Sound, Vibration and Design. ASME: New York, NY, USA; pp. 489–495.
22. de Almeida, F.C.L.; Brennan, M.J.; Joseph, P.F.; Dray, S.; Whitfield, S.; Paschoalini, A.T. Measurement of Wave Attenuation in Buried Plastic Water Distribution Pipes. *Strojniški Vestn. J. Mech. Eng.* **2015**, *60*, 298–306. [CrossRef]
23. Xu, J.; Chai, K.T.C.; Wu, G.; Han, B.; Wai, E.L.C.; Li, W.; Yeo, J.; Nijhof, E.; Gu, Y. Low-Cost, Tiny-Sized MEMS Hydrophone Sensor for Water Pipeline Leak Detection. *IEEE Trans. Ind. Electron.* **2019**, *66*, 6374–6382. [CrossRef]
24. Leal Sousa, R.; Vargas, E.; Chaminé, H.I.; Ribeiro e Sousa, L.; Karam, K. Risk Assessment on Landslides Focused on the Role of the Water: Examples from Model Regions (Rio de Janeiro State and Hong Kong). *SN Appl. Sci.* **2021**, *3*, 423. [CrossRef]
25. Visvikis, D.; Cheze Le Rest, C.; Jaouen, V.; Hatt, M. Artificial Intelligence, Machine (Deep) Learning and Radio(Geno)Mics: Definitions and Nuclear Medicine Imaging Applications. *Eur. J. Nucl. Med. Mol. Imaging* **2019**, *46*, 2630–2637. [CrossRef]
26. Shen, Y.; Cheng, W. A Tree-Based Machine Learning Method for Pipeline Leakage Detection. *Water* **2022**, *14*, 2833. [CrossRef]
27. Tariq, S.; Hu, Z.; Zayed, T. Micro-Electromechanical Systems-Based Technologies for Leak Detection and Localization in Water Supply Networks: A Bibliometric and Systematic Review. *J. Clean. Prod.* **2021**, *289*, 125751. [CrossRef]
28. Ullah, N.; Siddique, M.F.; Ullah, S.; Ahmad, Z.; Kim, J.M. Pipeline Leak Detection System for a Smart City: Leveraging Acoustic Emission Sensing and Sequential Deep Learning. *Smart Cities* **2024**, *7*, 2318–2338. [CrossRef]
29. Siddique, M.F.; Ahmad, Z.; Kim, J.M. Pipeline Leak Diagnosis Based on Leak-Augmented Scalograms and Deep Learning. *Eng. Appl. Comput. Fluid Mech.* **2023**, *17*, 2225577. [CrossRef]
30. Ullah, S.; Ullah, N.; Siddique, M.F.; Ahmad, Z.; Kim, J.M. Spatio-Temporal Feature Extraction for Pipeline Leak Detection in Smart Cities Using Acoustic Emission Signals: A One-Dimensional Hybrid Convolutional Neural Network–Long Short-Term Memory Approach. *Appl. Sci.* **2024**, *14*, 10339. [CrossRef]
31. Kang, J.; Park, Y.-J.; Lee, J.; Wang, S.-H.; Eom, D.-S. Novel Leakage Detection by Ensemble CNN-SVM and Graph-Based Localization in Water Distribution Systems. *IEEE Trans. Ind. Electron.* **2018**, *65*, 4279–4289. [CrossRef]
32. Ravichandran, T.; Gavahi, K.; Ponnambalam, K.; Burtea, V.; Mousavi, S.J. Ensemble-Based Machine Learning Approach for Improved Leak Detection in Water Mains. *J. Hydroinform.* **2021**, *23*, 307–323. [CrossRef]
33. El-Zahab, S.; Asaad, A.; Mohammed Abdelkader, E.; Zayed, T. Collective Thinking Approach for Improving Leak Detection Systems. *Smart Water* **2016**, *2*, 3. [CrossRef]
34. Babu, P.A.; Siva Nagaraju, V.; Vallabhuni, R.R. Speech Emotion Recognition System with Librosa. In Proceedings of the 2021 10th IEEE International Conference on Communication Systems and Network Technologies (CSNT), Bhopal, India, 18–19 June 2021; IEEE: New York, NY, USA, 2021; pp. 421–424.
35. Quy, T.B.; Kim, J.M. Leakage Detection of Water-Induced Pipelines Using Hybrid Features and Support Vector Machines. In *Advances in Computer Communication and Computational Sciences: Proceedings of IC4S 2018*; Springer: Singapore, 2019; pp. 377–387.
36. Barakat, N.; Hajeir, L.; Alattal, S.; Hussein, Z.; Awad, M. Air Leaks Fault Detection in Maintenance Using Machine Learning. *J. Qual. Maint. Eng.* **2024**, *30*, 391–408. [CrossRef]
37. Zadkarami, M.; Safavi, A.A.; Taheri, M.; Salimi, F.F. Data Driven Leakage Diagnosis for Oil Pipelines: An Integrated Approach of Factor Analysis and Deep Neural Network Classifier. *Trans. Inst. Meas. Control* **2020**, *42*, 2708–2718. [CrossRef]
38. Mohammed, K.K.; El-Latif, E.I.A.; El-Sayad, N.E.; Darwish, A.; Hassanien, A.E. Radio Frequency Fingerprint-Based Drone Identification and Classification Using Mel Spectrograms and Pre-Trained YAMNet Neural. *Internet Things* **2023**, *23*, 100879. [CrossRef]
39. Gemmeke, J.F.; Ellis, D.P.; Freedman, D.; Jansen, A.; Lawrence, W.; Moore, R.C.; Plakal, M.; Ritter, M. Audio set: An ontology and human-labeled dataset for audio events. In Proceedings of the 2017 IEEE International Conference on Acoustics, Speech and Signal Processing (ICASSP), New Orleans, LA, USA, 5–9 March 2017; IEEE: New York, NY, USA, 2017; pp. 776–780.
40. Hershey, S.; Chaudhuri, S.; Ellis, D.P.; Gemmeke, J.F.; Jansen, A.; Moore, R.C.; Plakal, M.; Platt, D.; Saurous, R.A.; Seybold, B.; et al. CNN architectures for large-scale audio classification. In Proceedings of the 2017 IEEE International Conference on Acoustics, Speech and Signal Processing (ICASSP), New Orleans, LA, USA, 5–9 March 2017; IEEE: New York, NY, USA, 2017; pp. 131–135.

Disclaimer/Publisher's Note: The statements, opinions and data contained in all publications are solely those of the individual author(s) and contributor(s) and not of MDPI and/or the editor(s). MDPI and/or the editor(s) disclaim responsibility for any injury to people or property resulting from any ideas, methods, instructions or products referred to in the content.

water

MDPI

Article

Predictive Rehabilitation of Clean Water Customer Connections Leveraging Machine Learning Algorithms and Failure Time Series Data

Milad Latifi [1], Shahab Sharafodin [2,*] and MohammadAmin Gheibi [3]

[1] Datatecnics, Anchorage One, Media City, Salford M50 3YL, UK; milad.latifi@yahoo.com
[2] Faculty of Civil and Environmental Engineering, Tarbiat Modares University, Tehran P.O. Box 14115-143, Iran
[3] School of Civil Engineering, Faculty of Engineering, University of Tehran, Tehran 1417613131, Iran; amingheibi@ut.ac.ir
* Correspondence: s_sharafodin@modares.ac.ir

Abstract

Failures in clean water service lines can disrupt supply, increase operational costs, and reduce customer satisfaction. This study develops a machine learning framework to predict such failures, providing a proactive tool for utility asset management. A case study was conducted on a water distribution network in Tehran, serving approximately 205,000 customers, with 11 years of service line data and over 88,000 recorded failures. Service line attributes, including length, diameter, material, age, demand, and pressure, were combined with historical failure data to train Random Forest, Extreme Gradient Boosting, and Long Short-Term Memory models. Model performance was assessed using F1-score, AUC-ROC, and AUC-PRC. A novel metric was introduced to quantify failure reduction when prioritising replacements. The results demonstrate that machine learning can effectively capture complex relationships between service line features and failures, offering significant benefits for tactical maintenance planning. This research underscores the potential of predictive approaches to improve reliability and reduce costs.

Keywords: failure prediction; machine learning; water service lines; predictive asset management

1. Introduction

Water distribution networks (WDNs) are essential infrastructure systems that transport treated potable water from treatment facilities to end users, including households, businesses, and industries. These systems typically consist of a network of interconnected pipes, pumps, valves, storage reservoirs, and service lines, all working together to ensure a reliable water supply. Ensuring the effective operation and maintenance of WDNs is crucial for public health, economic stability, and environmental protection. As WDNs age, maintaining them has become increasingly challenging, especially given the global trend of ageing infrastructure [1–4]. The importance of maintaining a WDN lies in its role in preventing issues such as water contamination, pressure imbalances, and supply shortages. Failures in the system, such as pipe bursts, leaks, and valve malfunctions, can lead to substantial water losses, infrastructural damage, and disruptions to essential services. Such failures often result from material degradation, external interference, or operational stress, highlighting the need for robust maintenance strategies [5–7]. Historically, reactive maintenance has been the predominant approach to managing water network failures, where

issues are addressed only after they occur. However, this approach often leads to higher costs, increased water loss, and service interruptions [8–10]. In contrast, predictive maintenance, which leverages data-driven techniques such as using sensors, pressure monitoring, and analytics, is emerging as a more efficient and proactive solution [11–13]. By predicting potential failures and addressing them before they escalate, predictive maintenance reduces operational costs and enhances system reliability [14–17].

The prediction of water pipe failures has evolved significantly, advancing from traditional statistical models to more sophisticated data-driven and machine learning (ML) approaches. This shift is driven by the increasing complexity of water distribution systems and the pressing need for more accurate predictive maintenance strategies [18]. In the early stages, statistical models, such as those based on Weibull and lognormal distributions, were widely used to predict pipe failures. These models primarily relied on historical failure data to forecast future events, providing a foundational method for understanding the structural deterioration of water mains. However, the reliability of such models was highly dependent on the availability and quality of historical data, posing challenges when data were scarce or incomplete. Studies have highlighted these limitations, noting the reduced accuracy of predictions under such conditions [19–21].

With advancements in technology, machine learning techniques have emerged as more effective tools for failure prediction in WDNs. Models such as Artificial Neural Networks (ANNs) and Support Vector Machines (SVMs) have been successfully applied to analyse complex patterns in operational data, enhancing the predictive accuracy of these systems [22–25]. Later, more advanced ML models, including tree-based models such as Random Forest (RF) and eXtreme Gradient Boosting (XGB), demonstrated improved performance in water pipe failure predictions [26]. Comparisons between traditional statistical models and ML approaches have shown that the latter, particularly tree-based models, often outperform earlier methods in predicting individual pipe failures [27,28].

Ensemble models, which combine multiple ML algorithms, have become essential for enhancing failure prediction accuracy in WDNs. These models often integrate supervised and unsupervised techniques, leveraging the strengths of each. For example, clustering (unsupervised) groups pipes based on failure patterns, while regression or classification (supervised) predicts the likelihood of failure [29]. Stacking, a common ensemble method, combines predictions from multiple models using a meta-learner, increasing overall accuracy and robustness, particularly in scenarios with high variability or noisy data [30].

In recent years, the integration of ML models with traditional statistical and physical models has further enhanced predictive capabilities. Combining these methods has been shown to improve the accuracy of condition predictions for water pipes, particularly in cases involving corrosion depth or structural degradation [31–34]. Additionally, optimised inspection schedules can now be developed using ML models, aiding maintenance planning by accurately predicting failure risks [17,35]. The use of diverse data sources, including environmental factors and historical failure records, has also refined predictive models, with techniques such as AutoML playing a crucial role in these advancements [13,36].

Although models have been developed for the condition assessment and failure prediction of mains, little attention has been given to failures in service lines. Service lines are small-diameter pipes branching from mains to deliver water to individual customers. The primary causes of service line failures include the use of low-quality materials, improper installation, and age-related deterioration. In most countries, the section of the service line between the main and the property boundary (public service line) is owned by the utility, while the remaining section within the property (private service line) is the responsibility of the customer. Although it is the customer's duty to address failures or leaks on the private line, such issues can still lead to supply disruptions on the customer's side. Therefore,

https://doi.org/10.3390/w18010110

investigating the failure modes of service lines and implementing predictive maintenance for these assets is essential.

The likelihood of failures in service lines is influenced by factors such as pipe material, age, diameter, service pressure, flow rate, and other hydraulic characteristics [37]. Additionally, water quality and microbiological factors are known contributors to many failures [38]. Service lines are also vulnerable to environmental conditions, including bedding quality, soil corrosivity, soil stability, stray electrical currents, and temperature fluctuations, particularly freezing soil. Other common causes of failure include external damage from third parties, such as contractors accidentally striking water pipes during excavation, as well as issues stemming from improper installation and inadequate installation supervision [39].

A recent survey of case study WDNs in various countries revealed significant differences in the proportion of total water network failures attributed to service lines.

In the UK and Italy, service lines account for less than 30% of total failures, whereas in Tokyo, Taiwan, the Philippines, Jordan, and New Zealand, this figure exceeds 80% [40]. In the US, Lee and Meehan [41] developed a model for predicting service line failures using nine years of failure data. They tested several statistical distributions, including exponential, Weibull, and lognormal, finding the Weibull distribution to be the most effective for generating survival functions across different pipe materials and ages. Their findings revealed distinct survival rates depending on material, with certain types, such as lead and copper, generally lasting longer than materials like polyethylene. Van Hecke [42] compared the benefits of using 316-stainless steel corrugated pipes for service lines with those of polyethylene pipes. For a life cycle cost analysis, they estimated the failure likelihood for service lines made from these materials by calculating the ratio of failures to the total number of service lines. Their findings reported a failure rate of 0.003 (failures per year) for the Tokyo WDN and 0.001 (failures per year) for an Australian utility. The analysis, however, did not account for additional factors such as pipe diameter, age, and other variables beyond material type.

Although many studies have focused on predicting failures in water mains, failures in service lines remain insufficiently understood and poorly predicted, despite their major contribution to overall network failures and customer disruptions. Existing models often rely on incomplete data and are not designed for the unique characteristics of service lines, such as material variability, installation quality, and environmental influences. This gap highlights the need for a reliable, data-driven predictive framework that can identify high-risk service lines and support proactive maintenance planning.

In this research, a machine-learning-based predictive maintenance model is developed to forecast failures in service lines, representing the main contribution of the study. The objectives of the research are as follows: (1) developing a predictive maintenance model using machine learning algorithms to predict service line failures; (2) enabling proactive decision-making by estimating the likelihood of service line failures; (3) supporting asset managers and utility operators in formulating short-, medium-, and long-term preventive investment plans; and (4) reducing supply interruptions and enhance the reliability of water distribution systems.

The article is organised as follows: The first section presents the introduction and literature review. The case study section focuses on a part of Tehran water distribution network. The methodology section details the machine learning modelling employed in the study. The results section highlights the findings and analyses, while the discussion section examines why the models behave as observed, data limitations, comparisons of model performance, and implications for utilities. Finally, the last section provides the conclusions and highlights the key findings, practical applications, and limitations of the study for water utilities.

https://doi.org/10.3390/w18010110

2. Case Study

To evaluate the performance of the proposed approaches, they were applied to the public service lines in a case study WDN in Tehran, Iran. This case study was chosen because service line failures accounted for 98% of all recorded bursts. Specifically in 2023, Only 100 out of more than 6000 failures involved the mains; the rest occurred on service lines. This network spans 1400 km of pipes across an 80 km^2 area, serving a population of approximately 1.5 million, equivalent to nearly 205,000 customers. The high number of people per customer is due to the use of a shared service line for all properties within a single building. The WDN has a total demand of around 4 m^3/s, supplied by 10 separate service reservoirs.

Customer data primarily includes information on the length, diameter, material type, installation date, and elevation of service lines. The utility had a calibrated and up-to-date hydraulic model, allowing for the determination of maximum and minimum daily pressures at each service line. Additionally, historical billing data was used to establish the minimum and peak demand for each service line. Figure 1a shows the distribution of service line lengths, with more than half of the pipes measuring between 6 and 12 metres. Figure 1b illustrates the installation years of the service lines, with a significant number installed between 1986 and 1994, indicating a period of rapid development in the area. Another phase of WDN expansion occurred between 2000 and 2004, as reflected in Figure 1b.

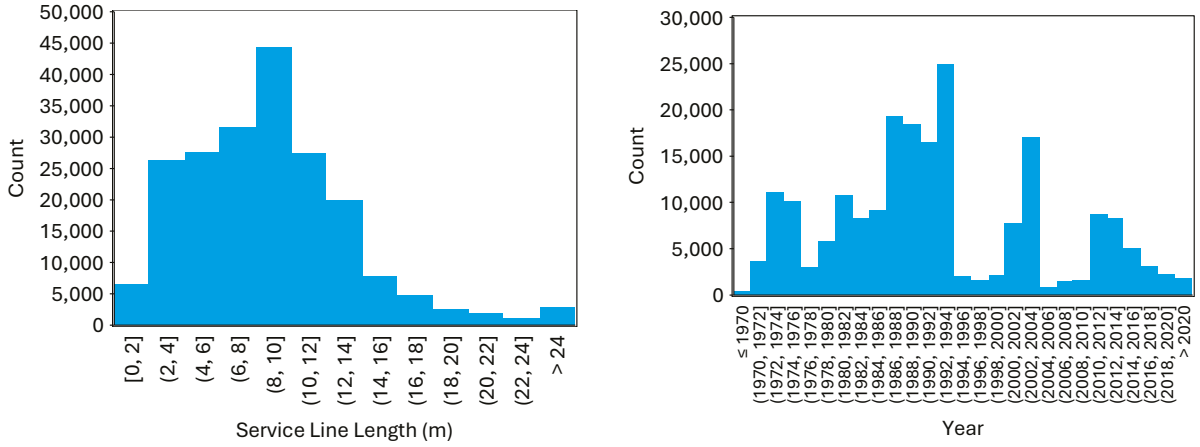

Figure 1. Distribution of service lines (**a**) length; and (**b**) year of installation.

Table 1 presents the distribution of the service lines based on their diameter and material. Around 80% of the service lines have a diameter of 1/2″ (12.7 mm), 15% a diameter of 3/4″, and only 5% are 1″ or larger. Half of the service lines are made of ductile iron (older generation), more than 30% were made of Polyethylene (newer generation), and 20% were made of other materials.

Figure 2a illustrates the distribution of minimum and maximum pressures across service lines. Over 50% of customers experience a minimum daily pressure between 15 and 25 m, while the maximum daily pressure shows a more even distribution. Furthermore, more than 88,000 failures were recorded in work orders between 2013 and 2023. Figure 2b displays the reported number of service line failures over this period. Excluding 2013, which contains incomplete data, the trend shows a general decline. The utility attributes this improvement primarily to the implementation of pressure management programmes, regular replacement of ageing service lines, fewer supply interruptions, and advancements in materials quality.

https://doi.org/10.3390/w18010110

Table 1. Distribution of the service lines based on their diameter and material.

Service Line Size	Percentage	Material	Percentage
1/2″ (12.7 mm)	79.50	Asbestos Cement	5.78
3/4″ (19.05 mm)	15.07	Cast Iron	12.05
1″ (25.4 mm)	4.48	Copper	1.71
1 1/2″ (38.1 mm)	0.77	Ductile Iron	48.92
2″ (50.8 mm)	0.14	Galvanised Iron	0.02
3″ (76.2 mm)	0.034	Polyethylene	31.30
4″ (101.6 mm)	0.008	Polyvinyl Chloride	0.13
6″ (152.4 mm)	0.002	Steel	0.10

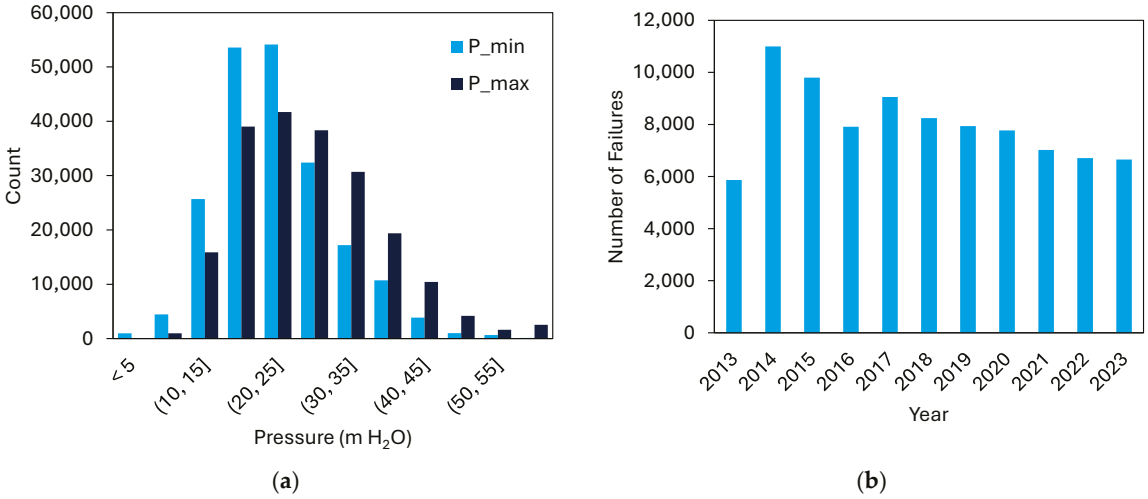

(**a**) (**b**)

Figure 2. (**a**) Distribution of service lines based on their minimum and maximum daily pressure; and (**b**) number of service line failures between 2013 and 2023.

3. Methodology

In this study, machine learning models were developed to predict the likelihood of failure (LoF) in service lines. The models were trained using service line failure data, capturing the complex relationships between service line attributes—such as length, age, diameter, material, demand, and pressure—and the LoF. Figure 3 presents the flowchart of the methodology used in this research. Failure data from 2013 to 2021 were used to train the classification models, which predict whether a pipe is likely to fail in the future.

To assess the impact of training data length on prediction accuracy, the training process was repeated eight times using datasets spanning 2 to 9 years. For example, failure data from 2013 to 2014 were used for the 2-year training, while data from 2013 to 2021 were used for the 9-year training. In all cases, failures occurring in 2022–2023 were used to validate the predictions.

3.1. Data Preparation

The utilised dataset comprised two distinct sub-datasets, as follows:

1. Asset Data: This dataset contained comprehensive details about the service line pipes, including the customer's unique ID number, as well as the diameter, length, age, installation depth, and material type of the service line. As outlined in the Case Study section, minimum and maximum pressures for each customer, obtained from the hydraulic model, were incorporated into the dataset. Historical customer data was also utilised to include the monthly consumption (demand) for each customer. Additionally, the dataset provided information on the reservoir supplying each service line and the diameter and material of the main pipe connected to it.

https://doi.org/10.3390/w18010110

2. Failure Data: This contained records of failures occurring on the service lines, including the customer's ID number, pipe diameter, and details of each failure, such as the date, type, and cause. Each failure was uniquely identified by the customer ID number, linking it to the corresponding asset data.

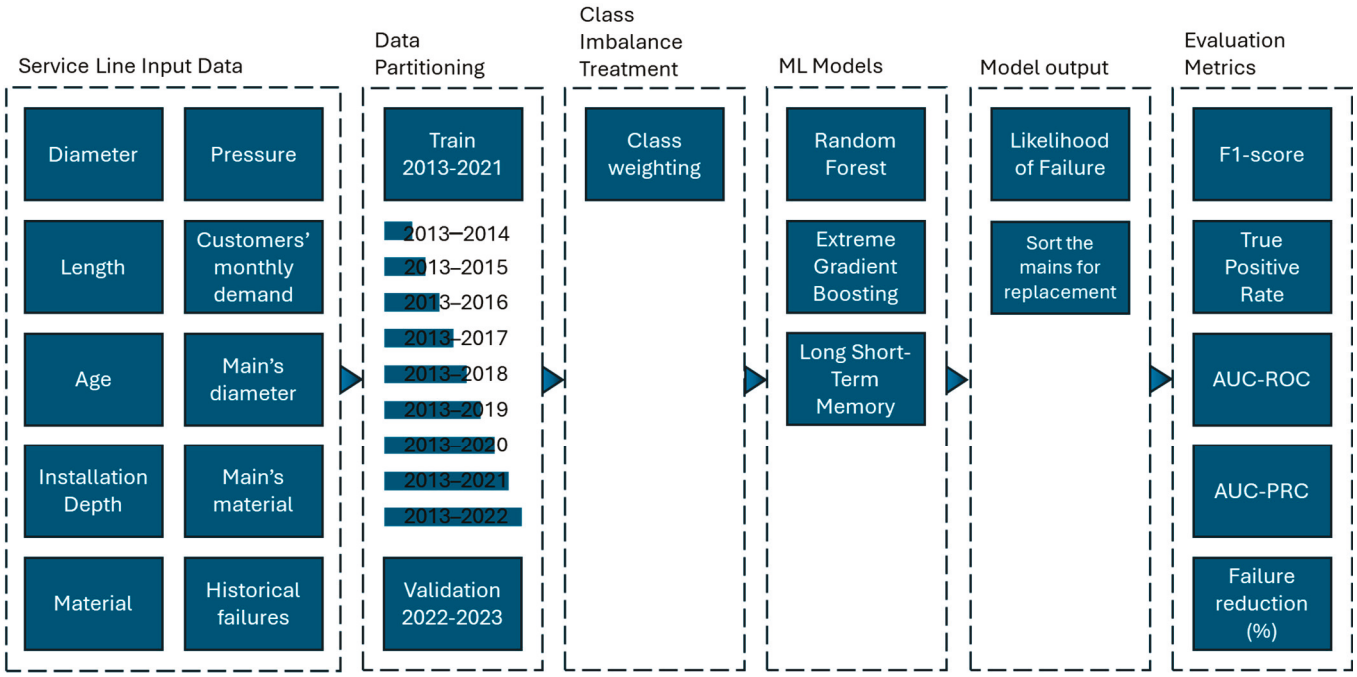

Figure 3. Flowchart of the methodology in the present study.

To streamline the modelling process, these two datasets were merged into a single comprehensive dataset. This integration enabled the identification of the number of incidents associated with each service line in the asset data for each year. Ultimately, event entries for each year were classified as binary, as multiple records for the same pipe within a single year likely indicate recurring incidents or repairs.

3.2. Classification

Classifiers are machine learning algorithms designed to learn from a subset of data and categorise unseen data into specific classes. These algorithms are widely used across various domains. In this research, Random Forest, Extreme Gradient Boosting, and Long Short-Term Memory models were employed to predict failures in service line pipes. Although the model prediction performance is evaluated in a two-year period, the purpose of this study is not to predict the exact timing of failures within a specified future time horizon. Instead, the models estimate the likelihood of failure based on historical asset attributes and failure records. The classification output indicates relative failure risk rather than a time-to-failure prediction.

3.2.1. Random Forest

Random Forest (RF) is an ensemble machine learning method commonly used for classification and regression tasks, built on the principle of aggregating multiple decision trees [43]. Ensemble algorithms are generally categorised into three types: bagging, boosting, and stacking. Bagging involves generating several individual estimators and combining their predictions through averaging (for regression) or majority voting (for classification) to produce the final ensemble prediction. Random Forest is a well-known example of a bagging technique [44].

https://doi.org/10.3390/w18010110

Conventional regression trees often suffer from overfitting, which leads to poor generalisation performance on unseen data [45]. Random Forest mitigates this issue by introducing randomness into the tree-building process. This is achieved by selecting a random subset of features at each split within the tree structure. The individual decision trees, trained on different subsets of data, are then combined to form a robust predictor. Predictions are made by averaging the outputs of the individual trees [43]. RF was selected for its ability to model complex nonlinear relationships in structured asset data while remaining robust to noise and overfitting [27,28].

3.2.2. Extreme Gradient Boosting

Extreme Gradient Boosting (XGB) is a highly efficient machine learning algorithm that combines the predictions of multiple weak tree models into a robust linear ensemble [46]. The final prediction output of the model is expressed as:

$$G(\mathbf{X}_i) = \sum_{k=1}^{r} g_k(\mathbf{X}_i) \quad (1)$$

where $G(\mathbf{X}_i)$ is the final prediction for sample i; $g_k(\mathbf{X}_i)$ is the contribution of the k-th stump; and r is the number of iterations.

While derived from Gradient Boosted Decision Trees (GBDT), XGB offers significant enhancements in two key aspects:

1. Optimisation Efficiency: XGB uses a second-order Taylor expansion to compute the loss function, allowing for faster and more accurate optimisation compared to the first-order approximation used by GBDT.
2. Overfitting Control: XGB incorporates a regularised model formulation, which helps manage overfitting and allows for adjustable model complexity, resulting in improved performance [47].

As with many machine learning models, XGB requires hyperparameter tuning to optimise its performance. XGB was chosen for its high predictive accuracy on tabular datasets and its effectiveness in handling imbalanced failure data through boosted learning and regularisation [46,47]. Given the large scale of the dataset in this research, XGB was selected as the preferred model for its efficiency and scalability.

3.2.3. Long Short-Term Memory

In this study, a Long Short-Term Memory (LSTM) model was used to classify service line failures based on available features of the pipes. The input data $X \in R^{n \times m}$, where n is the number of samples and m is the number of features, is reshaped into a 3-dimentional format $X_{LSTM} \in R^{n \times 1 \times m}$ to match the LSTM's input structure.

The LSTM processes the data sequentially by updating its internal state h_t at each time step t based on the current input x_t and the pervious hidden state h_{t-1}. The key operations in an LSTM cell, such as the forget gate, input gate, and cell state updates, allow it to capture long term dependencies in the data. Applying the three mentioned functions, the internal state at each time step can be calculated as:

$$h_t = o_t \odot \tanh(C_t), \quad \text{where } C_t = f_t \odot C_{t-1} + i_t \odot \widetilde{C}_t \quad (2)$$

where f_t is the forget gate which decides how much of the pervious cell state C_{t-1} to retain. i_t is the input gate which determines how much new information $\widetilde{C}_t$ from the current input x_t should be added to the cell state. o_t as known as output gate, controls how much of the cell state C_t is passed to the hidden state h_t. $\odot$ is element-wise (Hadamard) product of two matrices.

https://doi.org/10.3390/w18010110

After processing the input, a fully connected layer with a sigmoid activation function produces a probability $\hat{y} = \sigma(W \cdot h_t + b)$, where $\hat{y} \in [0, 1]$ represents the predicted probability of failure; σ represents the sigmoid activation function:

$$\sigma(z) = \frac{1}{1 + e^{-z}} \tag{3}$$

This function maps the input, z, to a range between 0 and 1, which is interpreted as a likelihood. W is a weight matrix that connects the hidden state h_t to the output layer. It defines how the hidden state contributes to the prediction. b is a bias term added to the linear transformation to provide flexibility in fitting the model.

The model is trained by minimising the binary cross-entropy loss:

$$L(y, \hat{y}) = -\frac{1}{n}\sum_{i=1}^{n}(y_i \log(\hat{y}_i) + (1 - y_i)\log(1 - \hat{y}_i)) \tag{4}$$

where y_i is true label for sample i; $\hat{y}_i$ is the predicted probability sample i, between 0 and 1, and n is the total number of samples in the training data [48,49].

LSTM is a robust algorithm designed for training on time-series data, making it particularly suitable for failure prediction in water pipes. Its ability to capture temporal dependencies, learn patterns from historical failure data, and detect subtle anomalies enables it to identify potential future failures effectively [50]. LSTM is theoretically well suited to this problem because service line failures exhibit temporal dependence, where past failure events and time-varying attributes influence future failure likelihood.

3.3. Data Partitioning and Treatment

To reflect the temporal nature of asset failures and avoid information leakage, the dataset was split chronologically into training and validation sets. Historical failure records from 2013 to 2021 were used for model training, while failures occurring between 2022 and 2023 were reserved as an unseen validation dataset. In this study, the temporal dimension is incorporated through the progressive expansion of the training period rather than through explicit multi-time-step sequence construction at the individual pipe level. To investigate the effect of training data length on model performance, multiple training windows were considered, ranging from 2 to 9 years. For example, the 2-year split included failures from 2013 to 2014, whereas the 9-year split covered the full 2013 to 2021 period. The validation dataset remained identical across all experiments to ensure consistent and comparable performance evaluation.

Cross-validation was not applied in this study due to the temporally ordered nature of the failure data. Random or repeated data splitting can lead to information leakage by allowing future observations to influence model training. Instead, a strict chronological split was adopted to reflect real-world deployment, where models are trained on historical data and applied to predict future failures.

The failure prediction problem is inherently imbalanced, with non-failure instances significantly outnumbering failures. To address this issue, a class weighting approach was adopted. Higher weights were assigned to the minority failure class during model training, increasing its contribution to the loss function. This encouraged the models to pay greater attention to failure events and improved their ability to identify high-risk service lines without altering the original data distribution. The class weighting was only applied to train dataset.

https://doi.org/10.3390/w18010110

3.4. Evaluation of Binary Classifiers

To assess the accuracy of predictions in binary classification, four key elements are considered: true positives (*TP*), false negatives (*FN*), false positives (*FP*), and true negatives (*TN*).

- True Positives (*TP*): Instances correctly predicted as positive.
- False Negatives (*FN*): Positive instances incorrectly predicted as negative.
- False Positives (*FP*): Negative instances incorrectly predicted as positive.
- True Negatives (*TN*): Instances correctly predicted as negative.

These elements are commonly visualised in a confusion matrix (Figure 4), which provides a clear summary of the model's classification performance.

Confusion Matrix		Predict Class	
		Positive	Negative
Actual Class	Positive	TP	FN
	Negative	FP	TN

Figure 4. A confusion matrix, presenting four key states regarding actual classes and prediction classes.

The F1-score is a metric used to evaluate the performance of a binary classification model by considering both precision and recall. Precision is the proportion of correctly predicted positive instances among all predicted positives:

$$\text{Precision} = \frac{TP}{TP + FP} \tag{5}$$

Recall is the proportion of correctly predicted positive instances among all actual positives:

$$\text{Recall} = \frac{TP}{TP + FN} \tag{6}$$

The F1-score is given as the harmonic mean of precision and recall, expressed mathematically as:

$$\text{F1-score} = 2 \times \frac{\text{Precision} \times \text{Recall}}{\text{Precision} + \text{Recall}} \tag{7}$$

This metric is particularly useful for imbalanced datasets, as it provides a balanced measure that accounts for both false positives and false negatives. A higher F1-score indicates better model performance, with a value of 1 representing perfect precision and recall.

The Receiver Operating Characteristic (ROC) curve is a graphical tool used to evaluate the performance of a binary classification model. It plots the True Positive Rate (*TPR*) also known as Sensitivity, against the False Positive Rate, *FPR*, which is equal to $1 - Specificity$, across various threshold levels. True Positive Rate ($TPR = TP/(FP + TN)$) is the proportion of actual positives correctly identified by the model, while False Positive Rate ($FPR = FP/(FP + TN)$) is the proportion of actual negatives incorrectly classified as positives. The ROC curve demonstrates the model's ability to distinguish between the two classes. An ideal classifier would have a point at the top-left corner of the plot ($TPR = 1$, $FPR = 0$), indicating perfect performance, while a random classifier would produce a di-

https://doi.org/10.3390/w18010110

agonal line. This makes the ROC curve a valuable tool for comparing and assessing classification models [51].

The Area Under the Curve (AUC) provides a single summary value of the ROC curve, where a value of 1 indicates a perfect model and 0.5 represents random chance. AUC-ROC is widely used to assess the performance of classification models. However, it has been shown to be biassed when dealing with imbalanced datasets, where one class significantly outnumbers the other [52]. For example, in datasets related to pipe breaks, non-break instances often outnumber those with breaks. To address this, the AUC of the Precision-Recall Curve (AUC-PRC) is used, as it is less influenced by class imbalances [53]. However, in highly imbalanced failure datasets, the baseline AUC-PRC of a random classifier is equal to the prevalence of the failure class; therefore, absolute AUC-PRC values should be interpreted relative to this baseline rather than in isolation [52]. Both the ROC and PR curves are derived from the confusion matrix at different threshold levels [54].

To evaluate the practical utility of the models developed in this study, a different approach was adopted. The classifiers provide a Likelihood of Failure (LoF) score between 0 and 1 for each service line, indicating the probability of failure. The higher the LoF score, the greater the likelihood of failure. All pipes were ranked based on their LoF values, and it was assumed that a certain percentage (p) of the pipes would be replaced. The top p percent of pipes, with the highest LoF scores, were selected as candidates for replacement. The number of actual failures in this subset during the validation period was then calculated. This value was compared with the expected number of failures if p percent of the pipes were randomly replaced within the WDN. In a random replacement scenario, replacing p percent of the pipes would typically capture p percent of the total failures. This metric helps quantify how many failures could be avoided in the validation period by replacing p percent of the pipes according to the model's predictions.

In this study, p ranged from 0.1% to 20%. Lower percentiles (e.g., 0.1%, 0.2%, 0.5%, 1%, and 2%) correspond to short-term, tactical pipe replacement plans, while higher percentiles (e.g., 5%, 10%, and 20%) align with long-term, strategic asset rehabilitation programmes. This evaluation method helps asset managers assess which model offers the most value for either tactical or strategic replacement decisions [13]. For this reason, model performance was additionally evaluated using a replacement-priority framework, which directly reflects operational decision-making and provides a more meaningful assessment than threshold-dependent metrics alone.

4. Results

After training each classification model on training sets ranging from 2 to 9 years in length, the predictive performance for service line failures was evaluated using the validation period (2022–2023). Figure 5a depicts the relationship between the F1-score and the number of years included in the training set. The F1-score was chosen as the evaluation metric due to its ability to balance precision and recall, which can often be at odds. As shown, the RF model achieves the highest performance, closely followed by the XGB model. Although the LSTM model demonstrates comparatively lower performance, it exhibits a notable increase in F1-score as the training set lengthens. This improvement is likely due to LSTM's capacity to process sequential data and retain information through its hidden state over time.

Figure 5b presents the ROC curve for the RF, XGB, and LSTM models trained over a 9-year period. The corresponding Areas Under the ROC Curve (AUC-ROC) for RF, XGB, and LSTM are 0.61, 0.58, and 0.60, respectively. These values suggest that all three models outperform a random baseline, demonstrating their ability to distinguish between the two classes.

https://doi.org/10.3390/w18010110

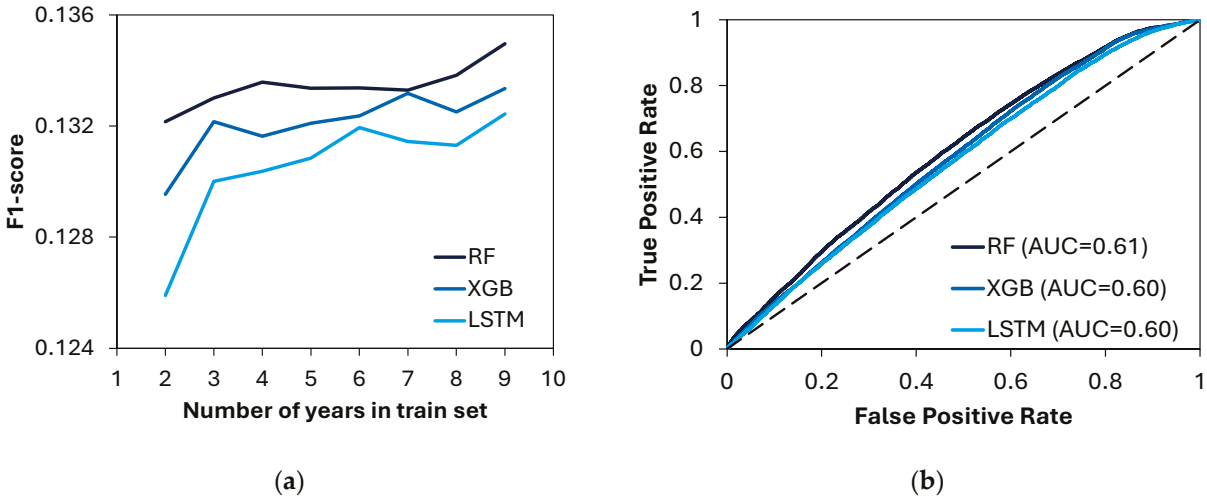

Figure 5. (**a**) F1-score; and (**b**) ROC curve for 9-year training; for RF, XGB, and LSTM models.

Figure 6a illustrates the relationship between the number of years in the training set and the AUC-ROC scores for all models. As the size of the training set increases, the AUC-ROC scores improve across all models. Notably, while the LSTM model initially exhibits weaker performance compared to RF and XGB, its performance shows significant improvement with a larger training set. This enhancement reflects the LSTM architecture's capacity to leverage sequential data and capture temporal dependencies effectively.

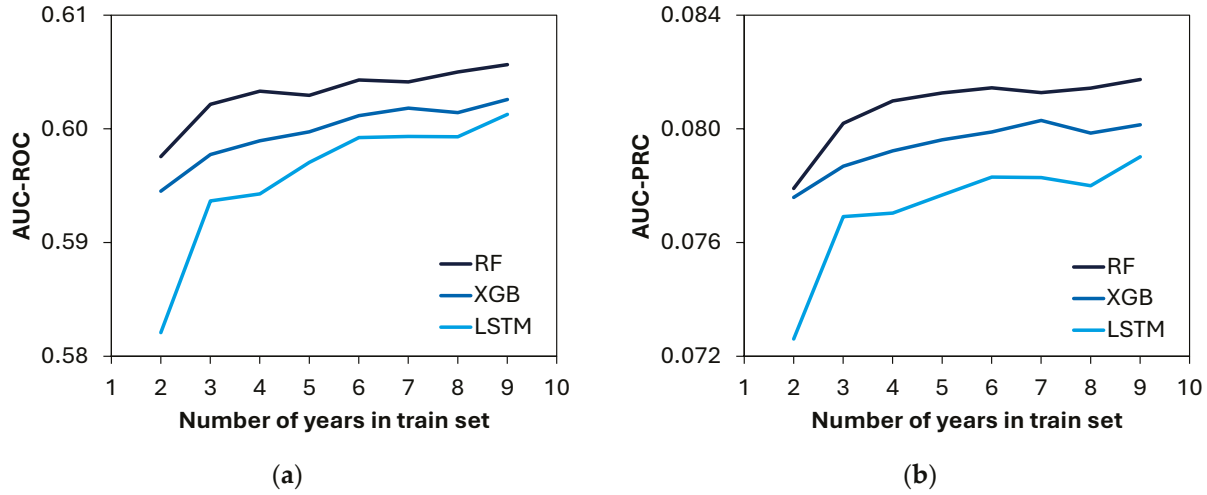

Figure 6. (**a**) AUC-ROC; and (**b**) AUC-PRC; values for RF, XGB, and LSTM models with various training data.

Figure 6b depicts the AUC-PRC scores as a function of the number of years in the training set. Although the absolute AUC-PRC values are relatively low, this outcome is expected due to the extreme class imbalance in service line failure data. Failure events constitute only a small fraction of the total observations, resulting in a very low random baseline AUC-PRC. The reported values therefore represent a meaningful improvement over random performance. The results indicate that the performance of all models improves with the inclusion of more years in the training set. Among the models, RF exhibits the highest performance, with XGB and LSTM following closely behind. This trend underscores the benefit of larger training datasets in enhancing model accuracy and reliability.

In this case study, the utility implements a preventive maintenance programme, replacing approximately 0.5% of service lines annually. This programme primarily targets service lines based on their age and material type, alongside replacing older service lines

https://doi.org/10.3390/w18010110

in newly developed areas. A 1% replacement of service lines corresponds to a two-year replacement cycle, while a 2% replacement aligns with a four-year schedule. Figure 7a illustrates the short-term replacement schedule, showing that prioritising 1% of service lines for replacement based on the models' recommendations results in an estimated 2% reduction in failures. Similarly, Figure 7b demonstrates that replacing 2% of service lines as suggested by the models leads to a projected 4% decrease in failures. Therefore, in tactical asset management, using a predictive machine learning model trained on less than 10 years of failure data can significantly enhance the effectiveness of investments, achieving twice the improvement compared to random asset replacement strategies.

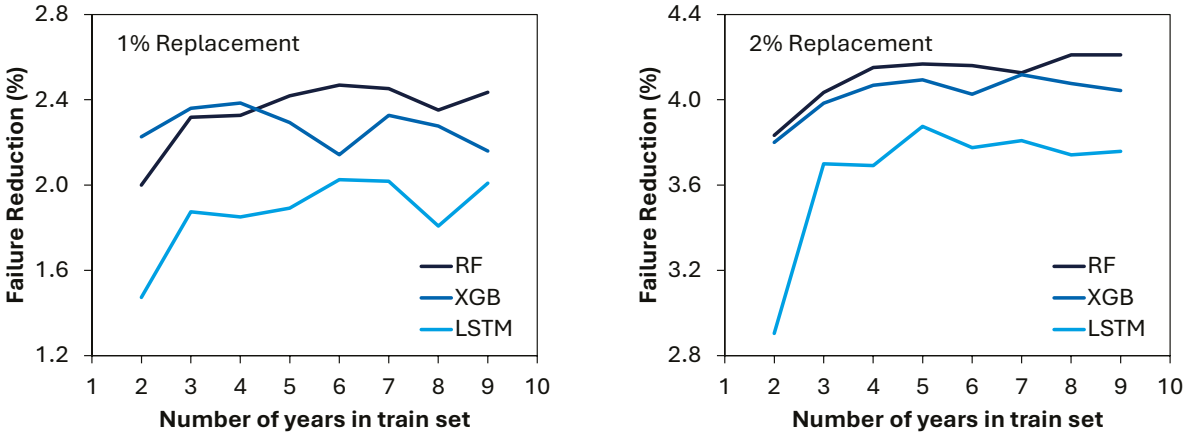

(**a**) (**b**)

Figure 7. Failure reduction in (**a**) 1%; and (**b**) 2%; pipe replacements for RF, XGB, and LSTM models with various training data.

Considering a replacement rate of 0.5% per year, a 5% replacement rate corresponds to a 10-year plan, while a 20% replacement rate aligns with a 40-year schedule. Figure 8 demonstrates the efficiency of the proposed models for strategic asset management. Figure 8a shows that replacing 5% of service lines, as recommended by all models, results in an approximate failure reduction ranging from 7.5% to 8.5%. Similarly, Figure 8b indicates that a 20% replacement, as suggested by the models, leads to a failure reduction of approximately 26% to 29%. These results reveal that the proposed models are more effective for tactical asset management programmes than for strategic ones.

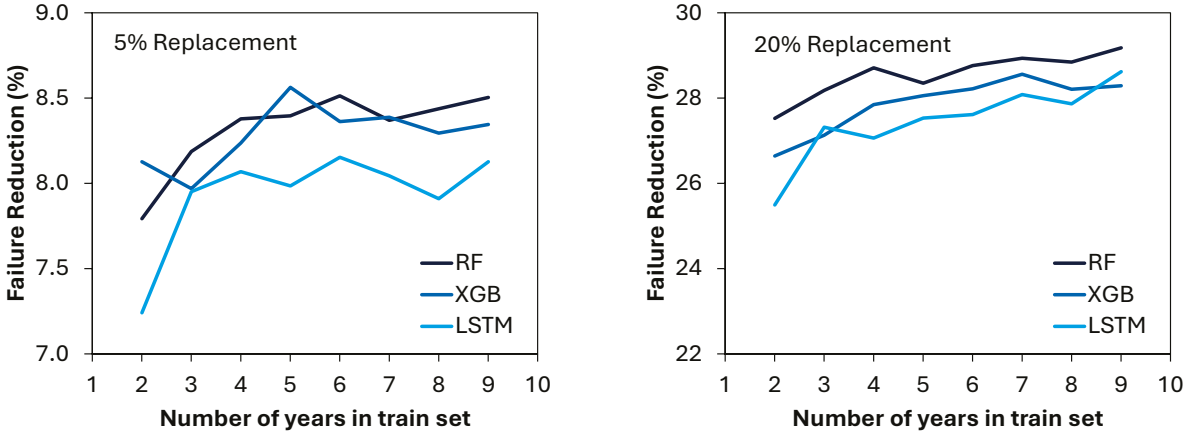

(**a**) (**b**)

Figure 8. Failure reduction in (**a**) 5%; and (**b**) 20%; pipe replacements for RF, XGB, and LSTM models with various training data.

https://doi.org/10.3390/w18010110

5. Discussion

Service lines comprise multiple elements, and failures may be attributed to different components. The varying proportion of failures across these elements helps identify the components most susceptible to failure in this case study. Figure 9 illustrates the various failure modes on a typical service line in the case study area. Over one-third of all service line failures occur in shut-off valves, primarily due to frequent use by customers. More than 21% of failures are associated with the components connecting the metre to the service line, which are also affected by their proximity to the frequently used shut-off valve. Additionally, 11% of failures were observed in the upstream joint of the metre. These joints experience higher wear due to the connection of two elements (metre and pipe) made from different materials. Non-homogeneous connections, such as curb box joints, exhibit lower failure rates as they are typically embedded in concrete or soil, offering additional protection. Overall, more than 75% of all service line failures in this case study occur within the metre box, highlighting the importance of careful installation and maintenance of its components. While out-of-box elements have lower failure rates, their repair is more time-consuming and costly due to their deep installation.

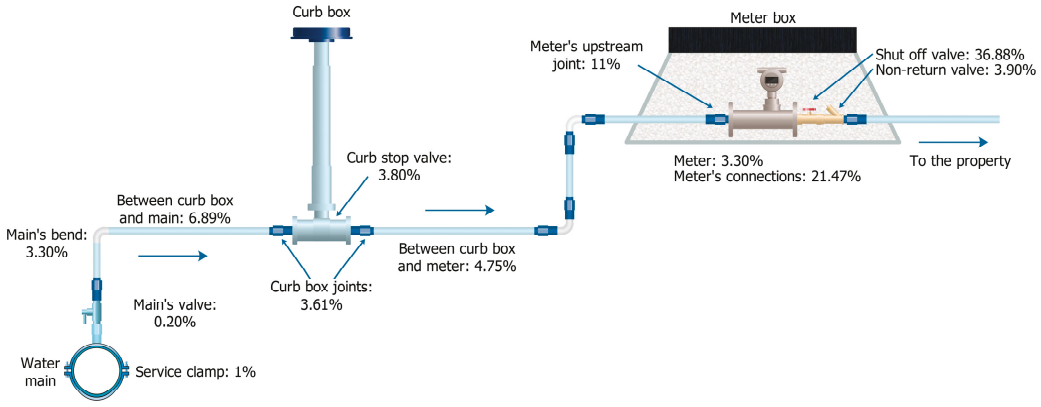

Figure 9. Failure modes on a typical service line in the case study area.

Although the models show minor performance differences, they produce broadly similar results, indicating that all are capable of capturing meaningful failure-related patterns. Random Forest achieved the highest performance, followed closely by Extreme Gradient Boosting, while Long Short-Term Memory showed lower but improving performance with longer training data. This similarity is largely due to the predominantly static nature of the input features, such as material, diameter, length, and pressure, which contain sufficient information to distinguish higher-risk service lines. Tree-based models effectively capture nonlinear relationships and handle class imbalance, whereas LSTM benefits mainly from longer historical records. Overall, the consistent performance improvement with increasing training data length highlights the importance of long-term failure data in capturing degradation trends and accumulated risk.

Most prior studies on pipe failure prediction have focused on water mains rather than service lines [18,19,22,27]. Reported AUC-ROC values for main failure prediction using machine learning models typically range between 0.60 and 0.75, depending on the richness of the feature set and network characteristics [26–28]. The AUC-ROC values achieved in this study (approximately 0.58–0.61) are therefore comparable, particularly given the limited feature set and the higher uncertainty associated with small-diameter service lines. In such rare-event prediction problems, precision inevitably declines as recall increases, which is a well-known characteristic of imbalanced classification rather than an indication of model inadequacy. International studies have shown that service lines often dominate failure statistics, accounting for more than 80% of failures in several utilities worldwide [40].

https://doi.org/10.3390/w18010110

Despite this, predictive modelling of service line failures remains scarce. Existing studies have largely relied on survival analysis or simplified statistical approaches [41,42], which typically focus on a limited number of explanatory variables.

As previously discussed, the available features for service lines did not fully capture all factors influencing failure. While attributes such as age, material, and pressure are primary determinants of failure rates, incorporating additional features—such as joint type, soil type, and weather data—could significantly enhance the predictive capabilities of the models. Material type, although included, is less informative since approximately half of the service lines share the same material. However, service lines with the same material but produced by different manufacturers often exhibit varying qualities and durability. Introducing a new feature, such as 'service line manufacturer,' could enable the models to account for the impact of production differences on failure rates.

The pressure data used in this study were derived from a hydraulic model; replacing this with actual pressure measurements, particularly capturing sudden pressure fluctuations, could further improve predictive accuracy. Additionally, in utilities where failure reasons are systematically recorded by technicians, failures could be categorised more precisely. This categorisation would provide valuable insights, enabling machine learning models to deliver more accurate and actionable predictions.

Most water utilities adopt a reactive approach to service line maintenance, addressing issues only after a failure occurs. This practice incurs substantial economic, environmental, and social costs. The methodology proposed in this study enables utilities to proactively identify and replace service lines with a high likelihood of failure, minimising unexpected disruptions and ensuring uninterrupted service for customers. Machine learning models have proven to be highly effective tools for planning predictive asset maintenance.

6. Conclusions

This study is among the first to evaluate machine learning-based failure prediction for clean water service lines while explicitly analysing the effect of training data length on model performance. A case study was conducted using a WDN serving over 200,000 customers. Data on service line attributes—including diameter, length, age, material, pressure, and demand—along with 11 years of historical failure records, were utilised. The first 9 years of data were employed for training the machine learning models, while the final 2 years were reserved for validation. RF, XGB, and LSTM algorithms were applied to estimate the likelihood of failure for each service line. Performance was evaluated using multiple metrics, including F1-score, ROC curve, AUC-ROC, and AUC-PRC. Additionally, a novel metric—failure reduction percentage relative to the replacement percentage—was introduced to quantify the effectiveness of the predictions in reducing failures by prioritising service lines with the highest likelihood of failure for replacement. The findings demonstrate that despite the limited feature set, the machine learning models successfully captured the complex relationships between service line attributes and failures. Furthermore, the models consistently improved with the inclusion of additional training data.

6.1. Key Findings

The results show that tree-based models (RF and XGB) outperformed the LSTM model, primarily due to the predominantly static nature of the service line attributes. Model performance improved consistently as longer training histories were used, underscoring the importance of historical failure data in capturing degradation patterns. The machine learning-based prioritisation strategy identified up to twice as many failures compared with random replacement for the same replacement rate. Furthermore, the predictive models

https://doi.org/10.3390/w18010110

demonstrated greater effectiveness for tactical, low-percentage replacement programmes than for long-term strategic asset planning.

6.2. Practical Implications

Utilities can use machine learning-derived likelihood-of-failure rankings to prioritise limited replacement budgets more effectively. Even when data are incomplete, predictive models provide measurable benefits compared with traditional reactive or age-based maintenance approaches. Moreover, the proposed evaluation metric directly links model outputs to operational outcomes, facilitating practical adoption by asset managers.

6.3. Limitations

Pressure data were model-based rather than measured, limiting the representation of transient effects. In addition, important explanatory variables such as soil properties, joint types, and manufacturer details were unavailable. Finally, representing failures as an annual binary outcome does not capture failure severity or recurrence frequency.

6.4. Future Research Directions

Future work should explore the integration of high-frequency pressure data, environmental variables, and detailed component-level information. Differentiating failure modes and incorporating cost–risk optimisation frameworks could further enhance strategic asset management. Additionally, hybrid models combining ML with physical or survival-based approaches may improve long-term failure prediction for service lines.

Author Contributions: M.L. and S.S. conceptualised the research. M.L. and S.S. developed the machine learning algorithms, while M.G. was responsible for data validation and preprocessing. S.S. executed the models and generated the results, which M.L. then visualised and validated. All authors contributed to drafting the manuscript, with M.L. finalising the submission. All authors have read and agreed to the published version of the manuscript.

Funding: This research received no external funding.

Data Availability Statement: The data are available from the authors upon reasonable request due to privacy and legal. The data involve customers' information and are owned by the water utility, so any access requests require the company's authorization.

Conflicts of Interest: The authors declare no conflicts of interest. Author M.L. was employed by the company Datatecnics. The remaining authors declare that the research was conducted in the absence of any commercial or financial relationships that could be construed as a potential conflict of interest.

References

1. Rahman, N.A.; Muhammad, N.S.; Abdullah, J.; Mohtar, W.H.M.W. Model Performance Indicator of aging pipes in a domestic water supply distribution network. *Water* **2019**, *11*, 2378. [CrossRef]
2. Perera, D.; Smakhtin, V.; Williams, S.; North, T.; Curry, A. *Ageing Water Storage Infrastructure: An Emerging Global Risk*; UNU-INWEH: Richmond Hill, ON, Canada, 2021. [CrossRef]
3. Ferdowsi, A.; Zolghadr-Asli, B.; AghaKouchak, A. Dangers of aging water infrastructure. *Science* **2024**, *386*, 158. [CrossRef] [PubMed]
4. Świetlik, J.; Magnucka, M. Aging of drinking water transmission pipes during long-term operation as a potential source of nano- and microplastics. *Int. J. Hyg. Environ. Health* **2024**, *263*, 114467. [CrossRef]
5. Zangenehmadar, Z.; Moselhi, O.; Golnaraghi, S. Optimized planning of repair works for pipelines in water distribution networks using genetic algorithm. *Eng. Rep.* **2020**, *2*, e12179. [CrossRef]
6. Lin, P.; Chen, X.; Huang, S.; Ma, B. An optimal maintenance and replacement strategy for deteriorating water mains. *Water* **2022**, *14*, 2097. [CrossRef]
7. Salehi, S.; Salamati Nia, S.P. A Qualitative-Risk-Based Model to Assess Group Decisions for Planning the Maintenance-Renewal Works of Water Pipelines with Unreliable Operational Data. *Water Resour. Manag.* **2024**, *38*, 3153–3177. [CrossRef]

https://doi.org/10.3390/w18010110

8. Barton, N.A.; Farewell, T.S.; Hallett, S.H. Using generalized additive models to investigate the environmental effects on pipe failure in clean water networks. *npj Clean Water* **2020**, *3*, 31. [CrossRef]
9. Barton, N.A.; Hallett, S.H.; Jude, S.R. The challenges of predicting pipe failures in clean water networks: A view from current practice. *Water Sci. Technol. Water Supply* **2021**, *22*, 527–541. [CrossRef]
10. Salehi, S.; Fontana, M.E.; Tscheikner-Gratl, F.; Herrera, M.; Sadiq, R.; Mian, H.R. A fuzzy group decision-making model for Water Distribution Network rehabilitation. *Urban Water J.* **2024**, *21*, 364–379. [CrossRef]
11. Rahbaralam, M.; Modesto, D.; Cardús, J.; Abdollahi, A.; Cucchietti, F.M. Predictive Analytics for Water Asset Management: Machine Learning and Survival Analysis 1–19. *arXiv* **2020**. [CrossRef]
12. Aslani, B.; Mohebbi, S.; Axthelm, H. Predictive analytics for water main breaks using spatiotemporal data. *Urban Water J.* **2021**, *18*, 433–448. [CrossRef]
13. Beig Zali, R.; Latifi, M.; Javadi, A.A.; Farmani, R. Semisupervised clustering approach for pipe failure prediction with imbalanced data set. *J. Water Resour. Plan. Manag.* **2024**, *150*, 04023078. [CrossRef]
14. Robles-Velasco, A.; Cortés, P.; Muñuzuri, J.; De Baets, B. Prediction of pipe failures in water supply networks for longer time periods through multi-label classification. *Expert Syst. Appl.* **2022**, *213*, 119050. [CrossRef]
15. Nunes, R.; Arraut, E.; Pimentel, M. Risk Assessment Model for the renewal of Water Distribution Networks: A Practical approach. *Water* **2023**, *15*, 1509. [CrossRef]
16. Minaei, A.; Hajibabaei, M.; Sabzkouhi, A.M.; Hesarkazzazi, S.; Abusamra, S.; Creaco, E.; Sitzenfrei, R. Asset Management Perspective in Long-Term Rehabilitation of Aged Water Distribution Networks. In Proceedings of the World Environmental and Water Resources Congress 2023, Henderson, NV, USA, 21–24 May 2023. [CrossRef]
17. Delnaz, A.; Nasiri, F.; Li, S.S. Asset management analytics for urban water mains: A literature review. *Environ. Syst. Res.* **2023**, *12*, 12. [CrossRef]
18. Barton, N.A.; Hallett, S.H.; Jude, S.R.; Tran, T.H. An evolution of statistical pipe failure models for drinking water networks: A targeted review. *Water Sci. Technol. Water Supply* **2022**, *22*, 3784–3813. [CrossRef]
19. Kleiner, Y.; Rajani, B. Comprehensive review of structural deterioration of water mains: Statistical models. *Urban Water* **2001**, *3*, 131–150. [CrossRef]
20. Dehghan, A.; McManus, K.J.; Gad, E.F. Probabilistic Failure Prediction for deteriorating pipelines: Nonparametric approach. *J. Perform. Constr. Facil.* **2008**, *22*, 45–53. [CrossRef]
21. Kabir, G.; Tesfamariam, S.; Sadiq, R. Predicting water main failures using Bayesian model averaging and survival modelling approach. *Reliab. Eng. Syst. Saf.* **2015**, *142*, 498–514. [CrossRef]
22. Jafar, R.; Shahrour, I.; Juran, I. Application of Artificial Neural Networks (ANN) to model the failure of urban water mains. *Math. Comput. Model.* **2010**, *51*, 1170–1180. [CrossRef]
23. Aydogdu, M.; Firat, M. Estimation of failure rate in water distribution network using fuzzy clustering and LS-SVM methods. *Water Resour. Manag.* **2014**, *29*, 1575–1590. [CrossRef]
24. Kutyłowska, M. Comparison of two types of artificial neural networks for predicting failure frequency of water conduits. *Period. Polytech. Civ. Eng.* **2017**, *61*, 1–6. [CrossRef]
25. Kutyłowska, M. Prediction of water conduits failure rate—Comparison of support vector machine and neural network. *Ecol. Chem. Eng. A* **2016**, *23*, 147–160. [CrossRef]
26. Latifi, M.; Zali, R.B.; Javadi, A.A.; Farmani, R. Customised-sampling approach for pipe failure prediction in water distribution networks. *Sci. Rep.* **2024**, *14*, 18224. [CrossRef]
27. Giraldo-González, M.M.; Rodríguez, J.P. Comparison of statistical and machine learning models for pipe failure modeling in water distribution networks. *Water* **2020**, *12*, 1153. [CrossRef]
28. Latifi, M.; Zali, R.B.; Javadi, A.A.; Farmani, R. Efficacy of Tree-Based Models for Pipe Failure Prediction and Condition Assessment: A Comprehensive Review. *J. Water Resour. Plan. Manag.* **2024**, *150*, 03124001. [CrossRef]
29. Kakoudakis, K.; Behzadian, K.; Farmani, R.; Butler, D. Pipeline failure prediction in water distribution networks using evolutionary polynomial regression combined with K-means clustering. *Urban Water J.* **2016**, *14*, 737–742. [CrossRef]
30. Beig Zali, R.; Latifi, M.; Javadi, A.A.; Farmani, R. A Weighted Likelihood Ensemble Approach for Failure Prediction of Water Pipes. *J. Water Resour. Plan. Manag.* **2025**, *151*, 04024066. [CrossRef]
31. Ji, J.; Robert, D.; Zhang, C.; Zhang, D.; Kodikara, J. Probabilistic physical modelling of corroded cast iron pipes for lifetime prediction. *Struct. Saf.* **2016**, *64*, 62–75. [CrossRef]
32. Mahmoodian, M.; Li, C.Q. Reliability-Based service life prediction of Corrosion-Affected cast iron pipes considering multifailure modes. *J. Infrastruct. Syst.* **2018**, *24*, 04018004. [CrossRef]
33. Heidary, R.; Groth, K.M. A hybrid population-based degradation model for pipeline pitting corrosion. *Reliab. Eng. Syst. Saf.* **2021**, *214*, 107740. [CrossRef]
34. Wang, W.; Wang, Y.; Zhang, B.; Shi, W.; Li, C. Failure prediction of buried pipe network with multiple failure modes and spatial randomness of corrosion. *Int. J. Press. Vessel. Pip.* **2021**, *191*, 104367. [CrossRef]

https://doi.org/10.3390/w18010110

35. Fan, X.; Yu, X. Machine learning-assisted optimal schedule of underground water pipe inspection. *J. Infrastruct. Preserv. Resil.* **2023**, *4*, 20. [CrossRef]
36. Zhang, C.; Ye, Z. Water pipe failure prediction using AutoML. *Facilities* **2020**, *39*, 36–49. [CrossRef]
37. Rajani, B.; Kleiner, Y. Comprehensive review of structural deterioration of water mains: Physically based models. *Urban Water* **2001**, *3*, 151–164. [CrossRef]
38. Song, X.; Zhang, G.; Zhou, Y.; Li, W. Behaviors and mechanisms of microbially-induced corrosion in metal-based water supply pipelines: A review. *Sci. Total Environ.* **2023**, *895*, 165034. [CrossRef]
39. AwwaRF (AWWA Research Foundation). *Installation, Condition Assessment, and Reliability of Service Lines*; AwwaRF: Denver, CO, USA, 2007.
40. IWA WLSG. *IWA WLSG Service Pipe Leakage Initiative Report*; International Water Association: London, UK, 2004.
41. Lee, J.; Meehan, M. Survival analysis of US water service lines utilizing a nationwide failure data set. *Am. Water Work. Assoc.* **2017**, *109*, 13–21. [CrossRef]
42. van Hecke, B. 316 stainless partially corrugated tube vs polyethylene for service lines. In Proceedings of the Water Loss 2022, Prague, Czech Republic, 19–22 June 2022.
43. Shirzad, A.; Safari, M.J.S. Pipe failure rate prediction in water distribution networks using multivariate adaptive regression splines and random forest techniques. *Urban Water J.* **2019**, *16*, 653–661. [CrossRef]
44. Cen, H.; Huang, D.; Liu, Q.; Zong, Z.; Tang, A. Application research on risk assessment of municipal pipeline network based on random Forest Machine learning algorithm. *Water* **2023**, *15*, 1964. [CrossRef]
45. Sadler, J.; Goodall, J.; Morsy, M.; Spencer, K. Modeling urban coastal flood severity from crowd-sourced flood reports using Poisson regression and Random Forest. *J. Hydrol.* **2018**, *559*, 43–55. [CrossRef]
46. Chen, T.; Guestrin, C. XGBOOST: A scalable tree boosting system. In Proceedings of the KDD '16: The 22nd ACM SIGKDD International Conference on Knowledge Discovery and Data Mining, San Francisco, CA, USA, 13–17 August 2016; Association for Computing Machinery: New York, NY, USA, 2016; pp. 785–794. [CrossRef]
47. Liu, W.; Chen, Z.; Hu, Y. XGBoost algorithm-based prediction of safety assessment for pipelines. *Int. J. Press. Vessel. Pip.* **2022**, *197*, 104655. [CrossRef]
48. Gers, F.A.; Schmidhuber, J.; Cummins, F. Learning to Forget: Continual Prediction with LSTM. *Neural Comput.* **2000**, *12*, 2451–2471. [CrossRef] [PubMed]
49. Pulver, A.; Lyu, S. LSTM with working memory. In Proceedings of the 2017 International Joint Conference on Neural Networks (IJCNN), Anchorage, AK, USA, 14–19 May 2017. [CrossRef]
50. Xiao, R.; Zayed, T.; Meguid, M.A.; Sushama, L. Dynamic risk assessment of natural gas transmission pipelines with LSTM networks and historical failure data. *Int. J. Disaster Risk Reduct.* **2024**, *112*, 104771. [CrossRef]
51. Fawcett, T. An introduction to ROC analysis. *Pattern Recognit. Lett.* **2005**, *27*, 861–874. [CrossRef]
52. Saito, T.; Rehmsmeier, M. The Precision-Recall Plot Is More Informative than the ROC Plot When Evaluating Binary Classifiers on Imbalanced Datasets. *PLoS ONE* **2015**, *10*, e0118432. [CrossRef]
53. McDermott, M.B.A.; Hansen, L.H.; Zhang, H.; Angelotti, G.; Gallifant, J. A Closer Look at AUROC and AUPRC under Class Imbalance. *arXiv* **2024**. [CrossRef]
54. Guo, H.; Li, Y.; Shang, J.; Gu, M.; Huang, Y.; Gong, B. Learning from class-imbalanced data: Review of methods and applications. *Expert Syst. Appl.* **2016**, *73*, 220–239. [CrossRef]

Disclaimer/Publisher's Note: The statements, opinions and data contained in all publications are solely those of the individual author(s) and contributor(s) and not of MDPI and/or the editor(s). MDPI and/or the editor(s) disclaim responsibility for any injury to people or property resulting from any ideas, methods, instructions or products referred to in the content.

https://doi.org/10.3390/w18010110

water

MDPI

Article

Key Calibration Strategies for Mitigation of Water Scarcity in the Water Supply Macrosystem of a Brazilian City

Jefferson S. Rocha [1], José Gescilam S. M. Uchôa [2], Bruno M. Brentan [3,4,*] and Iran E. Lima Neto [1]

[1] Department of Hydraulic and Environmental Engineering, Federal University of Ceará, Fortaleza 60451-970, Brazil; jeffersonrocha@alu.ufc.br (J.S.R.); iran@deha.ufc.br (I.E.L.N.)
[2] Department of Hydraulic and Sanitation Engineering, University of São Paulo, São Paulo 01246-904, Brazil; gescilam@gmail.com
[3] Fluing-Institute for Multidisciplinary Mathematics, Universitat Politècnica de València, 46022 Valencia, Spain
[4] Hydraulic Engineering and Water Resources Department, School of Engineering, Federal University of Minas Gerais, Belo Horizonte 31270-901, Brazil
* Correspondence: brentan@ehr.ufmg.br; Tel.: +55-85-3366-9776

Abstract: This study focuses on Fortaleza, the largest metropolis in Brazil's semi-arid region. Due to recurrent droughts, massive infrastructure like high-density reservoir networks, inter-municipal and interstate water transfer systems, and a seawater desalination plant have been implemented to ensure the city's water security. To evaluate the quantitative and qualitative impact of introducing these diverse water sources into Fortaleza's water supply macrosystem, adequate calibration of the operating and demand parameters is required. In this study, the macrosystem was calibrated using the Particle Swarm Optimization (PSO) method based on hourly data from 50 pressure head monitoring points and 40 flow rate monitoring points over two typical operational days. The calibration process involved adjusting the operational rules of typical valves in large-scale Water Distribution Systems (WDS). After parameterization, the calibration presented the following results: R^2 of 88% for pressure head and 96% for flow rate, with average relative errors of 13% for the pressure head and flow rate. In addition, with NSE values above 0.80 after calibration for the flow rate and pressure head, the PSO method suggests a significant improvement in the simulation model's performance. These results offer a methodology for calibrating real WDS to simulate various water injection scenarios in the Fortaleza macrosystem.

Keywords: water supply systems; calibration; PSO optimization

1. Introduction

Water Distribution Systems (WDS) play a strategic role in addressing water deficits. Through effective design, operational control, and the understanding of hydraulic parameters, it is possible to reduce losses throughout the system. These losses can reach millions of cubic meters yearly worldwide, with more severe impacts in developing countries [1,2]. Moreover, the rapid population growth driven by urbanization intensification and the adverse effects of extreme climate events pose significant challenges to ensuring the water supply for large urban centers [3,4]. These challenges are even more important in semi-arid regions, characterized by high temperatures and minimal annual precipitation. In such regions, investments in water infrastructure are essential to meet multiple uses and ensure an adequate water supply [5,6]. Computational hydraulic simulation models are useful as management tools for water systems, enabling visualizing and predicting hydraulic and quality indicators and enabling scenario anticipation.

Before using the results from hydraulic simulation, the calibration step is a key part of the process. It involves minimizing errors between monitored and calculated data by adjusting the input parameters of the hydraulic network model, often including pipe roughness, node base demand, water quality properties, and the operational rules of pumps and valves [7,8]. Calibration is frequently supported by optimization tools that adjust WDS model parameters to achieve optimal results and typically verified using pressure head, flow rate, and chemical concentration data. Reliable hydraulic models developed by various calibration and optimization methods can enhance WDS operations [9,10]. Such models may help reduce energy costs [11], expand the water supply with adequate pressure heads [12], detect leaks and pipeline obstructions [13–15], and rehabilitate WDS with fewer interventions and greater precision [16].

Calibration studies for WDS models are generally complex when applied to large-scale real networks (models with over 500 pipes and covering areas larger than 20 km^2, as classified by 17) due to limited data availability, operational rules complexity, network topology, and size uncertainties. These challenges lead many studies to focus on hypothetical or benchmark WDS models instead [7,17–19]. However, hypothetical WDS models introduce simplifications that may limit the application of proposed methodologies for real WDS calibrations. Real hydraulic model calibration presents various difficulties, including the large number of nodes and pipes to optimize, the limited distribution of monitored data, dynamic operational rules, and data errors or omissions that force researchers to disregard existing information [9,20]. Furthermore, despite optimization methods and modelers' knowledge, sensitivity and experience remain crucial in tasks such as parameter selection, anomaly identification, operational rule adjustments, network behavior analysis, and other aspects [21].

Several WDS calibration methods are highlighted in the literature, particularly automatic approaches known for their precision and efficiency in real networks [8,22]. These automatic calibration methods are broadly categorized into numerical and optimization-based approaches. Numerical approaches directly solve continuity and energy equations using numerical methods such as weighted least squares and singular value decomposition, making calibration complex and time-consuming for large-scale networks [20,23]. On the other hand, optimization-based approaches reduce differences between simulated and observed results by adjusting decision variables through nonlinear hydraulic equations, a highly complex process [22,24]. To address these challenges, Evolutionary Algorithms (EAs) have been employed due to their heuristic flexibility and ability to solve nonlinear, non-convex, and multimodal problems, making them particularly suitable for WDS calibration [22,25].

Particle Swarm Optimization (PSO) is one of the AEs with strong applicability in WDS, as it is particularly effective due to its ability to converge quickly to solutions, making it highly practical for real WDS hydraulic models [9,26]. PSO is a random global quasi-optimal solution search algorithm used to minimize the differences between monitored and simulated data. In addition, the method is inspired by the theory of swarm intelligence, which considers the exchange of information and the coevolution of species in a colony, as observed in bird migrations or fish schooling behaviors [7,26,27]. Over time, PSO and its more than 22 variants have been applied in WDS calibrations and other diverse hydraulic applications [28].

This study evaluates the PSO method for calibrating real, large-scale WDS by focusing on the water supply macrosystem of a major Brazilian city with water availability challenges. The calibration process incorporated 48 h monitoring data from 50 pressure head points and 40 flow rate points, as well as operational rules of 48 pressure head-reducing valves. This

approach mirrors real-world complexities, contrasting with many studies that overlook such operational data. However, it also emphasizes that classical calibration alone is insufficient for accurate model performance. Inferring a priori knowledge about system behavior, such as operational constraints and infrastructure specifics, is crucial for improving calibration outcomes. Calibration was assessed using five hydraulic modeling indicators and comparative pre- and post-calibration graphs. The results demonstrate significant hydraulic model improvement, enhancing its predictive capabilities and adaptability to various scenarios, such as integrating new water supply sources or responding to severe water crises.

2. Materials and Methods

2.1. Study Area

Fortaleza, the capital of Ceará state in Brazil, has approximately 2.5 million inhabitants and is located in the country's semi-arid Northeast region. This region is characterized by low annual precipitation, high evaporation rates, elevated temperatures, limited groundwater resources, intermittent rivers, and irregular rainfall patterns, resulting in water constraints throughout most of the year [29,30]. The city's water infrastructure includes two Water Treatment Plants (WTP Oeste and WTP Gavião) and eight reservoirs: Gavião, Pacoti, Riachão, Pacajus, Aracoiaba, Banabuiú, Orós, and Castanhão, with a combined storage capacity exceeding 11,000 hm^3. These reservoirs are integrated through two major water supply systems: the "Canal do Trabalhador" and the "Eixão das Águas" [31]. Together, the treatment plants have a maximum productivity of 15 m^3/s; however, during the multi-year 2012–2017 drought, this capacity was reduced to 8.2 m^3/s. In response to the city's ongoing water scarcity challenges, Fortaleza began the development of a seawater desalination plant project (DESAL) with a projected production capacity of 1 m^3/s, which is expected to supply water to approximately 300,000 inhabitants [32,33]. Figure 1 illustrates Fortaleza's water system.

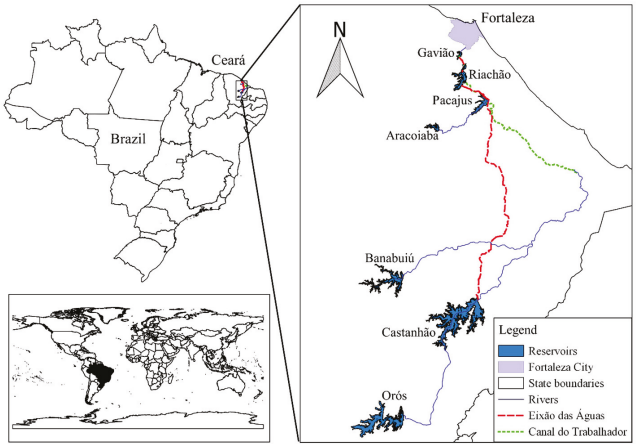

Figure 1. Location and water system of Fortaleza City, emphasizing the multiple reservoirs and hydraulic works that contribute to the city's water security.

2.2. Macrosystem of the Metropolitan Region of Fortaleza (MMF)

The water supply macrosystem model of Fortaleza comprises 479 junctions, one reservoir, and four tanks, resulting in 484 nodes. In addition, the model includes 393 pipes, 19 pumps, and 103 valves, resulting in 515 links. The total length of the pipes is 202.59 km and occupies an area of around 350 km^2, with most of this extension composed of pipes more than 1000 mm in diameter, as shown in Table 1. The average topographic elevation of the hydraulic elements is 33.6 m, with the highest point at an elevation of 103.4 m and the lowest point at an elevation of just 7.5 m. The base demand of the 84 consumption nodes

ranges from 0.37 to 868.3 L/s, according to information provided by the state water and sewage agency. In turn, the system is equipped with 48 pressure head-reducing valves governed by hourly operating rules.

Table 1. Pipes distribution in the analyzed network by diameter.

Diameter	Number	Extension (km)
≤200 mm	61	1.73
200–400 mm	43	9.94
400–600 mm	105	46.19
600–1000 mm	107	60.06
≥1000 mm	77	84.67
Total	393	202.59

The water supply macrosystem model was provided by the state water and wastewater agency (CAGECE) in a format compatible with EPANET 2.2 software. The schematic representation of this water distribution macrosystem model and the location of the monitored points are shown in Figure 2.

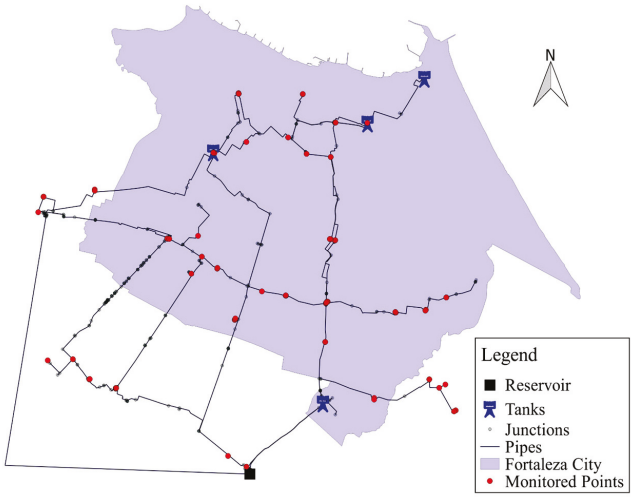

Figure 2. Analyzed macrosystem, along with the locations of the monitored points.

2.3. Methodology

This study calibrated the proposed WDS model using observed pressure head and flow rate data provided by the state water and wastewater agency (CAGECE). The calibration relied on data from 50 pressure head monitoring points and 40 flow rate monitoring points over two typical operational days, totaling 2400 pressure head data points and 1920 flow rate data points employed in the analysis. Hourly flow rate measurements were recorded by stations installed at the network nodes by the state water and wastewater agency (CAGECE). Since EPANET calculates flow rates only for pipes, it was necessary to transfer the measured flows from the outlet nodes to the upstream pipes of each node. Modifications to valve operation rules were also implemented. The model's 48 pressure head-reducing valves, each with hourly operation rules, introduced a level of complexity to the calibration process. This complexity was addressed through manual adjustments in EPANET software during the calibration in collaboration with the state water and wastewater agency. These adjustments involved analyzing the operational rules through generated graphs and assessing their influence on network nodes. The valve

operation rules were adjusted (e.g., increasing or decreasing pressure head control values) or, in some cases, removed to better match the observed monitoring point values while avoiding potential negative pressure heads at any network node during the modeled period. It is important to highlight that each pressure head-reducing valve has operational rules for each time step, meaning that 2304 operation rules were analyzed. Any modification to a single rule impacted the network's behavior. Therefore, for each calibration iteration, these operation rules were considered, as it would not have been possible to achieve a minimally calibrated model without these adjustments. This highlights the complexity of calibrating large-scale hydraulic WDS models [34].

Initially, the process relied on pre-calibration data provided by the state water and wastewater agency (CAGECE). That is, the initial values for absolute roughness and base demands were considered based on the agency's data and operational experience with the network. Moreover, this study prioritized the calibration of the base demand factors, ranging from 0.1 to 4, before addressing the calibration of pipe absolute roughness (ε), ranging from 0.0001 mm to 15 mm. After optimizing the objective function for base demand calibration, these values were updated in the hydraulic model, and the network conditions were checked for the presence of negative pressure heads. This sequence was chosen because base demand significantly influences flow rate behavior in hydraulic models, thereby affecting flow rates and hydraulic head losses. In addition, this parameter is more variable than roughness [35], introducing high uncertainty into the network, with any variation altering its behavior, making base demand a dominant factor in hydraulic networks [36]. Once the hydraulic model is adjusted, absolute roughness values can be calibrated, updated in the hydraulic model, and verified for negative pressure heads within the network. The precise determination of the pipe materials in the macrosystem was not possible due to the lack of detailed information about the materials used in each network segment. However, based on prior knowledge and the practices of the agency responsible for maintenance, PVC and Cast Iron are known to be the most commonly used materials. Additionally, it is important to highlight that absolute roughness values of 0.0001 mm are not realistic for water distribution networks. This value was used in this study solely to broaden the search for optimal results during the calibration process. Furthermore, it is noteworthy that the objective function scores were computed using the absolute difference between the modeled and simulated values and divided by the product of the number of monitored points and the total simulation time of 48 h. Additionally, no constraint was imposed on the equality between the Base Demand and the tank flow rates. In summary, the calibration process utilized in this study required pre-calibration operational adjustments to achieve a hydraulic model that closely represents real-world conditions.

The PSO method aims to minimize the objective function by iteratively changing and updating the position of particles within the search space, thereby seeking the best individual and collective positions. Thus, a particle i can be represented by two vectors: one representing the spatial position x_i and the other representing the search velocity v_i. Initially, the particles are randomly distributed, generating the first solution. Subsequently, the particles are moved so that those farther from the best solution converge toward it, storing the best position based on both individual and collective best-known position of the swarm [7,37,38]. This iterative process is described by Equations (1) and (2).

$$v_i^{t+1} = wv_i^t + c_1 r_1 \frac{\left(x_i^t - l_i^t\right)}{\Delta t} + c_2 r_2 \frac{\left(x_i^t - g_i^t\right)}{\Delta t}, \quad (1)$$

$$x_i^{t+1} = x_i^t + v_i^{t+1}\Delta t, \quad (2)$$

where i represents the particles of the swarm; r_1 e r_2 are the values of the random distribution, with values varying from 0 to 1; c_1 is the cognitive factor related to the information of the particle's best positions; c_2 is the social factor related to the information of the best positions experienced by the group; w is the inertia coefficient responsible for weighting the velocities of the particles; l_i^t represents the vector of the best local solution; and g_i^t represents the vector of the best global solution or the swarm's best solution.

The results of the calibrated network are compared with the results of the pre-calibration network using quantitative evaluation parameters in addition to a graphical analysis of the flow rate and pressure head behavior. The quantitative evaluation was conducted through the Mean Absolute Error (MAE), Average Relative Hourly Error (ARHE), Nash-Sutcliffe Efficiency Coefficient (NSE), Coefficient of Determination (R^2), and Percentual Bias (PBIAS). The MAE is calculated as the sum of the absolute difference between the monitored and modeled values divided by the total number of data points. The ARHE evaluates the absolute difference between the monitored and modeled values normalized by the monitored value and the number of simulated hours (48 h). In this way, the ARHE considers the deviation of the monitored and modeled data for each hour of the simulation, thus allowing a more detailed analysis of the deviation behavior. The NSE evaluates the model's efficiency by comparing the squared difference between the monitored and modeled values with the squared deviation of the monitored values from their mean. The range spans from 1 (perfect model representation) and $-\infty$ (the mean of observed data is a better predictor than the model itself). This metric is one of the main indicators of the accuracy of hydrological models, but it can also be applied in hydraulic modeling [39]. The R^2 reflects the proportion of variance explained by the model, representing the degree of alignment between observed and modeled values. It ranges from 0 (poor regression fit) to 1 (perfect regression fit), indicating how well the model predicts observed data [39]. The last indicator used was the PBIAS, which considers the trend of the mean modeled values in relation to the monitored values. For this indicator, the closer the value is to zero, the better the model. Negative PBIAS values indicate that the model is overestimating the results, while positive PBIAS values suggest an underestimated model [40]. Table 2 presents the list of equations used for the model indicators:

Table 2. Relationship of model indicators and their equations.

Indicators	Equations
Mean Absolute Error	$MAE = \frac{\sum_{i=1}^{n} abs(O_i - M_i)}{n \cdot h}$
Average Relative Hourly Error (%)	$ARHE = \frac{\sum_{i=1}^{n} abs\left(\frac{O_i - M_i}{O_i}\right)}{n \cdot h} \cdot 100$
Nash–Sutcliffe Efficiency Coefficient	$NSE = 1 - \frac{\sum_{i=1}^{n} (O_i - M_i)^2}{\sum_{i=1}^{n} \left(O_i - O_i^{mean}\right)^2}$
Coefficient of Determination	$R2 = \left(\frac{\sum_{i=1}^{n} \left(O_i - O_i^{mean}\right)\left(M_i - M_i^{mean}\right)}{\sqrt{\sum_{i=1}^{n} \left(O_i - O_i^{mean}\right)^2 \cdot \sum_{i=1}^{n} \left(M_i - M_i^{mean}\right)^2}} \right)^2$
Percentual Bias (%)	$PBIAS = \frac{\sum_{i=1}^{n} (O_i - M_i)}{\sum_{i=1}^{n} O_i} \cdot 100$

Notes: where O_i are the observed or monitored data and O_i^{mean} is their respective mean, M_i are the values obtained from the modeling and M_i^{mean} is their respective mean, n is the number of observed or monitored nodes, and h is the number of hours used in the simulation.

The calibration process lasted a year and a half, accounting for code adjustments, data collection from the state agency, outlier analysis, and modifications to the valve operation rules. Additionally, each execution of the calibration code took an average of seven days to produce results, even when using a computer with a Dell 12th Gen Intel(R) Core(TM) i7-12700 processor and 16 GB of RAM, Sobral, Brazil. Several modifications were made to

both the network and the code to achieve the results presented in this study, with the most exhaustive adjustment involving the operation rules of the various valves in the network.

3. Results

The results showed absolute roughness values ranging from approximately 15 mm to 0.0001 mm, with a mean of 6.2 mm and a median of 1.45 mm. For the base demands, the values ranged from 0.46 L/s to 868.3 L/s, with a mean of 90.2 L/s and a median of 30.38 L/s. Although the age of the pipes is unknown, the results, particularly the absolute roughness, suggest the presence of old or severely deteriorated pipes. In the monitored pipes, the flow velocities had a mean of 2.03 m/s and a median of 1.12 m/s. These values indicate relatively high flow velocities in the network, suggesting that the pressure in the pipes is not strongly dependent on the topographical elevations provided by the agency. In other words, the high flow velocity reduces the influence of terrain height variations on pressure distribution, implying that the network operates with less sensitivity to changes in topography. The values of the five chosen indicators used to evaluate the calibration of roughness and base demands through pressure heads and flow rates are summarized in Tables 3 and 4. The results indicate that the calibration process successfully met the proposed objectives. For the pressure heads, four out of the five indicators demonstrated a better fit between the proposed model and the monitored data. Similarly, all five indicators for flow rates showed an improved alignment between the model and the observations.

Table 3. General results of the calibration indicators for pressure heads.

	MAE	ARHE	NSE	R^2	PBIAS
Before Calibration	7.10 m	31.13%	0.597	0.623	2.64%
After Calibration	3.53 m	12.96%	0.873	0.879	3.38%

Table 4. General results of the calibration indicators for flow rates.

	MAE	ARHE	NSE	R^2	PBIAS
Before Calibration	43.7 L/s	320.79%	0.754	0.780	11.80%
After Calibration	16.3 L/s	13.09%	0.965	0.965	1.06%

Figure 3 shows an example of the typical average behavior of a monitored point for the pressure heads and flow rates of the analyzed WDS hydraulic model. Figure 3 shows the pressure head and flow rate scale presented in the Fortaleza microsystem and how well the calibrated model tracks the behavior of the monitored data over the two-day period. It is important to note that, in Figure 3, the *y*-axis does not start at zero to enhance visualization.

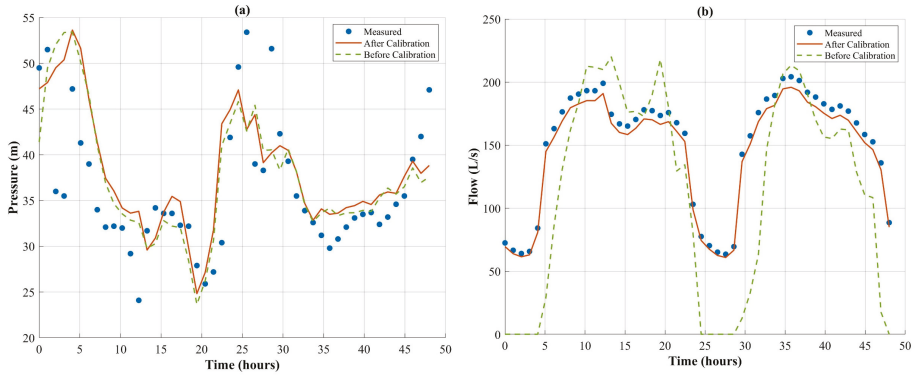

Figure 3. Analysis of the typical average behavior of the network through a monitored point for (**a**) pressure head and (**b**) flow rate.

Figures 4–7 show the behavior of the pipes and nodes represented by the Box and Whiskers diagram, which aims to represent the variability of the data and summarize various value distributions using the median, quartiles, minimum, maximum, and outliers [41,42]. Figures 8–13 consist of scatter plots addressing the relationship between a set of binary data, representing the behavior of the evaluation parameters for each monitored point and its respective modeled value, allowing the visualization of the network's overall behavior.

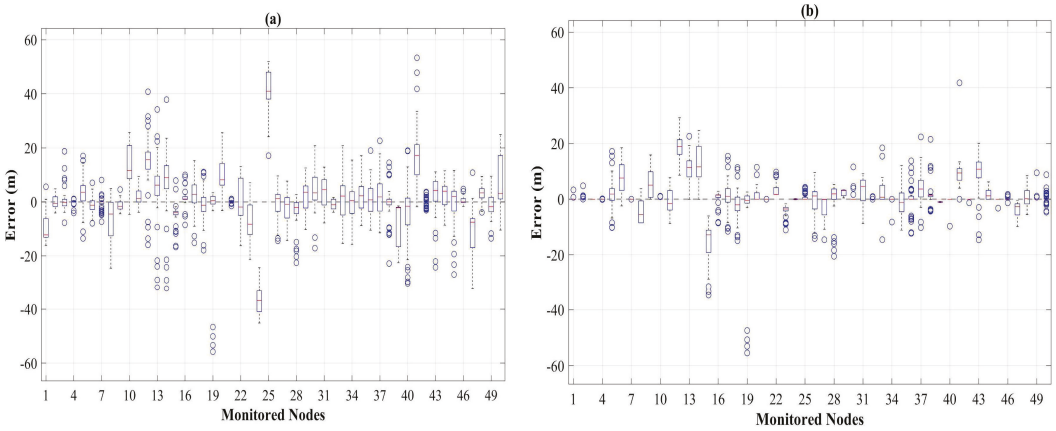

Figure 4. Box and Whiskers of the MAE for pressure heads (**a**) before calibration and (**b**) after calibration.

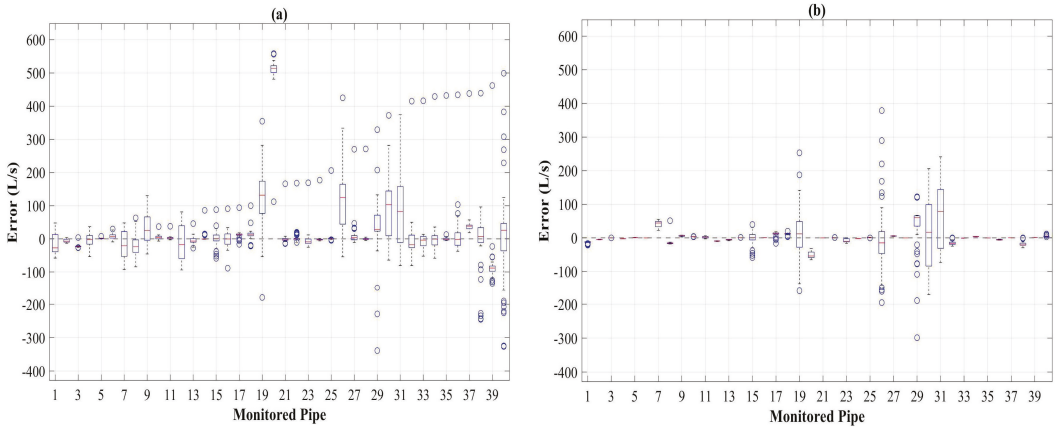

Figure 5. Box and Whiskers of the MAE for flow rates (**a**) before calibration and (**b**) after calibration.

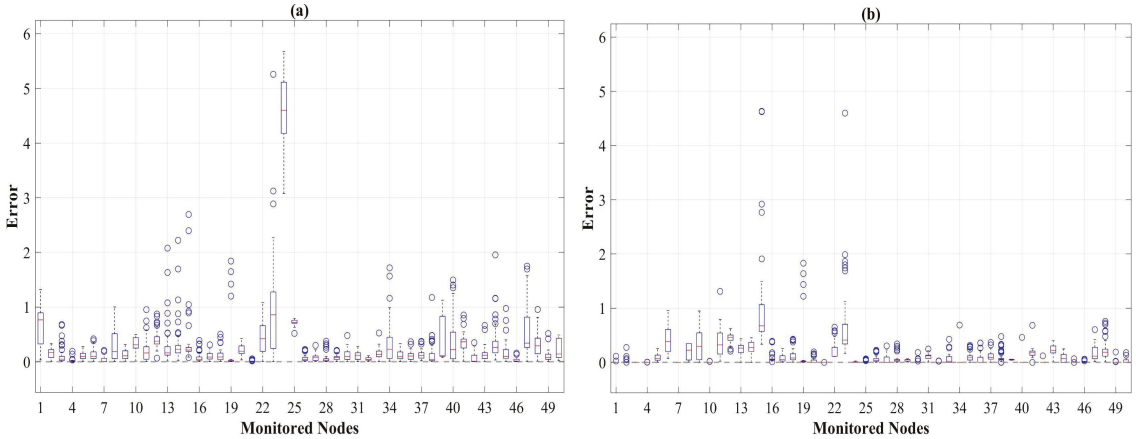

Figure 6. Box and Whiskers of the ARHE for pressure heads (**a**) before calibration and (**b**) after calibration.

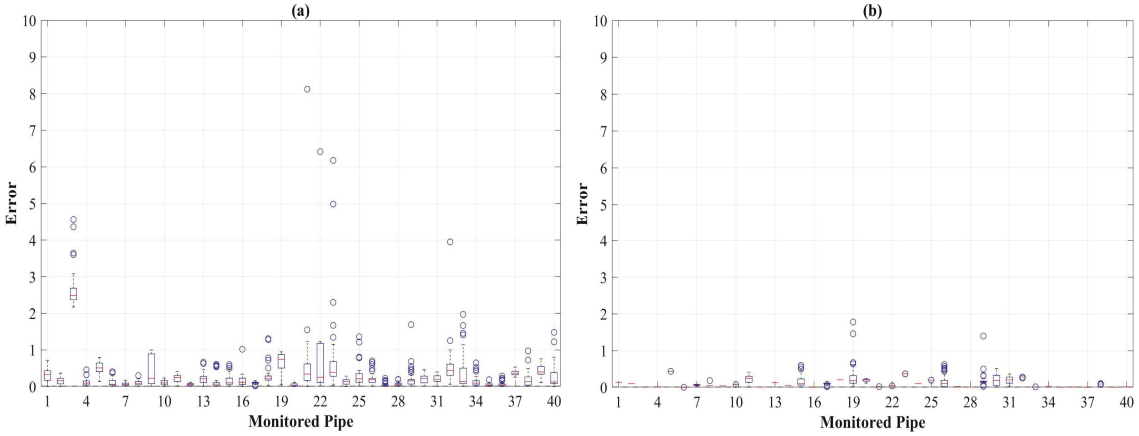

Figure 7. Box and Whiskers of the ARHE for flow rates (**a**) before calibration and (**b**) after calibration.

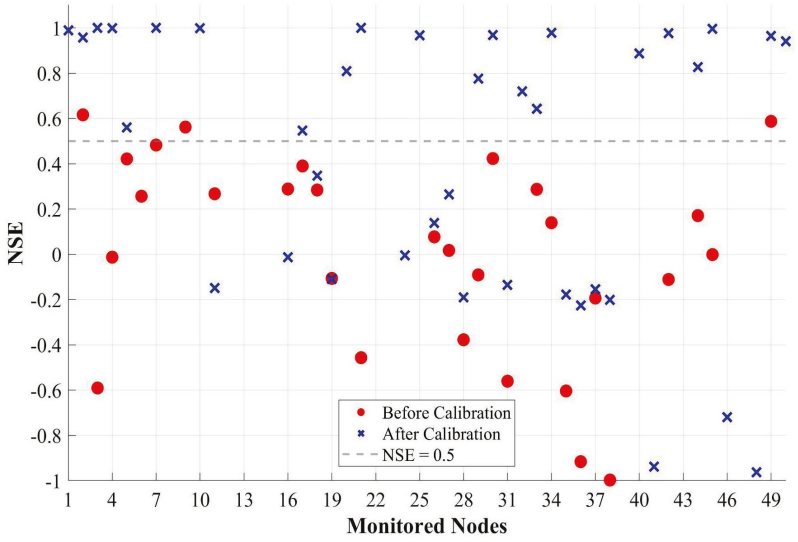

Figure 8. NSE plot for pressure heads before and after calibration.

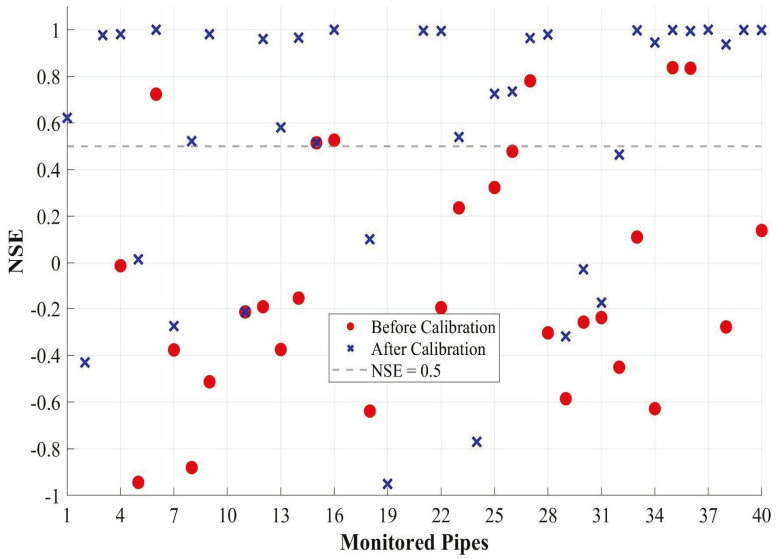

Figure 9. NSE plot for flow rates before and after calibration.

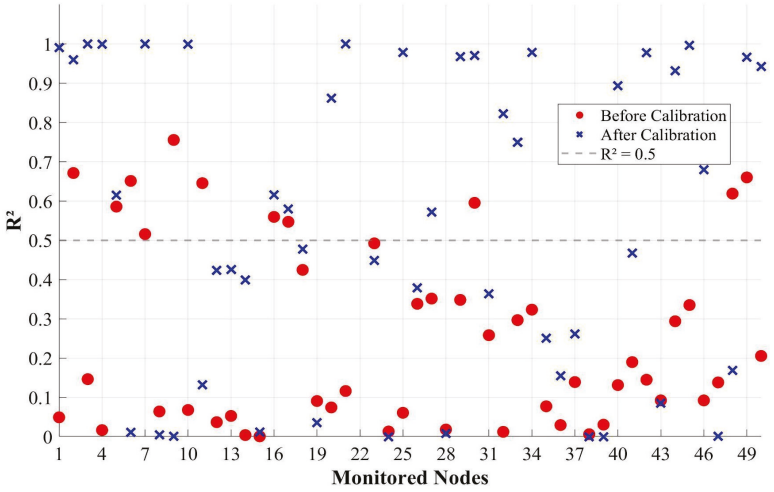

Figure 10. R^2 plot for pressure heads before and after calibration.

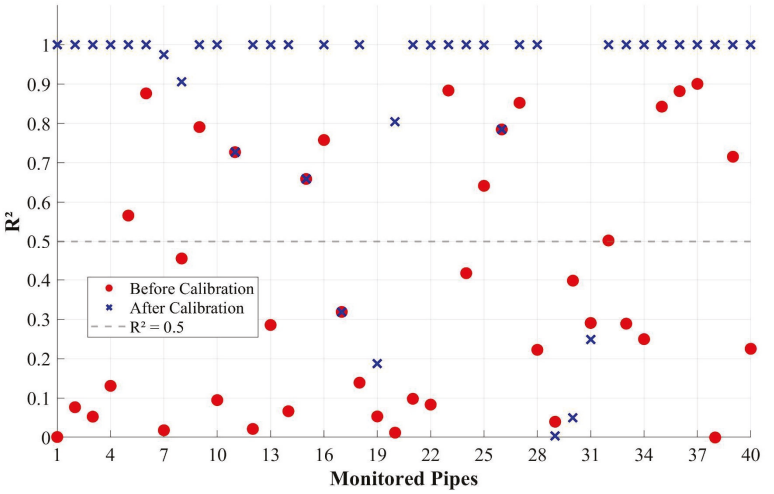

Figure 11. R^2 plot for flow rates before and after calibration.

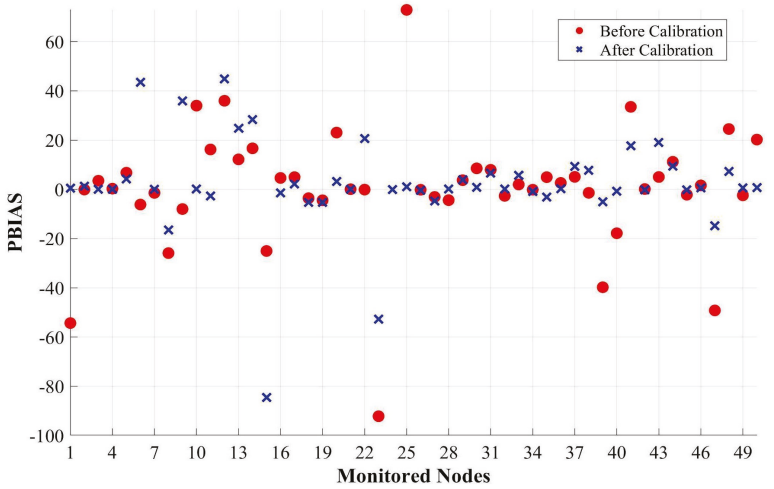

Figure 12. PBIAS plot for pressure head rates before and after calibration.

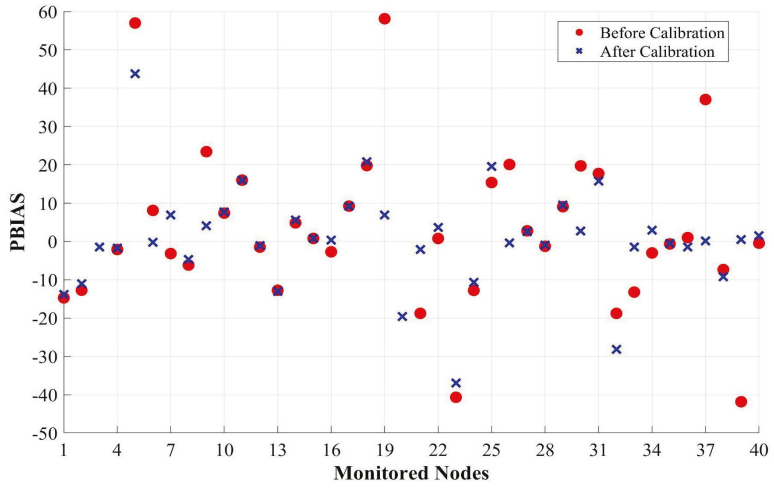

Figure 13. PBIAS plot for flow rates before and after calibration.

Figures 4 and 5 show the improvement in the hydraulic model after calibration, considering the error between the monitored and calculated data. The Box and Whiskers diagram for the MAE demonstrates a reduction in the number of outliers and a clustering of values closer to zero on the *y*-axis after calibration. In Figure 4, monitored points 24 and 25 highlight the reduction in pressure head errors after calibration. Similarly, Figure 5 shows a reduction of outliers above 300 L/s after calibration, a value that corresponds to nearly 30% of the highest monitored value for flow rates. For both pressure head and flow rate, the MAE was reduced by over 50%. Furthermore, considering the maximum allowable error of 2 m for pressure heads, as defined by the [43], the calibrated model achieves approximately 60% of pressure heads within this limit before calibration, compared to only 33% prior to calibration.

As the ARHE represents the average relative hourly error, this indicator reflects the behavior of the errors in hourly pressure heads and flow rates, allowing for a more detailed analysis of the parameters considered. Figure 6 shows the reduction in the number of relative errors above 1 for pressure heads after calibration compared to before. Similarly, Figure 7 highlights how much calibration reduced flow rate relative errors, which decreased from a maximum of approximately 8 m before calibration to below 2 m after calibration. Therefore, the improvement is more noticeable for the flow rates, as the reduction is higher than 95%.

The NSE and R^2 showed similar results, indicating that the calibration adequately represents the monitored values. The NSE and R^2 for the pressure head are 0.87, and for the flow rate, it is 0.96 after calibration. That is, values above 0.5 are considered acceptable for a model, and values above 0.8 indicate a very well-adjusted model [39]. Through Figures 8–11, it is possible to see the increase in the number of pipes and nodes above 0.5, with the most significant increase observed in Figure 8, where there are only three nodes above NSE = 0.5 before calibration, and after calibration, there are 22 nodes above this mark. For R^2, this increase in the number of values close to 1 is also visible in the graph, where a significant number of points near 0 can be seen before calibration. In comparison with the work by [44], which calibrated a hydraulic model of a WDS of a small town in the UK using 672 observed pressure heads and resulting in R^2 = 0.999, this work utilized more than three times the amount of observed pressure heads (2400) and obtained an R^2 of 0.87, indicating a hydraulic model close to ideal, despite the large amount of observed data. It is important to note that the scale of Figure 8 had to be expanded because some values

before calibration were quite divergent (with small NSE values), and it would not have been possible to view the graph in detail.

For the PBIAS, an adverse behavior was observed, as the value for the pressure head increased after calibration, while for flow rate, the reduction was predominant, as shown in Tables 3 and 4. This increase in PBIAS for pressure heads can be justified by the PBIAS equation itself, where the summation of the difference between observed and monitored data considers the sign of these subtractions. Thus, for the PBIAS value after calibration in the pressure heads to be higher than before calibration, it may indicate a slight tendency toward greater underestimation. Nevertheless, the PBIAS values after calibration can still be considered very good, as they are below 10% [45]. In Figure 12, it is emphasized that the graph had to be enlarged to view more details, as before calibration, the PBIAS values were significantly lower than the others. This highlights the improvement of the PBIAS indicator after calibration.

4. Discussion

It is also worth highlighting that several adjustments were made to the operating rules of the pressure head-reducing valves, including the removal of some rules and the hourly modification of certain valve operation rules. Moreover, for each modification made to the operating rules, it was necessary to check the consistency of the hydraulic model. These verifications involved modifying the valve operation rules, base demand factors, and absolute roughness values of the hydraulic model, followed by running the EPANET simulation for a 48 h period and checking for possible negative pressure heads at any point in the 484 nodes every hour. These analyses confirm that reaching the hydraulic model used in the calibration requires meticulous interventions by the modeler [21]. As a result, several modifications and preliminary calibrations were made to arrive at the final calibrated model, highlighting the inherent complexity of calibrating real, large-scale WDSs. The progress of this calibration process for both pressure heads and flow rates demonstrates the evolution of the indicator results alongside their respective calibration versions. For each version, the valve operation rules, the calibrated parameters, or the number of monitoring points were modified. For instance, from version 1 to version 2, the pressure head monitoring points were reduced from 57 to 56 due to inconsistent data at one point, in addition to changes made to the pressure head values of some valves. This procedure was repeated until version 8, which resulted in the final configuration of this study.

The exclusion of certain monitoring points and the increase in the values of the indicators were also evaluated. After excluding only six pressure head monitoring points based on the worst MAE results, leaving 44 monitoring points, it was observed that the evaluation parameters for the calibrated model presented the following results: MAE = 2.59 m, ARHE = 10.25%, NSE = 0.94, R^2 = 0.94, and PBIAS = 1.84%. When the same procedure was performed excluding only six flow rate monitoring points based on the worst MAE results and leaving 34 monitoring points, the following results were presented: MAE = 6.34 L/s, ARHE = 11.06%, NSE = 0.99, R^2 = 0.99, and PBIAS = −0.11%. Therefore, all indicators showed improvements in the results after the removal of just six monitoring points. Even with this removal, this work presents the number of monitored points used in the calibration as higher than that found in most of the analyzed literature, thus highlighting that the entire calibration process and the amount of data used in this work resulted in a consistent hydraulic model [7,46–49].

It is important to highlight that several innovative techniques for calibrating water supply networks have been developed, such as graph-based metamodels [12] and artifi-

cial neural networks [7], among others. However, the decision to calibrate the Fortaleza macrosystem using more traditional strategies from the literature was driven by the complexity of working with a real, dynamic system in collaboration with the state water and wastewater agency responsible for its management. Furthermore, the calibration's representativeness could be enhanced by incorporating additional parameters. One example is substitute roughness, which accounts not only for actual roughness but also for local resistances and eccentricities caused by reductions or cross-section changes [7,8,15]. Given the Brazilian context of increasing water demand and the impacts of climate change on water resources [50]—particularly in the largest metropolis of the Brazilian semi-arid region, which frequently experiences drought events [6]—this calibrated network represents a critical tool. It will support the state water and wastewater agency in evaluating the impacts of introducing new water sources, operational changes, and climate change scenarios, as well as increasing demand on the network's performance.

5. Conclusions

This study conducted a calibration of the absolute roughness (ε) and base demand multiplication factors of a large-scale real Water Distribution System (WDS) located in a metropolitan area of Brazil facing water risks. The calibration process involved 50 pressure head monitoring points and 40 flow rate monitoring points over a 48 h period. Additionally, the hydraulic model considered the operating rules of several pressure head-reducing valves within the network, highlighting the inherent challenges of real WDS and underscoring the importance of the modeler in calibrating large-scale hydraulic models with operational rules. The PSO method was used as the algorithm to minimize the objective function.

Moreover, the calibration development included adjustments to the valve operation rules, analyzing generated graphs and the influence of these rules on the network nodes. Modifications such as increasing, reducing, or eliminating pressure head control values were made to meet the monitored points and avoid negative pressure heads. In total, 2304 operation rules were evaluated, with each adjustment directly impacting the network behavior. These adjustments were essential for obtaining a minimally calibrated model, highlighting the complexity of calibrating large-scale WDS hydraulic models.

The results indicate that the calibrated model showed good performance for the five indicator parameters used (MAE, ARHE, NSE, R^2, and PBIAS), which were evaluated for both the entire network and each monitored point. Notably, 60% of the pressure head errors are below 2 m; the study includes a large number of monitoring points, highlighting the robustness of the calibration for a complex hydraulic model.

Finally, it is expected that the work in this study will contribute to improvements in the water distribution system of Fortaleza City by using the calibrated model for operation scenario analysis and network modifications. Moreover, it will support any analysis by the managing entities of the WDS on the impact of integrating new water supply sources into the network.

Author Contributions: Conceptualization, J.S.R., B.M.B. and I.E.L.N.; Methodology, J.S.R. and I.E.L.N.; Software, J.S.R. and B.M.B.; Validation, J.G.S.M.U.; Formal analysis, J.G.S.M.U. and I.E.L.N.; Data curation, J.G.S.M.U.; Writing—original draft, J.S.R.; Writing—review & editing, J.G.S.M.U., B.M.B. and I.E.L.N.; Supervision, B.M.B. and I.E.L.N.; Funding acquisition, I.E.L.N. All authors have read and agreed to the published version of the manuscript.

Funding: J.G.S.M.U. acknowledges the São Paulo Research Foundation—FAPESP (Grant 2020/15434-0 and 2023/13160-8) for the scientific and financial support. I.E.L.N. appreciates the financial support

from the National Council for Scientific and Technological Development-CNPq (#307680/2023–1) and the Coordination for the Improvement of Higher Education Personnel-CAPES (#2160/2024).

Data Availability Statement: The raw data supporting the conclusions of this article will be made available by the authors on request.

Acknowledgments: We thank the Companhia de Água e Esgoto do Ceará (CAGECE) for providing the data on pressures, flows, and the typology of the water supply system of the city of Fortaleza, which were essential for the development of this study.

Conflicts of Interest: The authors declare no conflict of interest.

References

1. Dighade, R.R.; Kadu, M.S.; Pande, A.M. Challenges in water loss management of water distribution systems in developing countries. *Int. J. Innov. Res. Sci. Eng. Technol.* **2014**, *3*, 13838–13846.
2. Kizilöz, B. Prediction model for the leakage rate in a water distribution system. *Water Sup.* **2021**, *21*, 4481–4492. [CrossRef]
3. Greve, P.; Kahil, T.; Mochizuki, J.; Schinko, T.; Satoh, Y.; Burek, P.; Fischer, G.; Tramberend, S.; Burtscher, R.; Langan, S.; et al. Global assessment of water challenges under uncertainty in water scarcity projections. *Nat. Sustain.* **2018**, *1*, 486–494. [CrossRef]
4. Rustam, F.; Ishaq, A.; Kokab, S.T.; de la Torre Diez, I.; Mazón, J.L.V.; Rodríguez, C.L.; Ashraf, I. An Artificial Neural Network Model for Water Quality and Water Consumption Prediction. *Water* **2024**, *21*, 3359. [CrossRef]
5. Campos, J.N.B.; Lima Neto, I.E.; Studart, T.M.C.; Nascimento, L.S.V. Trade-off between reservoir yield and evaporation losses as a function of lake morphology in semi-arid Brazil. *Ann. Braz. Acad. Sci.* **2016**, *88*, 1113–1125. [CrossRef]
6. Pereira, B.; Uchôa, J.G.; Freitas, G.; Meira Neto, A.A.; Anache, J.; Wendland, E.C.; Mendiondo, E.M.; Medeiros, P. Hydrological Heritage: A Historical Exploration of Human-Water Dynamics in Northeast Brazil. *Hydrol. Sci. J.* **2024**, *16*. [CrossRef]
7. Meirelles, G.; Manzi, D.; Brentan, B.; Goulart, T.; Luvizotto, E., Jr. Calibration model for water distribution network using pressure heads estimated by artificial neural networks. *Water Resour. Manag.* **2017**, *31*, 4339–4351. [CrossRef]
8. Zhao, Q.; Wu, W.; Simpson, A.R.; Willis, A. Simpler Is Better—Calibration of Pipe Roughness in Water Distribution Systems. *Water* **2022**, *14*, 3276. [CrossRef]
9. Savic, D.A.; Kapelan, Z.S.; Jonkergouw, P.M.R. Quo vadis water distribution model calibration? *Urban Water J.* **2009**, *6*, 3–22. [CrossRef]
10. Ferreira, B.; Antunes, A.; Carriço, N.; Covas, D. Multi-objective optimization of pressure head sensor location for burst detection and network calibration. *Comput. Chem. Eng.* **2022**, *162*, 107826. [CrossRef]
11. Maskit, M.; Ostfeld, A. Multi-Objective Operation-Leakage Optimization and Calibration of Water Distribution Systems. *Water* **2021**, *13*, 1606. [CrossRef]
12. Zanfei, A.; Menapace, A.; Brentan, B.; Sitzenfrei, R.; Herrera, M. Shall we always use hydraulic models? A graph neural network metamodel for water system calibration and uncertainty assessment. *Water Res.* **2023**, *242*, 120264. [CrossRef] [PubMed]
13. Nicolini, M.; Giacomello, C.; Deb, K. Calibration and Optimal Leakage Management for a Real Water Distribution Network. *J. Water Resour. Plann. Manag.* **2011**, *137*, 134–142. [CrossRef]
14. Salvino, M.M.; Carvalho, P.S.O.; Gomes, H.P. Calibração multivariada de redes de abastecimento de água via algoritmo genético multiobjetivo. *Eng. Sanit. Ambient.* **2015**, *20*, 503–512. [CrossRef]
15. Romero-Ben, L.; Alvez, D.; Blesa, J.; Cembrano, G.; Puig, V.; Duviella, E. Leak detection and localization in water distribution networks: Review and perspective. *Annu. Rev. Control* **2023**, *55*, 392–419. [CrossRef]
16. Osorio, D.A.J.; Lima, G.M.; Brentan, B.M. Hydraulic and economic analysis for rehabilitation of water distribution networks using pipes cleaning and replacement and leakage fixing. *Braz. J. Water Resour.* **2023**, *28*, e6. [CrossRef]
17. Garzón, A.; Kapelan, Z.; Langeveld, J.; Taormina, R. Machine Learning-Based Surrogate Modeling for Urban Water Networks: Review and Future Research Directions. *Water Resour. Res.* **2022**, *58*, e2021WR031808. [CrossRef]
18. Moasheri, R.; Ghazizadeh, M.J.; Tashayoei, M. Leakage detection in water networks by a calibration method. *Flow Meas. Instrum.* **2021**, *80*, 101995. [CrossRef]
19. Farghadan, A.; Zamani, M.S.; Ghazizadeh, M.J. A fault-injection-based approach to leak localization in water distribution networks using an ensemble model of Bayesian classifiers. *J. Process Control* **2023**, *132*, 103110. [CrossRef]
20. Chu, S.; Zhang, T.; Zhou, X.; Yu, T.; Shao, Y. An Efficient Approach for Nodal Water Demand Estimation in Large-scale Water Distribution Systems. *Water Resour. Manag.* **2022**, *36*, 491–505. [CrossRef]
21. Ostfeld, A.; Salomons, E.; Ormsbee, L.; Uber, J.G.; Bros, C.M.; Kalungi, P.; Burd, R.; Zazula-Coetzee, B.; Belrain, T.; Kang, D.; et al. Battle of the Water Calibration Networks. *J. Water Resour. Plann. Manag.* **2012**, *138*, 523–532. [CrossRef]

22. Zhang, Q.; Zheng, F.; Duan, H.-F.; Jia, Y.; Zhang, T.; Guo, X. Efficient Numerical Approach for Simultaneous Calibration of Pipe Roughness Coefficients and Nodal Demands for Water Distribution Systems. *J. Water Resour. Plann. Manag.* **2018**, *144*, 04018063. [CrossRef]
23. Chu, S.; Zhang, T.; Shao, Y.; Yu, T.; Yao, H. Numerical approach for water distribution system model calibration through incorporation of multiple stochastic prior distributions. *Sci. Total Environ.* **2020**, *708*, 134565. [CrossRef] [PubMed]
24. Zhang, Q.; Yang, J.; Zhang, W.; Kumar, M.; Liu, J.; Liu, J.; Li, X. Deep fuzzy mapping nonparametric model for real-time demand estimation in water distribution systems: A new perspective. *Water Res.* **2023**, *241*, 120145. [CrossRef] [PubMed]
25. Nicklow, J.; Reed, P.; Savic, D.; Dessalegne, T.; Harrell, L.; Chan-Hilton, A.; Karamouz, M.; Minsker, B.; Ostfeld, A.; Singh, A.; et al. State of the Art for Genetic Algorithms and Beyond in Water Resources Planning and Management. *J. Water Resour. Plann. Manag.* **2010**, *136*, 412–432. [CrossRef]
26. Zhang, L.; Jiang, H.; Cao, H.; Cheng, R.; Zhang, J.; Du, F.; Xie, K. Water Supply Pipeline Failure Evaluation Model Based on Particle Swarm Optimization Neural Network. *Water* **2024**, *16*, 3248. [CrossRef]
27. Minaee, R.P.; Afsharnia, M.; Moghaddam, A.; Ebrahimi, A.A.; Askarishahi, M.; Mokhtari, M. Calibration of water quality model for distribution networks using genetic algorithm, particle swarm optimization, and hybrid methods. *MethodsX* **2019**, *6*, 540–548. [CrossRef]
28. Jahandideh-Tehrani, M.; Bozorg-Haddad, O.; Loáiciga, H.A. Application of particle swarm optimization to water management: An introduction and overview. *Environ. Monit. Assess.* **2020**, *192*, 281. [CrossRef]
29. Souza Filho, F.A. *CEARÁ 2050: Diagnóstico dos Recursos Hídricos*; Ceará: Fortaleza, Brazil, 2018.
30. Walker, D.W.; Oliveira, J.L.; Cavalcante, L.; Kchouk, S.; Ribeiro Neto, G.; Melsen, L.A.; Fernandes, F.B.P.; Mitroi, V.; Gondim, R.S.; Martins, E.S.P.R.; et al. It's not all about drought: What "drought impacts" monitoring can reveal. *Int. J. Disaster Risk Reduct.* **2024**, *103*, 104338. [CrossRef]
31. Silva, S.M.O.; Souza Filho, F.A.; Cid, D.A.C.; Aquino, S.H.S.; Xavier, L.C.P. Proposta de gestão integrada das águas urbanas como estratégia de promoção da segurança hídrica: O caso de Fortaleza. *Eng. Sanit. Ambient.* **2019**, *24*, 239–250. [CrossRef]
32. Uchôa, J.G.S.M.; Almeida, P.P.; Marques, L.A.; Pereira, S.P.; Silva, S.M.O.; Lima Neto, I.E. Análise do impacto da usina de dessalinização no macrossistema de abastecimento de água da região metropolitana de Fortaleza—CE. In Proceedings of the I Simpósio Nacional de Mecânica dos Fluidos e Hidráulica, Ouro Preto, MG, Brazil, 22–24 August 2022.
33. CAGECE—Companhia de Água e Esgoto do Ceará. Planta de Dessalinização de Água Marinha. Available online: https://www.cagece.com.br/wp-content/uploads/PDF/EditaisContratacoes/PPP/Documentos-Relatorio/Relatorio_desempenho_de_projeto_PPP-Desal-1_assdpr.pdf (accessed on 7 January 2025).
34. Rathi, S.; Gupta, R.; Labhasetwar, P.; Nagarnaik, P. Challenges in calibration of water distribution network: A case study of Ramnagar elevated service reservoir command area in Nagpur City, India. *Water Sup.* **2020**, *20*, 1294–1312. [CrossRef]
35. Leinæs, A.; Simukonda, K.; Farmani, R. Calibration of intermittent water supply systems hydraulic models under data scarcity. *Water Sup.* **2024**, *24*, 1626–1644. [CrossRef]
36. Hossain, S.; Hewa, G.A.; Chow, C.W.K.; Cook, D. Modelling and Incorporating the Variable Demand Patterns to the Calibration of Water Distribution System Hydraulic Model. *Water* **2021**, *13*, 2890. [CrossRef]
37. Kennedy, J.; Eberhart, R. Particle swarm optimization. In Proceedings of the ICNN'95-International Conference on Neural Networks, Perth, WA, USA, 27 November–1 December 1995; Volume 4, pp. 1942–1948. [CrossRef]
38. Anchieta, T.F.F.; Meirelles, G.; Brentan, B.M. Optimal district metered areas design of water distribution systems: A comparative analysis among hybrid algorithms. *J. Water Process Eng.* **2024**, *63*, 105472. [CrossRef]
39. Rahman, N.A.; Muhammad, N.S.; Abdullah, J.; Mohtar, W.H.M.W. Model performance indicator of aging pipes in a domestic water supply distribution network. *Water* **2019**, *11*, 2378. [CrossRef]
40. Ghimire, A.B.; Magar, B.A.; Parajuli, U.; Shin, S. Impacts of Missing Data Imputation on Resilience Evaluation for Water Distribution System. *Urban Sci.* **2024**, *8*, 177. [CrossRef]
41. Farmani, R.; Savic, D.A.; Walters, G.A. Evolutionary multi-objective optimization in water distribution network design. *Eng. Optim.* **2005**, *37*, 167–183. [CrossRef]
42. Housh, M.; Jamal, A. Utilizing Matrix Completion for Simulation and Optimization of Water Distribution Networks. *Water Resour. Manag.* **2022**, *36*, 1–20. [CrossRef]
43. Water Research Centre. *Network Analysis—A Code of Practice*; WRc: Swindon, UK, 1989.
44. Kapelan, Z.S.; Savic, D.A.; Walters, G.A. Calibration of Water Distribution Hydraulic Models Using a Bayesian-Type Procedure. *J. Hydraul. Eng.* **2007**, *133*, 927–936. [CrossRef]
45. Moriasi, D.N.; Arnold, J.G.; Van Liew, M.W.; Bingner, R.L.; Harmel, R.D.; Veith, T.L. Model Evaluation Guidelines for Systematic Quantification of Accuracy in Watershed Simulations. *ASABE* **2007**, *50*, 885–900. [CrossRef]

46. Zarei, N.; Azari, A.; Heidari, M.M. Improvement of the performance of NSGA-II and MOPSO algorithms in multi-objective optimization of urban water distribution networks based on modification of decision space. *Appl. Water Sci.* **2022**, *12*, 133. [CrossRef]
47. Sabbaghpour, S.; Naghashzadehgan, M.; Javaherdeh, K.; Bozorg-Haddad, O. HBMO algorithm for calibrating water distribution network of Langarud city. *Water Sci. Technol.* **2012**, *65*, 1564–1569. [CrossRef] [PubMed]
48. Jadhao, R.D.; Gupta, R. Calibration of water distribution network of the Ramnagar zone in Nagpur City using online pressure head and flow rate data. *Appl. Water Sci.* **2018**, *8*, 29. [CrossRef]
49. Zanfei, A.; Menapace, A.; Santopietro, S.; Righetti, M. Calibration Procedure for Water Distribution Systems: Comparison among Hydraulic Models. *Water* **2020**, *12*, 1421. [CrossRef]
50. Ballarin, A.S.; Sousa Mota Uchôa, J.G.; Santos, M.S.; Almagro, A.; Miranda, I.P.; Silva, P.G.; Silva, G.J.; Gomes Júnior, M.N.; Wendland, E.; Oliveira, P.T. Brazilian water security threatened by climate change and human behavior. *Water Resour. Res.* **2023**, *59*, e2023WR034914. [CrossRef]

Disclaimer/Publisher's Note: The statements, opinions and data contained in all publications are solely those of the individual author(s) and contributor(s) and not of MDPI and/or the editor(s). MDPI and/or the editor(s) disclaim responsibility for any injury to people or property resulting from any ideas, methods, instructions or products referred to in the content.

water

MDPI

Article

A Method to Determine the Design Flow of Stormwater Pipe Networks Based on Dynamic Wave Simulation

Ying Tang [1], Yujie Zhao [2,3,*], Zhaoguang Li [1], Jinjun Zhou [2] and Hao Wang [2]

[1] Urban Construction School, Beijing City University, Beijing 100083, China; sugar201806035@bcu.edu.cn (Y.T.); lizhaoguang@bcu.edu.cn (Z.L.)
[2] College of Architecture and Civil Engineering, Beijing University of Technology, Beijing 100124, China; zhoujj@bjut.edu.cn (J.Z.); wanghao87@bjut.edu.cn (H.W.)
[3] Pearl River Water Resources Research Institute, Pearl River Water Resources Commission, Guangzhou 510610, China
* Correspondence: zhaoyujie5626@163.com

Abstract: The rational method (RM) adopting steady uniform flow assumption is a simple and mainstream approach for the design of urban stormwater-drainage systems (USDSs). However, when designing large-scale USDSs, the RM significantly deviates from the actual flow regime due to inappropriate assumptions. To improve the accuracy and reliability of the design method, a dynamic-wave-simulation-based method (DWSBM) is proposed. Firstly, a numerical model which is equivalent to the surface runoff yield process of RM is established and validated. Then the dynamic wave module is adopted for pipe flow calculations. This method integrates hydraulic models for the whole design process. Both DWSBM and RM are used for USDS design of two areas, and design comparison demonstrates that the design flow rates computed using DWSBM are greater than obtained by RM. With the increase in pipeline length, the design flow differences between the two methods in the two areas increased from 3.09% to 28.97% and from 16.01% to 45.40% respectively. Adopting the DWSBM for design flow rate calculation can effectively improve the design reliability and drainage capacity of USDSs.

Keywords: stormwater-drainage network design; dynamic wave method; SWMM

1. Introduction

The rationality of urban stormwater-drainage system (USDS) design is directly related to the drainage safety of an entire city [1]. Typically, the design of a USDS consists of two parts [2,3]: determination of the design flow rate and selection of pipe diameters and slopes. Among these components, the design flow rate is the basis for selecting the diameter and slope, and its accuracy directly influences the overall drainage performance of the USDS and the cost-effectiveness of the investment.

In conventional design processes of USDSs, the design flow rate is determined by the rational method (RM), which utilizes the Manning formula for hydraulic calculations [4,5]. This method only needs the rainfall intensity, runoff coefficient and catchment area, which is widely applied due to its simplicity and convenience. However, as a semi-empirical and semi-theoretical formula, the RM assumes the flow regime in the pipe network drainage process is steady and uniform, which deviates from actual flow conditions. Particularly when applied to the design of large-scale USDSs, its accuracy is notably insufficient. Furthermore, it can only calculate peak flow rates and fails to provide the entire flow hydrograph. Additionally, it is also unsuitable for pressure pipe networks. Therefore, for larger-scale USDSs, numerical models capable of simulating hydrological and hydraulic processes should be used to obtain more accurate design results.

With the development of hydraulic models, numerical simulations have been widely applied to verify existing USDS-design schemes. By utilizing hydraulic models to simu-

late existing USDSs and analyze deficiencies, support is provided for improving design schemes. Shao et al. [6] divided pipe network design into two stages based on the initial design scheme, and iteratively adjusted pipe diameters and slopes using a Storm Water Management Model (SWMM) according to pipe flow, velocity, and depth. To better reflect the flood resistance of urban pipe networks, Sañudo et al. [7] combined the Iber and SWMM, considering both hydrological and hydraulic processes during rainfall periods, and proposed a dual drainage model for urban drainage system design. Bisht et al. [8] utilized the MIKE URBAN model to simulate two-dimensional flooding, and modified drainage system designs according to flooding conditions.

In addition, many studies have utilized hydraulic model to optimize USDS-design schemes. Hydraulic models are used to assess the operational performance, and are further integrated with economic indexes to achieve more accurate and reasonable designs. Moussavi et al. [9] utilized SWMM for hydraulic simulation of drainage systems, combining it with adaptive genetic algorithms to obtain the most economic design scheme. Zaheri et al. [10] divided the design process into two stages using cellular automata, with pipe diameter and node elevation as decision variables, respectively. SWMM simulation was used to incorporate hydraulic performance into the constraints to select the optimal design scheme. Li et al. [11] combined online data-driven evolutionary algorithms with SWMM, aiming to minimize total overflow of the USDS. Flow velocity and design cost were used as constraints to accomplish the optimization of the USDS design.

With the development of multi-objective optimization algorithms, many studies considered the economic and hydraulic performance simultaneously to obtain the optimal solution. Based on SWMM and improved particle swarm optimization algorithm, Li et al. [12] employed a multi-objective optimization design method to minimize both engineering costs and flood risks. The feasibility and effectiveness of this approach were then validated through scenario simulations. Based on cellular automata, Guo et al. [13] took both network construction costs and overflow occurrences as objectives, determining the optimal design by optimizing pipe diameters. Lin et al. [5] conducted an SWMM-based simulation analysis, employing RM to establish an initial network. They proposed objective functions based on the average pipe fullness ratio, manhole overflow, and network construction costs to achieve a multi-objective optimization design. To enhance the efficiency of multi-objective optimization in network design, Wang et al. [14] conducted a comparative study of the non-dominated sorting genetic algorithm (NSGA), the MATLAB Global Optimization Toolbox (MLOT), and the genetically adaptive leaping algorithm for approximation and diversity (GALAXY) algorithms, and selected the most robust and simple one to assist in drainage system design.

The above methods effectively improve design precision through verification and optimization. However, the prerequisite for these methods is the availability of different design schemes, which offers the feasibility of finding the optimal design from multiple scenarios. This approach suffers from low computational efficiency, with computation time increasing as the scale of the USDS expands. Furthermore, if all runoff yield and flow concentration parameters within the design area cannot be accurately acquired, it is impossible to set model parameters accurately, thereby diminishing the reliability and universality of the hydraulic model.

To address the limitations of USDS design, this study proposes a dynamic-wave-simulation-based method (DWSBM) to deduce the design flow of the USDS. The DWSBM first establishes a runoff yield and flow concentration model which is equivalent to the RM. Then, utilizing the dynamic wave method, the design flow of pipes is calculated sequentially. By integrating the hydraulic model for USDS design, the method improves design efficiency and accuracy. By quantifying the differences in design results between RM and DWSBM, the impact of actual unsteady flow on the USDS design process is revealed, which provides support for the wider application of hydraulic models in USDS design.

2. Materials and Methods

2.1. The Rational Method to Compute the Design Flow Rate of Pipe Section

In USDS design, the most critical parameter is the design flow rate. Once the design flow rate is determined, other parameters such as pipe diameter, slope, fullness ratio, Manning's coefficient, and flow velocity can be determined according to the "Standard for design of outdoor wastewater engineering (GB 50014-2021)". Among these, the slope determines the pipe's elevation and flow velocity. The RM is the most commonly used approach for calculating design flow rates [15]. The RM posits that the design collection time of a pipe consists of surface collection time and pipe drainage time, assuming the flow of stormwater in the pipes is steady and uniform. When the duration of rainfall equals the time it takes for water to travel from the farthest point of the catchment to the manhole, the design flow rate of the pipe reaches its maximum. The calculation of the design flow rate of the stormwater pipe is achieved by multiplying the rainfall intensity, runoff coefficient, and drainage area. This method requires few parameters and is computationally simple [16].

The flow regime in actual stormwater pipes is unsteady, and employing the rational method can lead to inaccuracies. When the catchment area exceeds 2 km^2, the calculation accuracy of the RM is significantly reduced, rendering it unsuitable for adoption [17].

2.2. Pipe Drainage Simulation Based on Dynamic Wave Method

When designing pipe networks for larger catchments, it is imperative to employ dynamic wave method [18] which better represent the actual flow characteristics for calculating the pipe drainage process. The dynamic wave method solves Equations (1) and (2) which simulate the pipe drainage process.

$$\frac{\partial A}{\partial t} + \frac{\partial Q}{\partial x} = 0 \tag{1}$$

$$\frac{\partial Q}{\partial t} + \frac{\partial \left(Q^2/A\right)}{\partial x} + gA\frac{\partial H}{\partial x} + gAS_f = 0 \tag{2}$$

where x is the distance (m), t is the time (s), A is the cross-sectional area (m^2), Q is the flow rate (m^3/s), H is the water level in the pipe ($Z + Y$) (m), Z is the elevation of the inner bottom of the pipe (m), Y is the hydraulic head of water in the pipe (m), S_f is the friction slope, g is the gravitational acceleration (m/s^2).

The dynamic wave method fully considers various flow regimes and inlet and outlet losses, and simulates the complex actual water flow in the pipe by solving a complete set of Saint-Venant equations (Equations (1) and (2)) [19].

In the dynamic wave method for simulating flow process in drainage pipe networks, consideration is given to downstream boundary conditions. Specifically, when computing the hydraulic state for each time step, it is necessary to simultaneously solve the hydraulic equations for the entire pipe network. Consequently, when applying this model to the design and calculation of a USDS, it is essential to initialize a set of values for pipe diameters, slopes, and buried depths.

2.3. Parameters Setting of Runoff Yield Model and Flow Concentration Model

After determining a series of parameters, including rainfall initial loss parameters, infiltration parameters, and surface Manning's coefficient, the DWSBM can simulate the surface runoff yield and flow-concentration processes through the initial-continuing loss method and nonlinear reservoir method, respectively. However, it is common in many areas that required parameters cannot be unconditionally obtained during the design period. Considering the fairness of comparison and the relatively easy acquisition of RM parameters, the aforementioned parameters of DWSBM are set as equivalent to those of the RM. As for the surface runoff yield process, equivalence is achieved by adjusting infiltration parameters. For the flow-concentration process, it is achieved by the isochronous method.

2.3.1. Equivalent Setting of Surface Runoff Yield Model

Losses in the urban runoff yield process are dominated by surface infiltration. The depression storage and evaporation can be neglected [20]. Equation (5) is the φ index method to calculate the net rainfall (runoff) process line after determining the parameters of the Horton infiltration (Equations (3) and (4)). Through trial calculations, parameters of the Horton infiltration index are determined based on the principle of equivalence of discharge-runoff coefficient (Equation (6)) and rainfall volumetric runoff coefficient (Equation (7)) [21].

$$f_i = f_c + (f_0 - f_c)e^{-ki} \tag{3}$$

$$F_{(i)} = f_c \times i + \left[\frac{f_0 - f_c}{k}\right]\left(1 - e^{-ki}\right) \tag{4}$$

$$R_i = \begin{cases} P_i - F_i, & P_i > F_i \\ 0, & P_i \le F_i \end{cases} \tag{5}$$

$$\sum_{i=j+1}^{j+t_1} R_i = C_{max}\sum_{i=j+1}^{j+t_1} P_i \tag{6}$$

$$\sum_{i=1}^{n} R_i = C\sum_{i=1}^{n} P_i \tag{7}$$

where f_0 is the initial infiltration rate, mm/min, f_c is the equilibrium infiltration rate, mm/min, k is the decay coefficient, F_i is the infiltration intensity at time i, mm/min, R_i is the runoff volume at time i, mm, P_i is the rainfall volume at time i, mm, t_1 is the surface collection time in the sub-catchment area, min, C_{max} is the discharge runoff coefficient, n is the number of rainfall periods, and C is the rainfall volumetric runoff coefficient.

Due to the large number of sub-catchments, the manual trial calculation of Horton's infiltration parameters can be quite complex. To address this complexity, the particle swarm optimization (PSO) algorithm [22,23] is employed for automatic optimization adjustment of parameters. The objective function is shown in Equation (8).

$$\min F = \left|\sum_{i=j+1}^{j+t_1} R_i - C_{max}\sum_{i=j+1}^{j+t_1} P_i\right| + \left|\sum_{i=1}^{n} R_i - C\sum_{i=1}^{n} P_i\right| \tag{8}$$

Parameters to be optimized are f_0, f_c, and k. The initial population of particles is generated based on the reasonable range of each parameter (Table 1). Through multiple iterations, the optimized equivalent settings of the parameters for the runoff yield model are achieved.

Table 1. Reasonable range of each optimization variable.

Parameter	f_c (mm/min)	f_0 (mm/min)	k (min^{-1})
Alpha loamy sand	0.59	8.04	0.64
Carnegie sandy loam	0.75	6.25	0.33
Cowarts loamy sand	0.83	6.47	0.18
Dothan loamy sand	1.11	1.47	0.02
Fuquay pebbly loamy sand	1.02	2.64	0.08
Leefield loamy sand	0.73	4.80	0.13
Stilson loamy sand	0.66	3.43	0.11
Range	0.00~0.83	0.03~4.23	0.03~0.12

The particle swarm optimization (PSO) algorithm is used to optimize the objective function. The detailed process of the algorithm is shown in Figure A1. The maximum flying speed of particles in each dimension is $\pm 0.1 \times$ (upper bound $-$ lower bound) [24], with an acceleration coefficient of 2 [25]. The inertia weight follows a linearly decreasing weight (LDW) strategy [26], as shown in Equation (9):

$$w_i = w_{max} - (w_{max} - w_{min}) \times i/N \tag{9}$$

where w_i is inertia weight at the ith generation, w_{max} is 0.95, w_{min} is 0.45 [27], i is current generation number, and N is termination generation number.

2.3.2. Equivalent Setting of Flow-Concentration Model Parameters

The isochronal method [28], also known as the time-area method, assumes that the runoffs do not interfere with each other and consist of a linear superposition of the runoff on each isochronal block according to the confluence time in turn. The formula of the isochronal method is presented in Equation (10) [29], which requires only determination of the pipe drainage time and flow-concentration curve type.

$$Q_{(t_i)} = \frac{\alpha F}{t_k} \sum_{j=1}^{t_k} I_{t_{i-j}} \cdot \Delta t \tag{10}$$

where $Q(t_i)$ is the flow rate at the moment of t_i, m^3/s; $I_{t_{i-j}}$ is the net rainfall at the moment of t_{i-j}, mm. When $t_{i-j} \leq 0$, take $t_{i-j} = 0$. F is the area of catchment, ha; α is the unit conversion factor, 0.167.

Since the RM is based on rectangular catchments and the urban stormwater-catchment area can be mostly generalized to rectangular catchments, a linear flow-concentration curve is utilized. The surface collection time of the sub-catchment is considered the pipe drainage time. By setting the pipe drainage time and flow-concentration curve type of the DWSBM equivalent to the RM, the stormwater inlet process line of the DWSBM can be completed.

2.3.3. Coupling Setting of Runoff Yield Model, Flow-Concentration Model and SWMM Dynamic Wave Model

SWMM [30] is widely used for the simulation and analysis of USDSs. This study utilizes its dynamic wave module for simulating the pipe drainage process. For the surface runoff yield and flow-concentration process, SWMM provides the initial-continuing loss method and the nonlinear reservoir method, respectively. However, both the initial-continuing loss method and the nonlinear reservoir method require the determination of many parameters, which is unpractical in the design period. Thus, this study uses the runoff coefficient and the isochronous method instead. Hence, the runoff yield model and the flow concentration model proposed in this study need to be coupled with the dynamic wave module. Firstly, using the aforementioned two models, all sub-catchments are simulated once to obtain the full time stormwater inlet process line of each node. In the subsequent pipe drainage simulation process, the stormwater inlet process line of each node is used as the inflow property of SWMM. The process is illustrated in Figure 1.

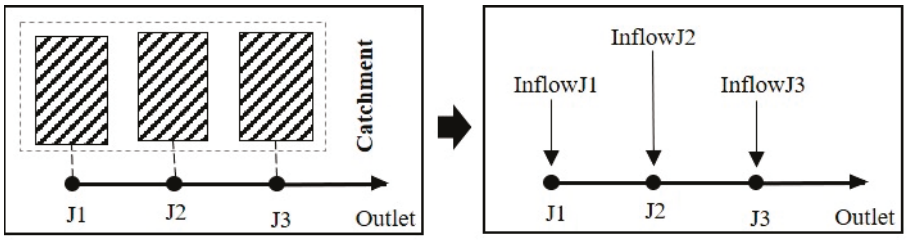

Figure 1. Model coupling schematic diagram.

2.4. Stormwater Pipe Network-Design Framework Based on Dynamic Wave Method

Utilizing the design equivalence method proposed in Section 2.3 for the stormwater inlet process line, and coupling it with the dynamic wave method, the design condition equivalence is achieved. Based on this, the design of the USDS is conducted, and the design process is shown in Figure 2.

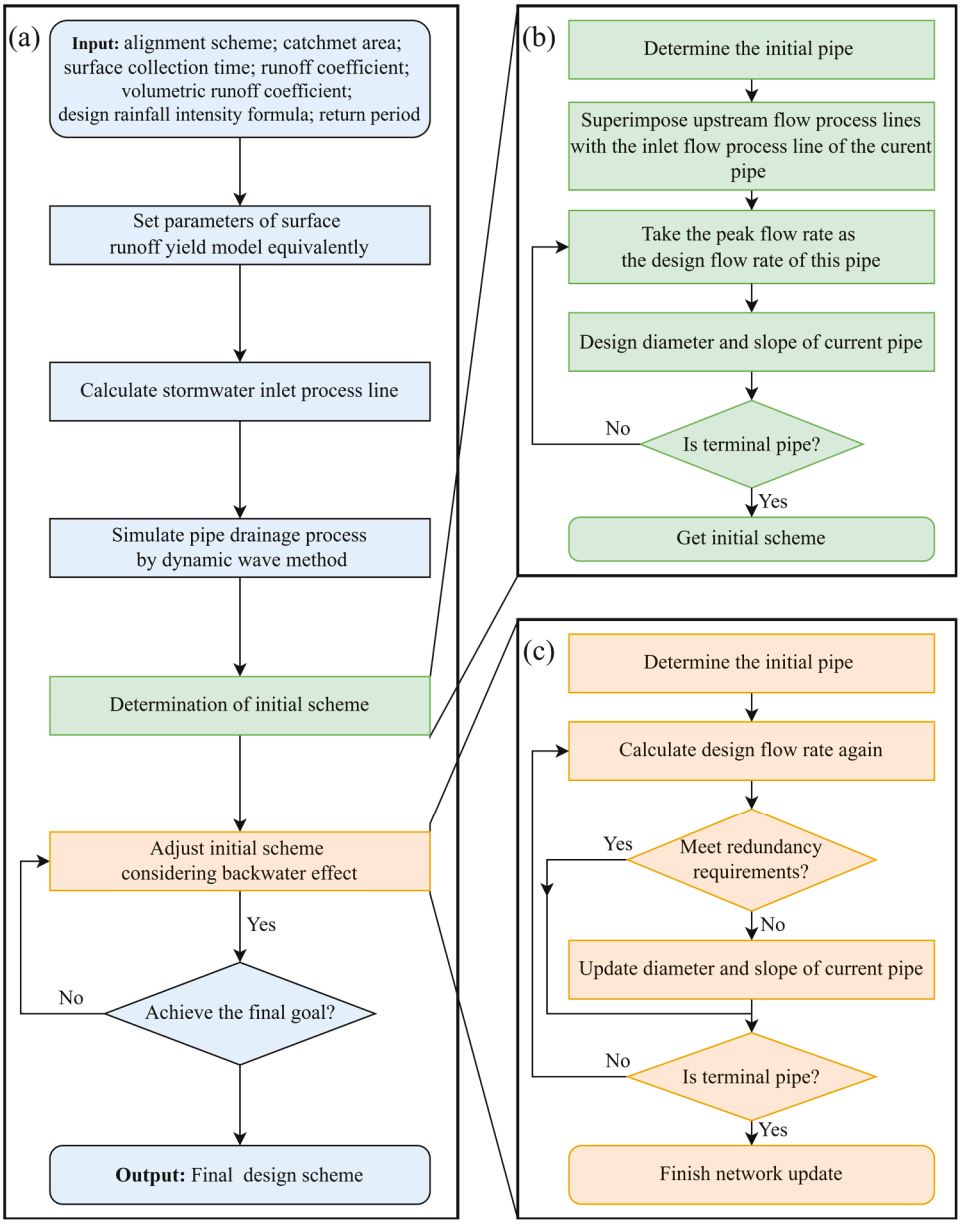

Figure 2. Design process of USDS based on DWSBM. (**a**) Main design process. (**b**) Design process of initial scheme. (**c**) Adjust process of initial scheme.

Starting from the upstream pipe, the initial pipe diameter, slope, and buried depth values are determined, and then the design adjustment of the USDS is carried out to establish the initial scheme.

Based on the dynamic wave method, the drainage process of the pipes is simulated. The flow process line for each pipe is then calculated. The peak flow rate Q_{max} of a flow process line is taken as the design flow rate for the pipe. Based on this, the initial design scheme is adjusted accordingly. The final objectives of the dynamic wave-based stormwater pipe network design are shown in Equations (11) and (12):

$$0.90 \leq min\left\{\left(\frac{Q_{max}}{Q_{full}}\right)_i\right\} i = 1, 2 \cdots, n \tag{11}$$

$$1 > max\left\{\left(\frac{Q_{max}}{Q_{full}}\right)_i\right\} i = 1, 2 \cdots, n \tag{12}$$

where Q_{full} is the full pipe flow of the pipe; $(Q_{full}/Q_{max})_i$ is the difference between the full pipe flow of pipe section i and the design flow; n is the number of pipes.

Compare Q_{max} and Q_{full}, and adjust the pipe diameter and slope accordingly until the final design scheme is obtained. The constraints in the design process are shown in Equations (13)–(15).

$$D_i \in Z \tag{13}$$

$$D_{i-1} \leq D_i \tag{14}$$

$$H_i > H_{min} \tag{15}$$

where D_i is the pipe diameter of design pipe i; Z is the set of commercial pipe diameters, D_{i-1} is the maximum upstream pipe diameter adjacent to the design pipe, D_0 is the initial pipe diameter of the design pipe; S_i is the slope of design pipe section i; H_i is the covered depth of design pipe section i; H_{min} is the minimum covered depth.

2.4.1. Determination of Initial Schemes

In order to simplify the initial parameter settings, in the process of determining the initial scheme, the influence of the backwater is ignored. Applying the dynamic wave model to simulate the drainage process of pipes, the initial design is completed section by section from the upstream. The process is shown in Figure 2b and the steps are described in detail as follows:

(1) Determine the initial pipe based on the alignment scheme;
(2) Simulate the flow process lines of all upstream pipes connected to this pipe using the dynamic wave method. Superimpose these lines with the inlet flow process line of the sub-catchment area of this pipe, and take the peak flow rate as the design flow rate of this pipe;
(3) Complete the hydraulic calculation of this pipe based on the design flow rate, and determine the pipe diameter and slope;
(4) Proceed from upstream to downstream, complete the design of the pipe diameter and slope for each section in sequence.

To improve the efficiency of selecting the initial scheme, the combination of diameter and slope of each pipe is determined according to the following rules:

(1) Determine the minimum slope S_{flow} allowed for each pipe according to its design flow rate, and determine the maximum slope S_1 and minimum slope S_2 according to the design velocity range and design buried depth range of the pipe section;
(2) Determine the allowable slope range S_{min}~S_{max} for each pipe according to the relative size between S_{flow}, S_1, and S_2; if $S_{flow} > S_1$, the design parameters selected for the pipe do not meet the design requirements;
(3) Determine the pipe slope according to the relative size between the ground slope S_0, S_{min}, and S_{max}.
    (1) If S_0 is greater than S_{max}, choose S_{max};
    (2) If S_0 is between S_{min} and S_{max}, choose S_0;
    (3) If S_0 is less than S_{min}, choose S_{min}.

2.4.2. Sensitivity Analysis of Parameters

The initial scheme requires further adjustment of diameter and slope according to the full flow conditions. In order to effectively determine the adjustment order of diameter and slope, a sensitivity analysis of the two parameters was performed in the study based on Manning's formula (Equation (16)) using the perturbation method [31].

$$Q = A_0 v = A_0 \frac{1}{n_c} R^{\frac{2}{3}} S_0^{\frac{1}{2}} \tag{16}$$

where Q is the flow rate (m^3/s); A_0 is the cross-sectional area of the pipe (m^2); v is the flow velocity of the pipe (m/s); n_c is the roughness coefficient of the pipe; R is the hydraulic radius; S_0 is the slope of the pipe.

The perturbation analysis method is commonly used for sensitivity analysis [32]. For example, the diameter of a pipe is kept constant and a perturbation is applied to the benchmark value of the slope. By observing the change of the flow rate calculated by Equation (16) when the slope changes, the sensitivity of the flow rate to the slope can be assessed. The influence of the diameter or slope change on the flow rates is quantified by calculating the change rate β. The perturbation is achieved by multiply perturbation multipliers α with the diameter or slope. Without loss of generality, perturbation multipliers used in this study are 0.80, 0.85, 0.90, 0.95, 1.00, 1.05, 1.10, 1.15, and 1.20, totaling nine values. To evaluate β under different perturbations, the sensitivity of the diameter and slope is then calculated using Equation (17).

$$\text{Sensitivity} = \frac{\sum_{j=1}^{9} (\alpha_j - \overline{\alpha})(\beta_j - \overline{\beta})}{\sum_{j=1}^{9} (\alpha_j - \overline{\alpha})} \quad (17)$$

where $\beta_j = (R_j - R_r)/R_r$, R_j is the flow rate with a specific perturbation multiplier α_j, R_r is the baseline flow rate without perturbation, $\overline{\alpha} = \sum_{j=1}^{9} \alpha_j/9$, $\overline{\beta} = \sum_{j=1}^{9} \beta_j/9$.

In the sensitivity analysis of the pipe diameter, considering two types of stormwater pipe, circular pipe and culvert, the influence of the pipe diameter (circular pipe) or canal width (culvert) on the flow rate is analyzed separately. In the sensitivity analysis of the slope, the same size of the round pipe or culvert is used and the slope 0.0020 is used as the benchmark value. The calculated statistical results are shown in Table 2.

Table 2. Statistics of perturbation results of pipe diameter and slope.

Diameter (mm)/ Cross-Sectional Size (mm × mm)	Slope	Sensitivity of Diameter	Sensitivity of Slope
DN1000	0.0020	2.681	0.502
DN2000	0.0020	2.681	0.502
2000 × 2000	0.0020	1.331	0.502
4000 × 2400	0.0020	1.248	0.502
6000 × 2600	0.0020	1.200	0.502

The results in Table 2 show that for the pipe diameter, the change in the diameter of the circular pipe has the greatest effect on the design flow. The sensitivity of the cross-sectional size of the culvert gradually decreases as the pipe section size increases. Relatively, the sensitivity of the slope is smaller and overall lower than the effect of the pipe diameter. Therefore, the pipe diameter or canal width should be prioritized in the design process.

2.4.3. Determination of the Final Design Scheme

After determining the initial scheme, the dynamic wave method is called again to simulate the drainage process in the pipe. The design scheme is adjusted considering the backwater effect upon the initial design scheme. According to Section 2.4.2, the pipe diameter should be adjusted first, followed by the slope. Eventually, the final design scheme is determined, meeting design objectives. The specific design process is shown in Figure 2c, with specific steps outlined as follows:

(1) Identify the upstream initial pipe section;
(2) Simulate the entire pipe network by the dynamic wave method, obtain the flow process line of this pipe, and use the peak value as the design flow rate Q_{max};
(3) Check whether the pipe section meets the design redundancy requirements as shown in Equation (18). If it meets the design requirements, proceed directly to the next step. If not, adjust the diameter and slope according to the design flow;

(4) Check whether the current pipe is the end pipe. If it is, finish the pipe network adjustment. If not, go to the next pipe section design and return to step 2;
(5) Adjust the pipe network according to the above steps until the final design scheme is determined.

$$0.90 \leq \left(\frac{Q_{max}}{Q_{full}}\right)_i < 1 \; i = 1, 2 \cdots, n \tag{18}$$

where Q_{full}, Q_{max}, i, and n are the same as Equations (11) and (12).

In the process of determining the final design scheme, the adjustment rules of the pipe diameter and slopes are as follows:

(1) According to the results of the sensitivity analysis, the pipe diameter should be adjusted first, starting from the initial value, according to the commercial pipe diameter, decreasing step by step;
(2) When the design flow meets the termination condition, the adjustment is completed. If the adjustment of the pipe diameter cannot reach the termination condition, the slope should be adjusted in steps of 0.001;
(3) In the process of adjusting the pipe diameter in decreasing steps, if the design flow rate and full pipe flow rate ratio is greater than 1 with reduction of the pipe diameter by one level and the ratio is less than 0.90 without reduction, it is necessary to adjust the slope of the pipe section and the ground slope. The principle is as follows: if the ground slope is less than the slope of the pipe (usually in flat terrain), only reduce the slope (without reducing the diameter); if the slope of the ground is greater than the slope of the pipe, then choose to reduce the diameter and increase the slope.

3. Results

The USDSs in two areas of Beijing, China, are used as examples to compare design results using different design methods.

3.1. Study Area

Case 1 (Figure 3a): The catchment area is 2.48 km^2 with 37 sub-catchments. The pipe network consists of 38 pipes totaling 10.41 km, with 38 nodes and 1 outlet, and the design standard is a 3-year event. The C_{max} of each sub-catchment is 0.60~0.80, and the C is 0.48~0.68 accordingly.

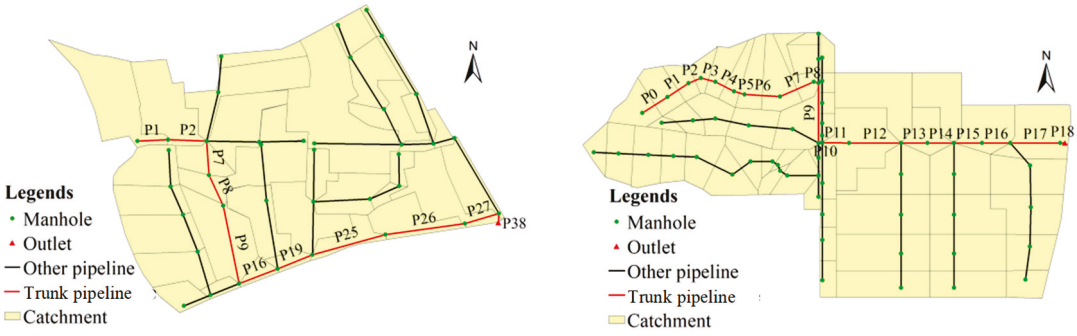

Figure 3. Plane figure of stormwater network; (**a**) Case 1; (**b**) Case 2.

Case 2 (Figure 3b): The catchment area is 4.506 km^2 with 56 sub-catchments. The pipe network consists of 61 pipes with a total length of 12.403 km, 61 nodes, and 1 outlet; and it follows the same standard as Case 1, with a C_{max} of 0.65 and a C of 0.53 for each sub-catchment.

3.2. Equivalent Settings for Model Parameters

Surface runoff simulations for sub-catchments of Cases 1 and 2, as well as the calculation of the rainfall inlet process line for each sub-catchment, were conducted sequentially. Taking a certain sub-catchment in Case 2 as an example, the process and results of the equivalent setting are elaborated below. Table 3 presents the relevant design parameters for this area.

Table 3. Initial design parameters of a sub-catchment in Case 2.

Catchment Area (ha)	C_{max}	C	Surface Collection Time (min)	Return Period (years)
2.73	0.65	0.53	8	3

Firstly, the infiltration parameters of sub-catchments are determined using the PSO algorithm to obtain their net rainfall process lines. Then, the isochronal method is applied to calculate the stormwater inlet process lines. The PSO algorithm is configured with a swarm size of 100, and the termination criterion is set to 50 generations. The optimization process is illustrated in Figure 4, and the stormwater inlet process line is illustrated in Figure 5. Table 4 shows that the optimal C_{max} and C obtained by PSO are equal to the initial parameters of the sub-catchment area with an objective function value of 0.0087, indicating equivalence of surface runoff. The peak flow rate of the stormwater inlet process line, calculated by the runoff yield model and flow-concentration model of DWSBM, is 0.5614 m^3/s. The difference of the peak flow rate between the DWSBM and the RM is 0.0011 m^3/s. A relative error of 2% demonstrates the equivalence setting of the surface runoff model.

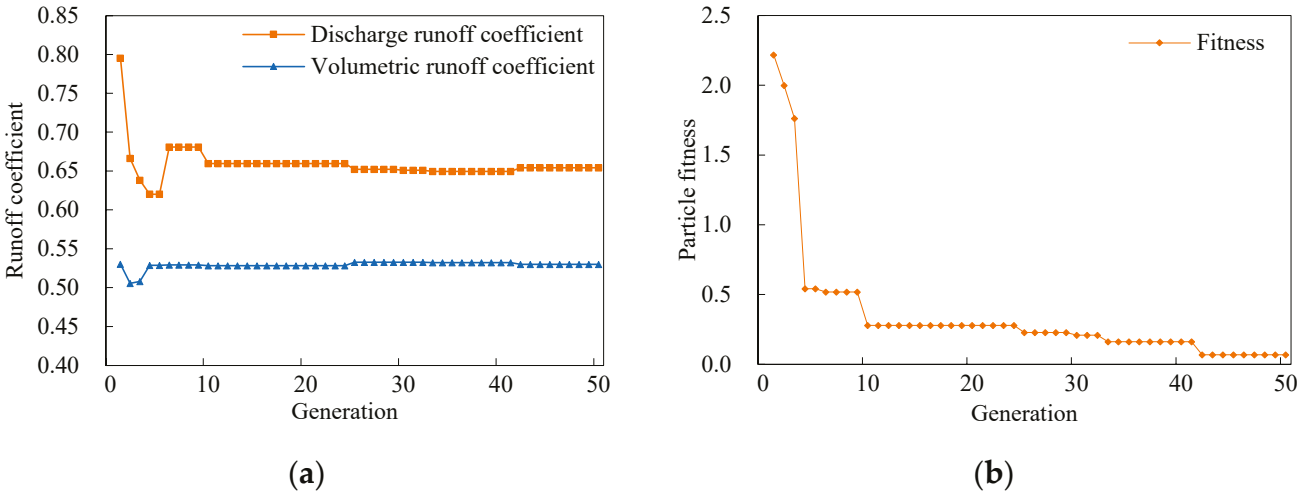

Figure 4. Optimization process; (**a**) C_{max} and C; (**b**) fitness.

Table 4. Results of a sub-catchment after design condition equivalence.

F_{min}	Outlet Flow Rate (m^3/s)		Absolute Error (m^3/s)	Relative Error (%)
	Rational Method	Equivalent Model		
0.0087	0.5603	0.5614	0.0011	2

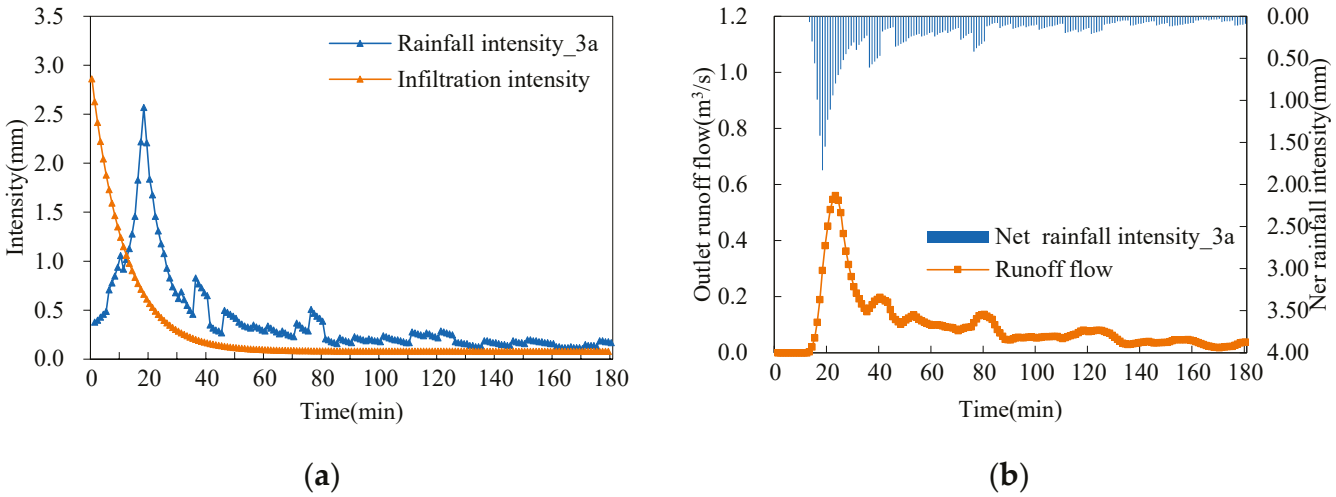

Figure 5. Calculation of runoff yield and flow concentration; (**a**) calculation of runoff yield; (**b**) calculation of flow concentration.

Based on the above method, the surface runoff parameters of all sub-catchments are equivalently set to obtain the stormwater inlet process line for each sub-catchment. These hydrographs are then coupled with the dynamic wave model of SWMM to facilitate the design of the USDS.

3.3. Analysis of the Backwater Effect

Since the backwater effect is influenced by many factors, such as pipe size, slope, and node inflow, it is difficult to quantify simply. Therefore, this section analyzes the impact of downstream backwater on upstream design from the perspective of the difference between initial scheme flow and final simulation results.

The flow calculated for each pipe during the determination of the initial scheme is taken as the "initial value". After applying the dynamic wave method to adjust the initial scheme, the peak flow calculated for each pipe is termed the "final value". The relative error of two flow values (Equation (19)) is used to characterize the influence of the pipe backwater effects on the design results.

$$\text{Relative Error} = \frac{\left(Q_{final} - Q_{initial}\right)}{Q_{initial}} \tag{19}$$

where $Q_{initial}$ is the pipe flow of the initial design scheme; Q_{final} is the peak pipe flow of the final design scheme.

Figure 6 illustrates the relative errors in design flows for each trunk pipe in Case 1 and Case 2. The relative errors of pipe flow fluctuate in two network instances, but they are all less than 0 except for the terminal pipe. To estimate the influence of backwater effects on flow calculations more precisely, average relative errors in the design flow rates for all pipes in the two instances are calculated. These averages were −0.027 for Case 1 and −0.020 for Case 2. In summary, within stormwater pipe networks of the same scale, the backwater effects generated by downstream pipes result in a reduction in the designed flow rates of upstream pipes. Therefore, to improve the accuracy in design calculations, it is imperative to consider the downstream backwater effect during flow rate computations.

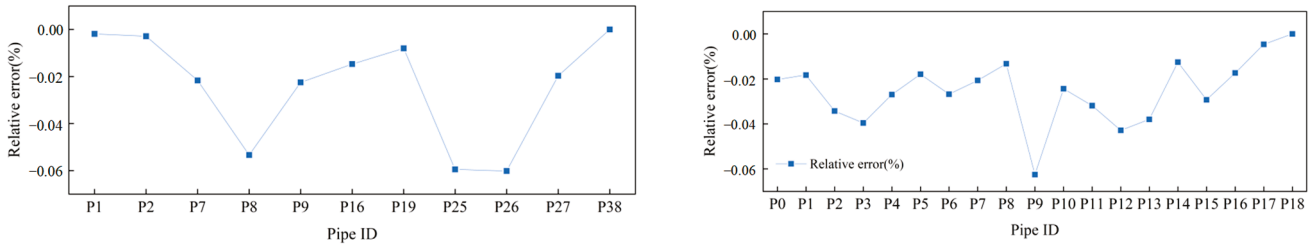

Figure 6. Relative error of design flow. (**a**) Case 1; (**b**) Case 2.

3.4. Comparative Analysis of the Design Results of Two Methods

When applying the DWSBM for a USDS design, the primary differences between the DWSBM and the RM arise from the calculation of the pipe drainage process, as parameters of the runoff yield model and the flow concentration model are set equivalently. To quantify differences between these two methods, the design results for trunk pipes in two cases are compared through design collection time, pipe drainage time, and design flow rate. The spatial distribution of the selected pipes for the two cases is illustrated in Figure 3.

3.4.1. Comparison Between USDS Capacity and Observed Runoff Data

The USDS should effectively drain runoff from the catchment. By comparing the runoff with the drainage volume of the pipe network, the drainage capacity of the USDS can be evaluated. Therefore, runoff data during a rainfall on 10 July 2022 were collected. In Case 1, the observed runoff volume is 1.03246×10^5 m^3, the runoff calculated by the RM is 9.8138×10^4 m^3 in total, and the DWSBM is 1.00224×10^5 m^3. In Case 2, the observed runoff volume is 1.88643×10^5 m^3, the runoff calculated by the RM is 1.84978×10^5 m^3, and the DWSBM calculates 1.85597×10^5 m^3. Table 5 shows the relative errors among the RM, the DWSBM, and the observed runoff data. Although RM can drain most of the runoff, the runoff volume drained by the DWSBM is larger than the RM, which proves the superiority of the DWSBM.

Table 5. Relative error among RM, DWSBM, and observed data.

Source of Runoff Data	Case 1	Case 2
Observed (m^3)	1.03246×10^5	1.88643×10^5
RM (m^3)	9.8138×10^4	1.84978×10^5
Relative error between observed and RM (%)	−4.95%	−1.94%
DWSBM (m^3)	1.00224×10^5	1.85597×10^5
Relative error between observed and DWSBM (%)	−2.93%	−1.61%

Note: Relative error = $(R_s - R_{obs})/R_{obs}$, where R_s is the simulated runoff data by RM or DWSBM, and R_{obs} is the observed runoff data.

3.4.2. Comparison of Design Runoff Yield Time and Pipe Drainage Time

The main difference in design collection time arises from the calculation of pipe drainage time. First, pipe drainage times are compared. As shown in Figure 7, the pipe drainage time calculated by the DWSBM is shorter, and the velocity is higher compared to the RM.

The difference in collection time is shown in Figure 8. From upstream to downstream, as the number of pipes increases and pipe drainage time accumulates, the difference in collection time calculated by the two methods gradually increases. In Case 1, the maximum difference is 12.15 min, while in Case 2, it is 16.87 min.

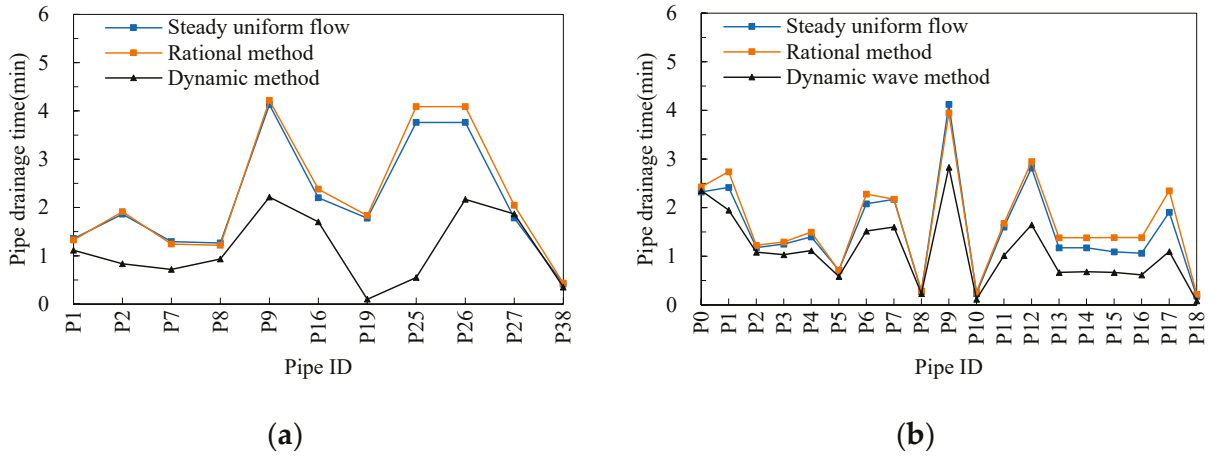

Figure 7. Comparison of pipe drainage time between dynamic wave method and rational method. (**a**) Case 1; (**b**) Case 2.

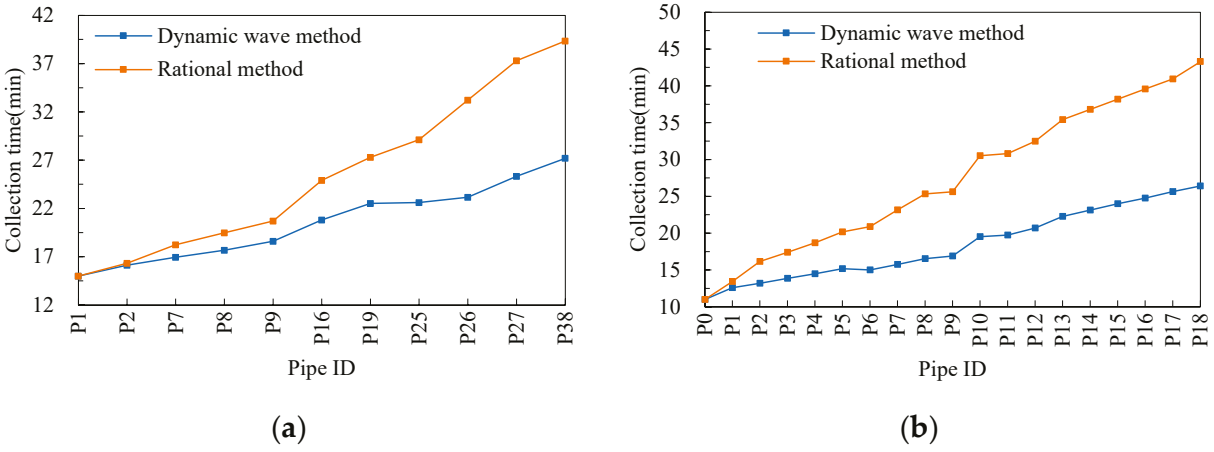

Figure 8. Comparison of collection time between dynamic wave method and rational method. (**a**) Case 1; (**b**) Case 2.

The RM simulates the pipe drainage process based on the steady uniform flow in the fully filled pipe. The dynamic wave method associates the pipe drainage time with water levels upstream and downstream. During the design process of the DWSBM, the water level in the pipe continuously rises, meaning a higher upstream water level compared to downstream, with the hydraulic gradient exceeding the pipe slope. Therefore, for the same diameter and slope, the time calculated by the dynamic wave method is shorter than that by RM.

3.4.3. Comparison of Design Flow

Based on the analysis in Section 3.4.2, when the DWSBM and the RM are applied to the design of USDSs, differences in pipe design flow rates are inevitable due to differences in the design collection time and pipe drainage time. Since the DWSBM reduces the time interval between the peak of the upstream flow process line and the peak of the stormwater inlet flow process line of the catchment, the calculated design flow rate of the pipe is greater than that of the RM.

To investigate differences in design flow rates by two methods under various design areas, the design flow values of trunk pipes are compared, as shown in Figures 9 and 10.

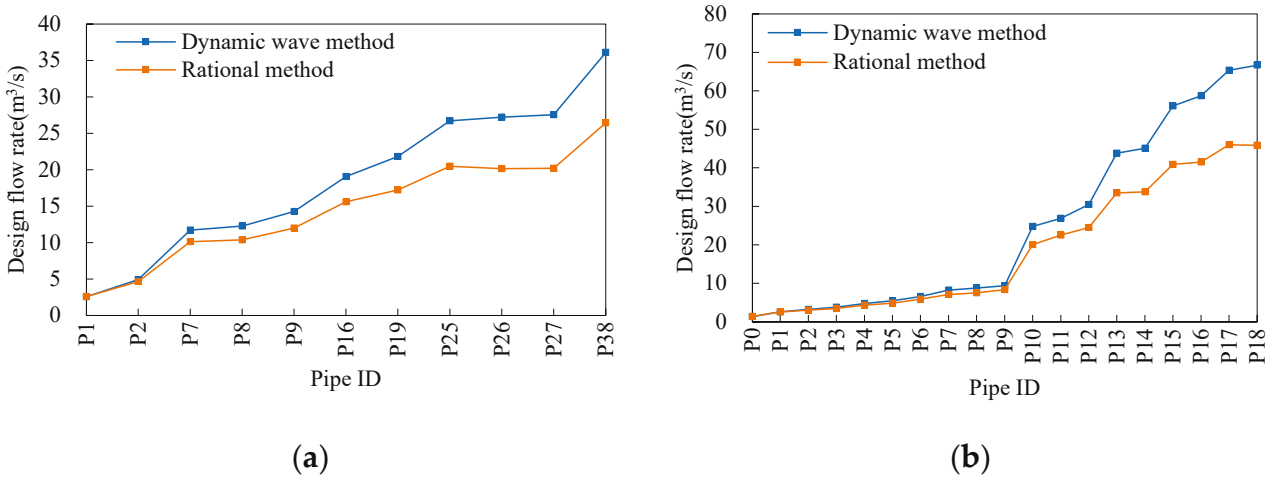

Figure 9. Comparison of design flow. (**a**) Case 1; (**b**) Case 2.

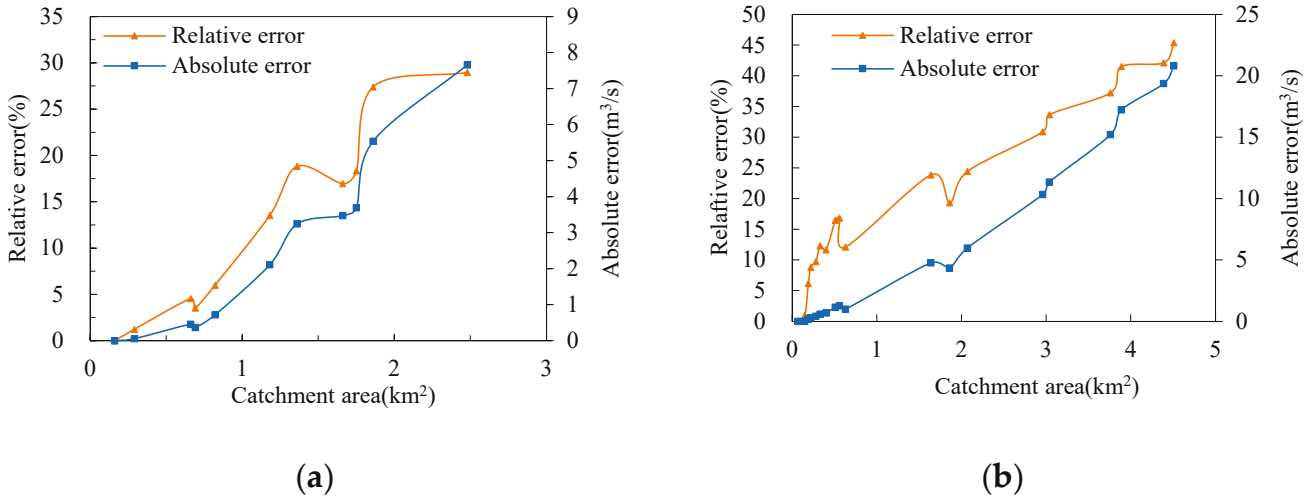

Figure 10. Relation between design flow difference and catchment area. (**a**) Case 1; (**b**) Case 2.

Figure 9 shows that, in both cases, as the number of pipes increases from upstream to downstream, the difference in design flow rates between the two methods gradually increases, and reaches a maximum at the terminal pipe. For Case 1, the maximum difference in design flow rates is 7.66 m^3/s, with the relative error increasing from 3.09% to a maximum of 28.97%. In Case 2, the maximum difference in design flow rates is 20.82 m^3/s, with the flow rate relative error increasing from 16.01% to a maximum of 45.40%.

Figure 10 compares the design flow between two methods for different catchment areas. For design catchment areas of 2 km^2, the flow differences calculated for Case 1 and Case 2 are 6.11 m^3/s and 5.42 m^3/s, respectively. And the flow calculated by DWSBM increased by 28.49% and 23.40% compared to the RM for the respective cases.

For a practical USDS, design conditions such as pipe layout can affect the results of hydraulic calculations. Hence, for USDSs with the same catchment area but located in different regions, the absolute and relative errors in flow calculated by the two methods may vary. However, the consistency lies in the DWSBM yielding a design flow greater than that derived from the RM.

4. Discussion

The design scheme for USDSs is not an actual drainage system but an engineered product developed under specific design conditions, lacking observed real-time network monitoring data. In the DWSBM, the simulation for the surface runoff process involves

numerous parameters, which are provided only within reasonable ranges. Therefore, during the design period, it is challenging to quantitatively and scientifically validate these parameters, and their unchecked application can lead to significant design deviations. To address this, our study proposes a method that combines runoff coefficients with the φ index method for runoff yield calculations. This method is coupled with the isochronal method to ensure that the parameters in the runoff model are equivalent to those in the RM. This method ensures the reliability of the simulation parameters and supports the application of the DWSBM in calculating design flows for USDSs.

To further analyze the influence of the pipe drainage process on the design results, the design flow, pipe drainage time, design collection time, and design redundancy (q/Q) (Q_{max}/Q_{full}) of the entire network of two cases are statistically analyzed. The design results of the DWSBM are considered the true value, and the relative error between the two methods and the rational method are calculated (Equation (20)). As shown in Table 6, the relative error of the design flow is positive, indicating that the design flow of the DWSBM is higher than that of the RM. Since the catchment area of Case 2 is 1.82 times that of Case 1, the design flow difference in this example is larger, and the relative error is higher. The relative errors of the pipe drainage time and design collection time are negative, which indicates that the pipe drainage time calculated by the DWSBM is shorter than that of the RM. The phenomenon is consistent with the conclusion of the pipe drainage time of the DWSBM and the RM.

$$\text{Relative Error} = \frac{V_{DWSBM} - V_{RM}}{V_{RM}} \tag{20}$$

where V_{DWSBM} is the value (design flow, pipe drainage time, design collection time, and design redundancy) obtained by the DWSBM, V_{RM} is the corresponding value obtained by RM. The numerator of Equation (19) is the absolute error.

Table 6. Relative error of design results between DWSBM and RM.

	Design Flow	**Pipe Drainage Time**	**Design Collection Time**	***q*/*Q***
Case 1	0.02	−0.45	−0.08	−0.03
Case 2	0.10	−0.43	−0.21	−0.33

The main reason for the difference between the two methods lies in the calculation of the pipe drainage process. In order to explain the generation of the design flow difference, the relative errors of the design flow (ΔQ), the pipe drainage time (Δt_2), and the design collection time (Δt_1) and q/Q ($\Delta(q/Q)$) in the two cases are statistically analyzed to ensure that all values provide a unified baseline. A multiple linear regression is performed on these four variables, and variables with p values less than 0.05 are eliminated. The regression equation is $\Delta Q = -0.0326 - 0.9238\Delta t_1 + 0.798\Delta(q/Q)$. The variables that significantly affect ΔQ include Δt_1 and $\Delta q/Q$, with a confidence level of 95%. The response coefficients and variance analysis results are shown in Tables 7 and 8. The analysis of variance (ANOVA) of the multiple linear regression is shown in Table 9. The F-statistic of 90.48 ($p < 0.001$) confirms that the model is statistically significant.

Table 7. Response coefficient.

Term	**Coefficient**	**Standard Error**	**T Value**	***p* Value**
Constant term	−0.0326	0.0133	−2.46	0.019
Δt_1	−0.9238	0.0716	−12.89	0.000
$\Delta q/Q$	0.798	0.316	2.53	0.016

Table 8. Regression results (DWSBM vs. RM).

	S	R-sq	R-sq (Modified)	R-sq (Predict)
Result	0.0415	83.79%	82.87%	80.50%

Table 9. ANOVA result.

	Degree of Freedom	Adj SS	Adj MS	F Value	*p* Value
Regression	2	0.31248	0.156238	90.48	0.000
Residual	35	0.06043	0.001727		
Total	37	0.37291			

Concerning the regression equation, the negative coefficient of Δt_1 indicates that underestimating the design collection time will lead to an overestimation of ΔQ, which is consistent with the conclusion that the dynamic wave method designs a shorter collection time leading to a higher design flow. The coefficient of $\Delta(q/Q)$ is positive, indicating that the closer the design redundancy in the design of DWSBM and RM, the lower the difference in their design flow.

Through practical application analysis, the limitations of RM based on the theory of steady uniform flow for USDS design have been identified. As the scale of the USDS increases, the difference in design flow between the DWSBM and the RM method becomes more significant. It is evident that for large-scale projects, the DWSBM is more suitable for calculating the design flow.

This study proposes a USDS design flow-calculation method based on hydraulic models and conducts a comparative analysis of design results using two cases. However, systematic analysis of the differences in design schemes and influencing factors is still lacking. Additionally, considering the needs of the project, combining the economic costs of different schemes can enhance the technical and economic analysis of the design methods, thereby increasing their practical value. To further illustrate the strengths and weaknesses of the DWSBM, a SWOT analysis was conducted, as shown in Table A1.

5. Conclusions

(1) The research proposes a USDS-design method focused on deducing pipe design flow based on the dynamic wave method. By constructing the runoff yield model and the flow-concentration model, whose model parameters are equivalent to existing design parameters, coupling the dynamic wave module of SWMM, and iteratively updating to solve for the design flow of each pipe, the design of the entire stormwater pipe network design is completed. This method not only directly applies hydraulic models to the USDS-design process but also enhances the reliability of the design. The feasibility of this method is confirmed through its application to two USDSs in Beijing.

(2) The prerequisite for applying the dynamic wave model to USDS designs is ensuring the equivalence between runoff yield parameters and initial design parameters. This research proposes taking the sub-catchment surface collection time as the surface runoff coefficient peak flow duration. the surface runoff process is simulated by combing with the runoff coefficient and the φ index method. The equivalent model is established by combining with the isochronous method. Through verification, this model can effectively achieve design condition equivalence.

(3) Case studies quantitatively analyze the differences in design flow between two methods from perspectives of topological relations and catchment areas. The comparison also reveals the extent to which actual unsteady uniform flow affects the design process. The design flow calculated using the DWSBM is consistently higher than that using the RM. Additionally, the difference in design flow between the two methods gradually increases with the catchment area (design scale). However, the difference

varies depending on the design conditions, such as pipe network layout. When the catchment area is 2 km^2, the design flow calculated using the dynamic wave method increases by 28.49% and 23.4% in Case 1 and Case 2, respectively. Compared to the RM, the proposed method aligns more closely with actual flow, resulting in a more reliable design.

(4) In USDS design, the design flow rate determines the design scale. The method proposed in this paper offers higher design accuracy compared to the traditional method (RM). However, the DWSBM involves the use of an optimization algorithm and a hydraulic model, making it relatively complex. In practical applications, design engineers require quick and convenient tools for design flow rate calculations. Therefore, it is still a challenge to apply the proposed method for practical application by developing a customization tool. In addition, the DWSBM focuses on the calculation of design flow rates. Pump stations, as critical facilities of USDSs, also play a significant role. Integrating the DWSBM with dynamic pump control to optimize stormwater pump station design will be a key topic for future research.

Author Contributions: Conceptualization, Y.T. and Y.Z.; methodology, Y.Z., Z.L. and H.W.; software, Y.T. and J.Z.; validation, Y.T. and Y.Z.; formal analysis, Y.T. and Y.Z.; resources, Y.T., Z.L. and H.W.; data curation, Y.Z. and J.Z.; writing—original draft preparation, Y.T. and Y.Z.; writing—review and editing, Y.Z., Y.T. and Z.L.; visualization, Y.Z. and J.Z.; supervision, Y.T., Z.L. and H.W. All authors have read and agreed to the published version of the manuscript.

Funding: This research was funded by Major Science and Technology Innovation Pilot Project for Water Resources Protection and Integrated-Saving Utilization in the Yellow River Basin of Inner Mongolia Autonomous Region, grant number 2023JBGS0007, General Program of National Natural Science Foundation of China, grant number 72373011, R&D Program of Beijing Municipal Education Commission, grant number KM202210005017.

Data Availability Statement: The data presented in this study are available on request from the corresponding author.

Conflicts of Interest: The authors declare no conflicts of interest.

Appendix A. SWOT Analysis of DWSBM

To better demonstrate the strengths and weaknesses of DWSBM, a SWOT analysis was conducted.

Table A1. SWOT analysis of DWSBM.

	Strengths	Weaknesses
Internal factors	DWSBM is more realistic and more accurate.	DWSBM requires lots of calculation and lacks consideration of cost-related factors.
	Opportunities	Threats
External factors	The acceleration of urban municipal infrastructure regeneration calls for a better USDS-design method.	RM is the mainstream method so far and is simpler.

Appendix B. Flowchart of PSO

The PSO algorithm used in this paper is illustrated in Figure A1.

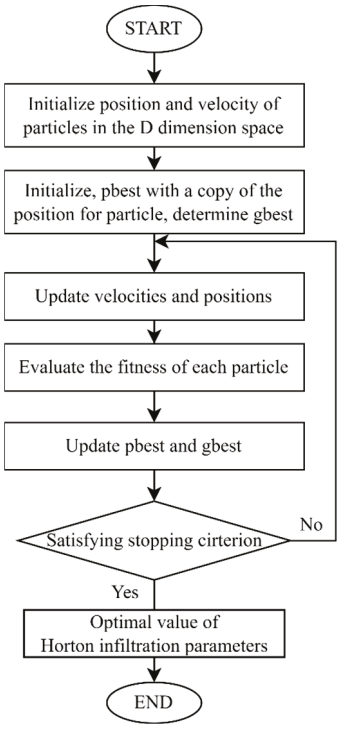

Figure A1. Flowchart of PSO.

References

1. Freire Diogo, A.; Antunes Do Carmo, J. Peak Flows and Stormwater Networks Design—Current and Future Management of Urban Surface Watersheds. *Water* **2019**, *11*, 759. [CrossRef]
2. Zhao, C.; Liang, H.; Tian, K.; Mo, L.; He, Z. Research and application of stormwater network modification of closed pond tailings pond based on ArcGIS and SWMM. *China Min. Mag.* **2024**, *33*, 91–99.
3. Hou, Y.; Wang, R.; Zhang, M.; Feng, Y. Design Process Optimization of Municipal Rainwater Pipe Network Based on ArcGIS and Excel. *China Water Wastewater* **2024**, *40*, 87–92. [CrossRef]
4. Liu, Z.; Zhang, X.; Wang, Q.; Xu, Z. The application of mathematical model in the planning and design of stormwater pipe network. *J. Beijing Norm. Univ. (Nat. Sci.)* **2024**, *60*, 651–658.
5. Lin, R.; Zheng, F.; Savic, D.; Zhang, Q.; Fang, X. Improving the Effectiveness of Multiobjective Optimization Design of Urban Drainage Systems. *Water Resour. Res.* **2020**, *56*, e2019WR026656. [CrossRef]
6. Shao, Z.; Zhang, X.; Li, S.; Deng, S.; Chai, H. A Novel SWMM Based Algorithm Application to Storm Sewer Network Design. *Water* **2017**, *9*, 747. [CrossRef]
7. Sañudo, E.; Cea, L.; Puertas, J. Modelling Pluvial Flooding in Urban Areas Coupling the Models Iber and SWMM. *Water* **2020**, *12*, 2647. [CrossRef]
8. Bisht, D.S.; Chatterjee, C.; Kalakoti, S.; Upadhyay, P.; Sahoo, M.; Panda, A. Modeling Urban Floods and Drainage Using SWMM and MIKE URBAN: A Case Study. *Nat. Hazards* **2016**, *84*, 749–776. [CrossRef]
9. Moussavi, A.; Samani, H.M.V.; Haghighi, A. A Framework for Optimal Reliability-Based Storm Sewer Network Design in Flat Areas. *Can. J. Civ. Eng.* **2017**, *44*, 139–150. [CrossRef]
10. Zaheri, M.M.; Ghanbari, R.; Afshar, M.H. A Two-Phase Simulation–Optimization Cellular Automata Method for Sewer Network Design Optimization. *Eng. Optim.* **2020**, *52*, 620–636. [CrossRef]
11. Li, X.; Hou, J.; Chai, J.; Du, Y.; Han, H.; Yang, S.; Gao, X.; Yang, X. An Online Data-Driven Evolutionary Algorithm–Based Optimal Design of Urban Stormwater-Drainage Systems. *J. Irrig. Drain. Eng.* **2022**, *148*, 04022041. [CrossRef]
12. Li, F.; Duan, H.-F.; Yan, H.; Tao, T. Multi-Objective Optimal Design of Detention Tanks in the Urban Stormwater Drainage System: Framework Development and Case Study. *Water Resour. Manag.* **2015**, *29*, 2125–2137. [CrossRef]
13. Guo, Y.; Walters, G.A.; Khu, S.T.; Keedwell, E. A Novel Cellular Automata Based Approach to Storm Sewer Design. *Eng. Optim.* **2007**, *39*, 345–364. [CrossRef]
14. Wang, Q.; Zhou, Q.; Lei, X.; Savić, D.A. Comparison of Multiobjective Optimization Methods Applied to Urban Drainage Adaptation Problems. *J. Water Resour. Plan. Manag.* **2018**, *144*, 04018070. [CrossRef]
15. Wu, S.; Zhao, Y.; Wang, H.; Qiang, W.; Liu, Z. Calculation method for stormwater network design flow based on kinematic wave simulation. *J. Tsinghua Univ. (Sci. Technol.)* **2023**, *63*, 1887–1896. [CrossRef]
16. Zhou, Y.; Zhao, H. *Theory and Calculation of Drainage Pipe Network*; China Architecture & Building Press: Beijing, China, 2000; ISBN 978-7-112-04475-7.

17. Shanghai Municipal Engineering Design Institute (Group) Co., Ltd. *Standard for Design of Outdoor Wastewater Engineering*; Shanghai Municipal Engineering Design Institute (Group) Co., Ltd.: Shanghai, China, 2021; p. 286.
18. Hou, J.; Zhang, Z.; Ma, L.; Zhang, D.; Xiang, L.; Wang, Y.; Li, J. Unstructured numerical model for rainfall-runoff process in watershed based on GPU acceleration technology. *Adv. Water Sci.* **2021**, *32*, 567–576. [CrossRef]
19. Shih, D.-S.; Yeh, G.-T. Studying Inertia Effects in Open Channel Flow Using Saint-Venant Equations. *Water* **2018**, *10*, 1652. [CrossRef]
20. Deng, P. Study on the Flood-Peak Runoff Coefficient Method of Urban Storm Water Pipe Design and Mathematic Model. *Water Wastewater Eng.* **2014**, *50*, 108–112. [CrossRef]
21. Hui, W. Research and Application on Calculation Model of Urban Waterlogging Water Accumulation. Master's Thesis, Taiyuan University of Technology, Taiyuan, China, 2015.
22. Siregar, Y.; Pardede, C. Study of Hybrid Transmission HVAC/HVDC by Particle Swarm Optimization (PSO). *Energies* **2022**, *15*, 7638. [CrossRef]
23. Wang, H.; Lei, X.; Khu, S.-T.; Song, L. Optimization of Pump Start-Up Depth in Drainage Pumping Station Based on SWMM and PSO. *Water* **2019**, *11*, 1002. [CrossRef]
24. Hu, J. Improved Particle Swarm Optimization Integrating Multiple Strategies. *Comput. Syst. Appl.* **2021**, *30*, 172–177. [CrossRef]
25. Xu, L.; Huang, Z.; Yang, Z.; Ding, W. Mixed Particle Swarm Optimization Algorithm with Multistage Disturbances. *J. Softw.* **2019**, *30*, 1835–1852. [CrossRef]
26. Pahlevi, R.; Murti, M.A.; Susanto, E. The Implementation of PID Using Particle Swarm Optimization Algorithm on Networked Control System. In Proceedings of the 2014 International Conference on Industrial Automation, Information and Communications Technology (IAICT), Bali, Indonesia, 28–30 August 2014; IEEE: New York, NY, USA, 2014; pp. 35–38.
27. Shi, Y.; Eberhart, R.C. Empirical Study of Particle Swarm Optimization. In Proceedings of the 1999 Congress on Evolutionary Computation-CEC99 (Cat. No. 99TH8406), Washington, DC, USA, 6–9 July 1999; Volume 3, pp. 1945–1950.
28. Xia, J.; Zhang, Y.; Liang, C.; Liu, J. Review on urban storm water models. *Eng. J. Wuhan Univ.* **2018**, *51*, 95–105. [CrossRef]
29. Liu, X.; Wang, T.; Zhang, Q.; Yuan, R.; Zhou, Y. Comparison of EPA SWMM and Mike Urban Isochrones Model. *China Water Wastewater* **2017**, *33*, 30–35. [CrossRef]
30. United States Environmental Protection Agancy; Rossman, L.A. Storm Water Management Model (SWMM). Available online: https://www.epa.gov/water-research/storm-water-management-model-swmm (accessed on 25 March 2024).
31. Wang, G.; Xia, J.; Chen, J. A multi-parameter sensitivity and uncertainty analysis method to evaluate relative importance of parameters and model performance. *Geogr. Res.* **2010**, *29*, 263–270.
32. Wang, L. The Research on Urban Drainage Network Inundation Evaluation and Control Based on Modeling Technology. Ph.D. Thesis, Beijing University of Technology, Beijing, China, 2010.

Disclaimer/Publisher's Note: The statements, opinions and data contained in all publications are solely those of the individual author(s) and contributor(s) and not of MDPI and/or the editor(s). MDPI and/or the editor(s) disclaim responsibility for any injury to people or property resulting from any ideas, methods, instructions or products referred to in the content.

water

MDPI

Article

Probabilistic Forecasting and Anomaly Detection in Sewer Systems Using Gaussian Processes

Mohsen Rezaee [1,2], Peter Melville-Shreeve [1,2] and Hussein Rappel [1,*]

[1] Department of Engineering, Faculty of Environment, Science and Economy, University of Exeter, Exeter EX4 4QF, UK; mr861@exeter.ac.uk (M.R.); p.melville-shreeve2@exeter.ac.uk (P.M.-S.)
[2] Centre for Water Systems, University of Exeter, Exeter EX4 4QF, UK
* Correspondence: h.rappel@exeter.ac.uk

Abstract: This study investigates the capability of Gaussian process regression (GPR) models in the probabilistic forecasting of water flow and depth in a combined sewer system. Traditionally, deterministic methods have been implemented in sewer flow forecasting and anomaly detection, two crucial techniques for a good wastewater network and treatment plant management. However, with the uncertain nature of the factors impacting on sewer flow and depth, a probabilistic approach which takes uncertainties into account is preferred. This research introduces a novel use of GPR in sewer systems for real-time control and forecasting. To this end, a composite kernel is designed to capture flow and depth patterns in dry- and wet-weather periods by considering the underlying physical characteristics of the system. The multi-input, single-output GPR model is evaluated using root mean square error (RMSE), coverage, and differential entropy. The model demonstrates high predictive accuracy for both treatment plant inflow and manhole water levels across various training durations, with coverage values ranging from 87.5% to 99.4%. Finally, the model is used for anomaly detection by identifying deviations from expected ranges, enabling the estimation of surcharge and overflow probabilities under various conditions.

Keywords: combined sewer system; urban drainage; Gaussian processes regression; blockage detection; data-driven forecasting; surcharge and overflow prediction

1. Introduction

Sewer systems convey domestic, industrial and commercial wastewater (and sometimes stormwater and groundwater) from their sources to a wastewater treatment plant (WWTP) or a discharge point. These systems can be mainly divided into combined and separate sewer systems [1]. Combined sewer systems are built to take both wastewater and stormwater from different sources and convey them to the final point of the system. Such systems are prevalent in the UK, with Victorian era infrastructure deployed in the form of combined drainage systems in many urban areas.

Wastewater flow contains various types of pollutants which should be effectively treated to provide a safe environment. However, for several reasons, there are untreated releases in almost every sewer system which are detrimental to the environment and health [2]. The most important case in untreated wastewater releases is the combined sewer overflow (CSO), which is a structure installed to spill wastewater into the environment to reduce the risk of backup discharges and manhole overflows [3]. Even though CSOs minimise the risk of manhole overflows, blockages or pump failures, caused by various factors such as sediment formation [4], may still lead to unintentional discharges [5].

Given the adverse effects that CSOs cause, sewer systems should be designed and maintained in such a way that overflows are reduced to a minimum. Moreover, water companies risk paying penalties due to regulatory requirements set by the Water Service Regulation Authority (OFWAT) in the UK (and similar authorities in other countries). Therefore, water companies seek methods and models to predict the flow and to be able to forecast overflows in the system because proactive responses are often more cost-effective and preferable for mitigating environmental risks. However, reactive control is the most frequently implemented approach [6].

There are three types of models that can be used in forecasting overflows and other characteristics of a hydraulic or hydrologic environment: simulators [7], data-driven surrogate models [8] and hybrid models [9]. The first models, also known as physical models, have been used for more than five decades; however, they have been considered computationally expensive for years [10]. These models simulate the underlying physics of the environment and represent it as a set of partial differential equations (PDEs) [11].

The mathematical modelling of every physical system often requires tremendous simplifications that lead to significant uncertainties in computation. Additionally, high computational cost [12], demand for updating model parameters in response to urban development [13], and lack of knowledge of every physical behaviour of the system [13] are known as drawbacks of these models. Confidence in input parameters like the network topology, invert levels and current levels of service (for example root ingress, sediment build up, etc.) creates uncertainty in such models which can typically be improved through calibration approaches using short-term flow surveys at key nodes in the network to some extent.

On the other hand, data-driven models are capable of making predictions with greater computational efficiency [14]. These models present an opportunity to capture relationships between parameters without considering interactions [15]. Nonetheless, data-driven modelling suffers from a lack of physical interpretation, which may make it unreliable or challenging to interpret [16]. Therefore, some researchers have come to a mixture of data-driven and physical models, called physics-informed surrogate models, taking advantage of both physical and data-driven models [17]. While these models benefit from physical constraints, development and integrity challenges along with added complexity make them challenging to implement in this study and similar works.

Data-driven models range from simple linear regressions to complex deep-learning architectures, each varying in computational complexity. These models can be classified into deterministic and probabilistic approaches based on the way they handle uncertainty in the modelling process. While deterministic models offer an explicit solution to a water-related issue, probabilistic models take the inherent uncertainties of the data and the model parameters into account.

In sewer system modelling, uncertainties arise from multiple sources, including variability in precipitation and water usage, simplifications in physical equations, and sensor inaccuracies [18]—all of which can significantly impact the reliability of predictions. While most research in uncertainty quantification has focused on water quality and treatment plant operations, some researchers have addressed flow-related uncertainty. For example, Breinholt [19] assessed the uncertainty in flow prediction and modelling in a sewer system with a frequentist stochastic approach. Raimondi et al. [20] adopted a deterministic framework to quantify uncertainty in flow rate and temperature, while Sriwastava et al. [21] employed stochastic sampling to evaluate CSO volume variability.

While many data-driven models, like artificial neural networks (ANNs) and support vector machines (SVMs), require large datasets and lack uncertainty quantification in pre-

dictions, the Gaussian processes (GPs) method provides an approach capable of handling complex and small datasets through a natural Bayesian interpretation [22]. This method makes predictions incorporating experts' prior knowledge with a model (called likelihood, i.e., a function showing the probability of data happening given a parameter) and provides uncertainty measures in its predictions [23]. Moreover, GP is known as a suitable method for working with rare and costly data, while it can provide good results with larger datasets with an $O(N^3)$ computational complexity (Computational complexity describes how the runtime of an algorithm scales with the size of the input data (N). An $O(N^3)$ complexity means the computation time increases with the cube of the number of training points) [16].

Gaussian process regression (GPR) has been implemented in many different fields of study due to its capability in uncertainty quantification and flexibility (i.e., the ability to emulate different function shapes). This capability has led GPR models to be used in engineering and scientific fields as surrogate models, such as in computational engineering [24], climate science [11], finance [25] and many time-series related forecasting models [26].

In water engineering, GP-based frameworks have been used in forecasting river streamflow [27] and reservoir streamflow [28], fault detection in wastewater treatment plants [29], evaluation of the flooded nodes in a sewer system [30], drinking water demand prediction [31], streamflow temperature forecasting [32], water level fluctuations forecasting [33] and approximating parameters of a storm water management model (SWMM) [12].

Due to the need for a model that combines computational efficiency with principled uncertainty quantification, this work presents a framework that deploys a GPR model for forecasting flow and depth in a sewer system. This model uses a custom-designed kernel to capture various patterns affecting flow and depth changes in different parts of the network. This probabilistic model aids water companies in making short- and mid-term asset management plans and responding proactively to potential issues in the network and treatment facilities.

In addition to what data-driven and particularly GPR models can forecast in wastewater systems, they offer valuable applications in real-time control and nowcasting. With abundant sensors placed in sewer systems, smart and monitored wastewater management is on the horizon [34]. One critical challenge in sewer systems is anomaly detection [35]. When a pump failure occurs or a blockage develops in a pipe, the water flow and depth suddenly decrease downstream while increasing upstream. The timely prediction of these anomalies plays an important role in urban water management [36] and reduces costs associated with pollution events driven by such issues [37].

Data-driven methods provide a more cost-effective alternative to hardware-based techniques (e.g., CCTV, acoustic sensing, etc.) [36,38]. Among them, probabilistic methods are credited for their ability to take complexities into account [39]. Nonetheless, there is no systematic research using GPR for detecting anomalies in a sewer system.

Accordingly, this research proposes a novel probabilistic method for anomaly detection using a GPR model. The method estimates the likelihood of blockage occurrences in real time, and raises alarms when discrepancies exceed predefined thresholds. This method can replace traditional deterministic approaches used by water companies, ensuring a safe environment with less uncontrolled overflows.

The remainder of this paper is organised as follows. Section 2 discusses the data and the hydraulic model used to prepare the training and test datasets. It also outlines the GPR model structure, its implementation within the framework, and the evaluation metrics applied to assess its performance.

Section 3 presents the results taken from the GPR model along with a discussion. It shows how the GPR model works with long- and short-term training periods and how

it can be used in presenting probabilistic results for the stakeholders. Finally, the paper concludes with remarks and suggestions for future work.

2. Materials and Methods

2.1. Data and the Case Study

The case study of this research is a hypothetical combined sewer system built by EPA SWMM v5.2 software [40]. The system is a skeleton sewer network serving 11,300 inhabitants of a city, assumed to be placed in the UK. The average water consumption is assumed to be 140 Litre per capita per day with a 100% wastewater generation rate. A snapshot of the system and the details are presented in Figure 1 and Table 1.

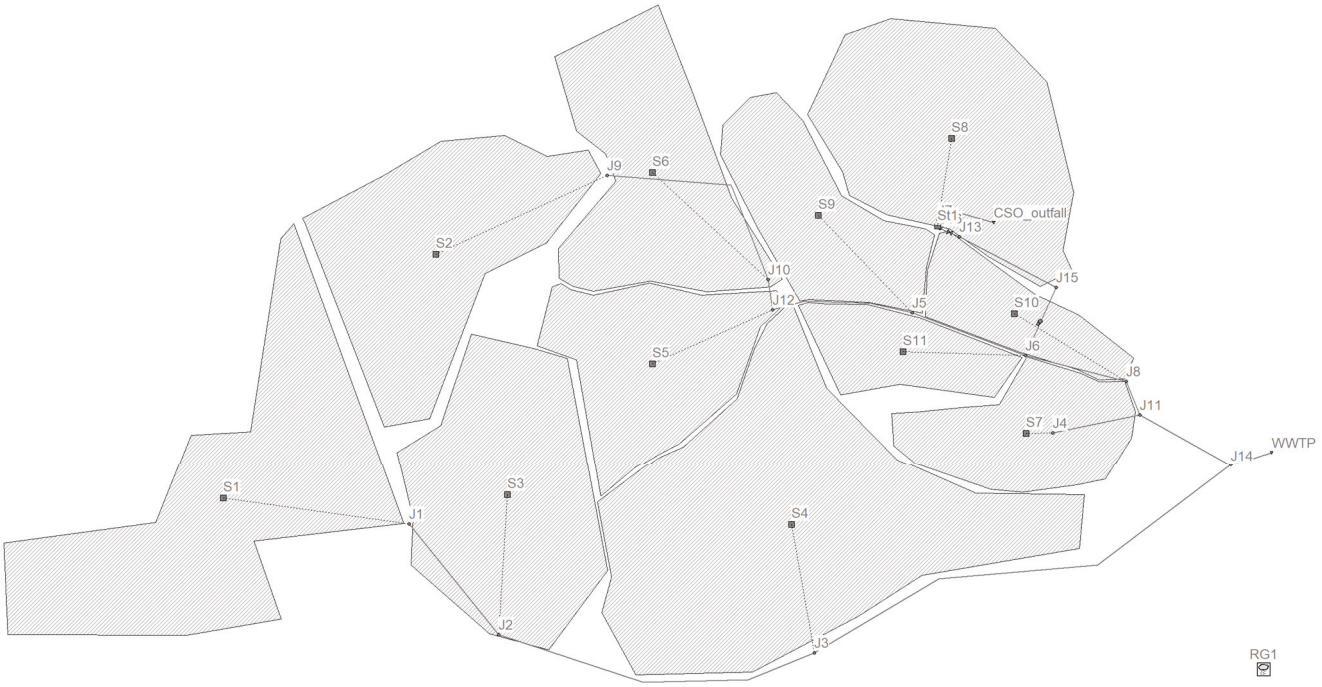

Figure 1. Skeleton sewer system terminating at the WWTP on the right side of the figure. The hatched areas show the sub-catchments, the links show the main sewers, and the square points are the Nodes labelled in the figure. The rain gauge (RG1) is shown at the right bottom of the figure.

A CSO is set in the network to release excess flows via a weir. There is also a storage tank and a pumping station set to regulate the flow in the network. The mains and trunk sewers have been designed based on the IDF curves of London [41] and have sizes between 500 mm and 1200 mm.

Groundwater infiltration can have a major contribution to the flow of a sewer system which makes it important when designing a sewer network and the treatment plant [42]. The seasonal effect of such can be complicated and driven by geological conditions such as soil porosity and bedrock characteristics. In this case study, the average value of groundwater infiltration is set as 25 per cent of the average annual dry-weather flow (DWF), which can be considered a normal value for a mid-life network based on recent research papers [43]. The groundwater infiltration is then distributed in different months of the year based on the average groundwater changes in the UK.

The average values of the infiltration are presented in Table 1. The sewer exfiltration is assumed to have negligible amounts in the network and has not been included in the calculations.

Table 1. Details of the wastewater production values and infiltration in each sub-catchment.

Sub-Catchment	Terminates at Joint	Population	Wastewater Production (L/s)	Infiltration (L/s)
S1	J1	1200	1.94	0.49
S2	J9	700	1.13	0.28
S3	J2	700	1.13	0.28
S4	J3	1200	1.94	0.49
S5	J12	1300	2.11	0.53
S6	J10	1200	1.94	0.49
S7	J4	900	1.46	0.36
S8	J7	1200	1.94	0.49
S9	J5	1000	1.62	0.41
S10	J8	1000	1.62	0.41
S11	J6	900	1.46	0.36
Total	**WWTP**	**11,300**	**18.31**	**4.58**

Different time patterns have been synthesised to approximate the model to a real-world case. These include daily, weekday, weekend and monthly water usage patterns, all constructed to reflect household wastewater production patterns. Moreover, a pattern is made for one of the sub-catchments showing that the water usage in the area is affected by a nearby university, and a groundwater infiltration pattern is constructed based on the UK groundwater fluctuation maps.

Finally, the hydraulic model is built in EPA SWMM, and the hydraulic simulation data are generated using PySWMM v.2.0.1 (the Python interface to SWMM) [44], allowing the authors to integrate the simulator and data-driven model within a single platform.

While rainfall data could have been synthetically generated at a specified resolution, this study uses open-access precipitation data from the Sheffield meteorological station [45]. With a 5 min resolution and 0.2 mm accuracy collected with an ARG-100 tipping bucket rain gauge, this dataset is ideally suited for the objectives of the research.

It should be noted that, as this research is based on a hypothetical network, the underlying hydraulic model is uncalibrated. Deploying this framework operationally would therefore first require training the GPR model on data from a hydraulic model of the target system that has been properly calibrated to field measurements.

2.2. Gaussian Process Regression

A GP is a collection of random variables, any finite number of which have a joint multivariate Gaussian density function [46]. GP is completely specified by its mean and covariance functions [47]. Mean (m($\boldsymbol{x}$) i.e., the central value of the set $\boldsymbol{x}$) and covariance ($k(\boldsymbol{x},\boldsymbol{x'})$, i.e., the measure indicating how two random variables depend on each other) functions of a real process, $f(\boldsymbol{x})$ (i.e., a function from real inputs to random outputs), are defined as:

$$m(\boldsymbol{x}) = \mathbb{E}\,(f(\boldsymbol{x})) \tag{1}$$

$$k(\boldsymbol{x},\boldsymbol{x'}) = \mathbb{E}\,((f(\boldsymbol{x}) - m(\boldsymbol{x}))(f(\boldsymbol{x'}) - m(\boldsymbol{x'}))). \tag{2}$$

Here, $\mathbb{E}$ denotes the expected value. Using the GP, we can define a distribution over functions $f(\boldsymbol{x})$,

$$f(\boldsymbol{x}) \sim \mathrm{GP}(m(\boldsymbol{x}), k(\boldsymbol{x},\boldsymbol{x}')), \tag{3}$$

where $\boldsymbol{x}$ and $\boldsymbol{x}'$ are two GP input vectors and $\boldsymbol{x} \in \mathbb{R}^N$ ($\mathbb{R}$ represents the set of real numbers).

Forecasting flow as a time-series can be performed by a GPR. In GPR, a GP is set as a prior for the latent function ($f(\boldsymbol{x})$) that maps the inputs into the output space and then updates the prior with the observations, using Bayes' rule [48]. In this work, the inputs are time and rainfall depth, and the output can be water flow or depth.

Let $\boldsymbol{X}$ and $\boldsymbol{X}_*$ denote training and test matrixes and $K(\boldsymbol{X}_*, \boldsymbol{X})$ shows the covariance matrix evaluated at all data points, the key predictive equations for GPR when there is noise in observations are as follows [46]:

$$\overline{\boldsymbol{f}_*} \;=\; K(\boldsymbol{X}_*,\, \boldsymbol{X})\left[K(\boldsymbol{X},\boldsymbol{X}) \;+\; \sigma_n^2\mathrm{I}\;\right]^{-1}\boldsymbol{y} \tag{4}$$

$$cov(\boldsymbol{f}_*) = K(\boldsymbol{X}_*,\, \boldsymbol{X}_*) - K(\boldsymbol{X}_*,\, \boldsymbol{X})\left[K(\boldsymbol{X},\, \boldsymbol{X}) + \sigma_n^2\mathrm{I}\right]^{-1}K(\boldsymbol{X},\, \boldsymbol{X}_*), \tag{5}$$

where I is identity matrix, $\boldsymbol{f}_*$ is the predicted test outputs according to the prior and the $\overline{\boldsymbol{f}_*}$ is the mean of the prediction on the test points, $\boldsymbol{X}*$. In Equation (4), observation values $y = f(\boldsymbol{x}) + \epsilon$ where ϵ is the Gaussian noise with variance σ_n^2.

In GPR, the prior mean function is often assumed to be zero, and the posterior mean is updated based on the observed data. To optimise the GPR, best hyperparameters are selected by maximising the log marginal likelihood. Hyperparameters are some free parameters in the covariance function that control how outputs vary with inputs.

$$log\; p(\boldsymbol{y} \mid \boldsymbol{X}) = -\frac{1}{2}\boldsymbol{y}^T\left(K + \sigma_n^2\mathrm{I}\right)^{-1}\boldsymbol{y} - \frac{1}{2}log\left|K + \sigma_n^2\mathrm{I}\,\right| - \frac{n}{2}log2\pi \tag{6}$$

$\left|K \;+\; \sigma_n^2\mathrm{I}\,\right|$ denotes the determinant of the covariance matrix containing noise. This optimisation process allows the model to best fit the observed data while avoiding high complexity of the model.

The most common hyperparameters are length scale, output variance and periodicity, found in Squared exponential (SE), Rational quadratic (RQ) and periodic kernels [49]. For further details on advanced kernels, the readers are referred to Wilson [50].

2.3. Constructing Forecasting Model

The overall workflow of this study is summarised in Figure 2. This figure demonstrates the steps of building this framework and its various applications. It also shows the iterative process of selecting the best kernel type for the GPR model. The hydraulic model data is used as training and testing datasets. To make the model closer to real-world conditions, random Gaussian noise with zero mean is added to the simulated data. The noise has a value between −3 and +3 standard deviation of this Gaussian noise which is set to be equal to 10% of the average dry-weather flow.

In this case study, the DWF has an average value of 25 L/s, so the 3 standard deviations are set to be 2.5 L/s (standard deviation = 0.8 L/s). It should be noted that the noise level remains the same for all dry- and wet-weather periods for simplicity.

The GPR model can be trained with a single input (only time) and forecast the flow or depth at future time steps (single-input, single-output model) or incorporate other influencing factors in forecasting (multi-input, single-output model). In this study, time as the primary input in the time-series and the precipitation as the key influencing factor

are considered as the inputs of the model. The output of the model is the desired flow or depth.

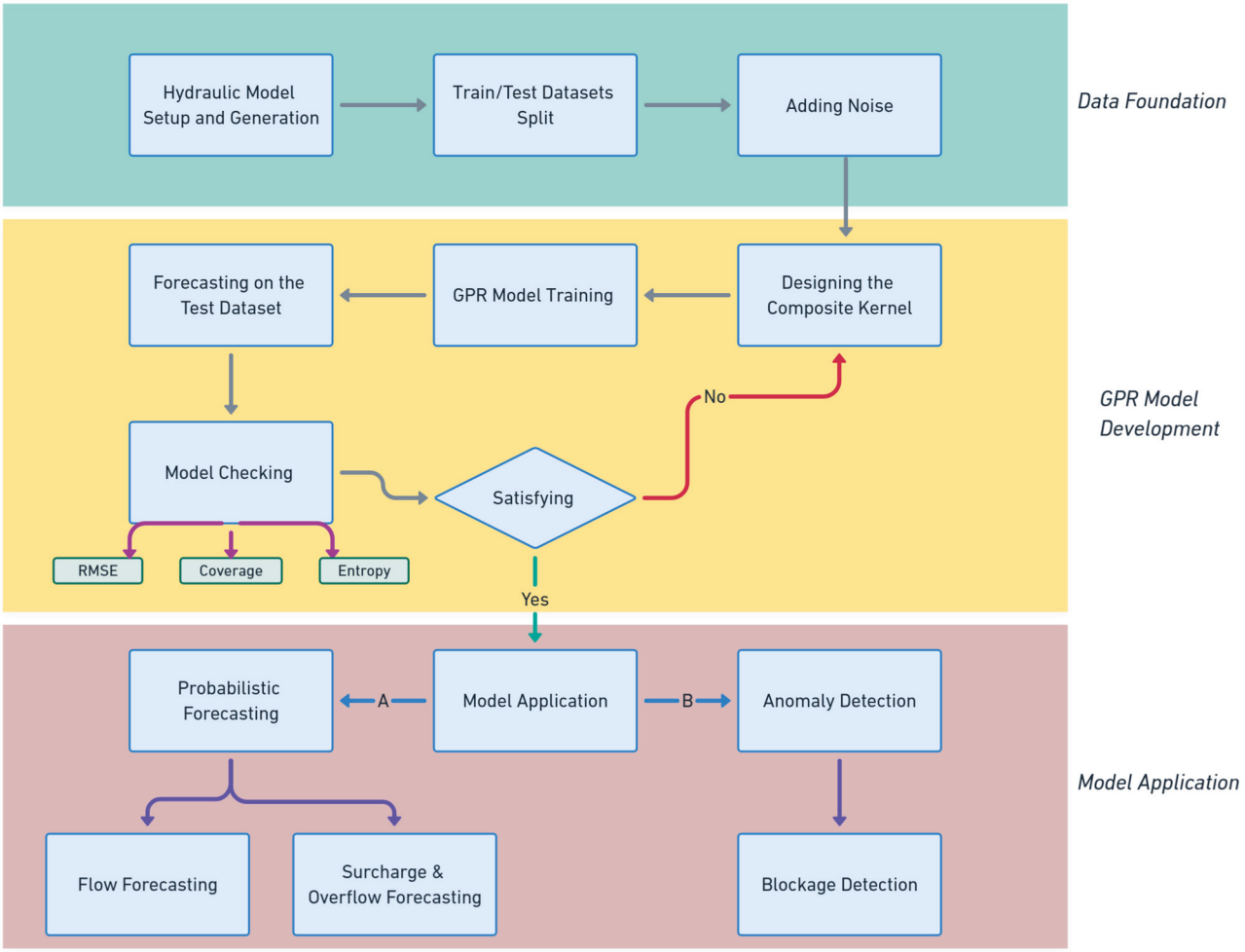

Figure 2. Flowchart of the research methodology, illustrating the stages from data foundation to the final applications. This process starts from preparing training and test datasets and then makes the composite kernel for the GPR model development. Finally, the built model comes to different applications.

The model can take more factors as inputs (e.g., population, land use, geometry, etc.) to increase the accuracy. Nonetheless, it is important to note that each new factor increases the model's dimensionality and, consequently, its computational demand which is not preferred in this research.

Once the data from PySWMM are collected and processed, they are imported into a GPR model constructed by the GPflow package in Python [51]. Depending on the data pattern and the dominant features of the time-series, a single or composite kernel, i.e., a combination of multiple covariance functions, is employed to capture different characteristics of the data.

Furthermore, as the wet-weather flow (WWF) is not as predictable as the dry-weather flow (DWF) due to the intense flows entering the sewers after each rainfall in a catchment, ordinary kernels may not fully capture these changes. So, a composite kernel designed to take stormwater and wastewater characteristics into account is needed.

2.4. Kernel Design

The selection of an appropriate kernel, or covariance function, is fundamental to the performance of a GPR model, as it encodes assumptions about the function being modelled. Various methods have been proposed for automatically selecting the optimal kernel for a GP model [52,53]. However, these methods add to the overall complexity of the model significantly which is not desirable in this study.

Moreover, from an overview of the water usage and sewer flow patterns, and the impact of the rainfall magnitude on the flow, it can be understood that the wastewater flow will follow some basic patterns that can be effectively captured within the main GP model by tuning the hyperparameters.

The main kernels used in this research are Periodic and Matérn kernels. Periodic kernel can be formulated as follows [46]:

$$k_{Per}(\boldsymbol{x}, \boldsymbol{x}') \;=\; \exp(-\frac{2Sin^2(\frac{x-x'}{2})}{l^2}), \tag{7}$$

where l is the length scale, and $\boldsymbol{x}$ and $\boldsymbol{x}'$ are GP input vectors.

Matérn kernel family can be formulated as [46]:

$$k_{Mat}(\boldsymbol{x}, \boldsymbol{x}') \;=\; \frac{2^{1-\nu}}{\Gamma(\nu)}\left(\frac{\sqrt{2\nu}|\boldsymbol{x}-\boldsymbol{x}'|}{l}\right)^{\nu} K_\nu(\frac{\sqrt{2\nu}|\boldsymbol{x}-\boldsymbol{x}'|}{l}), \tag{8}$$

where K_ν is the modified Bessel function [54]. l is the length scale and ν is a free parameter which is typically selected as 0.5, 1.5, or 2.5. Matérn kernels with higher value of ν are smoother, compared to smaller ν values.

The effectiveness of the designed kernel is assessed by the model checking metrics discussed in Section 2.5.

2.5. Anomaly Detection

To apply the GPR method for anomaly detection in sewer systems, the same training process used in the forecasting model is adopted, using the depths data of each manhole in the hydraulic model. These depth values serve as the training and testing datasets for the GPR model.

In a real-world case, a GPR model is trained using real-time depth measurements from the sensors and precipitation data obtained from the nearest online rain gauges. The trained model predicts expected depth values for each manhole in real-time. By comparing these predicted values with the actual sensor readings, discrepancies can be identified. If deviations exceed predefined thresholds set by the GPR model, an anomaly is detected. Anomalies typically manifest as unusually low or high depth values, indicating potential blockages—either downstream (causing increased water levels) or upstream (leading to sudden drops in depth).

In this study, two months of simulated depth data and precipitation are used as training data and the predictions in each timestep seek anomalies in the next 10 h. The anomaly detection process takes place separately for each manhole but the designed kernel can be used for all datasets.

In many cases, blockages only reduce the capacity of the pipe rather than fully obstructing the flow. Consequently, they do not lead to a surcharge, or a spike change in the depth enough to be flagged as an anomaly. However, GPR model can detect these changes as small deviations that can be considered as probable blockages and be put into inspection plans for early interventions.

The anomaly detection mechanism also considers data resolution. A single outlier may not always indicate an issue, so a predefined number of consecutive data points exceeding the threshold is required to trigger an alarm. The exact criteria can be adjusted based on case-specific conditions.

2.6. Model Checking

The role of predictive model checking is to assess the practical fit of a model [55]. Various techniques exist for assessing the fit of a model including statistic measures [56] and graphical checks [57]. Among them, root mean square error (RMSE), coverage and entropy are selected as three key metrics assessing the GPR model in this study. RMSE, coverage, and entropy together offer a balanced evaluation of the model by capturing its accuracy, the effectiveness of its uncertainty bounds, and the overall reliability of its probabilistic predictions.

2.6.1. Root Mean Square Error

RMSE measures the accuracy of the predictions by calculating the standard deviation of the residuals, providing a straightforward interpretation of the prediction error [58].

$$RMSE = \sqrt{\frac{1}{N}\sum_{i=1}^{N}(y_i - \hat{y}_i)^2} \tag{9}$$

where N is the number of test points, y_i is the actual value (flow, depth, etc.), and $\hat{y}_i$ is the predicted value.

2.6.2. Coverage

Coverage represents the percentage of data points that fall within the defined credible interval of the model. A good model is defined as a model having an α% coverage for an α% credible interval [56]. The typical value for α is 95, which is used in this research as well.

2.6.3. Entropy

Entropy quantifies the uncertainty associated with the predicted distribution, with higher entropy showing greater uncertainty [59]. For a univariate Gaussian probability density function with a variance of σ^2, the differential entropy $h(t)$ is given by the formula [60]:

$$h(t) = 0.5\log\left(2\pi e\sigma^2\right) \tag{10}$$

The overall differential entropy of the test points can be calculated as:

$$H = \frac{1}{N}\sum_{i=1}^{N} 0.5\log\left(2\pi e\sigma^2\right) \tag{11}$$

This value quantitatively reflects how narrow or wide the bounds are defined. A wider bound can increase the coverage but will result in higher entropy. Thus, a trade-off between these three measures—RMSE, coverage and entropy—is necessary in model evaluation.

It is noteworthy that the differential entropy used in this study is slightly different with the Shannon entropy used for discrete distributions. Unlike Shannon entropy, differential entropy can take negative values when the variance of the data is very small which completely depends on the unit of the data. Therefore, differential entropy values from different models are not directly comparable. Despite this drawback, differential entropy helps

identify which kernel configuration provides predictions with lower overall uncertainty, when evaluating different kernel designs using the same training and testing data.

3. Results and Discussion

3.1. Forecasting the WWTP Influent

The inflow of the WWTP is a critical metric for sewer system management, as it significantly influences the performance of the treatment plant. Accurate forecasting of WWTP influent enables proactive decision-making, allowing operators to optimise treatment processes, manage resources effectively, and mitigate potential issues such as overflows. Using a GPR model, flow predictions can be interpreted probabilistically, providing not only point predictions but also a measure of the associated uncertainty.

The WWTP influent values have been derived from the hydraulic simulator (PySWMM). To simulate real-world noise and variability, a zero-mean normal noise with a standard deviation of 0.8 L/s was added to the simulated values.

Once the simulations were complete and the noise was added to the dataset to make the synthetic data more realistic, train and test datasets were prepared and processed to construct the GPR model. The model's ability to capture the temporal dynamics of the influent, including both DWF patterns and the response to rainfall events, is crucial for effective wastewater management.

Figure 3 illustrates the WWTP influent and precipitation over the study period. The graph highlights the variability in influent flow, demonstrating the influence of rainfall events on peak flow rates. The total precipitation for the year is 875.6 mm.

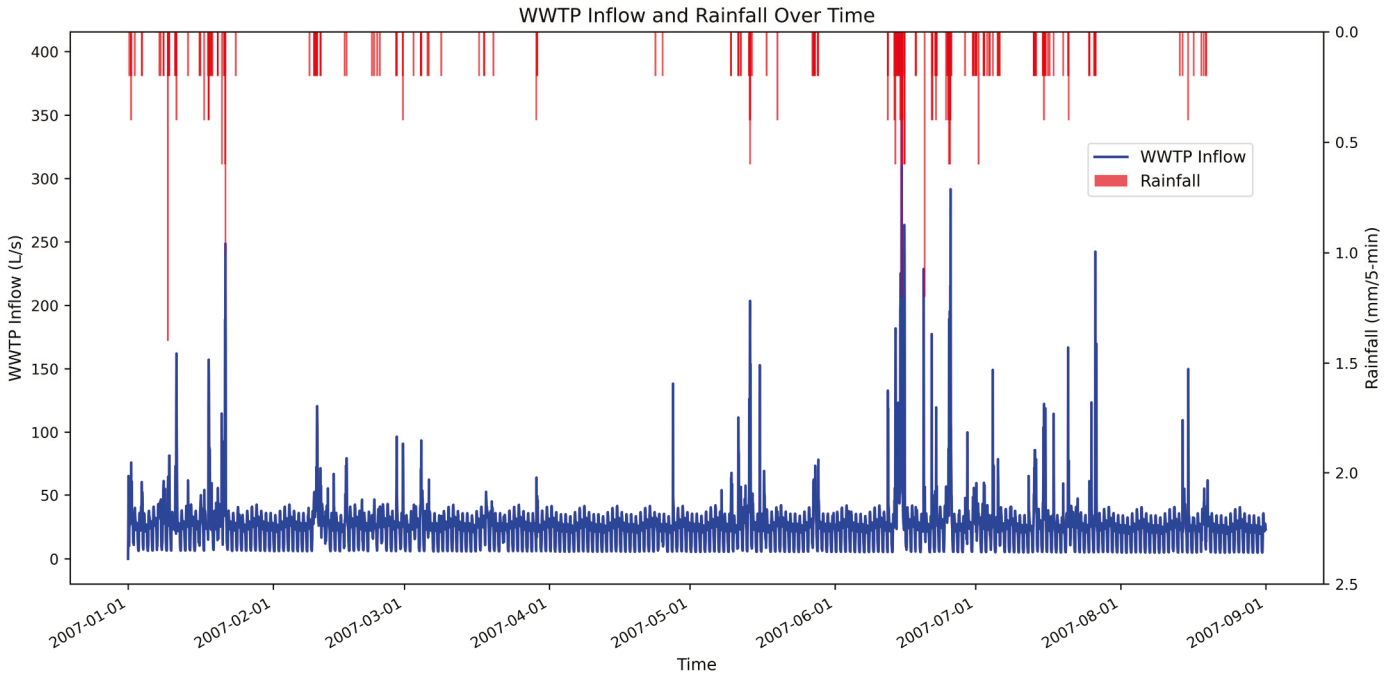

Figure 3. Simulated WWTP inflow without added noise and the precipitation in the case study. The blue line shows the inflow change overtime and the red line shows the precipitation depth in 5 min intervals.

To build and test the GPR model's predictions, 6 months of the study period were selected as the training dataset, and the subsequent 2 months for testing. The 6-month period allow the model capture daily, weekly and monthly patterns effectively. The interval

between the data points is one hour and the simulation timesteps are 180 s. The results of the GPR model are presented in Figure 4.

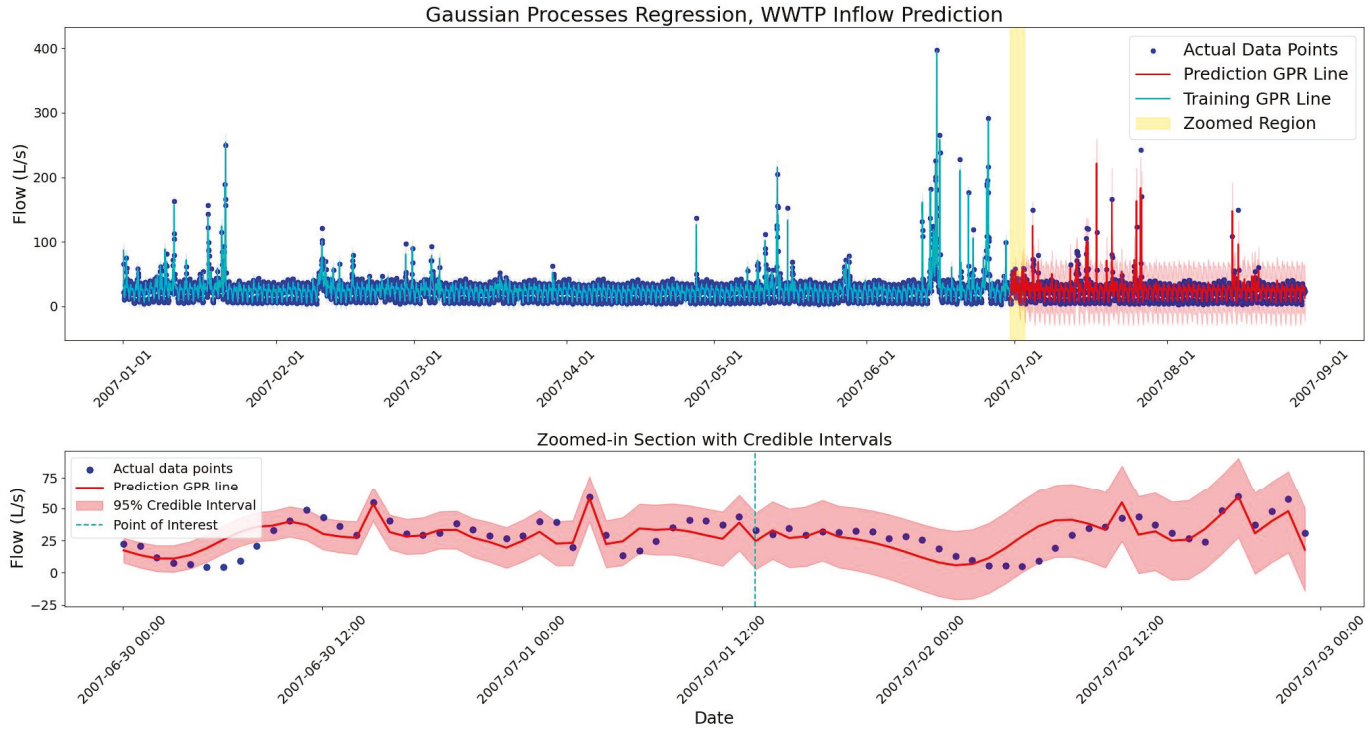

Figure 4. Gaussian process regression model on 6 months of training and 2 months of test data (**top**). The regression lines are shown in blue and red for training and test sets, respectively. The first 3 days of the test set is selected for a detailed illustration (**bottom**).

The bounds illustrate a 95% credible interval of the Gaussian distributions, corresponding to 1.96 standard deviations. Figure 5 illustrates the predicted distribution at a randomly selected point, from the zoomed-in section in Figure 4, showing how the Gaussian distributions work with the data.

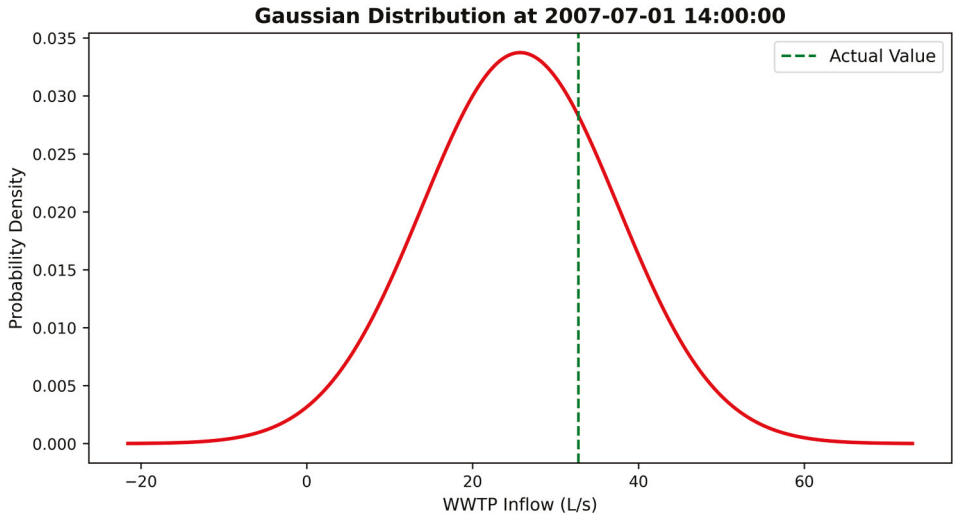

Figure 5. Gaussian distribution of the predicted WWTP inflow at 2007-07-01 at 14:00 p.m. The green dashed line shows the actual test point value. The distribution's domain is selected as ± 4 standard deviation of the distribution for a better illustration.

As shown in Figure 4, the predictive uncertainty in the GPR model increases as the predictions move further from the training data points, leading to a wider bound around the GPR mean. This occurs because the farther a prediction is from the training set, the less information the model has to constrain it. The mathematical reason behind this fact can be seen in Equation (5). As the distance between $\boldsymbol{X}$ and $\boldsymbol{X}_*$ increases, the $K(\boldsymbol{X}_*, \boldsymbol{X})$ becomes smaller and the covariance of the predictions achieves higher values. This complies with the fundamental principle that predictions become more uncertain as they extend beyond the observed data points.

The designed kernel for this model consists of four distinct covariance functions. The first two are periodic kernels, selected to capture the hourly and daily variations in the wastewater production pattern. These two kernels target the time input in the training data. The other kernel which is particularly designed to capture rainfall effect on the flow is a Matérn12 kernel (from the gpflow. GPR library in Python). This kernel belongs to the Matérn covariance family with $\nu = 1/2$ that makes the covariance function more rough compared to other ν values [46]. As a result, it can take the spike changes in flow caused by rainfalls.

The final kernel is a noise kernel used to handle the noise in observed data. The noise kernel is a two-dimensional function that is combined with other kernels by a simple addition.

The choice of this kernel structure is supported by model evaluation results and its ability to reproduce the observed data patterns. The model checking shows that over the 2-month test period, Coverage of the model is 99.4% for the 95% credible interval which indicates a perfect coverage. The RMSE between the actual data and the GPR's mean prediction for this 2-month period is 10.87 L/s. While this value seems high relative to the overall mean flow of 26.16 L/s, it reflects the significant errors that occur during high-magnitude, wet-weather events.

Additionally, the average differential entropy across the test points is 6.19, providing a measure of predictive uncertainty as defined in Section 2.6.3. While differential entropy's dependence on data scaling means its values are not directly comparable across different datasets and may not translate to an easily interpreted practical metric, it remains useful for model selection within a specific analysis.

The model's reliability highly depends on the range of values used in the training step. For this model, having rainfall events with greater depth values can train the model better, particularly for predictions at wet-weather periods. As shown in Figures 3 and 4, most of the large rainfalls happen at the 6th month of the year where it is placed in the training zone of the GPR model. To show the importance of the wide span of training data values, the training period is shifted back by one month and the model uses the first five months of the period for training. Hence, the sixth month with its heavy rainfalls is put into the test zone.

The results of this model show that some of the high flow values at the testing zone fall outside predicted bounds which indicates the importance of a representative value range in the training data for achieving accurate predictions. The model checking measures with the same kernel setting indicate 13.82 L/s of RMSE, 98.2% of coverage, and 5.98 of entropy. The increased value of RMSE shows a weaker fit of data which also can be proved by the visual GPR line in the predictions. The entropy and coverage values have not changed significantly; however, outliers exist in the high flow times.

As it is evident in Figure 4, a few outliers exist in the predicted data. These outliers mostly happen in the timesteps when there was an intense rainfall and consequently, a spike change has occurred in the flow. Also, some of the data fall outside the bounds at the

starting hours of the prediction when the model is adapting itself with the data and the bounds are narrower than the other predicted timesteps.

Moreover, it is important to note that the fact that Figures 4 and 5 show non-zero probability values for negative flow is due to the natural assumption of GPR that every data point is distributed Gaussian [46]. This can be highly unlikely and can be resolved by incorporating physical constraints. Addressing this limitation is beyond the scope of the current study but will be considered in future work to improve the model's physical consistency.

3.2. Forecasting Node Surcharges and Overflows

Using the same method, the water level in manholes—where the sensors are usually placed—can also be predicted. These predictions are useful in managing surcharges and overflows. Moreover, since the CSOs are spotlights of the sewer systems and water companies monitor them intently, forecasting CSOs would be another helpful application of GPR.

In this case study, the manhole with the most surcharge and overflow issues has been selected for the GPR forecasting. This selection ensures a sufficient number of data points are available for model evaluation. Also, it aligns with operational priorities, as manholes with persistent issues demand more attention over time. The results of the water depth prediction at the J15 node (the selected manhole) are presented in Figures 6 and 7.

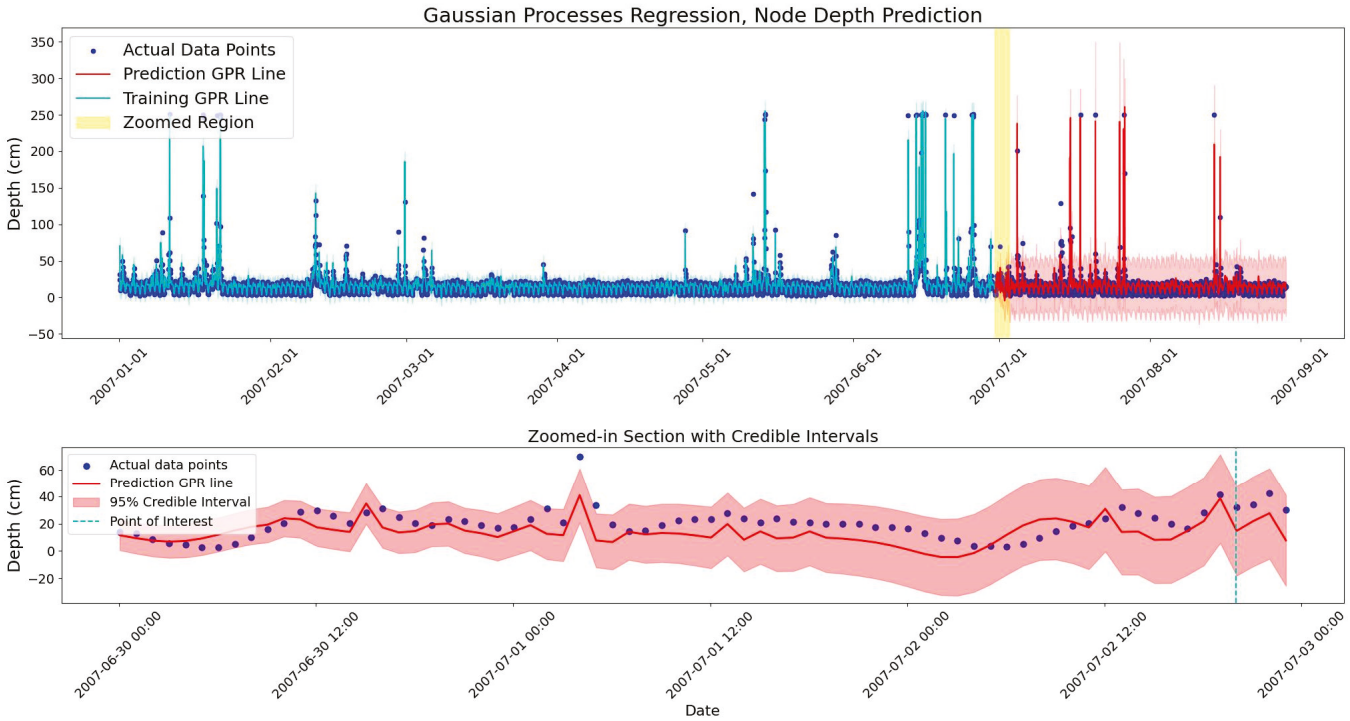

Figure 6. Water depth forecasting at node J15 for 2 months (**top**). GPR line at training and test datasets are illustrated in blue and red, respectively. The first 3 days of the test set is selected for a detailed illustration (**bottom**).

To demonstrate the model's capability on different but related time series, the same training and testing periods from the WWTP inflow analysis were used. The methodology remains consistent: a separate, single-output GPR model is trained for each manhole of interest, using that specific node's depth data as the target variable.

Given that the manhole depth is 2.5 m, the maximum observed values reach 250 cm in Figure 6, and the GPR model accounts for this range of variation during training. The results show that although significant rainfall events occurred during the test period, the GPR model does not predict excessively high water depths. This prediction can be restricted to certain values, but the model appears to do well without such constraints.

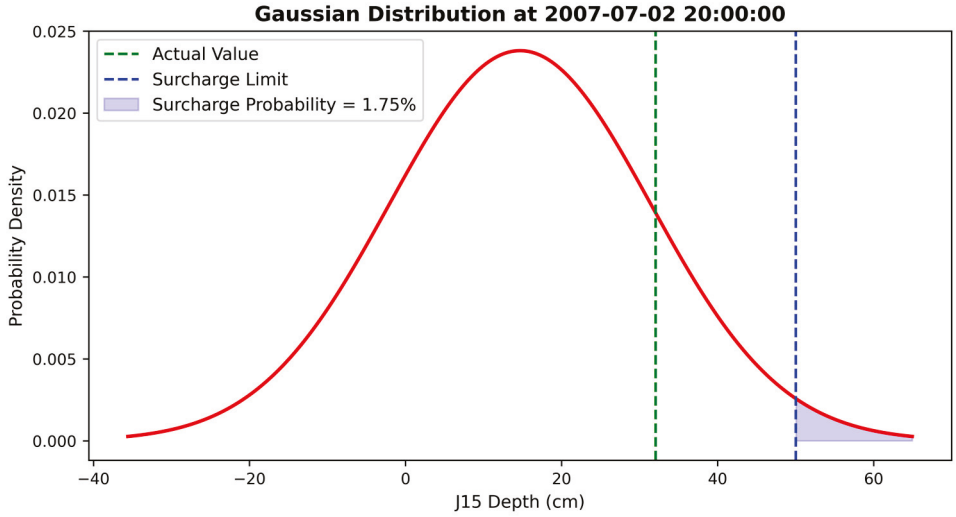

Figure 7. Gaussian distribution of the predicted node depth on 2007-07-02 at 8:00 p.m. The green dashed line shows the actual test point value. The purple dashed line also indicates the surcharge level which equals the pipe diameter. The area under the distribution for values greater than the surcharge limit is coloured in purple and shows the surcharge probability. The distribution's domain is selected as ± 4 standard deviation of the distribution for a better illustration.

Since the water level pattern closely resembles the flow pattern, the same composite kernel with tuned length scales and variances has been implemented in the GPR model. The model checking results show that the RMSE of the predictions is 10.9 cm, which is somewhat high compared to the 17.6 cm average water depth in the manhole over time. The coverage of the prediction is 99.4% that shows a perfect performance. Also, the differential entropy is calculated as 6.22.

In Figure 7, a predicted point is randomly selected for illustration. The pipe diameter is 50 cm, and water levels exceeding this threshold cause surcharges in the manhole. This value is marked with a dashed line, and the area under the predictive distribution exceeding this threshold is coloured to indicate the probability of surcharge. In this figure, the surcharge probability is 1.75%, which can be assumed to be negligible. The actual value at this point also confirms that no surcharge happened at this timestep.

This type of probabilistic output can be beneficial for developing a decision-making system which can be used in the water industry. With the same approach employed in finding the surcharge probability, manhole overflow probability can be predicted over time. These probabilistic forecasts allow operators to prioritise maintenance and allocate resources more efficiently, by focusing on locations and times with the highest risk. Figure 8 indicates the probability of surcharges and overflows in the 2-month test period of this case study.

In this figure, three thresholds (10, 25 and 50% probability) have been defined to indicate different levels of surcharge/overflow risk. These thresholds were defined based on the actual surcharge events in this case. In real-world scenarios, these thresholds would be defined based on the operator's specific risk tolerance.

Figure 8 shows one overflow prediction with probability greater than 50% and six predictions with 25 to 50% probability of happening. Among these seven predictions, four test points show that there is an actual overflow and the other three show no overflow. For predictions in the low-risk range, no overflow occurred in the simulation and the forecasts are made accurately.

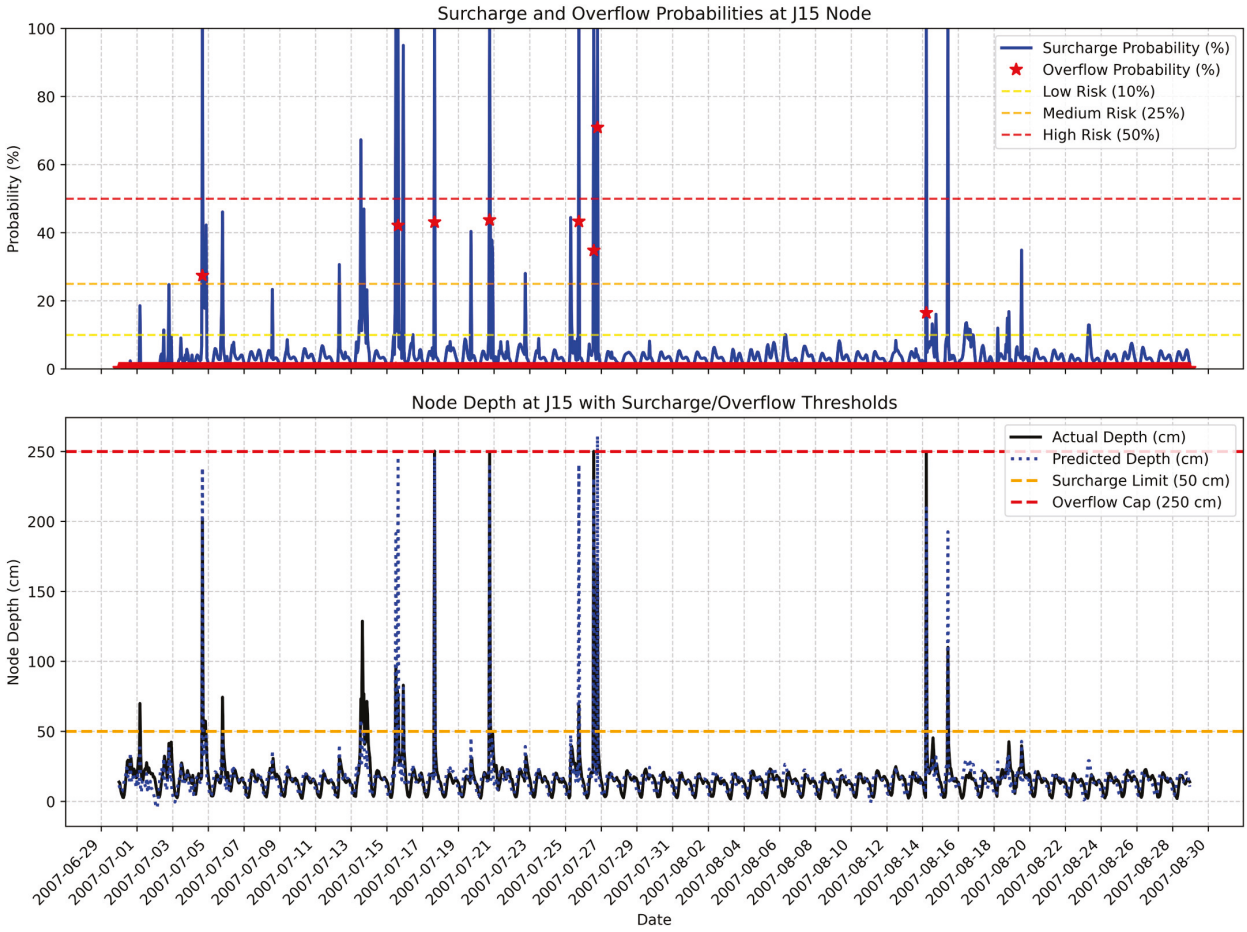

Figure 8. (**Top**): the probability of surcharge and overflow in the selected manhole. Blue line shows the probability of surcharge over time, and the red stars show the probability of an overflow from the manhole in each timestep. The dashed lines are drawn to divide the space into low, medium and high-risk zones. (**Bottom**): actual and predicted water depth at the selected manhole. Surcharge and overflow limits are shown with dashed lines.

During the 2-month period of the test period, surcharges occurred in 26 timesteps. The surcharge probability derived from the GPR model assigned different probabilities for each event, as presented in Table 2. Among the 26 surcharges, 5 events were not flagged as high- or medium-risk events while the remaining 21 timesteps were correctly identified with significant probability of surcharge. These surcharges occurred across 11 rainfall events and the model could predict 8 as high-risk and 2 as medium-risk events.

The same approach can be applied to forecast CSOs in the system. In this case study, the CSO is located downstream of a weir, which receives flow from an upstream manhole with an inlet offset. By predicting the water level at the upstream manhole, it becomes possible to estimate CSO occurrences more effectively. This approach allows the model to run more confidently using a continuous timeseries from the upstream manhole, which spans all training points and contains meaningful variation. In contrast, the CSO flow data

contains only a few non-zero values (eight, in the one-year simulation period of this study) during heavy rainfall events, with the majority of timesteps showing zero flow.

Table 2. Details of the actual surcharge events and the corresponding predicted probability values.

Surcharge Event Time	Node Depth (cm)	Probability of Surcharge (%)
2007-07-01 04:03	69.87	18.57
2007-07-04 16:03	200.96	100.0
2007-07-04 17:03	53.41	18.87
2007-07-04 18:03	57.83	29.83
2007-07-04 20:03	57.31	26.03
2007-07-05 19:03	74.39	46.10
2007-07-13 13:03	73.24	67.29
2007-07-13 14:03	56.46	11.23
2007-07-13 15:03	128.68	41.43
2007-07-13 16:03	74.78	45.86
2007-07-13 17:03	76.77	46.95
2007-07-13 21:03	71.39	23.23
2007-07-13 22:03	61.70	9.03
2007-07-15 12:03	95.31	100
2007-07-15 14:03	79.16	55.31
2007-07-15 15:03	75.72	100
2007-07-20 18:03	249.72	99.97
2007-07-20 19:03	59.88	47.38
2007-07-25 18:03	68.676	99.97
2007-07-26 14:03	250	99.99
2007-07-26 15:03	53.65	34.08
2007-07-26 19:03	169.6	100
2007-08-14 05:03	249.65	99.99
2007-08-15 10:03	110.05	100

Like the flow prediction, Figures 6 and 7 show a probability for negative depth values which seems unrealistic. It also shows non-zero probabilities for water depths exceeding the manhole's depth, which is physically impossible. The reason behind this matter is that the model is running purely data-driven without any physical constraint. Therefore, for more realistic predictions physical constraints will be added to the model in the future.

3.3. Anomaly Detection

The primary cause of anomaly in sewer systems is the blockage. In this study, an artificial spot, partial blockage is introduced in the C6 conduit of the hydraulic model, located between nodes J2 and J3. This blockage is simulated by increasing the roughness of the pipe instantly. This increase in roughness lowers the ability of the pipe to transfer water; therefore, the flow reduces, upstream depth increases, and downstream depth decreases.

These sudden changes in depth and flow can be considered as anomalies by comparing the observed values with GPR prediction results taken from the previous timesteps. When a sequence of observed values consistently falls outside the credible interval bounds of the predictions, it can serve as a reliable indicator of a potential blockage.

While simpler anomaly detection methods exist, such as fixed-level thresholds, the GPR framework provides a reliable approach by generating dynamic, probabilistic bounds that are conditioned on both time and precipitation, allowing for more sensitive fault detection.

The results of the depth prediction for the J2 node (the upstream manhole) are illustrated in Figure 9. For clarity, only the last two days of the training data from the 2-month training period are shown.

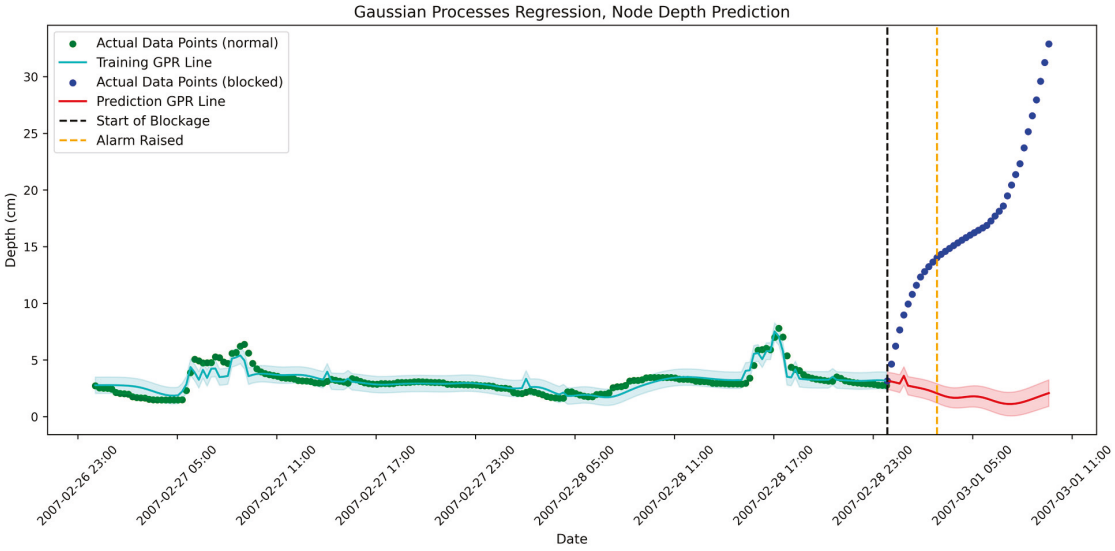

Figure 9. Blockage detection by water depth forecasting at J2 node. The prediction for 10 h has been presented by red line and the observed values have been presented by blue bullets. After three hours of consequent data points falling outside the bounds, an alarm is raised showing a probable blockage. The time interval between points is 15 min.

As shown in Figure 9, after 3 h of consequent data points falling outside the bounds, an alarm has been raised. This threshold is defined by the authors and can be adjusted based on the data points interval. Lowering this threshold would cause false alarms and lead to an increased inspection cost. However, false alarms are generally preferred over missed blockages [61].

The same approach can be applied to the downstream manhole (J3). Nonetheless, for the nodes receiving flow from multiple sources, blockage in one feeding pipe cannot be detected easily. A promising direction for future research is to use data-driven predictions from pairs of nodes that are directly connected or linked via the shortest paths. This can improve the ability of anomaly detection in the sewer system.

3.4. Prediction with Limited Data

As previously stated, GP models are capable of making predictions with minimal data for the training process and are more reliable in this case compared to other regression and classification methods among data-driven models. To demonstrate this, a flow prediction with one week of data has been made for a 3-day forecasting period. The test period is deliberately selected from the wet-weather periods to capture significant changes in the flow. The results are presented in Figure 10.

As the results show, the GPR line is fitted well on the data and the predictions seem reasonable. To further evaluate the model's robustness, four random 10-day segments were selected from the one-year dataset. The average results across these samples show 91.7% coverage, an RMSE of 8.44 L/s and an entropy of 4.54. These metrics suggest that the model trained with short periods can outperform longer-term models.

The primary limitation of using short training periods is the insufficient number of rainfall events available to train the model effectively. So, if a significant rain event occurs in the test points, the model is incapable of predicting the correct corresponding flow.

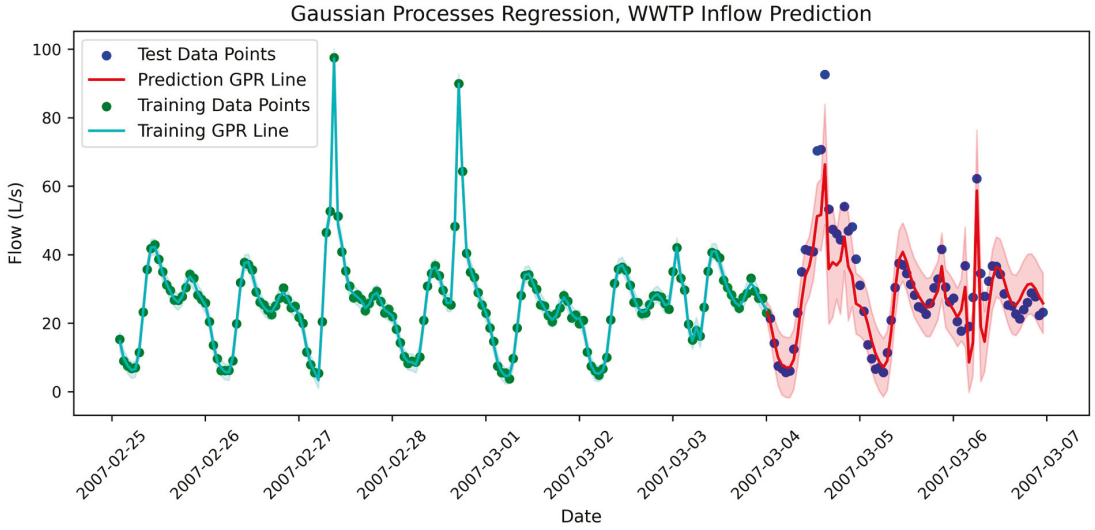

Figure 10. WWTP inflow prediction with seven days of training data using Gaussian process regression. The test period is three days, and the 95% credible interval is used to show the uncertainty around the predictions.

3.5. Further Discussion

The rainfall depths that have been used in this research were treated as deterministic inputs. However, in a predictive model, rainfalls will appear as probabilistic values with a likelihood of happening. Therefore, for an improved prediction, rainfall values can be set as Gaussian probability density function, each representing a level of uncertainty.

Moreover, standard GPR assumes Gaussian uncertainty, which may not reflect real-world conditions. This limitation can be addressed by employing more advanced techniques capable of capturing non-Gaussian distributions.

The predictions made in this study were all in a range of short- and medium-term periods because the main goal of this study was to detect flaws and anomalies, and to warn about high or low flows in a sewer system. The long-term predictions can be conducted with the aim of GPs, but the computational costs and high values of uncertainties may make other data-driven models more suitable for asset management applications.

In such cases, a kernel which captures annual cycles of groundwater infiltration can be added to the main kernel to enhance the model. Moreover, population increase and changes in water usage habits should be considered in long-term forecasts.

The GP regression model, shown in Figure 4, is built with hourly data, resulting in 4320 training points. For a more detailed prediction, data of the same period with a 5 min resolution can be used. However, this increases the number of training points to 51,840 which significantly increases the computational cost of the model due to the $O(N^3)$ complexity of the GP. In such cases, methods such as Sparse Variational Gaussian Processes (SVGP) can be beneficial in handling the large dataset [62].

It is important to note that rain gauge data is typically not available in real time and often arrives with a delay of 15 min or more. However, this latency does not significantly affect the performance of the anomaly detection model, as the alarm mechanism is designed to trigger only after a defined number of consecutive data points fall outside the credible bounds.

Additionally, the hydraulic simulations in this study were based on a single rain gauge, assuming uniform precipitation across the catchment. Future work should consider using spatially distributed rainfall data, which would provide more realistic and varied runoff inputs for training the GPR model, especially for large catchments.

The model's performance was defined by three metrics in this research. These metrics can be used separately for dry- and wet-weather periods to better show the model's performance during extreme events and the baseline.

Finally, incorporating physical constraints into the model can significantly enhance its realism and robustness. For example, the mean function which is commonly assumed to be zero in standard GPR can be replaced with a physics-informed prior that reflects expected system behaviour and is updated during posterior inference. Also, the geometry of a particular manhole, pipe or weir can be considered in producing predicted distributions for more precision.

Additionally, physical constraints, such as the continuity equation or operational limits like minimum flow rates and maximum water depth in each pipe or manhole, can be embedded into the model. These constraints help ensure that predictions remain within realistic and operationally acceptable bounds.

4. Conclusions

In this study, Gaussian processes regression (GPR) was implemented to predict flow and depth in a sewer system and flag anomalies. The case study was a hypothetical skeleton sewer system with different characteristics of a real-world system serving 11,300 inhabitants of a city in the UK.

The framework's novelty lies in its custom composite kernel, designed to capture key sewer flow dynamics, and its application for real-time blockage detection using predictive uncertainty bounds. The approach demonstrated high performance even when trained on limited data, highlighting its potential for real-world deployment in forecasting and real-time control, especially when historical data is sparse.

Based on the findings in sewer flow prediction, taking time and precipitation as two main inputs of the GPR model effectively captures flow patterns with the designed kernel. In contrast, having a single-input model cannot effectively reflect flow changes during wet-weather periods. Also, adding new inputs to the model only adds to the dimension of the covariance matrix, which is directly related to the computational cost of the GPs.

Designing a composite kernel that reflects the underlying physical processes in the system proved highly effective in this model. The kernel was optimised by maximising the log marginal likelihood, while additional evaluation metrics such as RMSE, coverage, and differential entropy helped identify the best kernel settings.

GPR can respond well to minimal training datasets and make reliable predictions. On the other hand, a high number of data points can reduce the model's speed and make it computationally inefficient.

Outliers may appear in every prediction, often due to a lack of wide range in training datasets, especially when dealing with precipitation data. In such cases, increasing the length of the training period helps.

The proposed probabilistic framework offers a new way for decision-makers to assess sewer system risks. By providing dynamic uncertainty bounds for its forecasts, the model allows for a quantitative assessment of risk (e.g., overflow probability), which can support more resilient infrastructure planning and help mitigate threats to public health and the environment.

In summary, this research offers a promising framework for probabilistic forecasting and anomaly detection in sewer systems. Future work can enhance this approach by incorporating physical constraints into the model and representing input variables, such as rainfall, as probability distributions to capture input uncertainty more accurately. Furthermore, this probabilistic platform has the potential to serve as an alternative to

real-time control and forecasting platforms currently used by water companies, offering a transparent and adaptable decision-support tool.

Author Contributions: Conceptualisation, M.R., H.R. and P.M.-S.; methodology, M.R. and H.R.; software, M.R.; validation, M.R.; formal analysis, M.R.; investigation, M.R. and H.R.; resources, M.R., H.R. and P.M.-S.; data curation, M.R.; writing—original draft preparation, M.R.; writing—review and editing, M.R., H.R. and P.M.-S.; visualisation, M.R.; supervision, H.R. and P.M.-S.; project administration, H.R. All authors have read and agreed to the published version of the manuscript.

Funding: This research received no external funding.

Data Availability Statement: The hydraulic model and the source code for forecasting flow are available through the GitHub repository: https://github.com/MohsenRz/Sewer_System_Forecasting_Emulator.git, accessed on 20 July 2025.

Acknowledgments: For the purpose of open access, the author has applied a Creative Commons Attribution (CC BY) licence to any Author Accepted Manuscript version arising from this submission.

Conflicts of Interest: The authors declare no conflicts of interest.

Abbreviations

The following abbreviations are used in this manuscript:

CSO	Combines Sewer Overflow
GP	Gaussian Process
GPR	Gaussian Processes Regression
SWMM	Storm Water Management Model
DWF	Dry-weather Flow
CCTV	Closed-circuit Television
RMSE	Root Mean Square Error
SVGP	Sparse Variational Gaussian Processes

References

1. Walski, T.M.; Barnard, T.E. *Wastewater Collection System Modeling and Design*; Haestad Press: Waterbury, CT, USA, 2004.
2. Owolabi, T.A.; Mohandes, S.R.; Zayed, T. Investigating the impact of sewer overflow on the environment: A comprehensive literature review paper. *J. Environ. Manag.* **2022**, *301*, 113810. [CrossRef] [PubMed]
3. Perry, W.B.; Ahmadian, R.; Munday, M.; Jones, O.; Ormerod, S.J.; Durance, I. Addressing the challenges of combined sewer overflows. *Environ. Pollut.* **2024**, *343*, 123225. [CrossRef]
4. Arthur, S.; Crow, H.; Pedezert, L. Understanding blockage formation in combined sewer networks. *Proc. Inst. Civ. Eng.-Water Manag.* **2008**, *161*, 215–221. [CrossRef]
5. Faris, N.; Zayed, T.; Aghdam, E.; Fares, A.; Alshami, A. Real-time sanitary sewer blockage detection system using IoT. *Measurement* **2024**, *226*, 114146. [CrossRef]
6. Balla, K.M.; Bendtsen, J.D.; Schou, C.; Kallesøe, C.S.; Ocampo-Martinez, C. A learning-based approach towards the data-driven predictive control of combined wastewater networks–An experimental study. *Water Res.* **2022**, *221*, 118782. [CrossRef] [PubMed]
7. Perez, G.; Gomez-Velez, J.D.; Grant, S.B. The sanitary sewer unit hydrograph model: A comprehensive tool for wastewater flow modeling and inflow-infiltration simulations. *Water Res.* **2024**, *249*, 120997. [CrossRef]
8. Zhang, Q.; Li, Z.; Snowling, S.; Siam, A.; El-Dakhakhni, W. Predictive models for wastewater flow forecasting based on time series analysis and artificial neural network. *Water Sci. Technol.* **2019**, *80*, 243–253. [CrossRef]
9. Li, S.; Tian, W.; Yan, H.; Zeng, W.; Tao, T.; Xin, K. Modeling transient mixed flows in sewer systems with data fusion via physics-informed machine learning. *Water Res. X* **2024**, *25*, 100266. [CrossRef]
10. Stieglitz, M.; Hobbie, J.; Giblin, A.; Kling, G. Hydrologic modeling of an arctic tundra watershed: Toward Pan-Arctic predictions. *J. Geophys. Res.-Atmos.* **1999**, *104*, 27507–27518. [CrossRef]
11. Donnelly, J.; Daneshkhah, A.; Abolfathi, S. Forecasting global climate drivers using Gaussian processes and convolutional autoencoders. *Eng. Appl. Artif. Intell.* **2024**, *128*, 107536. [CrossRef]

12. Machac, D.; Reichert, P.; Rieckermann, J.; Albert, C. Fast mechanism-based emulator of a slow urban hydrodynamic drainage simulator. *Environ. Model. Softw.* **2016**, *78*, 54–67. [CrossRef]
13. Troutman, S.C.; Schambach, N.; Love, N.G.; Kerkez, B. An automated toolchain for the data-driven and dynamical modeling of combined sewer systems. *Water Res.* **2017**, *126*, 88–100. [CrossRef] [PubMed]
14. Ge, J.; Li, J.; Qiu, R.; Shi, T.; Zhang, C.; Huang, Z.; Yuan, Z. A data-driven method for estimating sewer inflow and infiltration based on temperature and conductivity monitoring. *Water Res.* **2024**, *261*, 122002. [CrossRef] [PubMed]
15. Aliashrafi, A.; Zhang, Y.; Groenewegen, H.; Vanrolleghem, P.A. A Review of Data-Driven Modelling in Drinking Water Treatment. *Rev. Environ. Sci. Biotechnol.* **2021**, *20*, 985–1009. [CrossRef]
16. Swiler, L.P.; Gulian, M.; Frankel, A.L.; Safta, C.; Jakeman, J.D. A survey of constrained Gaussian process regression: Approaches and implementation challenges. *J. Mach. Learn. Model. Comput.* **2020**, *1*, 119–156. [CrossRef]
17. Raissi, M.; Perdikaris, P.; Karniadakis, G.E. Physics-informed neural networks: A deep learning framework for solving forward and inverse problems involving nonlinear partial differential equations. *J. Comput. Phys.* **2019**, *378*, 686–707. [CrossRef]
18. Thorndahl, S.; Willems, P. Probabilistic modelling of overflow, surcharge and flooding in urban drainage using the first-order reliability method and parameterization of local rain series. *Water Res.* **2008**, *42*, 455–466. [CrossRef]
19. Breinholt, A. Uncertainty in Prediction and Simulation of Flow in Sewer Systems. Ph.D. Thesis, Technical University of Denmark, Kongens Lyngby, Denmark, 2012.
20. Raimondi, A.; Sanfilippo, U.; Becciu, G. Uncertainty on flow rate and temperature measurement for the detection of illicit flows in sewers. *J. Hydrol.* **2024**, *632*, 130891. [CrossRef]
21. Sriwastava, A.K.; Tait, S.; Schellart, A.; Kroll, S.; Van Dorpe, M.; Van Assel, J.; Shucksmith, J. Quantifying uncertainty in simulation of sewer overflow volume. *J. Environ. Eng.* **2018**, *144*, 04018050. [CrossRef]
22. Ding, C.; Rappel, H.; Dodwell, T. Full-field order-reduced Gaussian Process emulators for nonlinear probabilistic mechanics. *Comput. Methods Appl. Mech. Eng.* **2023**, *405*, 115855. [CrossRef]
23. Wang, J. An intuitive tutorial to Gaussian process regression. *Comput. Sci. Eng.* **2023**, *25*, 4–11. [CrossRef]
24. Ding, C.; Chen, Y.; Rappel, H.; Dodwell, T. Functional order-reduced Gaussian Processes based machine-learning emulators for probabilistic constitutive modelling. *Compos. Part A Appl. Sci. Manuf.* **2023**, *173*, 107695. [CrossRef]
25. Gonzalvez, J.; Lezmi, E.; Roncalli, T.; Xu, J. Financial applications of Gaussian processes and Bayesian optimization. *arXiv* **2019**, arXiv:1903.04841. [CrossRef]
26. Roberts, S.; Osborne, M.; Ebden, M.; Reece, S.; Gibson, N.; Aigrain, S. Gaussian processes for time-series modelling. *Philos. Trans. R. Soc. A Math. Phys. Eng. Sci.* **2013**, *371*, 20110550. [CrossRef]
27. Sun, A.Y.; Wang, D.; Xu, X. Monthly streamflow forecasting using Gaussian process regression. *J. Hydrol.* **2014**, *511*, 72–81. [CrossRef]
28. Pastrana-Cortés, J.D.; Gil-Gonzalez, J.; Álvarez-Meza, A.M.; Cárdenas-Peña, D.A.; Orozco-Gutiérrez, Á.A. Scalable and interpretable forecasting of hydrological time series based on variational Gaussian processes. *Water* **2024**, *16*, 2006. [CrossRef]
29. Samuelsson, O.; Björk, A.; Zambrano, J.; Carlsson, B. Gaussian process regression for monitoring and fault detection of wastewater treatment processes. *Water Sci. Technol.* **2017**, *75*, 2952–2963. [CrossRef]
30. Ng, J.Y.; Fazlollahi, S.; Dechesne, M.; Soyeux, E.; Galelli, S. Robust optimal design of urban drainage systems: A data-driven approach. *Adv. Water Resour.* **2023**, *171*, 104335. [CrossRef]
31. Wang, Y.; Ocampo-Martinez, C.; Puig, V. Stochastic model predictive control based on Gaussian processes applied to drinking water networks. *IET Control. Theory Appl.* **2016**, *10*, 947–955. [CrossRef]
32. Grbić, R.; Kurtagić, D.; Slišković, D. Stream water temperature prediction based on Gaussian process regression. *Expert Syst. Appl.* **2013**, *40*, 7407–7414. [CrossRef]
33. Bonakdari, H.; Ebtehaj, I.; Samui, P.; Gharabaghi, B. Lake water-level fluctuations forecasting using minimax probability machine regression, relevance vector machine, Gaussian process regression, and extreme learning machine. *Water Resour. Manag.* **2019**, *33*, 3965–3984. [CrossRef]
34. Sweetapple, C.; Webber, J.; Hastings, A.; Melville-Shreeve, P. Realising smarter stormwater management: A review of the barriers and a roadmap for real world application. *Water Res.* **2023**, *244*, 120505. [CrossRef] [PubMed]
35. Patil, R.R.; Calay, R.K.; Mustafa, M.Y.; Ansari, S.M. AI-driven high-precision model for blockage detection in urban wastewater systems. *Electronics* **2023**, *12*, 3606. [CrossRef]
36. Rosin, T.R.; Kapelan, Z.; Keedwell, E.; Romano, M. Near real-time detection of blockages in the proximity of combined sewer overflows using evolutionary ANNs and statistical process control. *J. Hydroinf.* **2022**, *24*, 259–273. [CrossRef]
37. Jimoh, M.; Abolfathi, S. Modelling pollution transport dynamics and mixing in square manhole overflows. *J. Water Process Eng.* **2022**, *45*, 102491. [CrossRef]

38. Li, N.; Wang, X.; Li, Z.; Zhao, F.; Nair, A.; Zhang, J.; Liu, C. Real-time identification and positioning of sewer blockage based on liquid level analysis in rural area. *Processes* **2023**, *11*, 161. [CrossRef]
39. Kargar, K.; Joksimovic, D. Analysis of sewer blockage causes using open data. *Water Pract. Technol.* **2024**, *19*, 3855–3866. [CrossRef]
40. Rossman, L.A.; Simon, M.A. *Storm Water Management Model User's Manual Version 5.2*; US Environmental Protection Agency: Cincinnati, OH, USA, 2022.
41. Prodanovic, P.; Simonovic, S.P. *Development of Rainfall Intensity Duration Frequency Curves for the City of London under the Changing Climate*; Department of Civil and Environmental Engineering, The University of Western Ontario: London, ON, Canada, 2007.
42. Rezaee, M.; Tabesh, M. Effects of inflow, infiltration, and exfiltration on water footprint increase of a sewer system: A case study of Tehran. *Sustain. Cities Soc.* **2022**, *79*, 103707. [CrossRef]
43. Zeydalinejad, N.; Javadi, A.A.; Webber, J.L. Global perspectives on groundwater infiltration to sewer networks: A threat to urban sustainability. *Water Res.* **2024**, *262*, 122098. [CrossRef]
44. McDonnell, B.E.; Ratliff, K.; Tryby, M.E.; Wu, J.J.X.; Mullapudi, A. PySWMM: The python interface to stormwater management model (SWMM). *J. Open Source Softw.* **2020**, *5*, 1–3. [CrossRef] [PubMed]
45. Stovin, V. *Mappin Green Roof Test Bed Rainfall and Runoff Data 2007*; The University of Sheffield: Sheffield, UK, 2024. [CrossRef]
46. Rasmussen, C.E.; Williams, C.K.I. *Gaussian Processes for Machine Learning*; MIT Press: Cambridge, MA, USA, 2006.
47. Deshpande, S.; Rappel, H.; Hobbs, M.; Bordas, S.P.; Lengiewicz, J. Gaussian process regression + deep neural network autoencoder for probabilistic surrogate modeling in nonlinear mechanics of solids. *Comput. Methods Appl. Mech. Eng.* **2025**, *437*, 117790. [CrossRef]
48. Rappel, H.; Beex, L.A.; Hale, J.S.; Noels, L.; Bordas, S.P. A tutorial on Bayesian inference to identify material parameters in solid mechanics. *Arch. Comput. Methods Eng.* **2020**, *27*, 361–385. [CrossRef]
49. Duvenaud, D. Automatic Model Construction with Gaussian Processes. Ph.D. Thesis, University of Cambridge, Cambridge, UK, 2014.
50. Wilson, A.G. Covariance Kernels for Fast Automatic Pattern Discovery and Extrapolation with Gaussian Processes. Ph.D. Thesis, University of Cambridge, Cambridge, UK, 2014.
51. Matthews, A.G.; Van Der Wilk, M.; Nickson, T.; Fujii, K.; Boukouvalas, A.; Le, P.; Ghahramani, Z.; Hensman, J. GPflow: A Gaussian process library using TensorFlow. *J. Mach. Learn. Res.* **2017**, *18*, 1–6.
52. Duvenaud, D.; Lloyd, J.; Grosse, R.; Tenenbaum, J.; Ghahramani, Z. Structure Discovery in Nonparametric Regression through Compositional Kernel Search. In Proceedings of the International Conference on Machine Learning, Atlanta, GA, USA, 26 May 2013; pp. 1166–1174.
53. Kuok, S.C.; Yao, S.A.; Yuen, K.V.; Yan, W.J.; Girolami, M. Bayesian generative kernel Gaussian process regression. *Mech. Syst. Signal Process.* **2025**, *227*, 112395. [CrossRef]
54. Abramowitz, M.; Stegun, I.A. (Eds.) *Handbook of Mathematical Functions with Formulas, Graphs, and Mathematical Tables*; US Government Printing Office: Washington, DC, USA, 1948.
55. Gilks, W.R.; Richardson, S.; Spiegelhalter, D. (Eds.) *Markov Chain Monte Carlo in Practice*; CRC Press: Boca Raton, FL, USA, 1995.
56. Malde, S. Gaussian Process Emulators in Coastal Wave Modelling. Ph.D. Thesis, University of Sheffield, Sheffield, UK, 2018.
57. Gelman, A.; Carlin, J.B.; Stern, H.S.; Rubin, D.B. *Bayesian Data Analysis*, 3rd ed.; Chapman and Hall/CRC: Boca Raton, FL, USA, 2021.
58. Hyndman, R.J.; Koehler, A.B. Another look at measures of forecast accuracy. *Int. J. Forecast.* **2006**, *22*, 679–688. [CrossRef]
59. Hasegawa, Y.; Nishiyama, T. Thermodynamic entropic uncertainty relation. *arXiv* **2025**, arXiv:2502.06174. [CrossRef]
60. MacKay, D.J. *Information Theory, Inference and Learning Algorithms*; Cambridge University Press: Cambridge, UK, 2003.
61. Roghani, B.; Cherqui, F.; Ahmadi, M.; Le Gauffre, P.; Tabesh, M. Dealing with uncertainty in sewer condition assessment: Impact on inspection programs. *Autom. Constr.* **2019**, *103*, 117–126. [CrossRef]
62. Liu, H.; Ong, Y.S.; Shen, X.; Cai, J. When Gaussian process meets big data: A review of scalable GPs. *IEEE Trans. Neural Netw. Learn. Syst.* **2020**, *31*, 4405–4423. [CrossRef]

Disclaimer/Publisher's Note: The statements, opinions and data contained in all publications are solely those of the individual author(s) and contributor(s) and not of MDPI and/or the editor(s). MDPI and/or the editor(s) disclaim responsibility for any injury to people or property resulting from any ideas, methods, instructions or products referred to in the content.

water

MDPI

Article

Challenges of Urban Water Cycle Management in Small Spanish Municipalities: The Case of the Province of Granada

Francisco Javier García-Martínez [1,2], Francisco Osorio [2,3] and Francisco González-Gómez [3,*]

[1] Provincial Deputation of Granada, 18014 Granada, Spain; jgarcia@dipgra.es or fcojaviergarcia@ugr.es
[2] Department of Civil Engineering, University of Granada, 18071 Granada, Spain; fosorio@ugr.es
[3] Water Research Institute, University of Granada, 18071 Granada, Spain
* Correspondence: fcojose@ugr.es

Abstract: Urban water service management in Spain presents two very distinct realities: populated service areas and small population centres. Despite the professionalised management of resources to provide a comprehensive, high-quality service in the largest service areas, small population centres face significant deficits and shortcomings that pose a major challenge for the Spanish public administration. This article reviews the existing problems surrounding the management of urban water cycle services in small-population municipalities in the province of Granada. This case study describes a reality that can be extrapolated to a significant number of small municipalities in the rest of Spain, where the management of urban water cycle services is directly assumed by City Councils. Having reviewed the problems, the article concludes with a series of recommendations for improving urban water cycle management in small municipalities. The conclusions emphasise the study and creation of optimal service areas, as well as the creation of an independent regulatory body.

Keywords: urban water cycle; Spain; rural areas; governance

1. Introduction

Water and sanitation are fundamental to sustainable development; they are fundamental requirements, which underpin poverty reduction, economic growth, and environmental sustainability [1]. Within the framework of the 2030 Sustainable Development Agenda, states committed in 2015 to the goals of SDG 6: Clean Water and Sanitation [2]. Among the proposed targets are ensuring access to water, promoting the efficient and sustainable use of water resources, and improving water quality. To achieve these goals, the United Nations advocates for the adoption of a polycentric water governance model that engages all sectors of society [3]. This approach entails participation, dialogue, and coordination among the various stakeholders involved in decision making.

The challenges associated with accessing water and sanitation for residential use vary greatly across the world [4,5]. In developing countries, much progress needs to be made in order to fulfil the human right to access water and sanitation. At the other extreme, in Europe and North America, access to water and sanitation is virtually guaranteed for the entire population [6]. In these regions, the challenges are to advance water circularity, efficiency, and the decarbonisation of all phases of the process.

While water policies in Europe focus on circularity and decarbonisation, part of the population continues to suffer from a lack of access to water and sanitation. The second principle of the United Nations 2030 Agenda advocates "Leaving no one behind", which

entails combating poverty and avoiding situations of discrimination. Regarding access to water and sanitation, this principle is reflected in the United Nations World Report, published in 2019 [7]. In response to this call, the European Union's Directive 2020/2184 states that Member States must improve access to water for human consumption for vulnerable and marginalised groups [8]. Reference is made to the installation of outdoor and indoor equipment in public spaces, which allows these groups access to drinking water.

Likewise, without reaching situations of extreme vulnerability for certain groups, in terms of access to water, part of the European population is being left behind in the advances being made in urban water cycle services. Population centres with fewer inhabitants, typically located in rural areas and dependent on the agricultural sector, present significant deficiencies in public water and sanitation services. These deficiencies encompass material, financial, organisational, political, and technical aspects.

This situation is more evident in Member States with greater population dispersion among small municipalities. Spain is one example; there are 6813 municipalities with fewer than 5000 inhabitants, accounting for 84% of the total [9]. Faced with the difficulties in providing urban water cycle services, many of these municipalities have opted to form larger service areas under various forms of association. This is a way to take advantage of the industry's economies of scale. Other municipalities have opted for concessions as a way to professionalise service provision. Finally, there are municipalities where the service is provided directly by the city council. It is in these cases where the technical and financial deficiencies are most evident. In general, it can be said that, despite the professionalised management of resources providing a comprehensive, quality service in the largest service areas, small population centres face deficiencies and shortcomings that pose a challenge for public administration. This is a situation acknowledged by the Government of Spain in the Green Paper on Governance in Spain [10], as well as in the report [11] prepared for the section on the Integrated Water Cycle in Small and Medium-Sized Municipalities of the Green Paper on Water Governance in Spain.

Institutional reports and academic research tend to be biased toward the study of the management of the urban water cycle in large cities. One explanation is the easier access to data; another possible reason is a greater interest for addressing issues that affect a larger share of the population. From a socio-political perspective, the challenges faced by large urban areas tend to have a greater impact and attract more attention. This article analyses the different situations and challenges that may arise in the provision of residential water services in small municipalities. To this end, the case of the province of Granada is as a good example. The objective of this paper is to demonstrate that, while the focus and progress towards circularity and decarbonisation are being focused on in large service areas, much remains to be done in small municipalities. Therefore, there is a clear risk that the gap in the management of urban water cycle services between large and small service areas will further widen in the coming years. Internal documentation was consulted, and information was obtained from a working group of the Provincial Council of Granada.

The work is structured as follows. After this introduction, the research methodology is briefly explained. We then focus on the area of study. The distribution of the population in the province of Granada and the management method for urban water service provision are described. Section 4 then describes the problems and causes of urban water service management in small municipalities under direct management. A brief discussion and policy implications are included in Section 6. The article concludes with conclusions and recommendations.

2. Methodology

The research was conducted using information obtained from the Granada Provincial Council and is the result of a programme promoted by the Provincial Council in 2022,

in which the City Council and the University of Granada also participated. Within the framework of this programme, an intense debate has taken place in recent years with the aim of improving the management of urban water cycle services in municipalities under direct management. This covers 106 of the 174 municipalities in the Province of Granada.

The concern for urban water cycle services in Granada originated in a diagnostic report prepared in 2013 and entitled "Technical and Operational Study of the Urban Water Cycle in Various Municipalities of the Province of Granada" [12]. This report was supplemented by studies conducted in 2019 and 2020 [13–17]. This background evidence shows that concern about urban water cycle services in small municipalities has been ongoing for some time. This series of reports highlights many structural shortcomings in water service management in Granada.

At the same time, between 2016 and 2021, regular meetings were held by the Water Working Group of the Granada Network of Municipalities Towards Sustainability (GRAMAS Network), made up of mayors, municipal technicians, provincial council staff, and researchers from the University of Granada. The GRAMAS Network is an initiative promoted by the Granada Provincial Council that has the aim of incorporating the principles of sustainability and good environmental practices into municipal management through the exchange of experiences and institutional cooperation. In order to achieve the set objectives, a participatory methodology is used based on practical actions developed through working groups that seek common solutions to shared problems through the exchange of experiences and the adoption of good practices.

Based on this background, it was decided to launch the General Programme for the Improvement of the Complete Water Cycle [18]. Within the framework of this programme, two main objectives were established: the identification of the causes of the problems detected in the management of urban water services and the proposal of measures to improve the economic and technical performance of the services. For the development of this research, use has been made of the internal documentation of the Provincial Council of Granada, which was generated within the framework of the General Programme for the Improvement of the Integral Water Cycle [18], and the content of the information from the meetings that continued to be held in the GRAMAS Network until the completion of this research.

For the processing of information and the presentation of results, an exhaustive review was conducted of both the technical reports produced by the Provincial Council of Granada and the minutes from the GRAMAS Network. In Section 3, data extracted from the provincial council's reports are used to describe how urban water cycle services are managed across municipalities in the province of Granada, classified by population size. Additionally, the section highlights specific shortcomings in service provision, particularly in small municipalities operating under direct management models. Section 4 presents an analysis of the main factors that hinder the effective management of urban water cycle services. The methodological approach involved identifying the most frequently cited issues in the GRAMAS Network's discussion groups and in provincial council reports. These issues were compiled into a list of contributing factors that were subsequently classified and grouped based on their origin, with special attention given to the roles played by the various stakeholders involved.

3. The Provision of Urban Water Services in the Province of Granada, According to Population Size

3.1. The Distribution of the Population at the Municipal Level: Granada and Spain

The most commonly used indicator for determining whether a town is small is the number of inhabitants [19]; however, there is no consensus on this figure [20]. In Spain, the Ministry of Agriculture and Fisheries has defined small rural municipalities as those with

fewer than 5000 inhabitants [21]. Based on this definition, both Spain and the province of Granada are predominantly made up of small rural municipalities (Table 1).

Table 1. Distribution of municipalities by population size in Spain and the province of Granada, 2024 (prepared by the authors based on [9]).

	Spain				Granada			
	Municipalities		Inhabitants in Municipalities		Municipalities		Inhabitants in Municipalities	
Size of Municipalities According to Population	No	%	No	%	No	%	No	%
0–300	3155	38.87	405,142	0.85	9	5.17	2020	0.22
301–1000	1828	22.48	1,038,799	2.16	65	37.36	40,997	4.41
1001–2000	877	10.79	1,238,465	2.58	28	16.09	38,240	4.11
2001–5000	956	11.76	3,045,156	6.34	31	17.82	88,573	9.52
5001–10,000	544	6.69	3,859,439	8.04	20	11.49	138,496	14.89
10,001–20,000	347	4.27	4,877,169	10.16	12	6.90	173,690	18.67
20,001–50,000	272	3.35	8,032,859	16.73	7	4.02	158,651	17.06
50,001–300,000	140	1.72	15,483,019	32.24	2	1.15	289,534	31.13
>300,000	12	0.15	10,042,467	20.91	0	0.00	0	0.00
Total	8131	100.00	48,022,515	100.00	174	100.00	930,201	100.00

The population distribution in Spain and the province of Granada is similar, so Granada is considered a good example of the Spanish territory. The percentage of municipalities with fewer than 5000 inhabitants is slightly higher than 76% in Granada, while in Spain, it is around 84%. Considering the population living in these municipalities, this represents 18.26% in the province and 12.35% nationally. Figure 1 illustrates that, in most of the Spanish territory, a high concentration of the population inhabits provincial capitals. A significant portion of the remaining population is distributed across small municipalities—this is the so-called "emptied Spain". This pattern only differs in provinces with large metropolitan areas, such as Madrid and Barcelona, as well as along the coast.

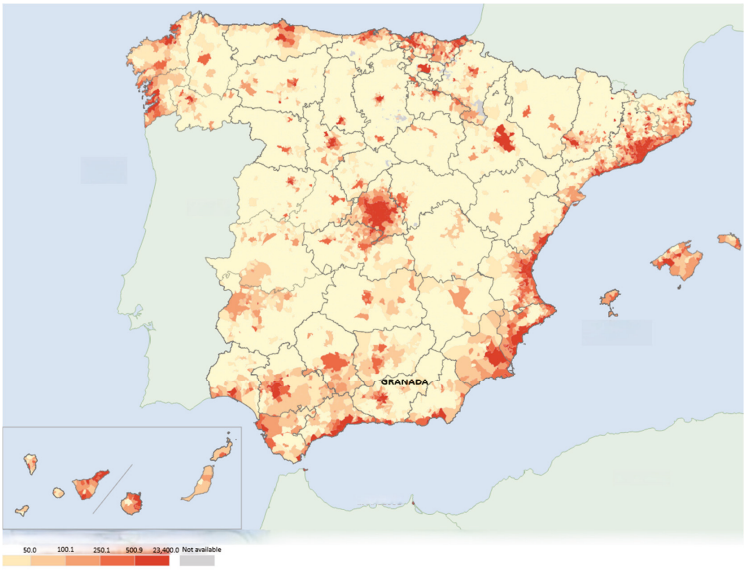

Figure 1. Population density in Spain, 2024. (Atlas Digital de las Áreas Urbanas del Ministerio de Vivienda y Agenda Urbana. Accessed on 5 June 2025: https://atlasau.mitma.gob.es/#c=indicator&i=pobevo.densidad&s=2024&view=map4).

3.2. Management of Urban Water Cycle Services in Granada

Population size is a determining factor in service management [22,23]. To take advantage of economies of scale in the industry, some municipalities have opted for municipal grouping [24,25]. In the province of Granada, up to three large supra-municipal management areas can be distinguished (Figure 2). In the Vega de Granada, two municipal groupings have been created for urban water cycle management: the Granada metropolitan area, made up of 15 municipalities and just over 390,000 inhabitants, and the Aguas de la Vega Sierra Elvira consortium, which includes 22 municipalities and provides services to 159,816 inhabitants. In both cases, the management of urban water cycle services has been delegated to a joint venture in which the private partner is a company from the multinational Veolia group. Additionally, on the Costa Tropical, a service area has been created comprising 16 municipalities and 115,000 inhabitants. In this case, the concession was awarded to a joint venture involving the multinationals Aqualia and Acciona.

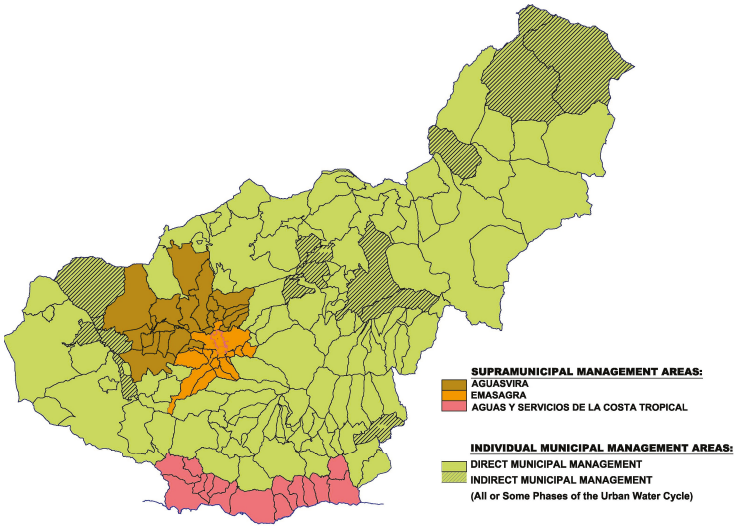

Figure 2. Geographical implementation of the different types of urban water cycle management in the province of Granada, 2024. (Own elaboration).

In contrast to these three large service areas, management in the rest of the province is at the municipal level. There are 15 municipalities where urban water cycle management is provided by a private company. The average population of these municipalities is 3700. The management companies are Aqualia (eight municipalities), Gestagua (six), and Acciona (one).

Finally, there are 106 municipalities where management is carried out directly (Figure 3); this represents almost two-thirds of the municipalities (60.92%) and one-fifth of the population (20.65%).

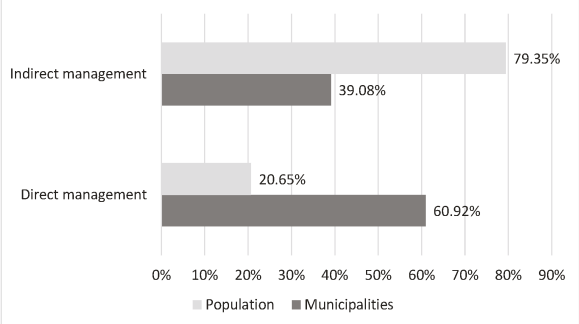

Figure 3. Types of urban water cycle management in the province of Granada, 2023. (Own elaboration).

3.3. First Approach to Urban Water Service Management in Small Municipalities Under Direct Management

Municipalities under direct management are characterised by small populations and limited financial and technical resources for providing water services. The main water resources come from wells [26]. Overall, there is a highly dispersed population, as well as significant decentralisation of infrastructure, which prevents the exploitation of industrial economies of scale and complicates the management of urban water cycle services.

There are multiple deficiencies. The first shortcoming is the widespread lack of both technical and economic–financial data, which hampers decision making. Basic information, such as the volume of water withdrawn and injected into the network, the volume of water consumed by users, and operating costs, is lacking. Among the reasons for the lack of data on water consumption are the absence of residential meters in 11.3% of smaller municipalities and the age of existing ones [13] (Table 2). It has also been found that 70.5% of tanks do not have outlet meters [14]. Furthermore, there is no independent economic accounting to quantify the costs of municipal water services and, consequently, determine whether the cost recovery principle is being met [17].

Table 2. Indicators of the urban water cycle service in municipalities with direct management of the water service in the province of Granada.

Description	Indicator
Percentage of municipalities in the province of Granada with direct management	60.92%
Percentage of the population in the province of Granada living in a municipality with direct management	20.65%
Percentage of municipalities are supplied by groundwater	92%
Percentage of groundwater bodies in danger	41%.
Percentage of municipalities with regulatory deposits in regular, poor, or very poor condition	21%
Percentage of municipalities that have problems of insufficient drinking water supply	17%
Percentage of municipalities with a supply network in poor or very poor condition	18%
Percentage of municipalities in the province of Granada with a deficit of household water meters	11.3%
Technical performance of the networks (ratio between the water recorded by the users' water meters and the water discharged from the regulating reservoirs)	32.7%
Number of wastewater treatment plants that are pending construction	90
Wastewater treatment plants that do not meet discharge parameters	>90%
Percentage of municipalities with sanitation networks in poor or very poor condition.	16%
Financial deficit for urban water cycle services	23 EUR/inhabitant/year

Despite the limited information available, the main problem with the supply service is the poor technical performance of the supply networks. On average, the technical performance of the networks is only at 32.7% (the ratio between the water recorded by the users' water meters and the water discharged from the regulating reservoirs). The reasons for the poor performance of the networks are leaks, problems with flow measurement, and illegal connections [17].

Another problem is that, in many small municipalities, wastewater treatment services are not provided, so the urban water cycle service is incomplete. Around 90 treatment plants are pending construction and more than 90% of the existing ones do not meet discharge parameters, resulting in a multitude of sanctions [16]. In the assessment of data

from the Survey of Local Infrastructure and Facilities conducted by the Provincial Council of Granada, 21% of the population lives in municipalities where the infrastructure for urban water management is in a fair, poor, or very poor condition [17].

The following sections delve into the problems surrounding the management of urban water services in small municipalities in the province of Granada. The analysis is conducted from the perspective of stakeholders. The perspectives of public administration, policymakers, and the public allow us to identify the causes of service deficiencies and shortcomings and the complexity of the decision-making scenario. Addressing the deficiencies and shortcomings of water services requires an understanding of their root causes.

4. Results

4.1. The Lack of Resources from the Public Administration Responsible for Providing Urban Water Cycle Services

The responsibilities for water supply and sanitation are divided between two levels of the Spanish public administration: the municipality and the provincial council. This distribution is established in Law 7/1985, of 2 April [27], Regulating the Foundations of the Local Government. Municipalities are required to guarantee the provision of residential drinking water supply and sewerage services. They are also recognised as having jurisdiction over wastewater treatment.

Additionally, provincial councils have a duty to assist municipalities with fewer than 20,000 inhabitants in the provision of urban water cycle services. Law 7/1985 [27] establishes that provincial councils may assume direct provision of the service or coordinate the provision of shared management through consortia, associations of municipalities, or other arrangements. This support for municipal governments is also contemplated in Law 5/2010, of 11 June [28], concerning local autonomy in Andalusia.

Within this framework of the distribution of power, municipal governments and provincial councils face two major limitations in providing urban water cycle services: financial and human.

4.1.1. Financial Insufficiency

Domiciliary water services are activities with significant economies of scale, and these are represented by the high proportion of fixed costs in the cost structure. The smaller the population over which the fixed costs are distributed, the higher the cost associated with each user of the service [29]. Since we are referring to municipalities with small populations, the costs per user are very high. However, it is common practice for water bills in small municipalities not to pass on all the costs of the service to users. De facto, the municipality bears the deficit of not passing on all service costs to the user [30]. This is paid for from other municipal revenues, so citizens are financing part of the water services as taxpayers, not as users. This is one of the factors that may help explain why the price of water in Spain is significantly lower in small municipalities with direct management of the service compared to municipalities that outsource management, whether to private or public companies [31].

In the small municipalities of the province of Granada as a whole, the financial deficit for urban water cycle services is estimated at EUR 3 million per year [17]. This is partly due to the limited tax collection capacity in small rural municipalities, driven by the small number of users and the low average incomes associated with agricultural activity [32].

The Granada Provincial Council, based on Law 7/1985 [27], cooperates and financially assists in the provision of urban water cycle services through several concerted programmes that subsidise a portion of the supplies and repairs required after breakdowns in the ur-

ban water cycle and implements remote management and digitalisation systems [33]. In the 2024/25 biennial period, these programmes cost a total of EUR 2,098,000 and were distributed among 106 municipalities under direct management upon request. As a complement to the support given to operating the water services described, the Granada Provincial Council made the urban water cycle improvement programme available to municipalities under direct management, enabling them to carry out actions aimed at solving the main deficiencies, co-financing 70% of the investments. The annual amount allocated to this programme is EUR 1 million [34].

Despite the financial resources that the Diputación de Granada allocates to small municipalities under direct management, the aid is insufficient because no substantial improvement in the technical performance of the services is observed (see Table 2). In addition, an increase in funding can improve infrastructure but it does not necessarily imply an improvement in service. This occurs if infrastructure is not managed professionally, due to the limitations of technical staff in the municipalities, as explained below.

4.1.2. Limitations and Deficiencies in Human Capital

A second limitation of small municipalities is the lack of personnel, both in number and training levels [17]. In the small municipalities of the province of Granada, there is no professionalised department for this public service. There are usually only two members of staff: a multi-services officer for field work, such as repairing leaks in the water supply network or cleaning and removing waste from the wastewater treatment plant, and an administrative officer for accounting management. In addition to meeting the needs of the urban water cycle, the staff also performs tasks in other services. The field officer also performs maintenance on public lighting and other municipal facilities, such as the school, the municipal swimming pool, the cemetery, and the town hall itself. The administrative officer is also responsible for other administrative tasks specific to the municipality, e.g., customer services, completing grant applications, and updating the municipal register. Furthermore, no one is usually responsible for the technical and financial oversight of the service, hence the poor technical efficiency of the service despite the aid received from other administrations. The lack of human resources is so evident that, in many cases, the political leader himself has to fill in these gaps. It is not uncommon for the mayor to dedicate part of his time to monitoring the chlorine dosage in drinking water and reading residential meters. Furthermore, the lack of a qualified technical manager often leads to ineffective measures being proposed. A recurring example of this is the proposal to implement new water intakes in response to the apparent problem of water resource scarcity when the real problem is the poor technical performance of the network due to a high percentage of leaks and fraud.

The provincial council offers local authorities a catalogue of technical assistance for urban water cycle services. This includes carrying out technical diagnoses and proposing service improvement plans, technical maintenance work on the remote-control system and wastewater treatment plants, and even wastewater analysis [33]. However, despite having a specific service dedicated exclusively to the urban water cycle, the provincial council does not have the necessary personnel to meet the demands of the 106 municipalities under its direct management. Therefore, in addition to funding, more specialised personnel are also needed.

4.2. Ignorance and Distance of Higher Levels of Public Administration with the Problem of the Urban Water Cycle in Small and Medium-Sized Municipalities

In general, there is a certain disconnection throughout Spain between the upper levels of administration and the existing problems surrounding urban water cycle services in

small municipalities. This is largely the result of the distribution of power between the various water services. As previously noted, Spanish regulations explicitly state that urban water cycle services are the responsibility of municipal governments, which are assisted by the provincial council in municipalities with fewer than 20,000 inhabitants. That the provision of urban water cycle services is a local responsibility is also evident in the institutional and political vision [10].

Although the responsibilities for water supply and sanitation are assumed by local governments, there are two areas of action by state and regional governments that impact the provision of urban water cycle services: regulation and assistance for infrastructure financing.

4.2.1. Regulation

Urban water service managers face multiple regulatory pressures. Central and regional governments approve regulations concerning the use of water, which impacts urban water cycle services. The regulations are extensive. For example, at the state level, the Royal Legislative Decree 1/2001, of 20 July [35], approves the revised text of the Water Law and contains references to the local level, primarily related to upstream water permits and wastewater discharges. With an impact on the quality of services provided at the local level, the following stand out: the Royal Decree 3/2023, of 10 January [36], established the technical and health criteria for the quality of drinking water and its control and supply; and the Royal Decree 509/1996, of 15 March [37] establishing the standards applicable to the treatment of urban wastewater.

Small and medium-sized municipalities are under pressure from increasingly demanding regulatory developments that are not accompanied by the means to comply with the new responsibilities. An example is the new requirement of Royal Decree 3/2023 [36] to install a filtration system in groundwater intakes when the water has a turbidity value greater than 1 nephelometric unit. This will require the installation of new equipment in most municipalities whose water source is groundwater. In the case of Granada, this will affect 92% of municipalities; however, the regulation is not accompanied by an aid programme.

In essence, the new regulations, which impose greater demands on service quality and sustainability in water resource management, pose greater difficulties for small municipalities. They make the technical, knowledge, and financial limitations in small municipalities more evident.

4.2.2. Aid for Infrastructure Financing

Central and regional governments transfer funds to local governments, partly from the European Union budget. Within the framework of various action plans, these funds have been used to invest in the infrastructure necessary to provide urban water cycle services in small municipalities.

Some aid has not been managed efficiently, which is partly due to the disconnection between the bodies that decide on the implementation of infrastructure and the local situation to be addressed. Much of the funding released for the construction of water treatment and wastewater treatment plants has become a problem for small municipalities [11]. The central and regional governments anticipated the investment but the operating and maintenance costs that these small population centres would have to face were not taken into account. The result is that some municipalities have opted to under-utilise expensive water treatment and wastewater treatment plants because they lack the resources to finance the current costs of the activity. It would have been more appropriate to invest from the outset in cost-effective infrastructure tailored to the specific intervention area. There are various alternatives for water purification and wastewater treatment.

This is the case in several municipalities in the province of Granada (Órgiva, Ventas de Zafarraya, Zafarraya, etc.), where activated sludge wastewater treatment plants (WWTP) were built in the 1990s but the high energy costs associated with them led to their abandonment [38]. Years later, new treatment plants using biofilm system technology had to be built, and these are currently in operation (Figure 4).



Figure 4. Water treatment plants in Órgiva. (Own elaboration). Note: **Left**: Old Órgiva WWTP using activated sludge technology, built in the 1990s and abandoned due to high energy costs. **Right**: New Órgiva WWTP using a bacterial bed system, built in 2004 and currently in operation.

A current trend is the promotion of nature-based solutions that are more environmentally sustainable and, in some cases, associated with lower costs [39,40]. In Torre-Cardela, a water treatment plant using reverse osmosis technology was built. High energy costs made it economically unviable, which led to the consideration of a more cost-efficient technology with a lower environmental impact. The solution was a water treatment plant based on a biological method that employs aerobic granular technology for the removal of nitrates and other contaminants present in water intended for human consumption [41]. A particular case in the municipalities of the Alpujarra region of Granada is the preservation of the water channel system known as acequias de careo. It is an ancestral method of aquifer recharge using meltwater from the snowmelt of the Sierra Nevada [42,43]. Additionally, in some municipalities of the province, contaminants from wastewater are removed in artificial wetlands that replicate the biological processes of natural wetlands.

4.3. Difficult Decision Making at the Local Level

The management of urban water cycle services involves decision making that can generate conflicts between the local government team and the population. In small population centres, these situations can transcend the ideological, political, and economic spheres and become a personal matter. The greater proximity of family and neighbourhood ties can influence the decisions of the government team and will prevent unpopular decisions [42,44]. In line with Agency Theory, guided by political and neighbourhood motives, the local government (the agent) may make decisions that are not aligned with the primary social interest [45]. In the local environment, three sources of conflict can be detected.

4.3.1. Service Delegation

The complexity of urban water cycle management leads small municipalities to choose to operate through associations of municipalities or supra-municipal entities [46]. However, the transfer of service management is a decision that can generate controversy. In

small municipalities, the urban water cycle is one of the most important areas of local government activity. The transfer of this local policy transcends the interests of citizens, as it requires external agents to make decisions about service quality, water quality, or water prices. Therefore, it entails a loss of power in matters that affect fellow citizens. The most controversial situation is when the privatisation of service management is proposed, especially at times when there is a trend toward municipalisation [47]. This option often generates political conflict and, occasionally, citizen backlash [48,49]. As noted in Section 2, in the province of Granada, most small municipalities are not grouped into service areas but retain direct management. The reasons for this are diverse. In some cases, grouping does not occur because they are isolated due to topographical reasons. In other cases, the service is not privatised because the municipalities are of little interest to private companies. Typically, these municipalities have low economic viability due to their small population and poor infrastructure. In other cases, although they are municipalities that could join existing associations and consortiums, they resist transferring the service to a higher authority or privatising the service. Avoiding integration into larger service areas or privatisation means failing to take advantage of the benefits associated with economies of scale and the professionalisation of the service.

4.3.2. Updating the Water Price

A second decision that affects citizens is the price of water. In small municipalities, the price of water takes on more political importance than in large municipalities. Few services are provided, so fewer tax ordinances are debated in the city council plenary sessions. Furthermore, in deprived areas, a change in water prices can have a greater impact on household budgets, as this is a basic service for citizens. In short, updating water prices is an unpopular measure that can influence the behaviour of local politicians [32,50].

Regarding water prices, in the province of Granada, two differentiating factors are observed between direct and indirect management:

1. Prices are updated less frequently under direct management (Table 3). Three-quarters of the municipalities with direct management have rates that are five years old or more; only 15.19% of municipalities published their current rates in the last two years. However, two-thirds of the municipalities under indirect management have tariffs that are valid for less than two years.

Table 3. Years of validity of the fiscal ordinances for urban water cycle services in the province of Granada, 2024. (Prepared by the authors based on data from Granada Provincial Council [13]; Official Gazette of the Province [51]).

Years of Validity of the Rates	Direct Management		Indirect Management		Total Province	
	No	%	No	%	No	%
rates for less than 1 year	15	14.15%	45	66.18%	60	34.48%
rates for less than 2 years	1	0.94%	2	2.94%	3	1.72%
rates for less than 3 years	6	5.66%	1	1.47%	7	4.02%
rates for less than 4 years	0	0.00%	0	0.00%	0	0.00%
rates for less than 5 years	3	2.83%	0	0.00%	3	1.72%
rates for equal to or more than 5 years	81	76.42%	20	29.41%	101	58.05%
Total	106		68		174	

2. The average water price is lower under direct management (EUR 0.85/m^3) than with indirect management (EUR 1.96/m^3), see Table 4. The water bill is lower under direct

management for two reasons: sanitation and treatment costs are not passed on to the user and/or not all service costs are allocated.

Table 4. Average price of urban water service by type of management in the province of Granada in 2024. (Prepared by the authors based on data from the Granada Provincial Council [13]; Official Gazette of the Province [51]).

	Direct Management	Indirect Management	Total Municipalities Analyzed
Number of municipalities	40	60	100
Highest price (EUR/m^3)	1.71	2.59	2.59
Lowest price (EUR/m^3)	0.05	0.38	0.05
Average price (EUR/m^3)	0.85	1.96	1.51
% Municipalities without wastewater sanitation or purification rates	65.00%	1.67%	27.00%

Note: Estimated price for a family of three with an average daily consumption of 128 litres per person.

4.3.3. Fraud Management

Fraud detection measures can have a positive effect on the service's financial balance. Revenue increases for two reasons: (1) users pay for the service and (2) new users sign up. Furthermore, they encourage sustainable water use. Paying for the water consumed prevents waste. Although the measure may be well received by residents who responsibly pay their bills, it will generate negative reactions among defrauding residents, which may have a political cost [52,53].

The Granada Provincial Council promoted the pursuit of fraud between 2021 and 2023. To this end, it offered municipalities under direct management a subsidy covering 70% of the costs of the anti-fraud campaign. In three years, only 30 out of 106 municipalities requested this aid. It is likely that local governments did not opt for this measure because they wanted to avoid conflict with their fellow citizens.

4.4. The Tragedy of the Commons

The relationship between humans and water is complex. This is largely due to the occurrence of the tragedy of the commons [54]. This theory is applied in cases where there is a private exploitation of common goods. In the short term, individuals tend towards the over-exploitation of natural resources for their own benefit, even when they are aware of the long-term harm this will cause to the interests of the community and even their own interests.

In small rural municipalities, a conflict of interest arises among the citizens when the population, in addition to being residents of the municipality, carry out agricultural activities in the immediate surroundings. Paradoxically, this population living in the municipalities is sometimes responsible for the water supply problems of domestic users. This occurs when they act as agents, generating negative externalities on water sources such as primarily aquifers.

Groundwater is the main source of water supply for small towns in Spain. Seventy percent of the population living in cities with fewer than 20,000 inhabitants consumes water from aquifers [46]. The same is true in the province of Granada, where 70% of its municipalities are supplied exclusively by groundwater. Furthermore, another 22% of municipalities use groundwater along with surface water. Therefore, up to 92% of Granada's municipalities use groundwater for their urban water supply [26].

4.4.1. Water Demand for Agricultural Uses

Agriculture is by far the largest net consumer of water in Europe and, if practices do not change, demand for irrigated agriculture is likely to increase with climate change [55]. This situation also occurs in Spain and Granada, where approximately 80% of the distributed water is used for irrigation. In the province of Granada, 536,223 hectares are dedicated to cropland, of which just under 30% is irrigated [56].

Furthermore, although dryland can only be irrigated with rainwater, illegal groundwater extraction is widespread in Spain. In southern Spain, an increase in illegal wells has been identified in recent years [57,58]. In the province of Granada, there have been recent cases of illegal well closures [59,60], but it is difficult to estimate the volume of water extracted illegally. What is evident is the decline in water levels in the province of Granada, with 41% of its water bodies being in danger [61–63].

The over-exploitation of water resources due to agricultural activity, both through legal and illegal consumption, is jeopardising urban supplies in some towns. This is the case in Alamedilla, a municipality in Granada, where the proliferation of illegal wells means that the municipality cannot use its usual sources and is forced to extract water from other bodies of lower quality. In other cases, the same wells are still being used but the deeper water is causing energy consumption to increase. Additionally, the drop in groundwater levels has contributed to an increase in the concentration of pollutants deposited at the bottom, such as arsenic.

4.4.2. The Nitrate Pollution Problem

Another challenge is the water pollution caused by excess nutrients from agricultural runoff. The main problem associated with agriculture and livestock farming is diffuse pollution due to the use of fertilisers—which may contain, among other chemical compounds, nitrates, phosphates, and potassium—and pesticides—which may contain, among others, organophosphates and glyphosate [64–66]. The main problem in the province of Granada associated with the use of fertilisers is the infiltration of the fertilisers into the ground. This increases nitrate levels in the aquifers from which water is extracted to supply households. As a result, in addition to the environmental impact, water becomes unfit for human consumption or incurs high purification costs.

The existing technologies for removing nitrates have high implementation and operating costs, making them unfeasible in small municipalities [67]. Specifically, in the Montes Orientales area of the province of Granada, the groundwater has high nitrate levels that require the implementation of very expensive technologies to treat the water. Therefore, more cost-efficient technologies are being opted for. This is the case in Torre Cardela, where a pilot plant has been installed with an alternative nitrate removal system based on aerobic granular technology [68].

In addition to agricultural activity, there is the impact of livestock farming. Studies show that poor manure management practices and occasional discharges of slurry from pig farms lead to the bacteriological and nitrate contamination of groundwater [69,70]. This is the case in the northern part of the province of Granada, where large pig farms are proliferating.

5. Discussion and Political Implications

In Spain, there is a notable knowledge gap regarding the situation and challenges related to the management of urban water cycle services in small municipalities. The National Statistics Institute provides only aggregated data on water supply and sanitation at the national and regional levels. The Asociación Española de Abastecimientos de Agua y Saneamiento (Spanish Association for Water Supply and Sanitation) partially addresses

this gap by publishing the Estudio Nacional de suministro de agua potable y saneamiento every two years [71]. However, due to a low response rate, the association acknowledges the limited representativeness of the data published for municipalities with fewer than 20,000 inhabitants.

Research with a limited thematic and territorial focus enables a closer analysis of the challenges associated with water service management in small Spanish municipalities. For instance, González-Gómez et al. [72] identify population dispersion as a critical factor contributing to the high levels of non-revenue water observed in small and medium-sized municipalities in Andalusia. In another study by González-Gómez et al. [73], based on a sample of 80 rural water utilities in southern Spain, it was found that environmental variables help explain why operators with private sector participation are more efficient than public operators. This may be attributable to a selection bias, whereby private capital tends to engage in the management of services under more favourable conditions. Additionally, Picazo-Tadeo et al. [74] identify the presence of dispersion diseconomies and economies of scale in municipal water services based on a sample of water utilities in southern Spain. Overall, the findings indicate that small service areas are predisposed to lower performance, largely as a result of the scale-related and spatial inefficiencies inherent in the sector. Size influences the ability to obtain financial resources and, in turn, the achievement of economic and environmental objectives. In the international context, research consistently highlights the importance of demographic and territorial factors [75–80]. There are economies of scale and density, but they are not unlimited; moreover, there are dispersion diseconomies that constrain the configuration of optimal service areas.

The research focuses on small municipalities in the province of Granada. It confirms the existence of shortcomings in the management of water services in small population centres. More importantly, and adding value to the study, it provides an in-depth analysis of the underlying causes of poor performance. The shortcomings of the water service in small municipalities in the province of Granada are due to various causes. In summary, they result from a combination of insufficient financial resources and human capital, a lack of coordination between local needs and capacities and higher-level policies and regulations, difficulties and conflicts of interest in decision-making processes within a poorly defined regulatory and institutional framework, and behaviours contrary to the general interest. This section provides improvement proposals and political implications, as well as the main lines of action maintained by the working group of Diputación de Granada.

Table 5 lists the various problems identified in this research, along with a set of measures that have been classified according to the proposed areas of action in [81]. This proposal was developed based on the exchange of experiences within the GRAMAS Network and the information generated during the development of the Granada Provincial Council's General Programme for the Improvement of the Integrated Water Cycle. The information contained herein highlights the need to address a multi-dimensional problem from very different perspectives. Consequently, its resolution requires the design of comprehensive action plans.

Considering the fact that the case study of the province of Granada can be extrapolated to most of Spain [10,11], the information contained in Table 5 gives an idea of the significant challenge facing public administration in Spain in terms of improving the management of urban water cycle services in small municipalities under direct management. It is unrealistic to think of undertaking actions that would resolve these problems in a short period of time. An action plan for gradual implementation would need to be designed. Table 6 shows a time-specific breakdown of the measures that could be undertaken in each of the six areas of action shown in Table 5.

Table 5. Classification of urban water challenges by area of action. The case of the province of Granada. (Prepared by the authors).

Problems in Urban Water Cycle Management in Small Municipalities	Scope of Action in the Face of the Challenges of the Urban Water Cycle					
	Governance/Regulation	Availability of Resources	Infrastructure	Financing	Agents Involved	Innovation/Technological Research
Urban water service provision in the province of Granada: Low service quality in small municipalities						
Population atomisation and dispersion in small towns.	X					
Generalised lack of both technical and economic–financial data, which makes decision making difficult.	X					
Low hydraulic performance of networks	X		X	X	X	X
Lack of supply and treatment infrastructure	X		X	X		X
Lack of resources from the public administration responsible for providing urban water cycle services						
Financial insufficiency: Failure to comply with the cost–recovery principle. The cost of the service is financed by other taxes. Inefficient subsidies	X				X	
Limitations and deficiencies in human capital: Lack of a professionalised service for efficient management. Limited support from provincial councils.	X					
Lack of awareness and distance between higher levels of public administration and the problem of the urban water cycle in small and medium-sized municipalities						
Regulation: New regulations that impose greater demands, in terms of service quality and sustainability, pose greater financial and technical difficulties for small municipalities	X		X	X		
Aid for financing infrastructure: Lack of coordination between different administrations when planning and implementing infrastructure. State and regional governments implement infrastructure without taking into account maintenance and operating costs	X		X	X		
Difficult making at the local leves						
Managing urban water cycle services involves making decisions that can generate conflicts between the local government team and the population. Local politicians avoid making unpopular decisions	X				X	
Service delegation: The transfer of authority to another administration or the privatisation of the service generates citizen reaction, which influences local policy decisions.	X				X	
Water price updates: The frequency of updating water rates and the price of water is lower with the direct management of the service	X				X	
Fraud management: Although taking measures to prevent fraud in the service may be well received by residents who responsibly pay their bills, it will generate contrary reactions among defrauding residents. In many cases, it prevents the political decision from being made	X				X	
Conflict of interest. A clear example of the Tragedy of the Commons						
The demand for water for agricultural uses: The subscribers themselves are involved in sectors that over-exploit common water resources for water supplies.	X	X			X	
The problem of nitrate pollution: The subscribers themselves are involved in sectors that cause a loss of quality in the water resources used for water supplies.	X	X			X	

Table 6. Measures to improve urban water cycle services according to the proposed scope of action. (Prepared by the authors).

1. Resource Availability: Demand, Availability (Quantity and Quality), and Accessibility
- Conduct an assessment of the regulations to identify areas where they are ineffective. - Provide administrations with more resources to establish an efficient monitoring and control system for the inappropriate use of water resources with the following objectives: controlling diffuse pollution and preventing illegal water withdrawals. To this end, digitalisation emerges as an indispensable tool. - Promote the diversification of water resources and resource recovery initiatives through wastewater regeneration. - Promote nature-based solutions. - Urban water cycle services themselves can contribute to these objectives by improving technical performance and properly treating urban wastewater before discharge.
2. Infrastructure
- Encourage the grouping of small municipalities to address the need for infrastructure with greater economies of scale. - Promote the professionalisation of services, with the aim of maintaining infrastructure improvements and extending their useful life. - Plan more efficient infrastructure adapted to specific local circumstances. - Promote the development of infrastructure master plans independent of the political times to ensure their implementation. - Ensure financing to address infrastructure renewal needs through tariffs that include amortisation costs and the efficient use of aid granted by higher administrations.
3. Financing
- Encourage the grouping of small municipalities to achieve viable economic dimensions. - Promote professionalisation to ensure services more efficiently manage all available funding: revenues via tariffs and subsidies. - Establish uniform criteria for both the cost structure and tariff calculations and monitor their application, with the goal of achieving economic sustainability for the service. - Create specific conditional solidarity funds for small and medium-sized municipalities where users' financial capacity sets a tariff ceiling that makes cost recovery impossible. Small municipalities must demonstrate that they are doing everything possible to manage the service efficiently (complete transparency of economic and technical indicators and justifying not needing to belong to a supra-municipal service area). - Create state-level funding lines for small and medium-sized municipalities to address the needs for renovation or construction of new infrastructure resulting from new regulatory requirements.
4. Agents Involved: Participation and Attitudes of Stakeholders
- Promote management through supra-municipal entities to decouple local politics from decision making. - Promote transparency and access to information. On the one hand, this will achieve improved service through the comparison effect; on the other hand, it will raise user awareness about the efficient use of resources and the true cost of service provision, increasing their willingness to pay more for these services. - Promote co-responsibility in urban water cycle management through participatory mechanisms, accountability, and urban–rural partnerships. - Encourage citizens to participate in establishing the optimal service level, since the price of the service will depend on this level. - Ensure that the relationship between public administrations and private operators is governed by specifications that include all the duties and rights that the owner transfers to the manager, as well as the instruments for monitoring their compliance.
5. Technological Innovation/Research
- Promote research into the appropriate technologies to comply with regulatory developments and achieve high efficiency, compensating for the limited economies of scale in small towns. - Ensure the efficient management of current and new technologies by promoting professionalised supra-municipal organisational structures that contribute to increasing economies of scale and the qualifications of professionals. - Promote training programmes to increase the availability of trained and competent professionals in new technologies in rural areas. - Expand the digitalisation of infrastructure in the rural areas of small municipalities to improve the efficiency of fragmented infrastructure.

Table 6. *Cont.*

6. Governance/Regulation
- Adapt the jurisdictional regime so that municipalities that do not meet quality standards are integrated into professionalised supra-municipal organisational structures. Local entities at the provincial or supra-municipal level, such as associations of municipalities (Mancomunidades) and provincial councils (Diputaciones), or even existing consortiums can be leveraged. Of all of them, the provincial councils appear to be the most prepared for this task, as they are mandated to provide technical support to small municipalities by law. - Design a set of easy-to-calculate and understand indicators that allow for objectively determining the standard to be achieved, both from a service quality and economic perspective. - Ensure transparency and citizen access to information on urban water cycle services. This information will be understandable and readily available to citizens. - Promote citizen participation in a regulated environment, especially in choosing the type of service they require, as this will influence pricing. - Establish the obligation to maintain segregated accounting at the municipal level for urban water cycle services to promote management efficiency and transparency. Uniform rules must be established to allow for comparison between services - Regulate the pricing characteristics of urban water services with the aim of recovering costs and incentivising savings and efficiency. - Create permanent cooperation forums between the various administrations in which the representation of small municipalities is ensured. These forums should comprise political leaders (decision-making sphere), technical and administrative staff (expert support), and social stakeholders (participatory sphere). - Create the regulatory body as an independent public body charged with enforcing the politically, legally, or contractually established standards and supervising the services.

In general, during the meetings held within the GRAMAS Network, different approaches to addressing the problem were noted. Municipalities maintain a position of greater demands for funding from other administrations to address infrastructure investment and the high operating costs of the service. The priority of local governments is to ensure the supply of drinking water to citizens, given the challenges of transparency, technical and economic efficiency, and environmental sustainability. A short-term and almost one-dimensional vision prevails. The objective is to meet citizens' demand for water delivery to their homes to satisfy basic needs.

In contrast to the more short-term vision of municipal politicians, the provincial council and the University of Granada are more concerned about making structural and far-reaching decisions. While acknowledging the complexity of the problem, they emphasise that the set of actions in the area of governance is a key element, as it is linked to all of the problems identified (Tables 5 and 6). This perspective aligns with [82], which concludes that in the city of Seville—as in Granada, also located in Andalusia—there is a need to improve the governance of water resource management. In fact, effective water governance is key to Integrated Water Resources Management [4,5]. In this context, two preferred lines of action are identified due to their expected positive impacts on the overall problems identified. However, these actions transcend the local level.

In a country with such a dispersed population, a study of optimal service areas should be a priority. This study should be a preliminary step to promoting municipal associations and delegating service delivery to supra-municipal entities. This would allow for the sector's economies of scale to be leveraged, local politics to be decoupled from decision making, and the technical and economic management of the service to be professionalised. Other actions would likely be resolved or complemented by this primary action. Furthermore, undertaking other types of actions without establishing optimal service areas are likely to result in inefficient solutions. Although there are supra-municipal service area initiatives in Spain, they are not the result of a nationally planned strategy, as has been implemented in other countries. In Italy, the reform of Law No. 36 of 5 January 1994 [83] introduced the municipal reorganisation into Optimal Territorial Areas (Ambiti

Territoriali Ottimali [ATO]) [84]. Subsequent legislative reforms aimed to, among other objectives, rationalise and increase the efficiency of the ATOs [85–87]. Currently, there are 62 ATOs, and local authorities are mandated to delegate the management of water services to the operator assigned to each ATO. In Portugal, the creation of optimal service management areas for urban water was state-led and progressively implemented over time. Initially, Decree-Law No. 379/93 [88] played a decisive role by establishing the legal framework for the creation of multi-municipal companies by private law to operate water supply and sanitation systems across multiple municipalities, as well as for the establishment of Águas de Portugal (AdP), which was responsible for designing optimal service areas. In the Portuguese case, municipalities voluntarily join the multi-municipal systems created for each service area. Despite the improvements brought about by the creation of optimal service areas, the significant challenge of financing water supply and sanitation services persists in both Portugal [89] and Italy [90].

In Spain, certain cases of inter-municipal cooperation emerge from opportunistic circumstances, such as when small municipalities are integrated into larger neighbouring municipalities or metropolitan areas with shared boundaries. In other instances, such cooperation stems from locally initiated efforts—at either the municipal or provincial level—facilitated by specific political alignments, such as when the involved local governments are governed by the same political party. Regardless of the existing cases of municipal aggregation, as long as the decision remains in the hands of local politicians, many municipalities will remain resistant to delegating management to a supra-municipal body. There are issues at the local level related to the creation of optimal service areas that are difficult to resolve and may become sources of conflict. Local municipalities express reluctance towards sharing service management with neighbouring municipalities, citing concerns over the loss of control of such an important local service. Additional concerns include the decision to set a uniform price or different prices for each municipality within the same service area, as well as the possibility of privatising service management. Moreover, questions remain regarding whether the way in which many municipal aggregations are being implemented in Spain is resulting in optimal service areas. It should be noted that such aggregation processes entail a trade-off between economies of scale and dispersion diseconomies.

At the same time, it is recommended to create an independent regulatory body. Among other functions, the regulatory body could design a system of incentives and penalties to improve the technical and economic efficiency. The body would be responsible for setting performance targets according to the initial situation of each service area. Management decisions would be linked to these targets and not to local political interests. One element that could be considered is to condition aid and subsidies for infrastructure investment on meeting the objectives proposed in each service area. The absence of effective mechanisms for controlling the local management of municipal water services means that city councils lack incentives to improve the technical and economic efficiency of the service. Once the service areas resulting from the first proposed measure have been established, the independent regulator would promote management efficiency. An alternative measure would be the establishment of a water observatory; however, its impact would remain limited in scope. Observatories primarily contribute to greater transparency in the sector through the dissemination of data on service management, pricing structures, and service quality. In Spain, such initiatives are spatially constrained. At the regional level, only the Water Price Observatory in Catalonia exists. At the local level, a few smaller-scale initiatives exist, such as the Water Observatory of Emasesa (Metropolitan Water Supply and Sanitation Company of Seville) and the Water Observatory of Terrassa. In these cases,

beyond improving transparency, citizen participation in debates and decision-making processes related to water services is also promoted [91].

Over time, regulatory bodies for urban water services, with varying scopes of authority and competencies, have been established in EU countries [92]: in Bulgaria (Energy and Water Regulatory Commission [EWRC]), Chipre (Water Regulatory Council [WRC]), Croatia (Croatian Regulatory Authority for Network Industries [HAKOM]), Denmark (Danish Water Regulatory Authority, integrated into Danish Competition and Consumer Authority), Slovakia (The Regulatory Office for Network Industries [URSO]), Estonia (Estonian Competition Authority [ECA]), Greece (General Secretariat of Natural Environment and Water [HEA]), Hungary (Hungarian Energy and Public Utility Regulatory Authority [HEA]), Ireland (Commission for Regulation of Utilities [CRU]), Italy (Regulatory Authority for Energy, Networks and Environment [ARERA]), Latvia (Public Utilities Commission [PUC]), Lithuania (The National Energy Regulatory Council [VERT]), Malta (Regulator for Energy and Water Services [REWS]), Poland (Polish Waters [WP]), Portugal (The Water and Waste Services Regulation Authority [ERSAR]), and Romania (National Regulatory Authority for Community Services of Public Utilities [ANRSC]). In Germany, Austria, Belgium, Slovenia, Finland, France, Luxembourg, the Netherlands, the Czech Republic, and Sweden there is no national regulator. Instead, observatories have been established at the national or regional level. For example, in France, there is the Observatoire National des Services d'eau et Assainissement, which compares the performance of urban operators using the following indicators: price, drinking water quality, network leakage losses, asset management, network renewal, financial management, and service quality.

Spain is the exception. It is the only country without an independent regulator or a national or regional water observatory. The Spanish Association of Water Supply and Sanitation, the leading industry association in the urban water sector—with over 300 members providing urban water cycle services to 80% of the Spanish population—has repeatedly advocated for the creation of a regulatory body. [93]. However, the Spanish government has not taken this step. The excessive decentralisation of water-related responsibilities across various levels of administration, the difficulty of reaching political agreements, and the high fragmentation of service areas, management models, and service characteristics are among the factors that help explain the challenges in establishing a regulatory authority.

There is a key issue with these two priority measures, as well as with others listed in Table 6. The initiative does not fall to the local government, i.e., to the city councils and provincial councils. The initiative for action falls to the Spanish Government.

6. Conclusions and Recommendations

In Spain, there are two very different realities regarding urban water cycle services. While the most populous service areas have sufficient resources to provide quality service, there are shortcomings in small municipalities where direct service management predominates. Currently, sectoral policies focus on promoting digitalisation, decarbonisation, and sustainability. There will likely be greater opportunities to advance these policies in more populous service areas, which will ultimately widen the gap in the provision of urban water cycle services. Without abandoning these lines of action, greater efforts must be made to address the structural problems in small municipalities.

This article analyses the causes of the problems surrounding urban water cycle service management in small municipalities. The study area is the province of Granada, a representative example of the existing situation throughout Spain. An initial conclusion is that the problems surrounding urban water cycle management in small municipalities are broad

and complex. Consequently, a first recommendation is to implement action programs that include a broad set of measures.

The research has identified various causes of deficiencies in the management of urban water cycle services. Generally speaking, and as a second conclusion, it is noted that these structural causes stem from a governance deficit. Therefore, as a second recommendation, it is necessary to conduct a comprehensive review of the regulatory and institutional framework regarding the management of urban water services. Until this important issue is addressed, many of the problems identified in service management in small municipalities cannot be resolved.

A third conclusion is the existence of a certain disconnection and lack of sensitivity on the part of the central administration regarding the situation of water services in small municipalities. Within the four-tier structure of Spanish public administration—central, regional, provincial, and municipal—the central government has delegated powers and responsibilities to city councils and provincial councils. Although this decentralisation of powers is consistent with the application of the European Union's principle of subsidiarity, it is not incompatible with greater involvement and sensitivity from central and regional governments. In this regard, decisive involvement by the central and regional governments is recommended for leading an action plan to foster a change in the regulatory and institutional context that addresses the current governance deficits. In fact, without greater involvement from central and regional governments in this regard, it will be difficult to correct the structural deficiencies and shortcomings detected in urban water cycle services in small municipalities.

In the current context of climate change—characterised by a trend toward lower and more irregular precipitation, as well as rising average temperatures—improvements in water resource management have become increasingly urgent to support adaptation to more adverse conditions. Consequently, within the urban water cycle, changes in the regulatory framework are guiding stakeholders in the polycentric water governance model in this direction. Notable examples include the recent Directive (EU) 2024/3019 of the European Parliament and of the Council of 27 November 2024 on urban wastewater treatment, which requires wastewater treatment in urban areas with more than 1000 inhabitants in all Member States [94], and Directive (EU) 2020/2184 of the European Parliament and of the Council of 16 December 2020 on the quality of water intended for human consumption, which raises water quality standards and sets out guidelines for the improved monitoring and efficiency of distribution networks [8]. In the coming years, it will be possible to assess whether adaptation to environmental conditions occurs at different speeds depending on the population size of service areas and therefore whether the gap between urban and rural areas in terms of urban water cycle services is narrowing or widening.

Author Contributions: Conceptualisation, F.J.G.-M., F.O. and F.G.-G.; methodology, F.J.G.-M.; investigation, F.J.G.-M., F.O. and F.G.-G.; resources, F.J.G.-M.; writing—original draft preparation, F.J.G.-M., F.O. and F.G.-G.; writing—review and editing, F.J.G.-M., F.O. and F.G.-G.; supervision, F.O. and F.G.-G.; project administration, F.J.G.-M.; funding acquisition, F.O. and F.G.-G. All authors have read and agreed to the published version of the manuscript.

Funding: This research is part of the project TED2021-132494B-I00, funded by MCIN/AEI/10.13039/-501100011033 ERDF/EU, and the project PID2022-136235NB-I00, funded by MICIU/AEI/10.13039/-501100011033 and by ERDF/EU.

Data Availability Statement: Data is contained within the article.

Acknowledgments: Thanks to the Granada Provincial Council, which provided the data within the framework of the general protocol for actions between the Granada University and the Granada Provincial Council to promote territory–university linkage actions.

Conflicts of Interest: The authors declare no conflicts of interest.

References

1. Brennan, M.; Rondon-Sulbaran, J.; Sabogal-Paz, L.P.; Fernandez-Ibañez, P.; Galdos-Balzategui, A. Conceptualising global water challenges: A transdisciplinary approach for understanding different discourses in sustainable development. *J. Environ. Manag.* **2021**, *298*, 113361. [CrossRef] [PubMed]
2. United Nations. *Transforming Our World: The 2030 Agenda for Sustainable Development. United Nations General Assembly, Resolution A/RES/70/1*; United Nations General Assembly: New York, NY, USA, 2015. Available online: https://undocs.org/en/A/RES/70/1 (accessed on 5 June 2025).
3. United Nations. *The United Nations World Water Development Report 2023: Partnerships and Cooperation for Water*; UNESCO: Paris, France, 2023. Available online: https://unesdoc.unesco.org/ark:/48223/pf0000384655 (accessed on 5 June 2025).
4. Grison, C.; Koop, S.; Eisenreich, S.; Hofman, J.; Chang, I.S.; Wu, J.; Savic, D.; Van Leeuwen, K. Integrated water resources management in cities in the world: Global challenges. *Water Resour. Manag.* **2023**, *37*, 2787–2803. [CrossRef]
5. Koop, S.H.; Grison, C.; Eisenreich, S.J.; Hofman, J.; van Leeuwen, K. Integrated water resources management in cities in the world: Global solutions. Sustain. *Cities Soc.* **2022**, *86*, 104137. [CrossRef]
6. WHO and UNICEF. Monitoring Programme for Water Supply, Sanitation and Hygiene (JMP) 2024. Available online: https://washdata.org/reports/jmp-2024-country-consultation-wash-households (accessed on 5 June 2025).
7. United Nations. Leaving No One Behind. The United Nations World Water Development Report. UN Water, 2019. Available online: https://www.unwater.org/publications/un-world-water-development-report-2019 (accessed on 5 June 2025).
8. EU. Directive (EU) 2020/2184 of the European Parliament and of the Council of 16 December 2020 on the Quality of Water Intended for Human Consumption (Recast) (Text with EEA Relevance). 2020. Available online: https://eur-lex.europa.eu/legal-content/EN/TXT/PDF/?uri=CELEX:32020L2184 (accessed on 5 June 2025).
9. INE (Instituto Nacional de Estadística). *Censo Anual de Población 2021–2023*; INE: Madrid, Spain, 2024.
10. Ministerio para la Transición Ecológica y el Reto Demográfico. *Libro Verde de la Gobernanza del Agua en España*; Ministerio para la Transición Ecológica y el Reto Demográfico: Madrid, Spain, 2020. Available online: https://www.miteco.gob.es/content/dam/miteco/es/agua/temas/sistema-espaniol-gestion-agua/libro-verde-gobernanza/libro-verde-gobernanza-agua_tcm30-517206.pdf (accessed on 5 June 2025).
11. García-Rubio, M.A.; González-Gómez, F. *Informe Sobre el Ciclo Integral del Agua en Pequeños y Medianos Municipios*; Ministerio para la Transición Ecológica y el Reto Demográfico, Gobierno de España: Madrid, Spain, 2020. Available online: https://www.miteco.gob.es/content/dam/miteco/es/agua/temas/sistema-espaniol-gestion-agua/libro-verde-gobernanza/informes-tematicos/11-informe-tematico-ciclo-integral-pequenos-municipios_tcm30-517277.pdf (accessed on 5 June 2025).
12. Diputación Provincial de Granada. *Estudio Técnico Operativo de Explotación del Ciclo Urbano del Agua en Varios Municipios de la Provincia de Granada*; Diputación Provincial de Granada: Granada, Spain, 2013.
13. Diputación de Granada. *Encuesta de Tarifas de Agua*; Diputación de Granada: Granada, Spain, 2019.
14. Diputación de Granada. *Proyecto ADAPTA Gramada: Plan Provincial de Adaptación al Cambio Climático de Granada. Resumen Ejecutivo*; Diputación de Granada: Granada, Spain, 2019. Available online: https://www.dipgra.es/export/sites/diputaciongranada/servicios/areas/agua-promocion-agraria-y-medio-ambiente/.galleries/AREAS-Medio-Ambiente-Educacion-Ambiental-Documentos/AREAS-Medio-Ambiente-Educacion-Ambiental-Plan-de-adaptacion-al-cambio-climatico-00001/Resumen-ejecutivo-ppaccgr-adapta-granada.pdf (accessed on 5 June 2025).
15. Diputación de Granada. *Informe Sobre la Situación de la Depuración en la Provincia de Granada*; Diputación de Granada: Granada, Spain, 2019.
16. Diputación de Granada. *Análisis de los Datos del Ciclo Urbano del Agua en la Encuesta de Infraestructuras y Equipamientos Locales de la Provincia de Granada*; Diputación de Granada: Granada, Spain, 2020.
17. Diputación de Granada. *Proyecto de Adaptación al Cambio Climático de los Servicios de Agua Potable en el Marco del Plan de Recuperación, Transformación y Resiliencia*; Diputación de Granada: Granada, Spain, 2020.
18. Diputación de Granada. *Memoria del Programa General de Mejora del Ciclo Integral del Agua*; Diputación de Granada: Granada, Spain, 2022.
19. Caplan, K.; Harvey, E. *Small Town Water and Sanitation Delivery: Taking a Wider View*; WaterAid: London, UK, 2010; Available online: https://www.ircwash.org/sites/default/files/Caplan-2010-Small.pdf (accessed on 5 June 2025).

20. Humphreys, E.; van der Kerk, A.; Fonseca, C. Public finance for water infrastructure development and its practical challenges for small towns. *Water Policy* **2018**, *20*, 100–111. [CrossRef]
21. Ministerio de Agricultura, Pesca y Alimentación. *Demografía de la Población Rural en 2020*; AgrInfo nº 31: Madrid, Spain, 2021. Available online: https://www.mapa.gob.es/es/ministerio/servicios/analisis-y-prospectiva/ayp_demografiaenlapoblacionrural2020_tcm30-583987.pdf (accessed on 5 June 2025).
22. González-Gómez, F.; Picazo-Tadeo, A.J.; Guardiola, J. Why do local governments privatize the provision of water services? Empirical evidence from Spain. *Public Adm.* **2011**, *89*, 471–492. [CrossRef]
23. Albalate, D.; Bel, G.; González-Gómez, F.; Picazo-Tadeo, A.J. Contract renewal in urban water services, incumbent advantage, and market concentration. *Public Adm. Rev.* **2022**, *82*, 314–324. [CrossRef]
24. Ferro, G.; Lentini, E.J.; Mercadier, A.C. Economies of scale in the water sector: A survey of the empirical literature. *J. Water Sanit. Hyg. Dev.* **2011**, *1*, 179–193. [CrossRef]
25. Gómez-Reino, J.L.; Lago-Peñas, S.; Martinez-Vazquez, J. Evidence on economies of scale in local public service provision: A meta-analysis. *J. Reg. Sci.* **2023**, *63*, 793–819. [CrossRef]
26. Peinado, T.; Fernández, M.; García-Martínez, F.J.; Jiménez, J.; González, M. El Uso de las Aguas Subterráneas para Abastecimiento Urbano: Estado de la Provincia de Granada. XI Simposio del Agua en Andalucía. Granada, Spain. Available online: https://digital.csic.es/handle/10261/358363 (accessed on 5 June 2025).
27. *Ley 7/1985, de 2 de Abril, Reguladora de las Bases del Régimen Local*; Jefatura del Estado: Madrid, Spain, 1985.
28. *Ley 5/2010, de 11 de Junio, de Autonomía Local de Andalucía*; Comunidad Autónoma de Andalucía: Seville, Spain, 2010.
29. Ndaw, M.F. *Private Sector Provision of Water Supply and Sanitation Services in Rural Areas and Small Towns. The Role of the Public Sector*; Water and Sanitation Program: Guidance Note; World Bank Group: Washington, DC, USA, 2016; Available online: https://documents1.worldbank.org/curated/en/450101468179030315/pdf/104505-WPS-Box394877B-PUBLIC-Add-series-WSP.pdf (accessed on 5 June 2025).
30. García-Rubio, M.A.; Ruiz-Villaverde, A.; González-Gómez, F. Urban water tariffs in Spain: What needs to be done? *Water* **2015**, *7*, 1456–1479. [CrossRef]
31. García-Valiñas, M.Á.; González-Gómez, F.; Picazo-Tadeo, A.J. Is the price of water for residential use related to provider ownership? Empirical evidence from Spain. *Util. Policy* **2013**, *24*, 59–69. [CrossRef]
32. Alguacil-Duarte, F.; González-Gómez, F.; del Saz-Salazar, S. Urban water pricing and private interests' lobbying in small rural communities. *Water* **2020**, *12*, 3509. [CrossRef]
33. Diputación de Granada. *Libro Digital de la Concertación Local 2024/2025*; Diputación de Granada: Granada, Spain, 2024.
34. Diputación de Granada. *Mejora de Infraestructuras del Ciclo Integral de Agua de Uso Urbano*; Diputación de Granada: Granada, Spain, 2024.
35. *Real Decreto Legislativo 1/2001, de 20 de Julio, por el que se Aprueba el Texto Refundido de la Ley de Aguas*; Ministerio de Medio Ambiente: Madrid, Spain, 2001.
36. *Real Decreto 3/2023, de 10 de Enero, por el que se Establecen los Criterios Técnico-Sanitarios de la Calidad del Agua de Consumo, su Control y Suministro*; Ministerio de la Presidencia, Relaciones con las Cortes y Memoria Democrática: Madrid, Spain, 2023.
37. *Real Decreto 509/1996, de 15 de Marzo, de Desarrollo del Real Decreto-ley 11/1995, de 28 de Diciembre, por el que se Establecen las Normas Aplicables al Tratamiento de las Aguas Residuales Urbanas*; Ministerio de Obras Públicas, Transportes y Medio Ambiente: Madrid, Spain, 1996.
38. Diputación de Granada. *Jornada Sobre Nuevas Competencias y Obligaciones de las Entidades Locales en la Gestión y Explotación de Infraestructuras de Saneamiento y Depuración*; Diputación de Granada: Granada, Spain, 2024.
39. Krauze, K.; Wagner, I. From classical water-ecosystem theories to nature-based solutions—Contextualizing nature-based solutions for sustainable city. *Sci. Total Environ.* **2019**, *655*, 697–706. [CrossRef] [PubMed]
40. Oral, H.V.; Carvalho, P.; Gajewska, M.; Ursino, N.; Masi, F.; Hullebusch, E.D.V.; Kazak, J.K.; Exposito, A.; Cipolletta, G.; Andersen, T.R.; et al. A review of nature-based solutions for urban water management in European circular cities: A critical assessment based on case studies and literature. *Blue-Green Syst.* **2020**, *2*, 112–136. [CrossRef]
41. Alguacil-Duarte, F.; González-Gómez, F.; Romero-Gámez, M. Biological nitrate removal from a drinking water supply with an aerobic granular sludge technology: An environmental and economic assessment. *J. Clean. Prod.* **2022**, *367*, 133059. [CrossRef]
42. Jódar, J.; Zakaluk, T.; González-Ramón, A.; Ruiz-Constán, A.; Lechado, C.M.; Martín-Civantos, J.M.; Custodio, E.; Urrutia, J.; Herrera, C.; Lambán, L.J.; et al. Artificial recharge by means of careo channels versus natural aquifer recharge in a semi-arid, high-mountain watershed (Sierra Nevada, Spain). *Sci. Total Environ.* **2022**, *825*, 153937. [CrossRef]
43. Zakaluk, T.; Jódar, J.; González-Ramón, A.; Civantos, J.M.; Lambán, L.J.; Martos-Rosillo, S. Ancestral managed aquifer recharge systems and their impacts on the flow regime of a semi-arid alpine basin (Sierra Nevada, Spain). *J. Hydrol. Reg. Stud.* **2024**, *54*, 101870. [CrossRef]

44. Klien, M. The political side of public utilities: How opportunistic behaviour and yardstick competition shape water prices in Austria. *Pap. Reg. Sci.* **2015**, *94*, 869–891. [CrossRef]
45. Smith, E.; Umans, T.; Thomasson, A. Stages of PPP and principal–Agent conflicts: The Swedish water and sewerage sector. *Public Perform. Manag. Rev.* **2018**, *41*, 100–129. [CrossRef]
46. De Stefano, L.; Fornés, J.M.; López-Geta, J.A.; Villarroya, F. Groundwater use in Spain: An overview in light of the EU water framework directive. *Int. J. Water Resour. Dev.* **2015**, *31*, 640–656. [CrossRef]
47. McDonald, D.A. Landscapes of remunicipalization: A critical literature review. *Urban Aff. Rev.* **2024**, *60*, 1898–1930. [CrossRef]
48. Akchurin, M. Contested Infrastructures: Water, Privatization, and Place-Based Protest in Greater Buenos Aires. *City Community* **2023**, *22*, 171–194. [CrossRef]
49. Berge, J.V.D.; Scheunpflug, L.; Vos, J.; Boelens, R. Social movements in defense of public water services: The case of Spain. *Front. Water* **2023**, *5*, 1200440. [CrossRef]
50. Picazo-Tadeo, A.J.; González-Gómez, F.; Suárez-Varela, M. Electoral opportunism and water pricing with incomplete transfer of control rights. *Local Gov. Stud.* **2020**, *46*, 1015–1038. [CrossRef]
51. Diputación de Granada. *Boletín Oficial de la Provincia de Granada 2024*; Diputación de Granada: Granada, Spain, 2024.
52. González-Gómez, F.; García-Rubio, M.A.; Guardiola, J. Why is non-revenue water so high in so many cities? *Int. J. Water Resour. Dev.* **2011**, *27*, 345–360. [CrossRef]
53. Farouk, A.M.; Rahman, R.A.; Romali, N.S. Non-revenue water reduction strategies: A systematic review. *Smart Sustain. Built Environ.* **2023**, *12*, 181–199. [CrossRef]
54. Hardin, G. The tragedy of the commons: The population problem has no technical solution; it requires a fundamental extension in morality. *Science* **1968**, *162*, 1243–1248. [CrossRef]
55. European Environment Agency. Pesticides in Rivers, Lakes and Groundwater in Europe. 2024. Available online: https://www.eea.europa.eu/en/analysis/indicators/pesticides-in-rivers-lakes-and (accessed on 5 June 2025).
56. Gobierno de España. *Encuesta Sobre Superficies y Rendimientos de Cultivos. Año 2023*; Ministerio de Agricultura, Pesca y Alimentación: Madrid, Spain, 2024. Available online: https://www.mapa.gob.es/es/estadistica/temas/estadisticas-agrarias/boletin20231_tcm30-690544.pdf (accessed on 5 June 2025).
57. Rupérez-Moreno, C.; Senent-Aparicio, J.; Martinez-Vicente, D.; García-Aróstegui, J.L.; Calvo-Rubio, F.C.; Pérez-Sánchez, J. Sustainability of irrigated agriculture with overexploited aquifers: The case of Segura basin (SE, Spain). *Agric. Water Manag.* **2017**, *182*, 67–76. [CrossRef]
58. Martínez-Santos, P.; Castaño-Castaño, S.; Hernández-Espriú, A. Revisiting groundwater overdraft based on the experience of the Mancha Occidental Aquifer, Spain. *Hydrogeol. J.* **2018**, *26*, 1083–1097. [CrossRef]
59. Confederación Hidrográfica del Gudalquivir. *La CHG Cierra el Tercer Pozo de los 15 Denunciados en la Comarca de Baza (Granada) por Captación Ilegal de Aguas*; Confederación Hidrográfica del Gudalquivir: Seville, Spain, 2023. Available online: https://www.chguadalquivir.es/-/la-chg-cierra-el-tercer-pozo-de-los-15-denunciados-en-la-comarca-de-baza-granada-por-captacion-ilegal-de-aguas (accessed on 5 June 2025).
60. Confederación Hidrográfica del Gudalquivir. *La CHG Precinta 10 Pozos en los TT.MM. de Huelma (Jaén) y Alamedilla (Granada) por Presunta Captación Ilegal de Aguas*; Confederación Hidrográfica del Gudalquivir: Seville, Spain, 2023. Available online: https://www.chguadalquivir.es/-/la-chg-precinta-10-pozos-en-los-tt-mm-de-huelma-jaen-y-alamedilla-granada-por-presunta-captacion-ilegal-de-aguas (accessed on 5 June 2025).
61. Ministerio para la Transición Ecológica y el Reto Demográfico. *Plan Hidrológico de la Demarcación Hidrográfica del Guadalquivir*; Tercer Ciclo: 2022–2027; Ministerio para la Transición Ecológica y el Reto Demográfico: Seville, Spain, 2023.
62. Ministerio para la Transición Ecológica y el Reto Demográfico. *Datos Espaciales de la Confederación Hidrográfica del Guadalquivir*; Ministerio para la Transición Ecológica y el Reto Demográfico: Madrid, Spain, 2024. Available online: https://idechg.chguadalquivir.es/nodo/index.html (accessed on 13 December 2024).
63. Ministerio para la Transición Ecológica y el Reto Demográfico. *Redes de Control de la Confederación Hidrográfica del Guadalquivir*; Ministerio para la Transición Ecológica y el Reto Demográfico: Madrid, Spain, 2024. Available online: https://idechg.chguadalquivir.es/nodo/Redes/index.html (accessed on 8 December 2024).
64. Akhtar, N.; Syakir Ishak, M.I.; Bhawani, S.A.; Umar, K. Various natural and anthropogenic factors responsible for water quality degradation: A review. *Water* **2021**, *13*, 2660. [CrossRef]
65. Abascal, E.; Gómez-Coma, L.; Ortiz, I.; Ortiz, A. Global diagnosis of nitrate pollution in groundwater and review of removal technologies. *Sci. Total Environ.* **2022**, *810*, 152233. [CrossRef]
66. European Environment Agency. Nitrate in Groundwater. 2024. Available online: https://www.eea.europa.eu/en/analysis/indicators/nitrate-in-groundwater-8th-eap (accessed on 5 June 2025).

67. Munoz-Palazon, B.; Rodriguez-Sanchez, A.; Gonzalez-Lopez, J.; Rosa-Masegosa, A.; Gorras, S.; Vilchez-Varga, R.; Link, A.; Gonzalez-Martinez, A. Granular biomass technology for providing drinking water: Microbial versatility and nitrate performance in response to carbon source. *Appl. Water Sci.* **2023**, *13*, 165. [CrossRef]
68. Hurtado-Martinez, M.; Muñoz -Palazon, B.; Robles-Arenas, V.; Gonzalez-Martinez, A.; Gonzalez-Lopez, J. Biological nitrate removal from groundwater by an aerobic granular technology to supply drinking water at pilot-scale. *J. Water Process Eng.* **2021**, *40*, 101786. [CrossRef]
69. Samper, J.; Naves, A.; Pisani, B.; Dafonte, J.; Montenegro, L.; García-Tomillo, A. Sustainability of groundwater resources of weathered and fractured schists in the rural areas of Galicia (Spain). *Environ. Earth Sci.* **2022**, *81*, 141. [CrossRef]
70. Capa-Camacho, X.; Martínez-Pagán, P.; Acosta, J.A.; Martínez-Segura, M.A.; Vásconez-Maza, M.; Faz, Á. Environmental Monitoring of Pig Slurry Ponds Using Geochemical and Geoelectrical Techniques. *Water* **2024**, *16*, 1016. [CrossRef]
71. Asociación Española de Abastecimientos de Agua y Saneamiento. *XVII Estudio Nacional de Suministro de Agua Potable y Saneamiento*; Asociación Española de Abastecimientos de Agua y Saneamiento: Madrid, Spain, 2022. Available online: https://www.daquas.es/component/content/article/52-estudios/estudios-suministro/301-xvii-estudio-nacional-aeas-aga?Itemid=101 (accessed on 5 June 2025).
72. González-Gómez, F.; Martínez-Espiñeira, R.; García-Valiñas, M.A.; García-Rubio, M.A. Explanatory factors of urban water leakage rates in Southern Spain. *Util. Policy* **2012**, *22*, 22–30. [CrossRef]
73. González-Gómez, F.; García-Rubio, M.A.; Alcalá-Olid, F.; Ortega-Díaz, M.I. Outsourcing and efficiency in the management of rural water services. *Water Resour. Manag.* **2013**, *27*, 731–747. [CrossRef]
74. Picazo-Tadeo, A.J.; Sáez-Fernández, F.J.; González-Gómez, F. The role of environmental factors in water utilities' technical efficiency. Empirical evidence from Spanish companies. *Appl. Econ.* **2009**, *41*, 615–628. [CrossRef]
75. Carvalho, P.; Marques, R.C.; Berg, S. A meta-regression analysis of benchmarking studies on water utilities market structure. *Util. Policy* **2012**, *21*, 40–49. [CrossRef]
76. D'Inverno, G.; Carosi, L.; Romano, G. Environmental sustainability and service quality beyond economic and financial indicators: A performance evaluation of Italian water utilities. *Socio-Econ. Plan. Sci.* **2021**, *75*, 100852. [CrossRef]
77. Goh, K.H.; See, K.F. Twenty years of water utility benchmarking: A bibliometric analysis of emerging interest in water research and collaboration. *J. Clean. Prod.* **2021**, *284*, 124711. [CrossRef]
78. Guerrini, A.; Romano, G.; Campedelli, B. Factors affecting the performance of water utility companies. *Int. J. Public Sect. Manag.* **2011**, *24*, 543–566. [CrossRef]
79. Guerrini, A.; Romano, G.; Leardini, C. Economies of scale and density in the Italian water industry: A stochastic frontier approach. *Util. Policy* **2018**, *52*, 103–111. [CrossRef]
80. Marques, R.C.; De Witte, K. Is big better? On scale and scope economies in the Portuguese water sector. *Econ. Model.* **2011**, *28*, 1009–1016. [CrossRef]
81. Wan Rosely, W.I.H.; Voulvoulis, N. Systems thinking for the sustainability transformation of urban water systems. *Crit. Rev. Environ. Sci. Technol.* **2023**, *53*, 1127–1147. [CrossRef]
82. Algaba, M.H.P.; Huyghe, W.; Van Leeuwen, K.; Koop, S.; Eisenreich, S. Assessment and actions to support integrated water resources management of Seville (Spain). *Environ. Dev. Sustain.* **2024**, *26*, 7347–7375. [CrossRef]
83. Governo di Italia. Legge 5 gennaio 1994, n. 36–Disposizioni in materia di risorse idriche. In *Gazzetta Ufficiale n. 6 del 10 Gennaio*; Governo di Italia: Rome, Italy, 1994.
84. Danesi, L.; Passarelli, M.; Peruzzi, P. Water services reform in Italy: Its impacts on regulation, investment and affordability. *Water Policy* **2007**, *9*, 33–54. [CrossRef]
85. Governo di Italia. Norme in materia ambientale. In *Decreto Legislativo 3 Aprile 2006, n. 152. Gazzetta Ufficiale n. 88 del 14 Aprile 2006-Supplemento Ordinario n. 96*; Governo di Italia: Rome, Italy, 2006.
86. Governo di Italia. Legge 26 marzo 2010, n.42. Disposizioni in materia di enti gestori di servizi pubblici locali di rilevanza económica. In *Gazzetta Ufficiale n. 75 del 31 Marzo 2010*; Governo di Italia: Rome, Italy, 2010.
87. Governo di Italia. Decreto-Legge 6 dicembre 2011, n. 201. Disposizioni urgenti per la crescita, l'equità e il consolidamento dei conti pubblici. In *Gazzetta Ufficiale n. 284 del 6 Dicembre 2011–Suppl. Ordinario n. 251*; Governo di Italia: Rome, Italy, 2011.
88. Governo de Portugal. Decreto-Lei n.º 379/93, de 5 de novembro. In *Diário da República n.º 259/1993, Série I-A de 1993-11-05, Páginas 6214–6218*; Ministério do Ambiente e Recursos Naturais: Lisboa, Portugal, 1993.
89. Marques, R.C.; Simões, P.; Marques, E. The Financial Model for Water and Sanitation Services in Portugal: Lessons from Decades of Subsidies and Questionable Public Policies. *Water* **2024**, *16*, 3087. [CrossRef]

90. Massarutto, A. Economic Regulation, Water Pricing, and Environmental and Resource Costs: The Difficult Marriage Between Financial Sustainability, Investment Requirements and Economic Efficiency. In *Water Law, Policy and Economics in Italy*; Turrini, P., Massarutto, A., Pertile, M., de Carli, A., Eds.; Global Issues in Water Policy, Springer: Cham, Switzerland, 2021; Volume 28. [CrossRef]
91. Gaya, J. *Informe Sobre la Regulación del Ciclo Urbano del Agua en España*; Ministerio para la Transición Ecológica y el Reto Demográfico, Gobierno de España: Madrid, Spain, 2020. Available online: https://www.miteco.gob.es/content/dam/miteco/es/agua/temas/sistema-espaniol-gestion-agua/libro-verde-gobernanza/informes-tematicos/10-informe-tematico-regulacion-ciclo-urbano-agua-en-espana_tcm30-517276.pdf (accessed on 5 June 2025).
92. WAREG-European Water Regulators. *Key Performance Indicators Frameworks in Wareg Member Countries*; Wareg Report; WAREG: Brussels, Belgium, 2023. Available online: https://www.wareg.org/documents/kpis-report-2023-wareg-pdf/ (accessed on 5 June 2025).
93. Asociación Española de Abastecimientos de Agua y Saneamiento. Datos Sobre los Servicios del Agua Urbana en España. Resultados del XIV Estudio Nacional de Suministro de Agua Potable y Saneamiento en España 2016. Nota de Prensa. 2016. Available online: https://www.daquas.es/images/publicaciones/estudios-suministros/2016-notadeprensa.pdf (accessed on 5 June 2025).
94. EU. Directive (EU) 2024/3019 of the European Parliament and of the Council of 27 November 2024 Concerning Urban Wastewater Treatment (Recast) (Text with EEA Relevance) 2024. Available online: https://eur-lex.europa.eu/legal-content/EN/TXT/PDF/?uri=OJ:L_202403019 (accessed on 5 June 2025).

Disclaimer/Publisher's Note: The statements, opinions and data contained in all publications are solely those of the individual author(s) and contributor(s) and not of MDPI and/or the editor(s). MDPI and/or the editor(s) disclaim responsibility for any injury to people or property resulting from any ideas, methods, instructions or products referred to in the content.

MDPI AG
Grosspeteranlage 5
4052 Basel
Switzerland
Tel.: +41 61 683 77 34

Water Editorial Office
E-mail: water@mdpi.com
www.mdpi.com/journal/water



Disclaimer/Publisher's Note: The title and front matter of this reprint are at the discretion of the Guest Editors. The publisher is not responsible for their content or any associated concerns. The statements, opinions and data contained in all individual articles are solely those of the individual Editors and contributors and not of MDPI. MDPI disclaims responsibility for any injury to people or property resulting from any ideas, methods, instructions or products referred to in the content.





Academic Open
Access Publishing

mdpi.com

ISBN 978-3-7258-8578-7